Folding Dynamics in the Very Preterm Brain : Longitudinal Characterization of Sulcal Shape with Developmental and Functional Implications

Héloïse De Vareilles

THESE DE DOCTORAT

NNT : 2022UPAST065

université PARIS-SACLAY

Folding Dynamics in the Very Preterm Brain: Longitudinal Characterization of Sulcal Shape with Developmental and Functional Implications

Les dynamiques de plissement dans le cerveau très prématuré : caractérisation longitudinale de la forme des sillons avec implications développementales et fonctionnelles

Thèse de doctorat de l'université Paris-Saclay

École doctorale n° 575 Electrical, Optical, Bio-Physics and Engineering (EOBE)
Spécialité de doctorat : Sciences de l'information et de la communication
Graduate School : Informatique et sciences du numérique. Référent : Faculté des sciences d'Orsay

Thèse préparée dans l'unité de recherche **BAOBAB (Université Paris-Saclay, CEA, CNRS)**, sous la direction de **Jean-François Mangin**, directeur de recherche, le co-encadrement de **Jessica Dubois**, chargée de recherche, et le co-encadrement de **Denis Rivière**, ingénieur-chercheur.

Thèse soutenue à Paris-Saclay, le 24 mai 2022, par

Héloïse DE VAREILLES

Composition du Jury

Olivier COULON Directeur de recherche, Université Aix-Marseille (INT)	Président
Arnaud CACHIA Professeur, Université Paris Cité	Rapporteur & Examinateur
Maria DEPREZ Professeure associée, King's College London (Angleterre)	Rapporteure & Examinatrice
Manon BENDERS Professeure des universités – praticienne hospitalière, University Medical Center, Utrecht (Pays-Bas)	Examinatrice
Julien LEFÈVRE Maître de conférences, Université Aix-Marseille (INT)	Examinateur
John SUCKLING Professeur, University of Cambridge (Angleterre)	Examinateur
Jean-François MANGIN Directeur de recherche, Université Paris-Saclay	Directeur de thèse

université PARIS-SACLAY
DOCTORAL SCHOOL
Electrical, Optical, Bio: Physics and Engineering (EOBE)

Titre : Les dynamiques de plissement dans le cerveau très prématuré : caractérisation longitudinale de la forme des sillons avec implications développementales et fonctionnelles

Mots clés : plissement cortical, développement, IRM anatomique, prématurité

Résumé : Chez l'homme, le cerveau se plisse principalement in utero, pendant le troisième trimestre de grossesse : la surface du cortex au moment de la naissance à terme présente alors des creux (sillons) et des bosses (gyri) dont la forme reste relativement stable au cours de la vie. Les motifs de plissement du cerveau, bien qu'uniques à chaque individu, présentent une organisation globalement cohérente au sein de l'espèce, permettant d'identifier et de comparer les sillons entre individus. La variabilité en forme des sillons et ses relations avec la spécialisation fonctionnelle (que le contexte soit pathologique ou non) sont de plus en plus étudiées dans le cerveau mature, mais les études dans le cerveau en développement restent rares à cause de nombreuses difficultés soulevées par la neuro-imagerie du tout-petit.

Pendant mon doctorat, j'ai étudié les dynamiques de forme du plissement cortical sur la base de données d'imagerie par résonance magnétique (IRM) acquises longitudinalement dans une cohorte de nouveau-nés extrêmement prématurés, imagés vers l'âge équivalent à 7 mois de grossesse et à l'âge équivalent de la naissance à terme. J'ai adapté une méthode établie pour le cerveau adulte de caractérisation de la forme des sillons au contexte complexe du développement, et je l'ai appliquée à quatre régions corticales distinctes : le sillon central, la scissure sylvienne, et les régions périsylvienne et frontale inférieure, ces deux dernières n'ayant été explorées qu'à l'âge équivalent du terme du fait de leur apparition tardive dans le cerveau.

À travers mes travaux, j'ai tout d'abord décrit la variabilité en forme du sillon central et de la scissure sylvienne. Ceci m'a amenée à découvrir que la forme de ces plis est cohérente entre les deux âges, ce qui suggère un encodage précoce. J'ai par ailleurs évalué si la forme du sillon central permettait de prédire le devenir moteur des sujets : faute d'être significative, elle a néanmoins suggéré la pertinence fonctionnelle de certaines signatures sulcales.

Tout en étant concordantes avec l'état de l'art, mes observations sur le sillon central et la scissure sylvienne ont permis de détailler les motifs spécifiques et la chronologie d'encodage de leur forme précoce. En ciblant la scissure sylvienne et ses régions environnantes, j'ai émis l'hypothèse de dynamiques différentes entre l'opercularisation (processus menant au recouvrement du lobe insulaire par les lobes frontaux, pariétaux et temporaux) et la sulcation (processus menant à la formation des sillons) : mes observations ont alors suggéré une avance de l'hémisphère gauche dans le cadre de l'opercularisation, contre une avance de l'hémisphère droit pour la sulcation.

Par ailleurs, j'ai capturé des asymétries conséquentes entre hémisphères cérébraux, en détaillant les caractéristiques de formes dans chacun des objets sulcaux considérés : ces travaux ont ainsi contribué à une meilleure compréhension des asymétries précoces qui pourraient être liées au développement de la latéralisation fonctionnelle du cerveau en liens avec la latéralité manuelle ou la perception du langage.

De manière à compléter mes contributions, différentes directions devraient être explorées, dont la description de la variabilité des motifs des sillons et leurs relations avec le fonctionnement cérébral à des stades plus tardifs de développement de l'enfant et dans le cerveau de l'adulte, la quantification des altérations de plissement liées à la prématurité, et l'investigation plus approfondie des rapports entre opercularisation et sulcation, qui pourraient interagir ensemble au cours du développement.

Title : Folding Dynamics in the Very Preterm Brain: Longitudinal Characterization of Sulcal Shape with Developmental and Functional Implications

Keywords : cortical folding, development, anatomical MRI, prematurity

Abstract : In the human, the folding of the brain takes place mostly in utero, during the last trimester of pregnancy, resulting in a convoluted cortical surface at term, displaying furrows (sulci) and crests (gyri), whose patterns remain relatively stable throughout life. The same global folding organization is found between individuals, allowing to identify and compare matching sulci, while the more refined individual folding pattern is unique. The variability of sulcal folding pattern and its relations to functional specialization (both in health and pathology) are increasingly investigated in the mature brain, while studies in the developing brain are still scarce because of the many challenges of early-life neuroimaging.

During my PhD, I have investigated the dynamics of folding pattern based on longitudinally acquired magnetic resonance imaging (MRI) images from a cohort of extremely preterm infants, imaged once around the equivalent of 7 months of pregnancy, and once at term-equivalent age (TEA). I have adapted a pipeline established for adult sulcal shape characterization to the context of developing folds and applied it to four sulcal objects: the central sulcus, the sylvian fissure, and the perisylvian region and the inferior frontal region (these last two were only investigated at TEA because of their late appearance in the brain).

Throughout my works, I have described the shape variability observed in the central sulcus and the sylvian fissure at both ages. This led me to observe a consistent encoding of pattern between both ages, suggesting an early expression of sulcal shape features. I have incidentally tested if the central sulcus's shape was able to predict later motor outcome: even though it did not achieve significant results, it still seemed to suggest some functional relevance in sulcal signatures.

My observations on the central sulcus and sylvian fissure were concordant with the state of the art and detailed additional pattern specificities and the chronology of shape encoding. My focus in and around the sylvian fissure additionally led me to hypothesize a different dynamic in opercularization (the process leading to the burial of the insular cortex under the frontal, parietal and temporal lobes) from that in sulcation (the process leading to the formation of sulci): opercularization seemed to show an advance in the left hemisphere while sulcation has previously been reported to show an advance in the right hemisphere.

Moreover, I have captured hemispheric asymmetries and detailed their shape characteristics in each fold-related object or region considered. These studies have therefore contributed to shedding more light on early-life asymmetries., which could be linked to the functional lateralization of the brain regarding handedness or language perception.

In order to complement my contributions, additional investigations should be led in different directions, including the description of pattern variability and its links with brain function in later developmental stages in the child and the adult, the quantification of prematurity-induced sulcal alterations, and the further investigation of the relation between opercularization and sulcation processes, which might interact together during development.

1 AKNOWLEDGEMENTS

First and foremost, I would like to thank my three PhD supervisors, Jessica Dubois, Denis Rivière and Jean-François Mangin, who walked me through the wonderful life experience that my PhD proved to be. Their excellent advice and thoughtful considerations guided my steps along the path of sulcal development, which was fascinating to observe and investigate. I am unable to give an extensive list of the multiplicity of domains in which my three supervisors gave me advice or solutions, but it includes technical concepts, fundamental considerations, and the pursuit of my career. This triple co-supervision was complementary in many aspects, and led me to a fulfilling PhD experience, both on a theoretical and human level.

I would thereafter like to thank my collaborators and colleagues who contributed actively to the works produced in this manuscript. I address all my gratitude to Professor Manon Benders who made this whole adventure possible by sharing the MRI imaging data and additional clinical information of the cohort studied during my PhD, and for the enthusiasm she showed for my works. I also thank her team, and more specifically Maria-Luisa Tataranno and Nuša Stopar, who were valuable collaborators despite the distance. By extension, I wish to thank my referees, Arnaud Cachia and Maria Deprez, and the other members of my jury, Olivier Coulon, Julien Lefèvre, and John Suckling for accepting to assess my PhD thesis.

I would also like to thank all my colleagues from NeuroSpin whose participation in my works was essential, Joy Sun, Clara Fischer, Sara Neumane, François Leroy and Marco Pascucci and my friend and colleague from Cambridge University, Marin Ballu. Along with them I express my gratitude towards the colleagues who contributed to my works through thoughtful advice, namely Yann Leprince, Hugo Peyre, WenQi Shu-Quartier-Dit-Maire, Clément Poiret, and David Germanaud. Their involvement in my works allowed me to carry out my research as it is.

Right after, I would like to also thank my colleagues from both of my teams, BAOBAB/GAIA and InDev, for welcoming me warmly by their

sides during these years, and for being a never-ending source of awe through their respective research questions. Work-life by your sides was extremely pleasant. I take the opportunity to include my past team-members, who will not witness the end of my PhD but most certainly contributed to its joyful course. I would additionally like to thank all NeuroSpin for the general atmosphere which makes the lab an extremely inspiring working environment, as well as the CEA Saclay more globally for the services it proposes such as the leisure library and oil-painting classes, which I fully enjoyed during my PhD.

Inside and outside of the lab, every one of my friends had a huge impact on my mental well-being, and therefore on the successful pursuit of my research. Even though the COVID crisis made communication harder, it was great to have them virtually by my side during the harder times and physically by my side during the easier times. Special thanks to Louise Guillon, Lisa Perus and Julie Victor, for brightening my days on a daily basis and providing essential guidance in all kinds of matters, including scientific ones. In parallel, for their conviviality, I would like to thank Parvaneh Adibpour, Laurie Devisscher, Andrea Gondova and Sara Neumane. Within NeuroSpin, I cannot list all the people who were great throughout my stay, but Alex Popov deserves a special place, as a true friend and the person with whom I shared the whole experience, starting my pre-PhD internship by his side and denfending almost at the same time. I would like to express my profound gratitude towards Louise Morin and Maxime Gorwitz, for receiving me on a weekly basis and being wonderful at all times. I also want to thank my very dear friends Christel Michel, Léonard Laiter and Marin Ballu, whom I did not see as frequently but whose friendship and support kept me going.

Moreover, I wholeheartedly thank my four companions in role-playing adventures, Nicolas Vasselin (dungeon master), Alexandre Goy (Bœuf), Pierre Lataillade (Braize) and Alexandre Bas (Ryze), with whom we shared one single role-playing campaign during my entire PhD. I wish I had leveled up half as much as my own warrior (Uleek) during this PhD, but hey, at least I don't have the fate of the world on my shoulders… The hours of fun, unexpected results of our (sometimes unorthodox) attempts at solving problems had a real cathartic effect on my PhD. I also acknowledge the necessity to thank my other friends

and family for their patience to endure my passionate recollection of the latest role-playing adventure.

Last but certainly not least, I wish to thank my family for their constant support and their general awesomeness, during my PhD but also since ever, leading me to where I am now. Special thanks to Papa, Maman, Léonard and Ferdinand, but also to the ones who joined us through love, Agnese Ghersi and Chiara Infantino. On the topic of family enlargement through love, I am most grateful to my second family, Philippe and Catherine Geoffroy, along with Felix, Silvère and Marin, for welcoming me to their family a while ago and continuously supporting me with enthusiasm. I also thank those who left too early to witness this thesis but who inspired me enormously and whose memory I keep fondly in my heart, especially Grangran and Jean Benabou. Finally, I address my deepest gratitude to Robin Geoffroy, my fiancé, who not only brings me joy everyday but continuously reminds me how to enjoy life better. He is an incredible companion in every aspect, including moral, psychological and emotional support, which were essential during this fantastic PhD experience.

Thank you all dearly.

2 TABLE OF CONTENTS

3 LIST OF FIGURES

3.1 CHAPTER I

3.2 CHAPTER III

3.3 CHAPTER IV

4 LIST OF TABLES

4.1 CHAPTER I

4.2 CHAPTER II

4.3 CHAPTER III

4.4 CHAPTER IV

5 List of Abbreviations

ACC: anterior cingulate cortex
AUC: area under the curve
BPD: broncho-pulmonar dysplasia
BWZ: birth-weight z-score
CADASIL: cerebral autosomal dominant arteriopathy with subcortical infarcts and leukoencephalopathy
dHCP: developing Human Connectome Project
GA (w GA): gestational age (weeks of gestational age)
ICP: iterative closest point
IUGR: intra-uterine growth restriction
IVH: intra-ventricular hemorrhage
MA: moving average
mABC: movement assessment battery for children
MICCAI: medical image computing and computer assisted intervention society
MNI: Montreal Neurological Institute
MRI: magnetic resonance imaging
OHBM: organization for human brain mapping
OTS: occipito-temporal sulcus
PIPPI: perinatal, preterm and paediatric image analysis
PMA (w PMA): post-menstrual age (weeks of post-menstrual age)
PR: precision recall
ROC: receiving operator curve
STAP: superior temporal asymmetrical pit
STS: superior temporal sulcus
SVC: support vector classifier
TE: echo time
TEA: term-equivalent age
TR: repetition time

6 INTRODUCTION

The folding of the brain results from complex and intricate phenomena which are yet to be fully understood. Basic inter-studies comparisons reveal that mammal brains show an intriguing variability of folding, ranging from an absence of folds in small mammals such as mice, to a complex folded surface with individual shape variability as in the human, with in-between situations, as in the ferret, whose brain is folded in a manner that does not vary between individuals. This raises questions about the implications of brain folds (which globally increase in complexity with the size of the brain) in brain function, especially since alterations of cortical folding have been related to neurological adversities. Yet, the specificities of human brain folding are still poorly understood for a number of reasons. Its complex variability, which displays individual traits within a common global architecture, has been out of reach because of previous computational limitations. Moreover, in the absence of functional implications, the investigation of its non-pathological variability did not carry out much meaning. In addition, the fact that its development happens mostly *in utero* made its observation overwhelmingly complicated.

Modern-day neuroscience technologies offer new opportunities to investigate cortical folding in the human and its functional implications. The possibility for precise non-invasive *in vivo* imaging of the brain, notably through magnetic resonance imaging (MRI), opened the door to large cohort studies, necessary to assess global brain pattern variability. In parallel, the emergence of functional neuroimaging enabled the investigation of brain function and its anatomical correlates, leading to new insights about folding implications. Thus emerged the field of sulcal analysis, which set out to explore the cryptic variability of brain folding patterns, through the study of the geometry of the crests (gyri) and furrows (sulci) of the cerebral cortex. Additionally, the evolution of computational power and the advent of sophisticated computational methods paved the way for refined sulcal pattern studies.

The brain folds in a manner that is globally stable within mankind. This allows to give a nomenclature to the different fissures and sulci, to

compare them, and to assess abnormal gyrification patterns. Consequently, a growing literature has begun describing sulcation and investigating its implications. I propose to differentiate subdomains focusing on complementary sulcal questions. Evolutionary sulcal neuroscience focuses on the inter-species variability in sulcation suggesting potential correlates to the specificities of human cognition. Clinical sulcal neuroscience quantifies aberrations in sulcal patterns correlated to neuropathologies. Cognitive sulcal neuroscience assesses the links between cognitive abilities and sulcal landmarks. More generally, sulcal neuroscience investigates global sulcal shape variability and its general links to function.

As mentioned previously, in the human, cortical folding develops *in utero*. It can be divided in two distinct processes, opercularization and three successive sulcation waves, which we will detail later, which are due to concurrent cellular, genetic and biomechanical events. The folding pattern remains globally stable after birth, in such a way that pattern alterations observed in the adult brain relay valuable developmental informations. Yet, this information has to be explored in light of neurodevelopmental processes, which are challenging to investigate. The investigation of folding dynamics in the very young brain, historically restrained to *post mortem* fetal studies, is becoming increasingly successful, thanks to the development of methodologies dedicated to the very young brain, going as far as precise *in vivo* fetal MRI. Since the majority of sulcation takes place during the third trimester of gestation, the fetus is the optimal model to study the development of sulcation. However, it is challenging to assess sulcation longitudinally in the fetus since repeated MRI scanning outside clinical requirements are not recommended (and not allowed in France) for ethical considerations. Moreover, the act of birth has an impact on brain shape and hydrance, making difficult the longitudinal comparability of pre- and post-natal evaluations of folding.

Hence, the current thesis focused on a population of infants born extremely preterm scanned longitudinally, in order to investigate folding dynamics in the very young brain at a first age during early sulcation and at a second age, close to normal-term birth, when the general folding pattern approaches a relatively developed configuration. The purpose of this thesis is to contribute to the characterization of the

dynamics of folding pattern in the developing brain, through the means of three full-length articles:

I. Chapter I: A review of the state of the art addressing, in a first time, the reasons and methods for sulcal pattern studies in the human brain, and in a second time, the current knowledge on cortical folding in the developing brain through model, *post mortem* and MRI exploration

II. Chapter III: An original research article investigating the development of the central sulcus through advanced shape considerations and its link to later motor development, providing insights about an early sulcation phenomenon and its relation to function.

III. Chapter IV: An original research article addressing early asymmetries in and around the developing sylvian fissure through advanced shape characterization, providing insights about the process of brain opercularization, an early folding mechanism distinct from sulcation.

Chapter II is consecrated to the contextualisation of my PhD in terms of motivation and methods available independently from my contributions. After the presentation of these three articles and their respective implications, I discuss in Chapter V the additive value of my contributions in the understanding of early-life brain folding pattern, some resulting considerations about general human folding pattern, as well as discussing the validity and limits of the methods employed. I will finally conclude on the perspectives opened by this PhD thesis.

7 CHAPTER I: DEVELOPMENT OF CORTICAL FOLDS IN THE HUMAN BRAIN: AN ATTEMPT TO REVIEW BIOLOGICAL HYPOTHESES, NEUROIMAGING INVESTIGATION AND MODELLING STUDIES. *(FULL-LENGTH ARTICLE 1)*

7.1 CONTEXTALIZATION

In order to locate the contribution of the original research articles that I wrote during my PhD within the current body of literature on sulcal pattern and sulcal development, I propose the following article as a review of the state of the art on sulcal pattern investigation. This review gives an overview of the rich universe of sulcal studies, capturing the ever-growing scope of application of this discipline, supported by a multi-domain research effort. In its first half, after introducing reasons why we study cortical folding, I review different methods and approaches that have been developed for adult sulcal studies, and I then interrogate the specificities of human sulcation. The second half is dedicated to the development of sulci in the human, first explaining our current understanding of the mechanisms responsible for brain opercularization and sulcation, then observing the methodological advances and the opportunities they open for sulcal studies, and finally summarizing our current understanding on cortical folding in the earliest stages of life.

The following article is not yet published. It is intended for submission to the Flux special issue of the Developing Cognitive Neuroscience journal (submission scheduled in July 2022).

7.2 FULL-LENGTH ARTICLE

7.2.1 Investigating cortical folding in the adult

7.2.1.1 Why investigate cortical folding in the adult ?

A notorious characteristic of the human brain is its involuted shape, displaying ridges (gyri) and furrows (sulci). The resulting pattern is globally stable across individuals, which allows us to identify analogue sulci within the population and to compare them (Fig. 1). Yet, even though one can identify the same sulcus in two different brains, the shape and orientation of this sulcus will differ. It has actually been demonstrated that our "cortical foldingprints" are unique and allow individual identification (Duan et al., 2019a; Duan et al., 2020).

The first reason to investigate the outer shape of the brain and the specificities of its sulcation is for descriptive anatomy. In the end of the 19th century, the chronology of appearance of the different sulci (which we will detail in the next section, consecrated to the development of cortical folding) has been established through thorough post mortem observation of foetuses, as well as their evolution after birth with specimens ranging from childhood to adulthood (Cunningham, 1892). This memoir described with increased attention the sylvian fissure, the insula, the central sulcus, the intraparietal sulcus, and the frontal lobe sulci. This seminal work was the starting point of brain sulcal descriptive anatomy. Advances in neuroimaging now allows the scientific community to investigate this subject further, in vivo, with more reliable measures on larger cohorts. A meticulous description of anatomical specificities and variability of the human brain sulci has been undertaken. Different sulci have been described in terms of strict morphological variability across individuals: the cingulate and paracingulate sulci (Paus et al., 1996), the orbitofrontal sulci (Chiavaras et al., 2001), the precentral sulcus (Germann et al., 2005), the occipital sulci (Ialria & Petrides, 2007; Ialria et al., 2008), the collateral sulcus (Huntgeburth & Petrides, 2008; Huntgeburth & Petrides, 2012; Huntgeburth & Petrides, 2016), the postcentral sulcus (Zlatkina & Petrides, 2010), the caudal rami of the superior temporal sulcus (Segal & Petrides, 2012), the rhinal sulcus (Huntgeburth & Petrides, 2016), the sulcus diagonalis and the anterior

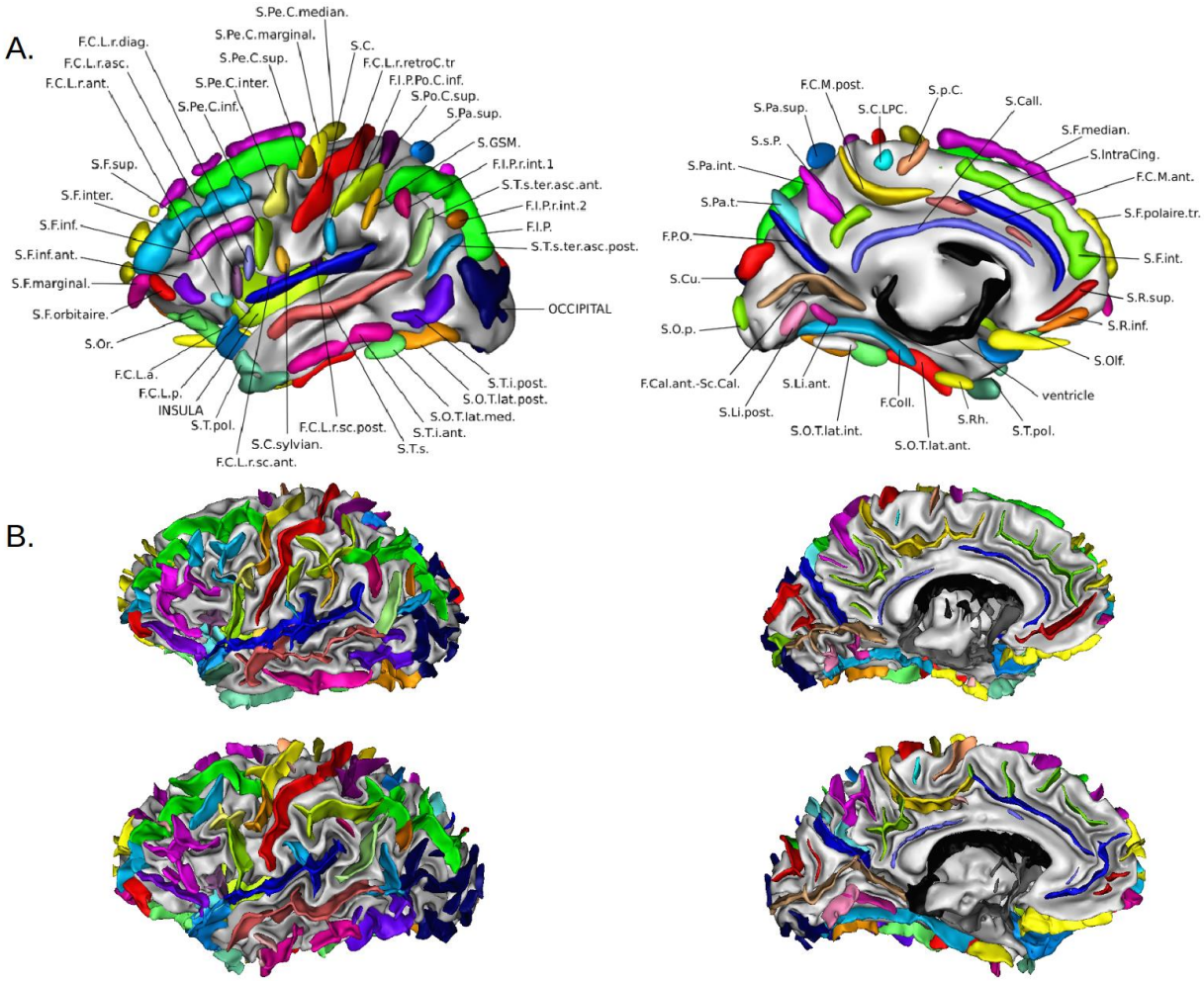

Figure 1: A. Sulcal nomenclature (Borne, 2019) represented on a thresholded statistical probabilistic anatomy map (Perrot et al., 2011) of a lateral (left) and medial (right) view of a left hemisphere. B. Lateral (left) and medial (right) views of two labelled left hemispheres.

Acronyms: S.Or.: orbital sulcus, S.F.orbitaire.: frontal orbary sulcus, S.F.marginal.: marginal frontal sulcus, S.F.inf.ant.: anterior inferior frontal sulcus, S.F.inf.: inferior frontal sulcus, S.F.inter.: intermediate frontal sulcus, S.F.sup.: superior frontal sulcus, F.C.L.r.ant.: anterior ramus of the sylvian fissure, F.C.L.r.asc.: ascending ramus of the sylvian fissure, F.C.L.r.diag.: diagonal ramus of the sylvian fissure, S.Pe.C.inf.: inferior precentral sulcus, S.Pe.C.inter.: intermediate precentral sulcus, S.Pe.C.sup.: superior precentral sulcus, S.Pe.C.marginal.: marginal precentral sulcus, S.Pe.C.median.: median precentral sulcus, S.C.: central sulcus, F.C.L..r.retroC.tr.: transverse retrocentral ramus of the sylvian fissure, F.I.P.Po.C.inf.: inferior postcentral sulcus, S.Po.C.sup.: superior postcentral sulcus, S.Pa.sup.: superior parietal sulcus, S.GSM.: sulcus of the supra-marginal gyrus, F.I.P.r.int.1: first interior ramus of the intraparietal sulcus, S.T.s.ter.asc.ant.: anterior terminal ascending branch of the superior temporal

sulcus, F.I.P.r.int.2: second interior ramus of the intraparietal sulcus, F.I.P.: intraparietal sulcus, S.T.s.ter.asc.post.: posterior terminal ascending branch of the superior temporal sulcus, OCCIPITAL: occipital sulci, S.T.i.post: posterior inferior temporal sulcus, S.O.T.lat.post.: posterior lateral occipito-temporal sulcus, S.O.T.lat.med.: medium lateral occipito-temporal sulcus, S.T.i.ant.: anterior inferior temporal sulcus, S.T.s.: superior temporal sulcus, F.C.L.r.sc.post.: posterior sub-central ramus of the sylvian fissure, S.C.sylvian.: central sylvian sulcus, F.C.L.r.sc.ant.: anterior sub-central ramus of the sylvian fissure, S.T.pol.: polar temporal sulcus, INSULA: insula, F.C.L.p.: posterior sylvian fissure, F.C.L.a.: anterior sylvian fissure, S.Olf: olfactive sulcus, S.R.inf.: inferior rostral sulcus, S.R.sup.: superior rostral sulcus, S.F.int.: internal frontal sulcus, S.F.polaire.tr.: transverse polar frontal sulcus, F.C.M.ant.: anterior cingulate sulcus, S.intraCing.: intracingulate sulcus, S.F.median.: median frontal sulcus, S.Call.: subcallosal sulcus, S.p.C.: paracentral sulcus, S.C.LPC.: paracentral lobule central sulcus, F.C.M.post.: posterior cingulate sulcus, S.Pa.sup.: superior parietal sulcus, S.s.P: sub-parietal sulcus, S.Pa.int.: internal parietal sulcus, S.Pa.t.: transverse parietal sulcus, F.P.O.: occipitoparietal sulcus, S.Cu.: cuneal sulcus, S.O.p.: occipitopolar sulcus, F.Cal.ant.-Sc.Cal.: calcarine sulcus, S.Li.post.: posterior intralingual sulcus, S.Li.ant.: anterior intralingual sulcus, S.O.T.lat.int.: internal occipitotemporal sulcus, F.Coll.: collateral sulcus, S.O.T.lat.ant.: anterior lateral occipitotemporal sulcus, S.Rh.: rhinal sulcus, S.T.pol.: polar temporal sulcus, ventricle: ventricle.

ascending ramus of the sylvian fissure (Sprung-Much & Petrides, 2018). Aside from strict anatomical description, looking into sulcation is useful for inter-subject alignment. In order to compare brain features (either morphological, microstructural or functional) between any number of individuals, a necessary step is to align brains in order to analyse analogous regions. Historically, because of the variability of folding patterns across individuals, brain registration was handled by spatial volume normalisation to a standard space implying little to no sulcal constraint, and resulted in template brains with blurry contours. This was not optimal since sulcation is an important marker for individual architecture and that such registration techniques dimmed out this individual variability. Therefore, numerous methods of brain registration involving sulci in a more or less direct manner have been developed. The context of the use of sulci as landmarks has already been detailed previously (Mangin et al., 2015a; Mangin et al., 2016), but we will give a quick overview of the major tools for brain registration and present the most recent solutions. We can differentiate two types of registration approaches taking sulci into account: those that aim for a global sulcal consistency and those that

try to match specific sulci together. To integrate global sulcal consistency, templates of average folding patterns have been built iteratively by using 2-D spherical representations of the cortex minimizing sulcal mismatch, as implemented in CIVET (Lyttelton et al., 2007) and FreeSurfer (Fischl, 2012). Their volumetric counterparts are ANTS (Avants et al., 2011) and DARTEL (Ashburner, 2007). Through curvature information, sulcal considerations have also been integrated in multi-modal surface matching (MSM), alongside myelin maps and resting-state networks (Robinson et al., 2014; Robinson et al., 2018). In terms of specific sulcal matching, both 2-D (HIPHOP; Auzias et al., 2013) and 3-D (DISCO, Auzias et al., 2011) approaches have been developed in order to focus on the diffeomorphic registration of individual folding patterns, matching corresponding pre-labeled sulci while producing correct alignments of grey and white matter volumes (Fig. 2). This sulcal approach, combined with the classic 3-D anatomical registration approach DARTEL (Ashburner, 2007), provides a valuable registration approach for heterogeneous datasets, such as datasets including *in vivo* and *post mortem* imagery at different developmental stages (Lebenberg et al., 2018).

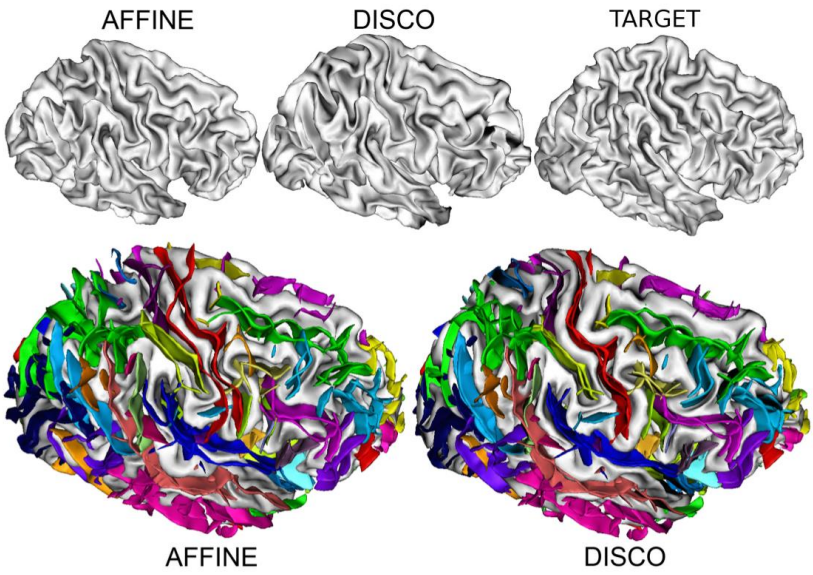

Figure 2: Comparison between the registration of two hemispheres using either affine or sulcally-constrained (DISCO) registrations (courtesy of Auzias et al., 2011)

Last but not least, the investigation of cortical sulcation is motivated by the search for ***anatomo-functional correlates***. This correlation is actually one of the motivations for sulcal-based registration. A recent study has reviewed the currently assessed links between sulcation and brain function, cognition and behaviour, which praised the multi-disciplinary investigation on the matter, yet concluded that our understanding of sulco-gyral link to function is still in its infancy (Jiang et al., 2021). In whole-brain studies, the match between regions delimited by sulci and architectonic areas, defined by localizable changes in either cytoarchitecture or myeloarchitecture (Brodmann, 1909; Vogt & Vogt, 1911), has been tested on histological data, and proved to be globally reliable, but with decreasing performance with increasing folding complexity in relation to brain development (i.e. cortical areas delineated by primary folds such as the central sulcus or the calcarine sulcus show a better link between sulcal-defined regions and Brodmann areas than the ones delineated by tertiary folds) (Fischl et al., 2008). Moreover, comparing subjects registration either in the Talairach space or using curvature-based cortical alignment showed that the latter technique issued significantly increased consistency in inter-subject functional activations, with better alignment in cortical regions delineated by primary folds once again (Frost & Goebel, 2012). Region- or sulcus-specific studies have also linked functional activation and sulcation in different brain areas: around the precentral gyrus (Fig. 3; Yousry, 1997; Amiez et al., 2006; Sun et al., 2016; Germann et al., 2019; Eichert et al., 2021), around the postcentral sulcus (Zlatkina et al., 2016), around the angular gyrus (Segal & Petrides, 2013), around the superior temporal sulcus (Sun et al., 2016), in the ventromedial prefrontal cortex (Lopez-Persem et al., 2019), and in the anterior cingulate cortex (Huster et al., 2009).

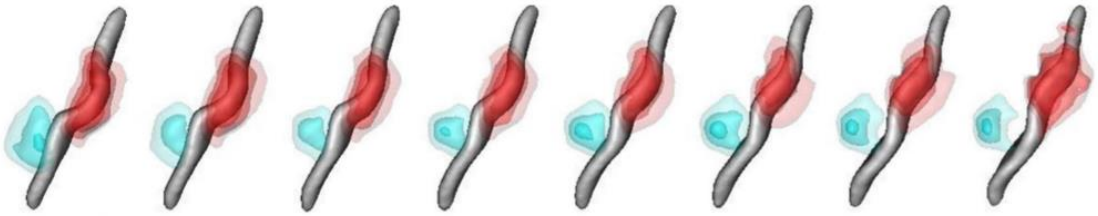

Figure 3: Group-average functional activations for motor (red) and reading (blue) tasks mapped with fMRI and superposed on the main variability trait of the central sulcus (courtesy of Sun et al., 2016). Note that the functional hand activation follows the hand knob's ascension along the axis, and that the reading activation moves farther away from the central sulcus as the second knob appears.

7.2.1.2 Methods to investigate sulcation

Now that we summarized the main reasons for exploring sulcal patterns, let us explore the means developed to do so. We can dissociate two types of methodologies: those that address the shape variability of sulci in a global approach, quantifying the shape of all the sulci in a given region or in the whole brain, and those that look into sulcus-wise shape variability, focusing on a given sulcus and assessing its shape variability within a given cohort. A challenge about these sulcus-specific shape studies is that they require accurate sulcal identification compared to the global approaches, which can rely on geometric considerations to quantify sulcation. Here, we will describe both methodologies, but following this section, we will mostly focus our attention on sulcus-wise shape variability.

7.2.1.2.1 Methods to investigate global shape variability

Without the necessity of identifying specific sulci, the standard method for quantifying regional or whole-brain sulcation specificities is to compute global or regional ***gyrification indices***. Initially relying on 2D coronal slices of frozen brains, the "historical" gyrification index is computed by dividing the pial length of the region of interest by the length of the outer envelope of the same region (Zilles et al., 1988). This method historically mostly relied on manual delineation of both of the surfaces, which has since then been automated (Moorhead et al., 2006). The gyrification index was subsequently refined by computing

it on 3D cortical reconstructions in order to ensure a better reconstruction of the pial surface and an easier interpretation of gyrification anomalies, including finer topological representations of anomalies and better capture of buried sulci (Schaer et al., 2008).

To go further in detail with regional gyrification, it is necessary to use a ***parametrization method*** on the brain to quantify individual gyrification. Such a method has been elaborated by spherical inflation in order to represent the whole cortex on a sphere, which is a simple parametrizable surface (Fig. 4; MacDonald et al., 1994; Fischl et al., 1999). Such spherical parametrisation paved the way to curvature-based methods, for example to estimate local gyrification more robustly (Luders et al., 2006). Furthermore, this concept of whole brain folding parametrization for fold analysis has been optimized through the definition of the depth potential function, which is both a faster and more precise folding parametrization process. This function is useful for registration with sulcal constraints as well as for detection of local sulcation differences between groups (Boucher et al., 2009).

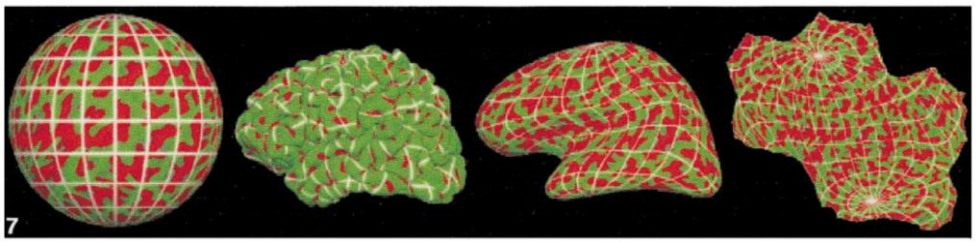

Figure 4: Spherical coordinate system mapped onto a variety of surface representations, from left to right: spherical, pial, inflated, and flattened spherical (courtesy of Fischl et al., 1999)

A more specific field has been derived from these depth parametrization methods: the study of ***sulcal roots or sulcal pits***. The sulcal root model is based on the hypothesis that sulcation develops from stable elementary folds appearing during the fetal stage (see next section), with sulci resulting from the merging of these stable elementary folds. This implies that the variability of sulcal pattern is due to variations in the way sulcal roots merge and not to their initial position or number, which is stable across individuals. These sulcal roots can thereafter be inferred by investigating the resulting curvature of sulcal walls and

fundi (Cachia et al., 2003; Régis et al., 2005). A similar yet slightly different concept is that of sulcal pits, which are defined as the local depth maxima of sulci, in order to provide more stable landmarks than sulci (Fig. 5; Lohmann et al., 2008; Im et al., 2010). A precursor approach for sulcal pits used the watershed algorithm to automatically extract sulcal regions (Rettmann et al., 2002). The two objects (sulcal roots and pits) are very similar and vary mostly in terms of concept: the sulcal roots are defined as the first atomic folding entities, which happen to get buried in the deepest parts of the sulci during development, while the sulcal pits are defined as the deepest parts of sulci, which are inferred to match the earliest, most stable folding units. The sulcal pit automatic extraction method has thereafter been refined to ensure increased inter-subject reliability and to extract pits from shallower folds than the initial method (Auzias et al., 2015). The method is suited for whole brain studies of variability and asymmetry in the presence of *plis de passage* (gyri buried inside a sulcus connecting its two walls), which have been quantified in regard to their heritability (Le Guen et al., 2018). In continuity of the detection of sulcal pits, the structural graph-based morphometry (SGBM) framework has been elaborated, representing folding patterns as pit-graphs, in order to be able to quantify folding shape differences and to spatially scale these differences (Takerkart et al., 2017). The latest curvature-based approach for describing regional patterns of sulcation is based on multi-view curvature features (Duan et al., 2019b). The method derives multiple curvature features from a curvature map by decomposing it by frequency and by building a gyral crest map, leading to an extensive description of cortical folding. This method is then pushed further to generate clusters of region-specific typical folding patterns, which we will address in the section about sulcus-specific shape characterization since it implies regional labelling which is similar to sulcus labelling.

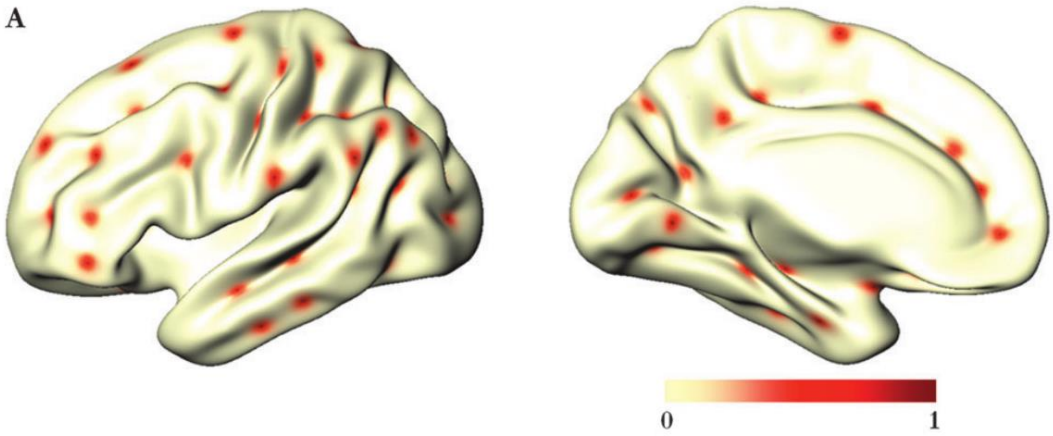

Figure 5: Sulcal pits of an individual brain projected on an averaged surface template (courtesy of Im et al., 2010)

Specialized methods for whole brain analysis have also been developed based on other parametrization approaches relying on ***curvature maps***. Based on the mean curvature of the grey-white interface, computed using curvature and diffusion flow (Desbrun et al., 1999), the spectral analysis of gyrification (SPANGY) has been developed to question and quantify the spectral distribution of the global and local shapes of the brain, including the folding patterns (Germanaud et al., 2012). This tool highlighted that different folding frequencies might correspond to the different waves of cortical folding, with lower frequencies corresponding to the primary sulci and increasing frequency corresponding to secondary, then tertiary folding (Dubois et al., 2019). Adopting a different approach, a more refined tool than the local gyrification index has been derived from curvature maps: the local shape complexity index. This index measures local shape complexity by computing the surface shape index (Koenderink & van Doorn, 1992) in the whole brain and computing the local variance of this index, offering finer and more localized shape complexity quantification (Kim et al., 2016a).

To transition between global shape variability approaches and sulcus-specific approaches requiring sulcal identification and labelling, let us present a global approach relying on sulcal identification: the subclinical abnormal gyration pattern (Régis et al., 2011). This method relies

on automatic labelling of sulci integrating a confidence metric for labelling. A number of neural networks trained on manually labelled control brains identify sulci on patient brains expected to show abnormal gyrification. Abnormal gyration patterns are thereafter identified by splitting the confidence metric by sulcus, and by selecting the sulci with scores inferior to the fifth percentile of sulcal scores of the training brains.

7.2.1.2.2 Methods to investigate sulcus-specific shape variability

Before addressing the methods for shape characterization of specific sulci, let us have a quick overview on the current methods for ***sulcal identification and labelling***. Obviously, the most natural yet time-consuming method for sulcal labelling is manual labelling by a trained expert based on reference atlases (Ono et al., 1990; Petrides, 2019). Manual labelling is still widely used despite the advances in automated labelling, either for correction of automatic labelling in variable or ill-defined sulci, because the great variability of cortical folding patterns makes it impossible to achieve perfect automatic performances, or for the definition of more refined specific labels for sub-sections of sulci. Yet, manual labelling is complex and sometimes ambiguous, even for trained experts, and it is not sustainable for studying large cohorts. This motivated the development of increasingly reliable automated labelling methods, which in addition improve reproducibility compared to non-experts. The different approaches for sulcal automatic labelling have been reviewed a few years ago (Mangin et al., 2015b). As many methods have been developed, we do not pretend to be exhaustive on the matter. Typical approaches include using a congregation of neural networks trained on manually labelled brains (Rivière et al., 2002), or graph matching using shape, orientation, location, and neighbourhood information (Yang & Kruegel, 2009). Another method was developed by using a Bayesian framework based on a probabilistic atlas (Perrot et al., 2011), and a more recent whole-brain approach achieves a better preformance using convolutional neural networks, both in accuracy and computation time (Borne et al., 2020). It should be noted that sulcus-specific methods are also developed to focus on specific elements of brain folding, such as the paracingulate sulcus for example (Yang et al., 2019).

Once the conundrum of sulcal labelling is resolved, the ***shape variability of specific sulci*** can be assessed. Examples of applications of different methods are highlighted below, but are by no means exhaustive of the very abundant literature in the domain. Simple metrics are useful for shape characterization and readily used in literature thanks to their automatic extraction in the openly-distributed brain analysis software BrainVISA (https://brainvisa.info). Using this software, sulci are defined through a watershed algorithm based on MRI intensities which detects a surface within the cerbrospinal fluid filling up the folds, the superior limit being delimited by the brain hull (Mangin et al., 2004a). Recent studies have characterized sulcal shape in terms of length alone (Yang et al., 2019), length and depth (Hotier et al., 2017; Mangin et al., 2020), length and surface area (Hopkins et al., 2014), depth and width (Kochunov et al., 2005), and a combination of length, mean depth, width, and surface area (Pizzagalli et al., 2020). Another metric that can be derived from these automatically extracted measures is the ***local sulcal index***, defined as the ratio between a sulcus's surface area and the outer cortical area (Cachia et al., 2008; Sarrazin et al., 2018).

These methods offer basic shape metrics but fail to capture more advanced shape properties such as pattern and location. An option to include ***pattern information*** in the sulcal analysis is by eye. Still today, visual classification of patterns in post mortem brains is informative (Wysiadecki et al., 2021). Either directly based on the MRI images (Steinmetz, 1990; Chiavaras & Petrides, 2000; Germann et al., 2005; Amiez et al., 2006; Zlatkina & Petrides, 2010; Huntgeburth & Petrides 2012; Sprung-Much & Petrides, 2018; Lopez-Persem et al., 2019; Eichert et al., 2021), or on volumetric reconstructions of the brain (Mellerio et al., 2015; Cachia et al., 2016; Cachia et al., 2017; Gay et al., 2017; Cachia et al., 2018; Del Maschio et al., 2019), *in vivo* visual classification of sulcal pattern is more practical to link it to function. Yet, the visual assessment directly based on MRI images normally requires manual tracing and identification of the sulci. Thankfully, automated methods for tracing are being developed in specific regions, such as in the occipito-temporal cortex (Snyder et al., 2019). On volumetric representations, sulcal detection and labelling are more advanced, as stated earlier. For example, the occipito-temporal sulcus of a cohort

has been manually classified between continuous, interrupted in the anterior part, and interrupted in the posterior part. The length of the interruption was also captured, and both the pattern and the length of this sulcus were associated to reading skills (Cachia et al., 2018). The sulcal shape investigation using more than simple metrics is also possible with automated methods. While comparing schizophrenia subjects with inner and outer-space hallucinations, after the observation of a significant difference in voxel-based morphometry around the right superior temporal sulcus, a group of researchers decided to compare the relative positioning of this sulcus in each group (Plaze et al., 2011). Thus, they superimposed the sulci on a Montreal Neurological Institute (MNI) referential and, at a given depth, averaged the position of each subgroup's superior temporal sulci using barycentres. By doing so, they demonstrated that patients suffering from outer space hallucinations had a significantly higher superior temporal sulcus in the right temporoparietal junction than patients suffering from inner space hallucinations.

Another option to characterize shape with more detail than length or depth is by quantifying its ***shape features***. An interesting approach, applicable on continuous sulci without branching, is quasi-isometric length parametrization (Fig. 6; Coulon et al., 2015). Applied to the central sulcus, it is able to quantify the position of the extremities of the hand knob (a characteristic bulk of the central sulcus), and therefore to compare the hand knob's location in different subgroups. It also opens up the possibility for depth parametrization along the sulcus, with which it is possible to observe subtle regional depth variations, for instance in the main branch of the superior temporal sulcus (Leroy et al., 2015) or in the central sulcus (Gajawelli et al., 2021). Alternatively, the sulcal depth profile, which we already addressed in the section about global shape variability, can also be used for shape characterization in a given sulcus such as the superior temporal sulcus (Le Guen et al., 2018).

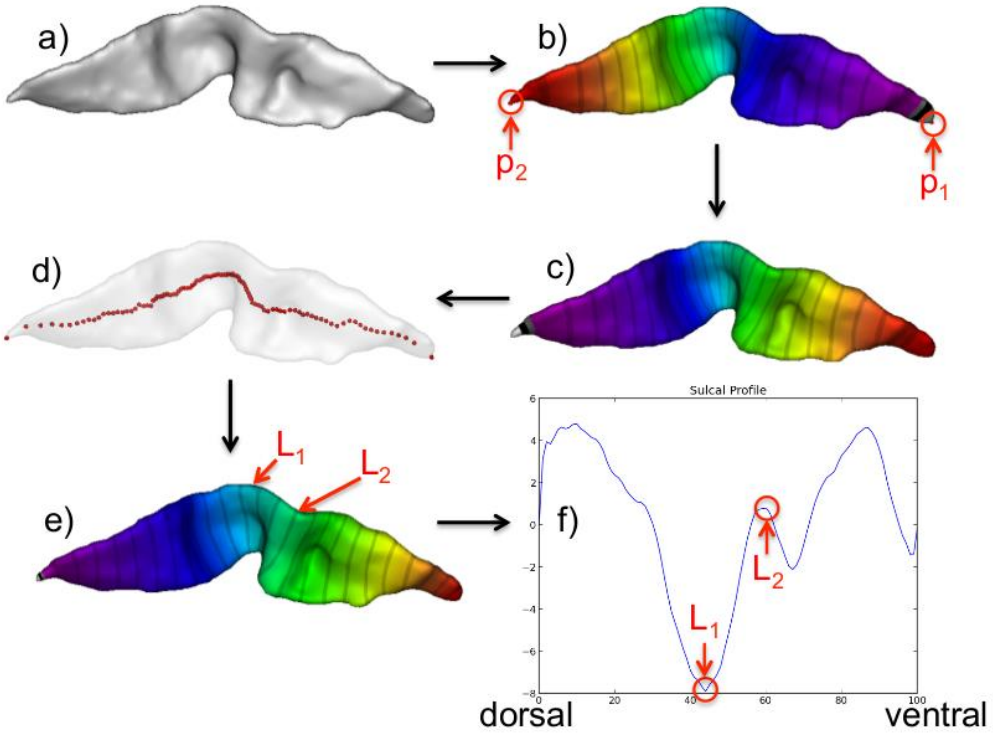

Figure 6. Illustration of the pipeline for quasi-isometric shape parametrisation. a) Central sulcus's mesh; b) Fielder vector and its extrema; c) initial length parametrization; d) medial axis; e) quasi-isometric length parametrisation; f) resulting sulcal profile with L_1 and L_2 the hand-knob marker positions. Stripes indicate isocontours (courtesy of Coulon et al., 2015).

In order to go further into shape characterization, we can also rely on ***machine learning to extract pattern information*** from a given population. A first approach consists of extracting 3-D moment invariants as descriptors of sulcal shape (which have interesting mathematical properties but are not easily interpretable) and classifying the results through dimension reduction using a principal component analysis (PCA), interpreting shape variability afterwards (Mangin et al., 2004b; Sun et al., 2007). The concept of classifying sulci based on shape dissimilarity was then pushed further by capturing the overall shape similarity between the sulci, rather than limiting the comparison to a finite number of parameters (the 3D moment invariants), and by adopting a dimensionality reduction algorithm more suited to the differentiation of sulcal shape (Sun et al., 2009). The overall shape similarity is then

captured by considering every possible pair of sulci in the cohort, applying a pairwise registration using the iterative closest point algorithm, and computing the residual distance after registration as the dissimilarity metric between the sulci. After aggregating the resulting metrics from the whole cohort, the Isomap algorithm (Tenenbaum, 2000) is applied for dimension reduction, which leads to the extraction of dimensions capturing the main shape variability of the studied sulcus. For example, this method captured a transition from a "single knob" (sulcus with one hump) to a "double knob" (sulcus with two humps) configuration of the central sulcus (Sun et al., 2012; Sun et al., 2016). The approach based on multi-view curvature feature briefly introduced before in the global shape characterization section also generates regional shape clustering, which do not strictly correspond to sulci yet yield valuable information about sulcation (Duan et al., 2019b). Once the multi-view curvature features are computed, by extracting the features from a specific region of interest, it is possible to compute the folding difference between every pair of subjects, and convert the resulting inter-subject distance matrices into similarity matrices. Then the matrices are fused together into a matrix containing both shared and complementary information from the cohort, on which is applied an "affinity propagation" clustering method (Frey and Dueck, 2007) which automatically sets the number of clusters. The resulting clusters differentiate subtypes of folding patterns, allowing description of the variability of folding patterns in the brain in a discontinuous approach.

7.2.1.3 Specificities of sulcation of the human brain

Now that we have discussed why and how we study cortical folding, let us have a rapid overview of what we now know about sulcation of the human brain, without mentioning either its cause or its development, which will be addressed in the second section of this manuscript. The human brain is not the only one with convolutions; in fact, many mammals show cortical folding, with their specificities depending on the species (Fig. 7; Van Essen et al., 2019). Studying the gyrification process and variability across animals contributes preciously to the understanding of sulcation in general, and has been historically investigated in parallel to human sulcation (Gratiolet, 1854; Cunningham, 1892; Welker, 1990). In this perspective, studying animals is motivated by two main reasons: to investigate the evolutionary process of brain

folding, and to be able to proceed to invasive experimental set-ups (such as gene knock-out or corticectomy) which are essential to explore and better understand the mechanisms driving the folding process but are unacceptable in the human for obvious ethical reasons.

7.2.1.3.1 Comparative description of brain folding across mammal brains

Several reviews detail the ***evolution of cortical folding*** across species and discuss the underlying mechanisms, either as the main topic (Zilles et al., 2013) or as a subtopic in the context of biological considerations (Borrell, 2018; Llinares-Benadero & Borrel, 2019). Interesting facts include the observation that gyrification index linearly increases with brain volume, but with different scales depending on the order (Zilles et al., 2013), that different experimentations on animals led to the appearance of folds on an initially flat brain, but some of them did not produce plausible underlying organisation (Borrell, 2018), and that gyrencephaly is an ancestral mammalian trait, lost by some species since then (Llinares-Benadero & Borrell, 2019).

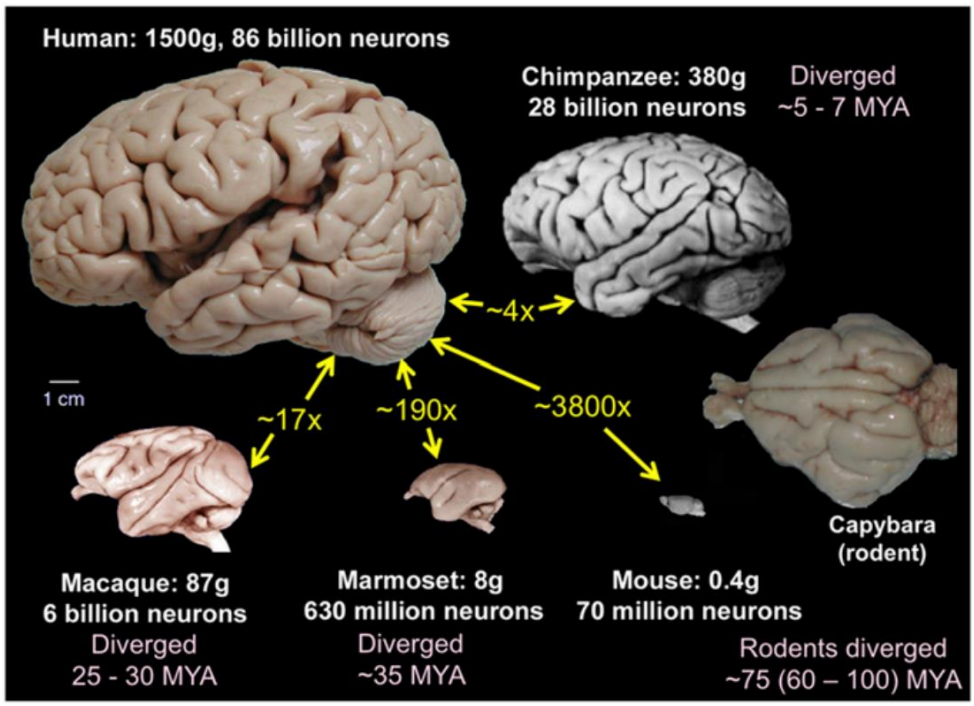

Figure 7: Scaled pictures of brains of four primate and two rodent species. Size ratios (in yellow) are based on brain weight (courtesy of Van Essen et al., 2019).

To interrogate the specificities of the human brain, the most relevant animal comparison is found in ***non-human primates***. A recent review of literature gives a comprehensive depiction of the primate brain evolution, including a section on gyrification and one on sulcal anatomy (Friedrich et al., 2021). We here summarize the main findings about sulcal shape in non-human primates and the way in which the human brain differs from theirs. An interesting concept was inferred from a comparison including macaques, human term-born infants, and adults (Hill et al., 2010). It pointed out that regional expansion of cortical surface area is similar during human development and primate evolution, and consequently suggested that regions of recent evolutionary expansion may benefit from maturing after birth, either for post-natal environment integration, or to prioritize early-life resources on regions optimizing early-life survival. Focusing more specifically on sulci, different studies have quantified either the similarities or the differences in the shape or patterns of sulci across species. In particular, the orbitofrontal cortex showed the same pattern variability in humans and macaques, even though the human brain showed some additional sulci inducing more complex configurations (Chiavaras & Petrides, 2000). The central sulcus's morphology was compared within ten species of primates (including humans), which suggested that the central sulcus's surface area showed a linear trend relative to the overall cortical area, within all primates except for the human (Hopkins et al., 2014). Moreover, the middle *frontoparietal "pli de passage""* (a buried gyrus within the central sulcus which has been observed in the human) was only present in great apes and was deeper than humans' for chimpanzees, gorillas and bonobos but not for orangutans, suggesting a more prominent "pli de passage" in humans and orangutans, and therefore possibly a greater connectivity and sensory-motor integration between the pre and post-central gyri.

Moreover, comparisons between humans and chimpanzees unveiled ***human-specific sulcal asymmetries***. Using sulcal depth profiles on the superior temporal sulcus, a rightward depth asymmetry (i.e. a significantly more important depth in the right than in the left hemisphere) in the superior temporal asymmetrical pit (STAP), was present in humans as soon as birth, as well as in children and adults, while it

was absent in chimpanzees (Leroy et al., 2015). Comparing length, positioning and bending of the sylvian fissure, it was shown that the leftward length asymmetry found in human adults was not reciprocated in the chimpanzee, with notably the sylvian fissure ending more posteriorly in the left hemisphere than the right only in humans (Hou et al., 2019). This study also reported a more frequent bifurcation of the sylvian fissure in humans, which tends to show an upward posterior branching, when chimpanzees show a less frequent bifurcation rate, and favour a configuration where the ascending ramus faces anteriorly. Nevertheless, it should be reminded that other asymmetries are shared between different species. For example, handedness was historically believed to be human-specific, including its anatomical correlates in terms of sulcal depth (with a deeper contralateral central sulcus in the region of the hand). Similar handedness-related depth asymmetries have been demonstrated in great apes (Hopkins et al., 2014) and olive baboons (Margiotoudi et al., 2019). Similarly, a recent study dismissed a sulcal asymmetric landmark previously thought to be human-specific, by identifying it in the chimpanzee, and assessing its functional relevance compared to humans: the paracingulate sulcus (Amiez et al., 2021). This finding led to a more in-depth study of the chimpanzee's cingulate cortex, which observed that the chimpanzee's oro-facial motor control was linked to the presence of a paracingulate sulcus, and identified asymmetries in the depth of the cingulate sulcus, with a leftward asymmetry in its anterior part and a rightward one in its posterior part (Hopkins et al., 2021). Similarly, a recent study reported a leftward asymmetry of the planum temporale (adjacent to the sylvian fissure) in the macaque brain, undermining the proposition that leftward planum temporale asymmetry constitutes a human-specific developmental marker for language development (Becker et al., 2020). These different observations highlight the relative complexity of the human brain compared to its closest phylogenetic cousins, with a differentiation mostly found in higher-order (associative) cortical regions, such as the lateral temporal or parietal cortices, or the prefrontal cortex, and the fact that cortical asymmetries are not all human-specific

7.2.1.3.2 Folding specificities in the human brain

Let us now return to the human brain and have an overview of its folding specificities, from broader to finer considerations. A first global observation is that ***the degree of gyrification scales with brain size***. Larger brains show more augmentation in surface area than in cortical thickness, even if both increase (exponent after log-regression inferior to one third for the cortical thickness, superior to two thirds for the surface area), and this increase in surface area is due to a higher number of folds rather than deeper folds (Im et al., 2008). This allometric scaling of gyrification compared to brain size is also valid locally on small cortex patches (Leiberg et al., 2021). Through spectral decomposition of folding, this positive allometric scaling was quantified for total folding power, and it showed different values based on the folding waves (Germanaud et al., 2012): the contribution of primary folding was constant, that of secondary folding increased similarly to total folding power, and that of tertiary folding increased almost twice as much, inducing additional pattern elements.

Still on a general point of view, as aforementioned, one of the specificities of the human brain lies in some of its ***asymmetries***, yet it is important to keep in mind that some asymmetries are also found in great apes, implying that the notion of hemispheric asymmetry is not strictly human-specific. In a pioneer sulcal shape study, the mean shape and evolution of major sulci has been assessed in children, adolescents and adults, which revealed shape asymmetries in the superior temporal sulcus, sylvian fissure, and postcentral sulcus at the three ages, with an important increase of asymmetry in the sylvian fissure between childhood and adulthood (Fig. 8; Sowell et al., 2002). A rightward asymmetry in the superior temporal sulcus's depth (around mid length, under Heschl's gyrus), the superior temporal asymmetrical pit (STAP) has been demonstrated to be human specific by comparison with chimpanzees (Leroy et al., 2015). Through a whole-brain sulcal pit and depth profile study, it was evidenced that the rightward asymmetry of the STAP is associated with more frequent interruptions of the left superior temporal sulcus through *"plis de passage"* (Le Guen et al., 2019). More globally, more "*plis de passage*" were detected in the left hemisphere along the whole superior temporal sulcus (except in its polar extremity), the superior part of the postcentral sulcus, and the

polar part of the inferior temporal sulcus. In the right hemisphere, more "*plis de passage*" were captured in the posterior part of the intraparietal sulcus and in the superior part of the precentral sulcus. This extended a previous study which already compared the relative distribution of sulcal pits in both hemispheres, and reported that the left hemisphere shows one more sulcal pit than the right one because the frequency of pits was too low in the anterior but not polar region of the right superior temporal sulcus (Im et al., 2010). This study additionally reported differences in sulcal pit distributions depending on the hemisphere: in the left one, the upper part of the postcentral sulcus, parts of the superior temporal sulcus, and the lower part of the calcarine sulcus; in the right one, the upper part of the parieto-occipital sulcus. In addition, the pits of the posterior part of the right superior temporal sulcus were more spatially variable than the left one's. Incidentally, to complement these anatomical observations about sulcal pit distribution with related functional findings, it has been reported that the depth pits of the superior temporal sulcus within the STAP are landmarks for the position of voice functional peaks along the length of the superior temporal sulcus, and that while not statistically significant, there was a trend towards a higher activity on the right side, suggesting a link between anatomical and functional asymmetries (Bodin et al., 2018).

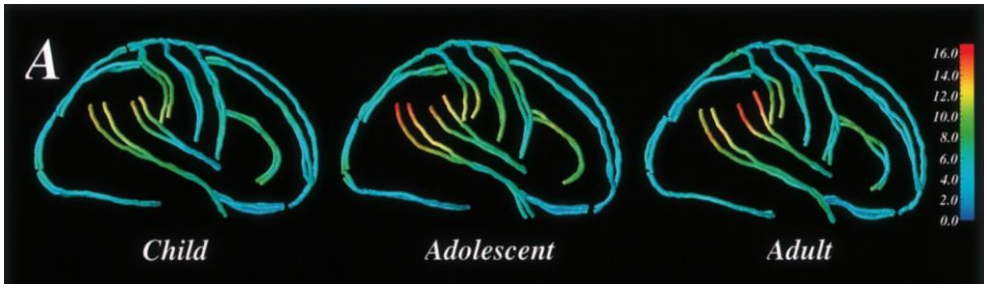

Figure 8: Superposition of the average sulcal shape profile of the left and right hemisphere at during childhood, adolescence and adulthood. The colour bar indicates average sulcal displacement asymmetry (courtesy of Sowell et al., 2002).

7.2.1.3.3 Sulcal patterns as proxy of early developmental mechanisms

These sulcal patterns, globally matching within the population yet specific to each individual, happen to remain stable during lifespan. Yet, it

should be noted that during childhood, a length increase of the left inferior frontal sulcus and a posterior shifting of the left precentral sulcus have been reported (Blanton et al., 2001), and that during adolescence, the cortex flattens, inducing reduced sulcal depth and increased sulcal width mostly in the frontal and occipital cortices (Aleman-Gomez et al., 2013). During adulthood, sulci widen and become shallower with age, with a significant sex effect, inducing a more pronounced effect in males in the superior temporal, collateral, and cingulate sulci (Kochunov et al., 2005). Yet, this does not seem to affect significantly the sulcal patterns that appear early on; a striking example is the longitudinal stability of the pattern of a variable tertiary sulcus – namely the paracingulate sulcus – which has been tested in a longitudinal cohort of subjects spanning ages 7 to 32 years, and has been reported to be fixed in childhood in every single case (Cachia et al., 2016).

This longitudinal stability of folding patterns erects sulcal pattern as a lead macroscopic ***anatomical proxy for in utero development*** (Mangin et al., 2010; Cachia et al., 2021). Thanks to this longitudinal stability, sulcal pattern has been reported to correlate to prenatal dispositions to cognition, response to later-life neurological adversities, and predisposition to psychiatric or neurological disorders. In terms of healthy cognitive variability, a number of studies have focused on the shape of the anterior cingulate cortex (ACC) regarding the presence or absence of a paracingulate sulcus in one or both hemispheres. With a battery of verbal and spatial tasks as assessment, adults with a leftward asymmetry in the ACC (i.e. a strictly more pronounced paracingulate sulcus in the left hemisphere than in the right) showed better performances than those with symmetrical or rightwards asymmetrical ACC (Fornito et al., 2004; Fornito et al., 2008). Using the Stroop test, it was found that a leftward asymmetrical ACC pattern leads to a better inhibitory control in adults (Huster et al., 2009), in children (Borst et al., 2014) and to a higher cognitive control efficiency in children (Cachia et al., 2014). Using the Flanker test, monolinguals with a leftward asymmetrical ACC pattern showed better cognitive control efficiency, while the opposite trend happened in bilinguals (Cachia et al., 2017; Del Maschio et al., 2019). In addition to the ACC, an asymmetry of the inferior frontal sulcus's pattern (either interrupted or continuous) also led to a better inhibitory control both in children and young adults (Tissier et al., 2018).

The folding pattern of the occipito-temporal sulcus (OTS, either continuous, interrupted anteriorly, or posteriorly), for its part, has been associated with reading accuracy (Cachia et al., 2018). Adults with a left OTS interrupted in the posterior region (matching the functional localization of the visual word form area) showed a better reading fluency than adults with a continuous left OTS; additionally, the length of this interruption correlated with the reading skills (Fig. 9). In the lateral prefrontal cortex, the sulcal depth of specific tertiary sulci was associated with individual differences in reasoning scores (Voorhies et al., 2021). This corpus of evidence demonstrates the intricate relation between sulcal pattern and normal cognitive development such as cognitive control or reading efficiency, in which individual environment can play a part, such as bilingualism.

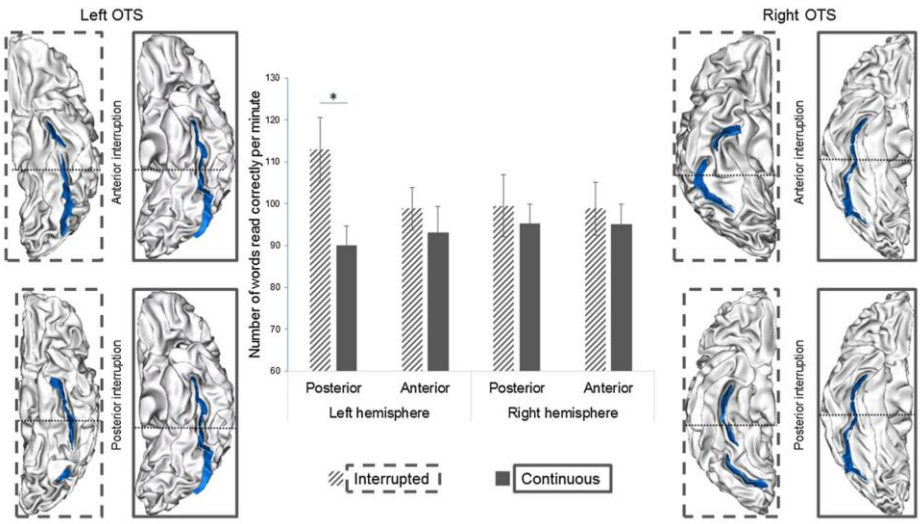

Figure 9. Relationship between the interruption of occipitotemporal sulcus (OTS, in blue) and reading ability. For the different individual hemispheres, the black dashed line represents the frontier between an anterior or posterior interruption. The error bars depict one standard error to the mean, and the * highlights the significantly different result (at $p<0.05$) between interrupted and continuous sulci (courtesy of Cachia et al., 2018).

At the interface of normal and pathological development lies the ***susceptibility to neurological adversities***. In the context of schizophrenia, the shape of the superior temporal sulcus in the right temporoparietal junction (functionally related to the "where" auditory pathway)

presented opposite deviations between subjects with inner space hallucinations and outer space hallucinations compared to healthy controls (Plaze et al., 2011). Under the hypothesis that both of these displacements of the right superior temporal sulcus can be observed in the general population (inducing an average positioning of the control subjects between the inner and outer space positioning), it can be interpreted that this whole folding variability is normal, but yet relates to the inner or outer perception of auditory hallucinations if they occur. Again in the schizophrenia spectrum, it was reported that a specific orbitofrontal sulcal pattern (medial orbital rostral and caudal regions disconnected with a continuous lateral orbital sulcus) in the right hemisphere is related to the absence of transitioning to psychosis in subjects at high risk, suggesting that displaying this pattern is advantageous against transition to psychosis (Lavoie et al., 2014). In the context of cerebral autosomal dominant arteriopathy with subcortical infarcts and leukoencephalopathy (CADASIL; a severe cerebral small vessel disease), the severity of the disability affecting subjects has been associated with the shape of the central sulcus, and more specifically with cumulative shape of the left and right central sulci in terms of height and size of the hand knob (higher and smaller hand-knobs were linked to more severe outcomes; Jouvent et al., 2016). Such variability of the central sulcus's shape appears as non-pathological since it concurs with that observed in a control cohort (Sun et al., 2012), yet it appears to be related to the severity of outcome in this pathological situation (Jouvent et al., 2016), suggesting an association between sulcal shape and a motor reserve in which to draw from in case of adversarial events.

In terms of links between pathological outcomes and sulcal pattern, we transition from a sulcal variability which can be considered as normal, with an impact on outcome in case of an adversarial context, to a sulcal pattern variability which is pathological, as suggested by the following non-exhaustive examples. In Turner syndrome subjects, the right intraparietal sulcus shows decreased maximal depth and a tendency towards reduced length, with additional pattern anomalies such as missing portions, aberrant branches or ending, unusual interruptions and a lack of downward convexity, accompanied by an anterior displacement of the central sulcus (Molko et al., 2003). In the context

of congenital unilateral limb absence, the central sulcus contralateral to the absent limb is significantly flatter than in acquired amputation and control situations, which implies that folding pattern signatures can be specific to developmental events (Sun et al., 2017). Contrarily to typical control subjects, ramifications of the precentral sulcus merging into the central sulcus have been reported in type 2 focal cortical dysplasia, a subtype of epilepsy (Mellerio et al., 2015), as well as a symmetrical sylvian fissure in length in patients suffering from Huntington disease, along with sulcal widening in different sulci (Mangin et al., 2020). Sulcal widening is not our focus since it relates to neurodegenerative processes, while the absence of length asymmetry in the sylvian fissure is certainly related to altered neurodevelopmental events.

This overview of folding studies suggests that sulcal patterns, which develop mainly *in utero*, are a reliable biomarker for neurodevelopment, be it in health or in pathology.

7.2.2 Folding progression during development

In the human, the folding of the brain occurs mainly *in utero*, during the third trimester of pregnancy. Before detailing its chronology of appearance and specificities (2.3), first of all I had a general overview of the current knowledge on folding mechanisms (2.1), and I then reviewed the specific MRI-based methods which have been developed to investigate the developing brain, be it in the foetus or the neonate (2.2).

7.2.2.1 Folding mechanisms

A number of different scientific fields have tried to understand why the brain folds for certain but not all mammals and have brought to light concurring mechanisms. Before assessing their causes, let us differentiate two different types of folding: the brain opercularization and sulcation. Opercularization is due to a greater development of the frontal, parietal and temporal lobes compared to the insular lobe, inducing a folding of these regions over the insula (implying that the frontal and parietal lobes become neighbours to the temporal lobe, over the insula), and resulting in the Sylvian Fissure. On the reverse, sulcation *per*

se seems to be due to intricate cellular phenomena inducing a mechanical buckling within a given region, resulting in the apparition of sulci.

Cellular biology, genetics and biomechanics have proposed different models to describe and explain these folding mechanisms, initially investigated separately. A number of reviews have brought together these different findings, which I have summarized here in order to gain a better overall understanding of the process. Among them, some have focused on the combination of cellular biology and biomechanics (Lewitus et al., 2013; Ronan et al., 2015), including a dual perspective review with both a cellular biology (Borrell 2018) and a biomechanistic (Kroenke & Bayly, 2018) point of view, with comments from the other perspective. Others have rather focused on the combination between cellular biology and genetic processes, which seem to orchestrate the biological events leading to cortical folding (Sur & Rubenstein, 2005). More recent reviews have combined the three approaches for a more global understanding of the overall folding mechanisms (Fernández et al., 2016 ; Llinares-Benadero & Borrell, 2019). Here, we will summarize the main cellular, genetic and biomechanical events underpinning cortical folding.

7.2.2.1.1 Cellular biology

In terms of ***cellular biology***, a comprehensive review precisely depicts the detailed organization of the fetal and neonatal brain (Kostović et al., 2019). Here, we will focus on processes which are directly linked to cortical folding. A first observation is that in the mature brain, the cortex is thicker in gyral crests and thinner in sulcal fundi. The morphology and distribution of the cortex's components differ between crests and fundi: in crests, the "column and layer" neuronal organization is more precise, the density of cell bodies is lower, the myelinated fibres are denser, oriented more vertically, and the pyramidal neurons show a vertically oriented configuration, with longer and more elaborated dendrites than their counterparts in sulcal fundi (Llinares-Benadero & Borrell, 2019). In gyrencephalic species, these specificities arise from the multiple neurogenetic events concurring in the developing brain,

including neuronal and glial cell proliferation and migration. Regarding proliferation, in the ferret, a heterogeneous rate of neurogenesis has been reported in the developing cortical mantle, with regions of higher neuronal density matching future gyral crests and regions of lower neuronal density matching future sulcal fundi, resulting in a homogeneous neuronal density across the cortex in the mature brain (Rockel et al., 1980). Migration is also an important factor in sulcation: the inhibition of intercellular adhesion of migrating cortical neurons induces folding without progenitor cell amplification in mice (a normally lissencephalic species), while preserving layered organization and radial glial morphology (del Toro et al., 2017). Incidentally, a recent review article has assessed different animal models inducing cortical folding and differentiated the ones which resulted in realistic folding properties from those which did not (Borrel, 2018). The migration of neurons during neurodevelopment from the ventricular and subventricular proliferative zones to the cortical mantel is guided by radial glial cells. These also seem involved in cortical folding: in lissencephalic species, the radial glial cells are parallel, while they are distributed in a heterogeneous manner in gyrencephalic species, with fan-shaped configurations in the regions undergoing greater folding expansion inducing a greater tangential expansion of radially migrating neurons (Llinares-Benadero & Borrell, 2019). This divergence of radial glial cells can be linked to the relative abundance of *basal* radial glial cells in gyrencephalic species compared to lissencephalic ones, whose cell somas are located both in the inner and outer subventricular zones where they undergo mitosis. The large number of basal glial cells, which extend their basal fibre in the pre-existing radial glial scaffold, cause a divergence in it (Fig. 10). A recent review further suggests that the subplate (a transient layer between the cortical plate and the intermediate zone – future white matter) may drive cortical folding through directional cues to guide fibres (Rana et al., 2019).

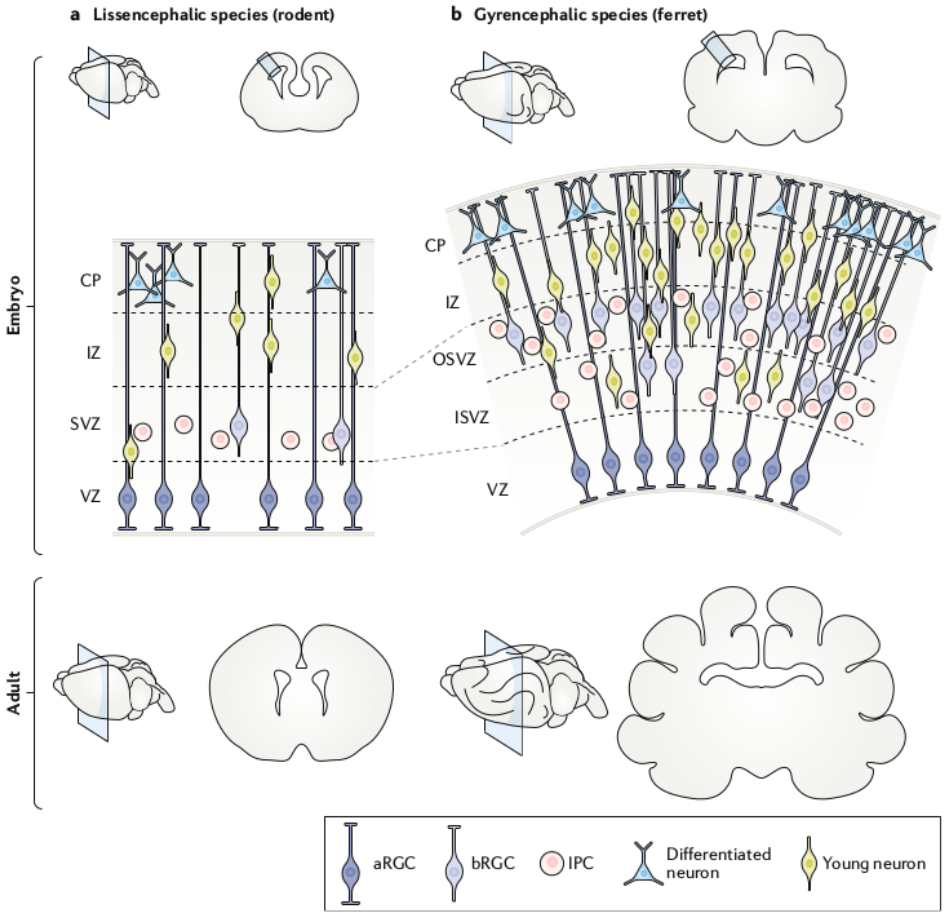

Figure 10. Illustration of cellular organisation during cortical development in the embryonic stage and resulting gyrification in the adult in a. a lissencephalic species and b. a gyrencephalic species (courtesy of Llinares-Benadero & Borrell, 2019). CP: cortical plate; IZ: intermediate zone; SVZ: subventricular zone; VZ: ventricular zone; OSVZ: outer subventricular zone; ISVZ: inner subventricular zone; aRGC: apical radial glial cell; bRGC: basal radial glial cell; IPC: intermediate progenitor cell.

7.2.2.1.2 Genetics

These biological events seem to be thoroughly ***genetically constrained***. For example, as mentioned above, the ferret brain shows heterogeneous neurogenesis rates along the germinal layers which seem to match the future location of sulci and gyri: genetic patterning has concurrently been observed, with specific genes displaying similarly heterogeneous degrees of expression which matched future folds, and

which were associated to differences in proliferation and neuronal migration (Llinares-Benadero & Borrell, 2019). In link to the opercularization mechanism, in the human, it was reported that the frontal, parietal and temporal lobes show differences in transcriptome compared to the insula, including genes related to neuronal proliferation and differentiation (Mallela et al., 2020). These are refined clues that genetics and cellular mechanisms linked to folding are intertwined. Previously, less refined clues suggested the implication of genetics in cortical folding. For example, in pathology, an association has been reported between bilateral frontoparietal polymicrogyria (inducing abnormally small and numerous gyri in the frontal and parietal regions) and the mutation of a given gene encoding a G-protein coupled receptor (Piao et al., 2004). In the general population, males have been reported to show longer sulci than females after correcting for brain size (while sex chromosome dosage did not show specific impacts on overall folding architecture; Fish et al., 2016).

More generally, the heritability of various sulcal metrics have been tested, which led to conclude that earlier forming sulci show higher heritability and that the most heritable sulcal metric is sulcal width (Pizzagalli et al., 2020). Although these different results suggest some genetic implication in cortical folding, it seems far from explaining the complexity of sulcal shape: when comparing monozygotic twins to dizygotic twins, it was observed that while brain size is highly heritable, the heritability of sulcal pattern is lower, even though monozygotic twins show more similar patterns than dizygotic twins (Bartley et al., 1997). The higher sulcal similarity between monozygotic twins have been reproduced comparing them to unrelated pairs of subjects using sulcal graph matching based on sulcal pits (Im et al., 2011). It is interesting to assess genetic constraints using the sulcal pits model, since sulcal pits or roots have been hypothesized to be anatomical correlates of the "protomap" folding model, according to which the early cells of the embryonic vesicle carry their intrinsic program for species-specific cerebral regionalization (protomap: Rakik, 1988; link to sulcal roots: Régis et al., 2005). To go further, the heritability of deep sulcal pits has been tested, and it was shown to have some small yet relevant symmetric genetic influences on the left and right hemispheres (Le Guen

et al., 2018). Moreover, this study reported a specific heritability asymmetry across the two hemispheres, in the superior temporal sulcus, with the left one being more genetically constrained. Further investigation found an association between the anatomy of superior temporal regions and a given genomic region, in the depth of the left STAP (Le Guen et al., 2019). A recent review focusing on sulcal pits and the developing brain suggested a link between the stability of sulcal pits distribution and the stability of the human-specific protomap (Im & Grant, 2019). From this corpus of evidence, we can conclude that genetic influence is crucial for the formation of folds, but not sufficient to explain the variability of folding patterns in the human brain.

7.2.2.1.3 Biomechanics

The missing piece of the puzzle is perhaps ***biomechanics***. Diverse biomechanical models considering different tissues with different viscoelastic properties have been proposed to simulate cortical folding, and recent models have highlighted that changing some parameters (such as initial geometry, or cortical thickness) induce folding variations which can both justify intra and inter-species variability. A number of reviews have discussed the different models in relation to supporting or opposing evidence from a number of fields, including animal, mathematico-physical, and computational models (Toro & Burnod, 2005; Bayly et al., 2014; Garcia et al., 2018; Kroenke & Bayly, 2018; Foubet et al., 2019; Heuer & Toro, 2019; Van Essen 2020). We tried to summarize these different theories here.

In ***computational modelling of brain folding***, the classic approach is to consider the brain before sulcation as composed of two layers: the outer layer representing the cortical plate, and the inner layer representing the tissue between the cortical plate and the proliferative ventricular surface, i.e. the intermediate zone (Kroenke & Bayly, 2018). Theories for cortical folding can be dichotomized between those which consider that *the governing forces arise from either the outer or the inner layer*. A first hypothesis of *outer-layer governing forces* is that the skull and meninges constrained the outer expansion of the cortex, forcing it to fold in order to fit in its container. This theory was disproved, notably through the observation of gyration after relieving cranial pressure in cats (Welker, 1990). Another outer-layer governing

forces theory, which is, this time, well supported by a number of domains, is that of tangential and greater expansion of the outer zone compared to the inner zone, the differential expansion of the two zones inducing a mechanical buckling which results in cortical folding (Toro & Burnod, 2005). This theory is supported by biophysical models using swelling gels (Tallinen et al., 2014; Tallinen et al., 2016) and numerical simulations (Xu et al., 2010; Tallinen et al., 2016). The consistency of this theory and experimental results pushed further investigation on how different parameters of such models imply variations in sulcation which concur with observations, including stiffness, growth rate, initial cortical plate thickness, and initial geometry (Wang et al., 2019; Wang et al., 2021). Independently from the two-layer model, additional computational efforts have been deployed to model the variability of brain folding pattern through reaction-diffusion mechanisms based on Turing morphogens to mimic the differential growth of sulci and gyri (Lefèvre & Mangin, 2010). This model resulted in developmentally consistent patterning of the brain and in variations in sulcal pattern matching some observed in real-life (such as sulcal interruptions).

In terms of ***inner-layer governing forces***, a first hypothesis was that radial growth of the inner zone occurs at different rates, and that gyri arise from more growth of the inner zone than in sulci. This has been disproved: if gyri were formed by the inner zone pushing the outer zone outwards, a compressive radial force should arise at the centre of gyri, while a tensile force is observed (Xu et al., 2010). Another inner-zone governing forces theory, more popular than the previous one, is the axon tension theory. In its original form, it hypothesized that the tension along axons pulled the sulcal walls together, inducing folds (Van Essen, 1997). Axonal tension has indeed been reported in the developing ferret brain, yet not in the direction which would induce folding (Xu et al., 2010), apparently disproving the axon tension theory. Nevertheless, an updated version of the tension-based morphogenesis has been proposed with the "differential expansion sandwich plus" (Van Essen, 2020), which offers to solve the apparent contradiction between tension-based models and experimental observations.

In any case, biomechanical forces may fill in the last brick of cortical folding dynamics, with plausible causes for inter-individual variability.

Yet, it should not be reduced to the final brick, coming after cellular and genetic considerations, since all three are deeply intertwined: mechanical forces, in turn, affect cellular activity. Biological forces affect geometry through mechanical stress, impacting the pathways of morphogens and signalling molecules (Foubet et al., 2019; Heuer & Toro 2020). Therefore, even though at first, these different fields were brought together mainly to validate or invalidate a given model based on its compatibility with the other fields, it appears that the mechanisms are not only concurrent but also interactive, and recent reviews advocate the combination of the three domains to understand the complex mechanisms at play (Fernández et al., 2016 ; Llinares-Benadero & Borrell, 2019).

In order to validate the different models proposed to explain folding mechanisms, refined *in vivo* analysis of human development have to be conducted. These require specific methodological developments because of the many hurdles in acquisition and processing of fetal and neonatal MRI.

7.2.2.2 Specific methods for the analysis of cortical folding through MRI in the fœtus/neonate brain

Now that we have clarified the current understanding of the folding mechanisms, we will address the difficulties of studying sulcation *in vivo* in the foetus, newborn (post-natal age below 28 days) or infant (below 1 year of age) through the means of MRI (it should be noted that MRI is not the exclusive means of anatomical imaging in these populations, as, for example, ultrasound allows sulcal investigation to some extent, though limited; Ginsberg et al., 2021). Recent reviews have brilliantly assessed the situation and explored the limits and perspective of early-life neuroimaging (Vasung et al., 2019; Li et al., 2019), with the second one focusing more on computational developments to adapt methodologies developed for more mature brains to the infant brain. In order to summarize the difficulties arising from the study of early folding, we discussed some considerations concerning acquisition of MRI data, segmentation, registration, and some ulterior computational methods which have required methodology adaptations.

The present listing of methodologies requiring special attention because of specificities of the developing brain is far from exhaustive. Our purpose here was mostly to highlight the reach of methodological complexities induced by the study of the brain during its major folding dynamics, and to sensitize the reader to hidden bias that may be neglected when projecting adult methodologies to such young brains.

7.2.2.2.1 MRI acquisition

MRI ***acquisition*** in the foetus is complex for a number of reasons, including the size of the object imaged, requiring a high spatial resolution in order to capture the details of brain structures, the presence of the foetus in the womb, which both prevents the operator from choosing the angle of acquisition and induces important movement artefacts since the foetus can freely move during the acquisition, added to the motions of the womb due to the mother's breathing, to the presence of the mother's tissues, and the maturational stage and the water environment of the brain, which is responsible for lower contrast in brain images between grey and white matter tissues (for review, see: Studholme, 2015). This requires the development of ultra-short imaging sequences (less than 30 seconds) to minimize motion.

In the neonate, the motion complexity caused by the *in utero* environment is relieved, especially around birth when the baby can easily be put to sleep during acquisition (after been fed). Yet the problems of brain size and maturational stage remain, requiring special efforts in resolution and contrast. The immaturity of the cerebral tissues and the high water content of the brain in the neonate reverses the classic adult contrasts. T2 weighted sequences are generally preferred in infants before 4-6 months of age as it enables a better contrast between grey and white matter than T1w MRI, even though it generally suffers from thicker slices (Dubois et al., 2014). The period between 6 months and a year is particularly challenging since the maturation of cerebral tissues and myelination of the white matter induce a reversal of contrast, which temporarily blurs the frontier between grey and white matter, heterogeneously within different regions which mature at different tempos. Yet in the scope of this review, we will focus on the fetal and early neonate period, before this challenging time-window.

7.2.2.2.2 Pre-processing and tissue segmentation

In fetal MRI, the first step is to correct 3D head movements during fast multi-slice imaging, enabling general fetal imagery rather than limiting fetal studies to small subsets with limited movements. This can be achieved through the use of super-resolution tools, increasing contrast and resolution in T2 weighted imagery (Rousseau et al., 2006; Gholipour et al., 2011; Kuklisova-Murgasova et al., 2012; Rousseau et al., 2013 ; Fig. 11). Motion correction (Cordero-Grande et al., 2018) and super-resolution tools are also suited for neonatal imagery (Makropoulos et al., 2018a).

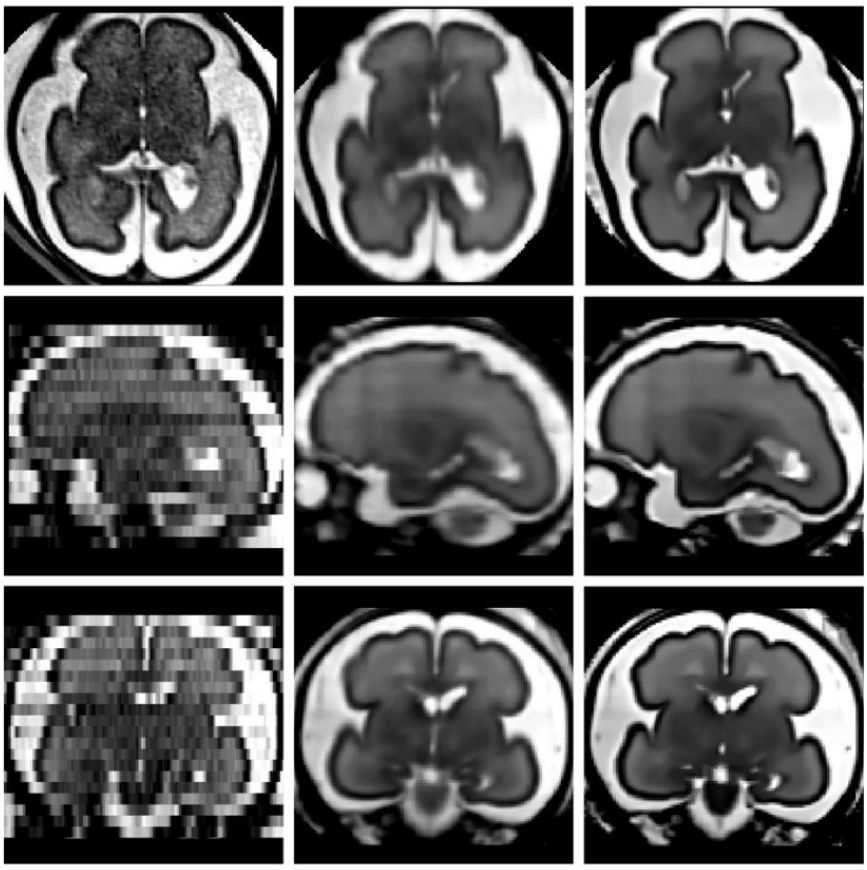

Figure 11. Illustration of reconstructed fetal brain MRI images. Top row: axial, middle row: sagittal, bottom row: coronal, left column: original images, middle columns: reconstructed images using local sparse interpolation, right columns: super-resolution reconstruction coupled with non-local denoising (courtesy of Rousseau et al., 2013)

After acquisition, correction of motion artefacts and reconstruction of super-resolved images, the MRI images need to be ***segmented*** to allow analyses, by differentiating the different components of the image (such as grey matter, white matter and cerebrospinal fluid) based on their contrasts and morphology. This process needs special adjustments in the very young brain for the same reasons as stated above: the objects are small for the resolution (inducing reduced precision as well as partial volume effects), the images are altered by motion, which cannot always be corrected during pre-processing, and the ongoing maturational process induces contrast specificities. Segmentation can be operated manually, yet to gain time and improve consistency and reproducibility in group studies, automatic segmentation methods are required, both in the foetus and neonate (for review, see: Makropoulos et al., 2018b). There are two main categories of segmentation pipelines, either atlas-based or not. For concision, we will prevent from detailing the technicalities of atlas construction, but it should be noted that impressive efforts are deployed to build ever more refined atlases, in the foetus, the preterm, and the neonate (Kuklisova-Murgasova et al., 2011; Wu et al., 2021). Once produced, brain atlases (which can be sophisticated probabilistic atlases computed over a group or within a given age-range, but also single subject labelled images) are useful for segmentation: they can be used (through registration) to initialize tissue delineation in MRI images, as a source of spatial information to guide local tissue labelling, enhancing intensity-based subsequent tissue recognition (in the foetus: Habas et al., 2010; in the preterm: Cardoso et al., 2013; Kim et al., 2016b; Liu et al., 2016; in the TEA preterm: Anbeek et al., 2013; in the term-born neonate: Prastawa et al., 2005; Shi et al., 2010; Wang et al., 2011; Wang et al., 2015). The direct use of atlas registration for segmentation can be achieved using longitudinally acquired images and through extrapolation of neonatal tissues based on images of the same brain at 1 or 2 years old, but this method is restricted to longitudinally-acquired datasets (Shi et al., 2010). Apart from this specific case, the methods following atlas priors are diverse, such as level set methods (Wang et al., 2011), expectation-maximisation algorithms (Cardoso et al., 2013; Makropoulos et al., 2014; Makropoulos et al., 2018), multi-atlas texture patches and joint proba-

bility-based label fusion (Kim et al., 2016b), combination of expectation-maximisation and patch-based methods (Liu et al., 2016), or fuzzy c-means thresholding (Bae et al., 2021).

Inclusion of multi-modal images for refined segmentation has also been achieved in the neonate (Wang et al., 2015). The use of atlases (which can be costly to create, in terms of manual segmentation, number of images required, and age-specificity requirements) is convenient for prior definition, but can be problematic if the image requiring registration differs too much from the template. In particular, for sulcal studies, the selection of an appropriate template in terms of sulcal variability can be challenging. Automatic segmentation can also be achieved without relying on atlases, through intensity based classification with topological constraints and mathematical morphology-based tools (in the foetus: Gholipour et al., 2011; in the preterm: Moeskops et al., 2015; in the term-born neonate: Hill et al., 2010; Leroy et al., 2011; Gui et al., 2012). These methods can require manual interventions, such as manual selection of parameters (which are necessarily age-dependent; Hill et al., 2010), identification of labels after automatic tissue-type classification because of maturational discrepancies (Gholipour et al., 2011). They can also use geometrical properties and anatomical knowledge to constrain the registration (Leroy et al., 2011; Gui et al., 2012; Moeskops et al., 2015). An interesting way to compare such methods is through benchmarks: the NeoBrainS12 challenge proposed comparisons of various methods cited here, among others, based on images acquired on preterm infants at 30 and 40 weeks of post-menstrual age (w PMA) (Išgum et al., 2015). More recently, deep learning algorithms have gained popularity in the field of segmentation. In this line, a recent article proposing an open dataset of manually segmented fetal brains (including healthy and pathological subjects), offered a benchmark of ten different segmentation algorithms which were produced by four different teams, and which included a multi-atlas segmentation approach (which repeatedly applies atlas based segmentations using multiple individual images as atlases) along with a number of deep learning approaches, based on multiple 2D U-Nets, 3D U-Nets, or mask R-CNN deep neural networks (Payette et al., 2021).

The resulting segmentations allow the extraction of different objects and measures useful for subsequent analyses, including cortical surfaces necessary for sulcal detection.

7.2.2.2.3 Sulcal detection, identification and analysis

Sulcal detection in the very young brain is challenging because of its rather smooth configuration in its early developmental stages. Their detection, usually based on local curvature properties, can be biased by acquisition noise, and classic object-based approaches used in the adult are not always suitable. Moreover, automatic sulcal labelization is challenging in the foetus because of age-related changes in brain size, sulcation, and relative position and size of cortical regions (Fig 12). Hence the development of an automated sulcal labelling for the fetal brain is particularly challenging: with the help of fetal atlases, spatial probability maps have been elaborated and after capturing the similarity between an individual's folding pattern and the corresponding age-matched template, sulcal labelling was attained with the sulcal basin approach (Yun et al., 2019). For sulcal pit extraction, the changes in brain size prevent from using fixed threshold parameters (as in Im et al., 2010). The detection of sulcal pits in the infant therefore required to perform "exhaustive searching from a range of each parameter" based on infant images with manually labelled sulcal pits (Meng et al., 2018).

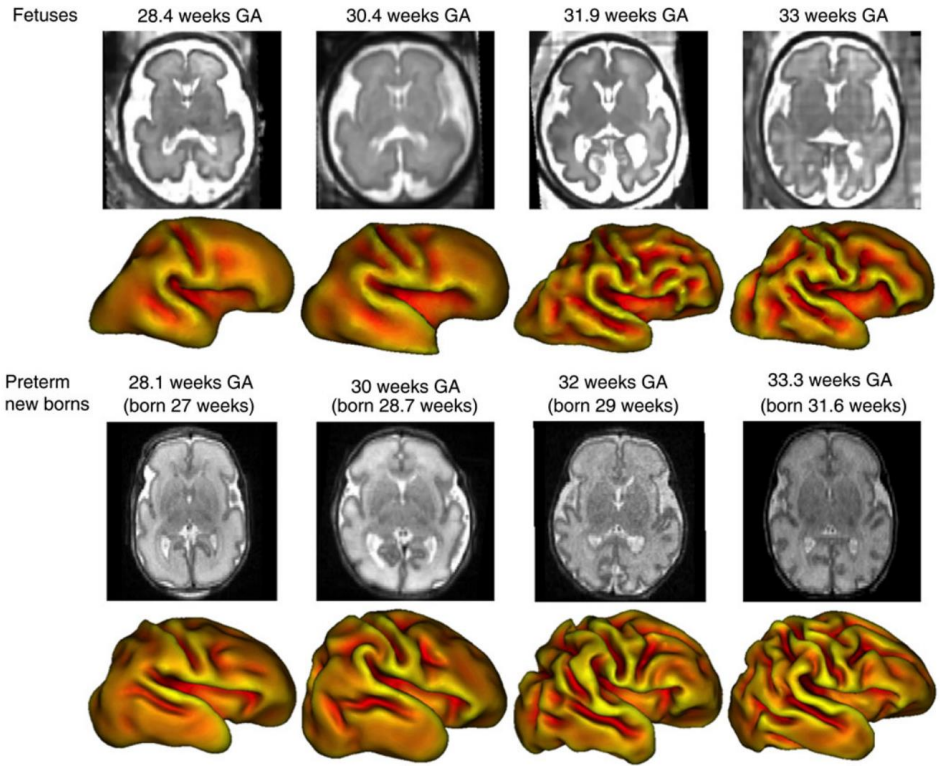

Figure 12. Representation of axial MRI slice and corresponding volumetric reconstructions of cortical meshes at multiple ages in the fetus (Top rows) and in the preterm (bottom rows) (courtesy of Lefèvre et al., 2016)

Sufficiently-refined sulcal detection methods allow for the investigation of global folding dynamics during development. A tool dedicated to the analysis of gyrification (SPANGY; presented in *1.2.1: Methods to investigate global shape variability*) has been applied to the developing brain, leading to a refined comparison of sulcal dynamics between the preterm and term newborn (Dubois et al., 2019). The SPANGY tool relies on spectral decomposition of folding pattern in 7 spectral bands (B0 to B6), in which B0 to B3 capture the global shape of the brain and B4, B5, and B6 seem to match sulci corresponding to primary, secondary and tertiary folding waves. Another approach, focused on pattern clustering, inferred similarity between multi-view curvature features (decomposed curvature maps at multiple spatial-frequency scales and gyral crest curves) using a similarity network fusion method and a hierarchical affinity propagation clustering approach (Duan et al., 2019b;

Fig. 15). This allowed for folding pattern clustering in the neonate, uncovering representative folding patterns in several brain regions.

7.2.2.2.4 Registration methods

Group studies require the images to be comparable, which is achieved through ***registration*** between subjects. Brains with sufficient anatomical landmarks are compatible with classic MRI registration methods, developed for the adult brain but eventually transposed to the infant, such as atlas-driven registrations using a neonate atlas rather than an adult one (Hill et al., 2010). Yet, when aligning either poorly folded brains or brains at different developmental stages, special care should be taken. Specifically, in the young fetus, anatomical landmarks are missing for surface based registration requiring volume-based approaches to ensure consistent inter-subject registration, such as volumetric group-wise registration of tissue mass (Habas et al., 2012). Alternatively, when more anatomical landmarks are present, it is possible to adapt existing methods to the fetal brain when the objects they are based on are detectable. For example, the DISCO tools for registrating adult brains as presented in *1.1: Why investigate cortical folding in the adult* have been adapted to enable preterm, infant and adult brain registration (Lebenberg et al., 2018). Alternately, the HIP-HOP tool (a landmark-based registration approach; Auzias et al., 2013) is compatible with early-stage sulcation pattern, since it does not impose the registration of specific sulci together by instead optimizing the match between sulci and iso-coordinates in a whole-brain approach, therefore managing the coregistration of brains with fewer and less developed sulci (Fig. 13; Auzias et al., 2015). Similarly, joint-spectral matching techniques (Lombaert et al., 2013) are compatible with the matching of brains which show different growth and folding stages: applied to preterm images acquired at 30w PMA and 40w PMA, registrations are qualitatively satisfactory and show consistency between lobe-specific matching and whole-brain white matter matching (Orasanu et al., 2016). Registration based on spectral surface matching to a fetal surface atlas has been demonstrated to present improvements in sulcal alignment compared to 3D alignment methods and similar ones yet cheaper computationally than spherical demons (Wright et al., 2015). Multi-modal surface matching (MSM, Robinson et al., 2014), considering sulcal, curvature and myelin features, has also been refined in order

to upgrade its regularization penalty, inducing improved alignment, and making it suited for longitudinal neonatal registration between 33 and 41w PMA (Robinson et al., 2018).

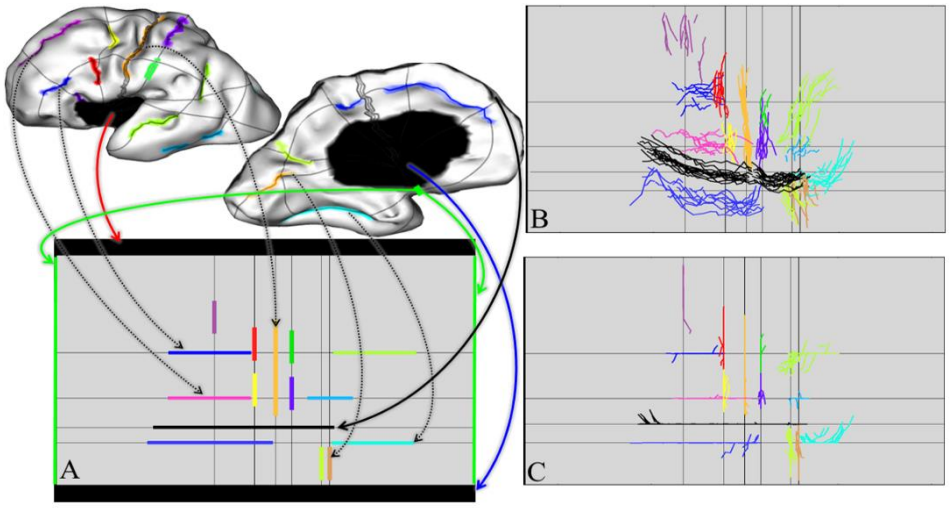

Figure 13. Representation of the HIP-HOP method applied to fetal brains. A. Each sulcus is mapped to a rectangular domain B. Superposition of 15 individuals after unconstrained mapping C. corresponding model with constrained mapping (courtesy of Auzias et al., 2015)

The development of refined methods to enable precise *in vivo* imaging and preprocessing of fetal and neonatal brain development allow for an increasingly precise investigation of the developing brain.

7.2.2.3 Progression of sulcation in the developing human brain

Now that the context of sulcal studies in the developing brain has been set, we will detail the progression of sulcation in the human, relying on both *post mortem* and *in vivo* data obtained in foetuses, in preterm and full-term neonates and infants, and focusing on the current knowledge about folding dynamics in the developing brain, before 2 years of age. We will finally review the folding specificities related to premature birth. A review on fetal and postnatal development of the cortex addresses cortical folding in a subsection (Dubois & Dehaene-Lambertz, 2015), and a review specifically explores it in the light of sulcal pits (Im & Grant, 2019).

7.2.2.3.1 Chronology of the development of folds

Let us first expose the chronology of folds' development. The first observations about the developing folds were made on *post mortem* specimens. A pioneer study explored 207 serially sectioned brains after excluding brains with obvious malformations, and reported the age of apparition of major fissures and sulci (Chi et al., 1977a). These develop in three successive folding waves, the primary folds appearing from 20w PMA , the secondary folds from 32w PMA, and the tertiary folds from 38w PMA (Chi et al., 1977a; Feess-Higgins & Laroche, 1987). This question was thereafter reinvestigated using MRI in different populations, including post mortem foetuses (Chi et al., 1977b; Hansen et al., 1993), in vivo foetuses (Garel et al., 2001; Habas et al., 2012), and extremely preterm neonates, in which hemispheric differences in apparition were also reported (Dubois et al., 2008a). The results of these different studies are summarized in Table 1. The chronology of folding reported are not strictly the same between studies (we can highlight a lag in the study by Dubois et al., 2008a, which may be due to the minimal depth required to detect a forming sulcus with their methodology, along with partial volume effects present in MRI and not in *post mortem* visual inspections, and the possibility of damaged or deformed *post mortem* specimen) yet relay similar trends, which are further confirmed by additional studies which did not explicitly detail the chronology of appearance of specific folds, but describe the time-line of sulcation by region.

The relative speed of sulcation has been assessed in the different brain regions (Fig 14; in the foetus: Habas et al., 2012; Wright et al., 2014; in the preterm: Dubois et al., 2008a; Kim et al., 2016b), and these report that the dynamic of sulcation is slower (and linear) in the insula and anterior temporal region compared to the other regions, which show a non-linear folding increase between 20 weeks of gestational age (w GA) and 40w GA) (Wright et al., 2014). Sulcation first develops in the area just around the central sulcus and the medial occipital regions, before the parietal, occipital, and posterior temporal regions, which themselves show advances in sulcation compared to the frontal and anterior temporal regions (in the preterm: van der Knaap et al., 1996; Dubois et al., 2008a; in the term-born neonate: Hill et al., 2010). When comparing growth rates by measuring cortical folding features such as

sulcal depth and mean curvature, the ordering of regions is as follows: posterior temporal, parietal, fusiform and parahippocampal, occipital, frontal, temporal medial, and cingulate (in the foetus: Wright et al., 2014; in the preterm: Kim et al., 2016b). As a result, at the age equivalent to full-term birth (~40w GA), all primary and secondary sulci are formed, as well as the majority of tertiary sulci; the overall sulcal shape is the same in neonates and adults and shows the same folding variability, with the exception of less convoluted anterior cingulate and anterior temporal cortices, and a higher sulcal depth variability of the mid temporal sulcus in neonates than in adults (Hill et al., 2010).

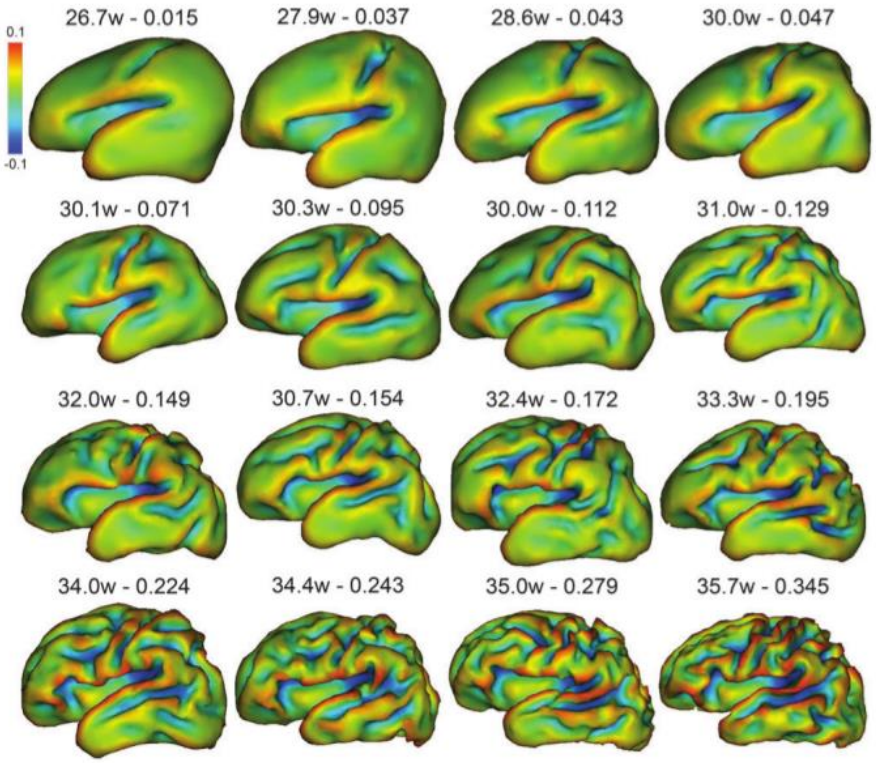

Figure 14. Reconstructions of inner cortical surface of preterm newborns of different gestational ages (left number) and whole-brain sulcation index (right number). Colours indicate surface curvature (courtesy of Dubois et al., 2008a)

Table 1: Chronology of appearance of sulci according to different studies, ordered by apparition age in Chi et al., 1977a

Sulcus or fissure	Date of apparition (w GA/PMA)				
	Chi et al., 1977a *post mortem, visual*	Hansen et al., 1993 *post mortem, MRI*	Garel et al., 2001 *in vivo, MRI, fetal*	Dubois et al., 2008, *in vivo, preterm, MRI*	Habas et al., 2012
				Left/Right	
Interhemispheric fissure	10	8-13			
Transverse cerebral fissure	10				
Callosal sulcus	14	8-13			
Sylvian fissure	16	8-13			
Calcarine sulcus	16	14-17	22-23		
Olfactory sulcus	16	14-17		32/34	
Parieto-occipital sulcus	16	14-17			
Insula[1]	18				22
Cingulate sulcus	18	14-17	Posterior[2]: 22-23 Anterior: 22-23		Posterior: 20 anterior: 23
Rhinal sulcus					23
Central sulcus[3]	20	18-22	24-25		24
Superior temporal sulcus	23	18-22	Posterior: 26, anterior: 30	27/26.7	25/24
Collateral sulcus	23	18-22	24-25	29/30	24
Uncinate sulcus				30/30	
Precentral sulcus[4]	24	22-25	26	29/29	27
Postcentral sulcus[5]	25	22-25	27	28/27	27
Superior frontal sulcus	25	22-25	24-25	30/29	24

Sulcus or fissure	Date of apparition (w GA/PMA)				
	Chi et al., 1977a *post mortem, visual*	Hansen et al., 1993 *post mortem, MRI*	Garel et al., 2001 *in vivo, MRI, fetal*	Dubois et al., 2008, *in vivo, preterm, MRI*	Habas et al., 2012
				Left/Right	
Intraparietal sulcus	26	22-25	27	30/29	
Inferior temporal sulcus[6]	26	22-25	30	30/29	
Occipital sulcus	27	22-25			
Inferior frontal sulcus	28	26-29	26	30/30	
Occipito-teporal sulcus[7]	30	26-29	29		
Secondary cingular sulci*	32		31		
Secondary occipital sulci*	34		32		
Insular sulci*	34-35		33		

Some sulci are given different names. We adopted the nomenclature from section 1.1, but the other possible names are the following: 1: Circular sulcus, 2: Marginal sulcus, 3: Rolandic sulcus, 4: Prerolandic sulcus, 5: Postrolandic sulcus, 6: middle temporal sulcus, 7: inferior temporal sulcus. *groups of sulci preventing us from using matching nomenclature

7.2.2.3.2 Evolution of folding pattern

These shape asymmetries, captured at different ages, are sometimes transient and characteristic of a maturational delay between hemispheres, and sometimes permanent in the sense that they remain asymmetric throughout life: hence the use for an assessment of the evolution of pattern. In terms of global folding measures (by that, we mean non sulcus-specific, including measures such as local gyrification indices), the region-wise evolution of curvature measures have been reported between 22 and 39w GA in the foetus (Wright et al., 2014), and longitudinally, yet with surprisingly opposite results, in the preterm between 30w and 40w PMA: one study reported the highest gyrification change in the parietal and occipital lobes (Moeskops et al., 2015), while the other one reported that these two regions showed the least increase of folding, and that the highest gyrification change was observed in the prefrontal and temporal lobes (Orasanu et al., 2016). These discordant results are probably due to methodological discrepancies between the two studies, as, for example, region-averaged values are used in Moeskops et al., 2015, which may decrease noise effects against a loss in precision. After normal-term birth, sulcation is reported to evolve differently between 0-1 year and 1-2 years of age, and unsurprisingly to show that sulcation rates decrease with development (Li et al., 2014). The increase of sulcal complexity was similarly reported between 6 months and 2 years of age (Kim et al., 2016b). Even though the different cortical regions show delayed sulcal growth, the global stability of the folding pattern between birth and 2 years of age has been assessed using sulcal pits, whose location and concentration were kept almost unchanged (Meng et al., 2014). Moreover, a study assessed whether brains which looked alike at birth evolved similarly at 1 year of age, and obtained relevant correlations (Rekik et al., 2018), suggesting that dynamic consistency of folding pattern is extendable to inter-subject considerations. On a more sulcus-focused approach, some studies reported sulcus-specific measures on a number of sulci, either in a longitudinal setting on preterm, reporting the relative growth of sulci in terms of length and surface area between 30 and 40w PMA (Kersbergen et al., 2016), or in a cohort of foetuses ranging from 20 to 28w GA, reporting the evolution of mean curvature (Habas et al., 2012). These studies give valuable overview of sulcation on the

whole-brain-scale. Using a multi-age fetal atlas, a study focusing on the links between genetics and opercularization beautifully characterized the growth dynamics around the insula through Jacobian vector fields in foetuses between 21 and 38w GA, showing the volumetric expansion of the frontal, temporal and parietal opercula (Mallela et al., 2020).

7.2.2.3.3 Asymmetries in the developing brain

In terms of hemisphere-wise development, the right hemisphere shows sulcal complexity earlier than the left one (Chi et al., 1977a; Dubois et al., 2008a; Habas et al., 2012). This sulcation delay is the most striking developmental asymmetry. Yet, the left hemisphere globally catches up to the right one later on. This approximate 2-week lag may explain the increased inter-individual variability observed in the right hemisphere between 27 and 36w PMA (Dubois et al., 2010). During the perinatal period, two sulcal asymmetries are most consistently reported: the left Sylvian Fissure is longer and less curved than the right one (post mortem: Chi et al., 1977a; in the foetus: Habas et al., 2012; in the preterm: Dubois et al., 2010; Kersbergen et al., 2016; in the term-born neonate: Hill et al., 2010; Glasel et al., 2011), and the superior temporal sulcus – more specifically its medium part – is deeper in the right hemisphere (in the foetus: Habas et al., 2012; in the preterm: Dubois et al., 2008a; Dubois et al., 2010; Kersbergen et al., 2016; in the term-born neonate: Hill et al., 2010; Glasel et al., 2011; Li et al., 2014; Bozek et al., 2018). Interestingly, Glasel et al., 2011 reported an absence of correlation between the rightward superior temporal sulcus and leftward sylvian fissure asymmetries, suggesting a difference in morphogenetic processes inducing both phenomena. Additional sulcal asymmetries have been reported using classical length and depth measures: in terms of right-deeper-than-left asymmetries, we can name the dorsolateral portion of the right central sulcus, as soon as 27w GA (Habas et al., 2012) and in the full-term neonate (Li et al., 2014), the insula in the preterm infant at term-equivalent age (TEA) (in terms of surface rather than depth; Kersbergen et al., 2016), the inferior frontal sulcus at 30w PMA and TEA in the preterm (Kersbergen et al., 2016), and the lateral occipito-temporal sulcus in full-term neonates (Bozek et al., 2018). In terms of leftward asymmetries, we can mention the parieto-occipital sulcus at 26w GA in the fetus (Habas et al., 2012),

and the anterior part of the temporal lobe, both medial and lateral, in the term born infant (Bozek et al., 2018). One asymmetry showed an inter-study reversal of trend with age: the superior frontal sulcus has been reported to be deeper in the left hemisphere at 27w GA (Habas et al., 2012) but deeper in the right hemisphere at 40w PMA (Kersbergen et al., 2016).

Finer asymmetries can be captured by looking further into shape and pattern: capturing only sulcal length, the asymmetries of the Sylvian fissure are limited to a longer left Sylvian fissure (Chi et al., 1977b), while a voxel-based analysis also showed a longer left sylvian fissure, both extending more anteriorly and posteriorly (Dubois et al., 2010). Looking into the localization of sulcal pits, hemispheric differences have been revealed in the neonate: the superior temporal sulcus showed more anterior pits in the right temporal pole, the superior part of the postcentral sulcus, a sulcal pit cluster on the left and not on the right, and the left central sulcus, higher sulcal pits than its right counterpart (Meng et al., 2014). This central sulcus asymmetry can be paralleled with the asymmetry previously reported in the adult (Sun et al., 2012). In a mix of TEA preterm and term-born neonates, pattern-specific asymmetries have also been reported in the superior temporal gyrus and in the cingulate cortex, in which some pattern occurrences seem to develop only in a given hemisphere (Duan et al., 2019b; Fig. 15).

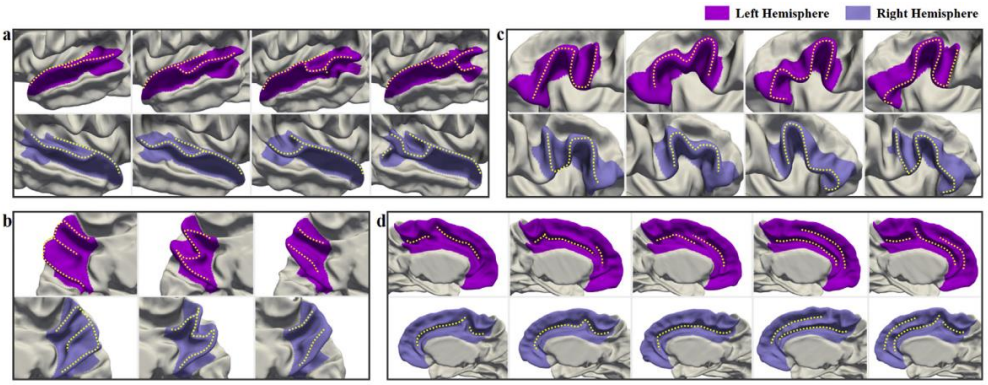

Figure 15. Representative gyral patterns captured in the (pink) left and (purple) right hemisphere matched by similarity in the (a) superior temporal gyrus, (b) precuneus, (c) inferior frontal gyrus, (d) cingulate cortex. Note the dissimilarity between the 3rd feature superior temporal gyrus in both hemispheres and between the 2nd and 3rd features in the cingulate cortex (courtesy of Duan et al., 2019b).

7.2.2.3.4 Folding alterations linked to prematurity

To be exhaustive, we have presented jointly results of cortical folding observed in the foetus, in the premature infant, and in the term-born infant. Yet, it should be noted that some clinical conditions lead to folding alterations, even in the case of non-pathological situations: for example, being a twin was associated with a delay in folding dynamics (Chi et al., 1977a; Dubois et al., 2008b). More importantly, ***altered sulcation has been reported in premature infants and children***. Prematurity *per se* is a motive of altered sulcal dynamics because of the difference between *in utero* and *ex utero* environment during sulcal development. When compared to same-age foetuses, the preterm brain without any obvious brain anomaly still shows less cerebrospinal fluid, more pronounced folds, and a more compact global shape (Lefèvre et al., 2016; Fig 12). This study additionally reported that preterm birth is linked to increases in intensity and sharpness of folding, as well as altered sulcal shape; this is modulated by GA at birth. When comparing extremely preterm newborns to moderate preterm newborns, extremely premature infants showed reduced cortical growth in a number of different regions (namely: the superior frontal, occipital, basal

temporal, precuneus, right superior and middle temporal and parahippocampal gyri as well as the right central sulcus area ; Kim et al., 2016b). Yet, this study design did not allow the authors to differentiate direct effects of prematurity on sulcation from indirect effects linked to adversarial situations linked to prematurity, as it did not exclude preterm subjects with brain injuries or clinical factors susceptible to alter cortical development. Additionally, the regions reported did not overlap with those observed in an alternative study set-up, comparing extremely preterm infants – selected to exclude periventricular leukomalacia, intra-ventricular haemorrhage of grade III and IV, focal brain lesions and persistent ventricular dilatation at TEA – with term-born controls, reporting reduced grey matter in the bilateral temporal lobes, pre and post-central gyri, orbitofrontal cortex, amygdala, para-hippocampal gyrus, hyppocampus and left insula (Padilla et al., 2015). Finally, when comparing extremely preterm neonate at TEA and term-born neonates, the TEA preterms showed a less complex gyrification (captured through the whole cortex convolution index: Ajayi-Obe et al., 2000; the gyrification index: Engelhardt et al., 2015; Shimony et al., 2016; the folding power in B4, B5 and B6 spectral bands: Dubois et al., 2019). A specific impact on the insula, superior temporal sulcus, and ventral pre- and postcentral sulci was reported (Engelhardt et al., 2015), compatible with the observation that the B4 spectral wave, most likely corresponding to primary sulci, shows the most significant decrease in TEA preterms compared to term-born infants, suggesting that sulci developing during the period of preterm birth are most impacted, when later developing sulci are still impacted but less, probably because of the condition of their *ex utero* development (Dubois et al., 2019).

In addition to the environmental difference between *in utero* and *ex utero* brain development, extreme prematurity is often associated with clinical disturbances which may affect normal brain development, including sulcal development, such as gestational age at birth, multiple pregnancies, intra-uterine growth restriction (IUGR), early-life severe illness indicators (such as necessity for prolonged mechanical ventilation, exposure to critical illness in the first 24 hours of life, and early exposure to steroids), and presence of brain injuries. Gestational age at birth impacts sulcal development in preterms, with decreasing divergence from control fetal development with increasing gestational

age at birth (Lefèvre et al., 2016). In extremely preterm populations, being part of a multiple pregnancy led to a delayed but harmonious maturation (Dubois et al., 2008b; Kersbergen et al., 2016). IUGR, either reported as such, as low birth-weight according to GA, or as smaller head circumference at birth, was linked to a discordant folding trajectory, either through disproportionate alterations in sulcation index compared to a decreased surface and volumetric growth (Dubois et al., 2008b), or through lower gyrification index and cortical surface area (Engelhardt et al., 2015), but also through decreased Sylvian fissure and insula surface area at 30w PMA, and smaller left insula, left superior temporal sulcus, and bilateral central sulcus at TEA (Kersbergen et al., 2016). In terms of early-life severe illness indicators, decreased cortical surface area was also reported in infants with higher critical illness in the first 24 hours, exposure to postnatal steroids, and to prolonged mechanical ventilation (Engelhardt et al., 2015). Prolonged mechanical ventilation was linked to reduced surface area of the insula and sylvian fissure as well as to reduced depth in the right central sulcus at 30w PMA, and to a smaller right superior temporal sulcus and a shallower left precentral sulcus at TEA (Kersbergen et al., 2016). Finally, different types of brain injuries were reported in links to altered sulcation. Extremely preterm infants with cortical grey matter anomalies showed increased cortical thickness and decreased cortical folding at TEA, which was more pronounced than at 30w PMA (Moeskops et al., 2015). This concurs with the observation that preterms with brain injury can be differentiated from those without (Shimony et al., 2016). Severe intraventricular haemorrhage (IVH) was reported to only be associated with a reduced presence of secondary sulci at 30w PMA (Kersbergen et al., 2016), in agreement with another study which linked IVH, periventricular leukomalacia, and ventriculomegaly to reduced cortical folding before 31w PMA but not later (Kim et al., 2020).

Imaging the developing brain is essential to understand the mechanisms underlying its formation and patterning. Multi-domain efforts are undertaken to describe early sulcal development and investigate its causes and implications. Methodological advances pave the way for

the characterization of normal sulcal pattern variability in the developing brain, fundamental to both abnormal trajectory detection and theoretical understanding of cortical organization.

7.2.3 References

Ajayi-Obe, M., Saeed, N., Cowan, F., Rutherford, M., Edwards, A., 2000. Reduced development of cerebral cortex in extremely preterm infants. The Lancet 356, 1162–1163. https://doi.org/10.1016/S0140-6736(00)02761-6

Aleman-Gomez, Y., Janssen, J., Schnack, H., Balaban, E., Pina-Camacho, L., Alfaro-Almagro, F., Castro-Fornieles, J., Otero, S., Baeza, I., Moreno, D., Bargallo, N., Parellada, M., Arango, C., Desco, M., 2013. The Human Cerebral Cortex Flattens during Adolescence. Journal of Neuroscience 33, 15004–15010. https://doi.org/10.1523/JNEUROSCI.1459-13.2013

Amiez, C., Kostopoulos, P., Champod, A.-S., Petrides, M., 2006. Local Morphology Predicts Functional Organization of the Dorsal Premotor Region in the Human Brain. J. Neurosci. 26, 2724–2731. https://doi.org/10.1523/JNEUROSCI.4739-05.2006

Amiez, C., Sallet, J., Novek, J., Hadj-Bouziane, F., Giacometti, C., Andersson, J., Hopkins, W.D., Petrides, M., 2021. Chimpanzee histology and functional brain imaging show that the paracingulate sulcus is not human-specific. Commun Biol 4, 54. https://doi.org/10.1038/s42003-020-01571-3

Anbeek, P., Išgum, I., van Kooij, B.J.M., Mol, C.P., Kersbergen, K.J., Groenendaal, F., Viergever, M.A., de Vries, L.S., Benders, M.J.N.L., 2013. Automatic Segmentation of Eight Tissue Classes in Neonatal Brain MRI. PLoS ONE 8, e81895. https://doi.org/10.1371/journal.pone.0081895

Ashburner, J., 2007. A fast diffeomorphic image registration algorithm. NeuroImage 38, 95–113. https://doi.org/10.1016/j.neuroimage.2007.07.007

Auzias, G., Colliot, O., Glaunes, J.A., Perrot, M., Mangin, J.-F., Trouve, A., Baillet, S., 2011. Diffeomorphic Brain Registration Under Exhaustive Sulcal Constraints. IEEE Trans. Med. Imaging 30, 1214–1227. https://doi.org/10.1109/TMI.2011.2108665

Auzias, G., Lefevre, J., Le Troter, A., Fischer, C., Perrot, M., Regis, J., Coulon, O., 2013. Model-Driven Harmonic Parameterization of the Cortical Surface: HIP-HOP. IEEE Trans. Med. Imaging 32, 873–887. https://doi.org/10.1109/TMI.2013.2241651

Auzias, G., Brun, L., Deruelle, C., Coulon, O., 2015. Deep sulcal landmarks: Algorithmic and conceptual improvements in the definition and extraction of sulcal pits. NeuroImage 111, 12–25. https://doi.org/10.1016/j.neuroimage.2015.02.008

Avants, B.B., Tustison, N.J., Song, G., Cook, P.A., Klein, A., Gee, J.C., 2011. A reproducible evaluation of ANTs similarity metric performance in brain image registration. NeuroImage 54, 2033–2044. https://doi.org/10.1016/j.neuroimage.2010.09.025

Bae, I., Chae, J.-H., Han, Y., 2021. A brain extraction algorithm for infant T2 weighted magnetic resonance images based on fuzzy c-means thresholding. Sci Rep 11, 23347. https://doi.org/10.1038/s41598-021-02722-0

Bartley, A., Jones, D., Weinberger, D., 1997. Genetic variability of human brain size and cortical gyral patterns. Brain 120, 257–269. https://doi.org/10.1093/brain/120.2.257

Bayly, P.V., Taber, L.A., Kroenke, C.D., 2014. Mechanical forces in cerebral cortical folding: A review of measurements and models. Journal of the Mechanical Behavior of Biomedical Materials 29, 568–581. https://doi.org/10.1016/j.jmbbm.2013.02.018

Becker, Y., Sein, J., Velly, L., Giacomino, L., Renaud, L., Lacoste, R., Anton, J.-L., Nazarian, B., Berne, C., Meguerditchian, A., 2021. Early Left-Planum Temporale Asymmetry in newborn monkeys (Papio anubis): A longitudinal structural MRI study at two stages of development. NeuroImage 227, 117575. https://doi.org/10.1016/j.neuroimage.2020.117575

Blanton, R.E., Levitt, J.G., Thompson, P.M., Narr, K.L., Capetillo-Cunliffe, L., Nobel, A., Singerman, J.D., McCracken, J.T., Toga, A.W., 2001. Mapping cortical asymmetry and complexity patterns in normal children. Psychiatry Research: Neuroimaging 107, 29–43. https://doi.org/10.1016/S0925-4927(01)00091-9

Bodin, C., Takerkart, S., Belin, P., Coulon, O., 2018. Anatomo-functional correspondence in the superior temporal sulcus. Brain Struct Funct 223, 221–232. https://doi.org/10.1007/s00429-017-1483-2

Borne, L., 2019. Design of a top-down computer vision algorithm dedicated to the recognition of cortical sulci. PhD thesis, Université Paris-Saclay.

Borrell, V., 2018. How Cells Fold the Cerebral Cortex. J. Neurosci. 38, 776–783. https://doi.org/10.1523/JNEUROSCI.1106-17.2017

Boucher, M., Whitesides, S., Evans, A., 2009. Depth potential function for folding pattern representation, registration and analysis. Medical Image Analysis 13, 203–214. https://doi.org/10.1016/j.media.2008.09.001

Bozek, J., Makropoulos, A., Schuh, A., Fitzgibbon, S., Wright, R., Glasser, M.F., Coalson, T.S., O'Muircheartaigh, J., Hutter, J., Price, A.N., Cordero-Grande, L., Teixeira, R.P.A.G., Hughes, E., Tusor, N., Baruteau, K.P., Rutherford, M.A., Edwards, A.D., Hajnal, J.V., Smith, S.M., Rueckert, D., Jenkinson, M., Robinson, E.C., 2018. Construction of a neonatal cortical surface atlas using Multimodal Surface Matching in the Developing Human Connectome Project. NeuroImage 179, 11–29. https://doi.org/10.1016/j.neuroimage.2018.06.018

Brodmann K. 1909. Vergleichende Lokalisationslehre der Großhirnrinde in ihren Prinzipien dargestellt auf Grund des Zellenbaues. Leipzig (Germany): Verlag von Johann Ambrosius

Barth.

Cachia, A., Mangin, J.-F., Riviere, D., Kherif, F., Boddaert, N., Andrade, A., Papadopoulos-Orfanos, D., Poline, J.-B., Bloch, I., Zilbovicius, M., Sonigo, P., Brunelle, F., Regis, J., 2003. A primal sketch of the cortex mean curvature: A morphogenesis based approach to study the variability of the folding patterns. IEEE Trans. Med. Imaging 22, 754–765. https://doi.org/10.1109/TMI.2003.814781

Cachia, A., Paillère-Martinot, M.-L., Galinowski, A., Januel, D., de Beaurepaire, R., Bellivier, F., Artiges, E., Andoh, J., Bartrés-Faz, D., Duchesnay, E., Rivière, D., Plaze, M., Mangin, J.-F., Martinot, J.-L., 2008. Cortical folding abnormalities in schizophrenia patients with resistant auditory hallucinations. NeuroImage 39, 927–935. https://doi.org/10.1016/j.neuroimage.2007.08.049

Cachia, A., Borst, G., Vidal, J., Fischer, C., Pineau, A., Mangin, J.-F., Houdé, O., 2014. The Shape of the ACC Contributes to Cognitive

Control Efficiency in Preschoolers. Journal of Cognitive Neuroscience 26, 96–106. https://doi.org/10.1162/jocn_a_00459

Cachia, A., Borst, G., Tissier, C., Fisher, C., Plaze, M., Gay, O., Rivière, D., Gogtay, N., Giedd, J., Mangin, J.-F., Houdé, O., Raznahan, A., 2016. Longitudinal stability of the folding pattern of the anterior cingulate cortex during development. Developmental Cognitive Neuroscience 19, 122–127. https://doi.org/10.1016/j.dcn.2016.02.011

Cachia, A., Del Maschio, N., Borst, G., Della Rosa, P.A., Pallier, C., Costa, A., Houdé, O., Abutalebi, J., 2017. Anterior cingulate cortex sulcation and its differential effects on conflict monitoring in bilinguals and monolinguals. Brain and Language 175, 57–63. https://doi.org/10.1016/j.bandl.2017.09.005

Cachia, A., Roell, M., Mangin, J.-F., Sun, Z.Y., Jobert, A., Braga, L., Houde, O., Dehaene, S., Borst, G., 2018. How interindividual differences in brain anatomy shape reading accuracy. Brain Struct Funct 223, 701–712. https://doi.org/10.1007/s00429-017-1516-x

Cachia, A., Borst, G., Jardri, R., Raznahan, A., Murray, G.K., Mangin, J.-F., Plaze, M., 2021. Towards Deciphering the Fetal Foundation of Normal Cognition and Cognitive Symptoms From Sulcation of the Cortex. Front. Neuroanat. 15, 712862. https://doi.org/10.3389/fnana.2021.712862

Cardoso, M.J., Melbourne, A., Kendall, G.S., Modat, M., Robertson, N.J., Marlow, N., Ourselin, S., 2013. AdaPT: An adaptive preterm segmentation algorithm for neonatal brain MRI. NeuroImage 65, 97–108. https://doi.org/10.1016/j.neuroimage.2012.08.009

Chi, J.G., Dooling, E.C., Gilles, F.H., 1977a. Gyral development of the human brain. Ann Neurol. 1, 86–93. https://doi.org/10.1002/ana.410010109

Chi, J.G., Dooling, E.C., Gilles, F.H., 1977b. Left-Right Asymmetries of the Temporal Speech Areas of the Human Fetus. Archives of Neurology 34, 346–348. https://doi.org/10.1001/archneur.1977.00500180040008

Chiavaras, M.M., LeGoualher, G., Evans, A., Petrides, M., 2001. Three-Dimensional Probabilistic Atlas of the Human Orbitofrontal Sulci

in Standardized Stereotaxic Space. NeuroImage 13, 479–496. https://doi.org/10.1006/nimg.2000.0641

Chiavaras, M.M., Petrides, M., 2000. Orbitofrontal sulci of the human and macaque monkey brain. J. Comp. Neurol. 422, 35–54. https://doi.org/10.1002/(SICI)1096-9861(20000619)422:1<35::AID-CNE3>3.0.CO;2-E

Cordero-Grande, L., Hughes, E.J., Hutter, J., Price, A.N., Hajnal, J.V., 2018. Three-dimensional motion corrected sensitivity encoding reconstruction for multi-shot multi-slice MRI: Application to neonatal brain imaging: Aligned Multi-Shot Multi-Slice MRI. Magn. Reson. Med. 79, 1365–1376. https://doi.org/10.1002/mrm.26796

Cunningham, D.J., 1892. Cunningham Memoirs - Contribution to the surface anatomy of the cerebral hemispheres by D.J. Cunningham with a chapter upon cranio-cerebral topography by Victor Horsley.

Del Maschio, N., Sulpizio, S., Fedeli, D., Ramanujan, K., Ding, G., Weekes, B.S., Cachia, A., Abutalebi, J., 2019. ACC Sulcal Patterns and Their Modulation on Cognitive Control Efficiency Across Lifespan: A Neuroanatomical Study on Bilinguals and Monolinguals. Cerebral Cortex 29, 3091–3101. https://doi.org/10.1093/cercor/bhy175

del Toro, D., Ruff, T., Cederfjäll, E., Villalba, A., Seyit-Bremer, G., Borrell, V., Klein, R., 2017. Regulation of Cerebral Cortex Folding by Controlling Neuronal Migration via FLRT Adhesion Molecules. Cell 169, 621-635.e16. https://doi.org/10.1016/j.cell.2017.04.012

Desbrun, M., Meyer, M., Schröder, P., Barr, A.H., 1999. Implicit fairing of irregular meshes using diffusion and curvature flow, in: Proceedings of the 26th Annual Conference on Computer Graphics and Interactive Techniques - SIGGRAPH '99. Presented at the the 26th annual conference, ACM Press, Not Known, pp. 317–324. https://doi.org/10.1145/311535.311576

Duan, D., Xia, S., Wu, Z., Wang, F., Wang, L., Lin, W., Gilmore, J.H., Shen, D., Li, G., 2019a. Cortical Foldingprints for Infant Identification, in: 2019 IEEE 16th International Symposium on Biomedical Imaging (ISBI 2019). Presented at the 2019 IEEE 16th International Symposium

on Biomedical Imaging (ISBI), IEEE, Venice, Italy, pp. 396–399. https://doi.org/10.1109/ISBI.2019.8759429

Duan, D., Xia, S., Rekik, I., Meng, Y., Wu, Z., Wang, L., Lin, W., Gilmore, J.H., Shen, D., Li, G., 2019b. Exploring folding patterns of infant cerebral cortex based on multi-view curvature features: Methods and applications. NeuroImage 185, 575–592. https://doi.org/10.1016/j.neuroimage.2018.08.041

Duan, D., Xia, S., Rekik, I., Wu, Z., Wang, L., Lin, W., Gilmore, J.H., Shen, D., Li, G., 2020. Individual identification and individual variability analysis based on cortical folding features in developing infant singletons and twins twins. Human Brain Mapp. 41, 1985–2003. doi: https://doi.org/10.1002/hbm.24924

Dubois, J., Benders, M., Cachia, A., Lazeyras, F., Ha-Vinh Leuchter, R., Sizonenko, S.V., Borradori-Tolsa, C., Mangin, J.F., Huppi, P.S., 2008a. Mapping the Early Cortical Folding Process in the Preterm Newborn Brain. Cerebral Cortex 18, 1444–1454. https://doi.org/10.1093/cercor/bhm180

Dubois, J., Benders, M., Borradori-Tolsa, C., Cachia, A., Lazeyras, F., Ha-Vinh Leuchter, R., Sizonenko, S.V., Warfield, S.K., Mangin, J.F., Hüppi, P.S., 2008b. Primary cortical folding in the human newborn: an early marker of later functional development. Brain 131, 2028–2041. https://doi.org/10.1093/brain/awn137

Dubois, J., Benders, M., Lazeyras, F., Borradori-Tolsa, C., Leuchter, R.H.-V., Mangin, J.F., Hüppi, P.S., 2010. Structural asymmetries of perisylvian regions in the preterm newborn. NeuroImage 52, 32–42. https://doi.org/10.1016/j.neuroimage.2010.03.054

Dubois, J., Dehaene-Lambertz, G., Kulikova, S., Poupon, C., Hüppi, P.S., Hertz-Pannier, L., 2014. The early development of brain white matter: A review of imaging studies in fetuses, newborns and infants. Neuroscience 276, 48–71. https://doi.org/10.1016/j.neuroscience.2013.12.044

Dubois, J., Lefèvre, J., Angleys, H., Leroy, F., Fischer, C., Lebenberg, J., Dehaene-Lambertz, G., Borradori-Tolsa, C., Lazeyras, F., Hertz-Pannier, L., Mangin, J.-F., Hüppi, P.S., Germanaud, D., 2019. The dynamics of cortical folding waves and prematurity-related deviations

revealed by spatial and spectral analysis of gyrification. NeuroImage 185, 934–946. https://doi.org/10.1016/j.neuroimage.2018.03.005

Eichert, N., Watkins, K.E., Mars, R.B., Petrides, M., 2021. Morphological and functional variability in central and subcentral motor cortex of the human brain. Brain Struct Funct 226, 263–279. https://doi.org/10.1007/s00429-020-02180-w

Engelhardt, E., Inder, T.E., Alexopoulos, D., Dierker, D.L., Hill, J., Essen, D., Neil, J.J., 2015. Regional impairments of cortical folding in premature infants. Ann Neurol. 77, 154–162. https://doi.org/10.1002/ana.24313

Feess-Higgins, A., Laroche, J.C., 1987. Development of the Human Foetal Brain: an Anatomical Atlas. Inserm-CNRS, Masson.

Fernández, V., Llinares-Benadero, C., Borrell, V., 2016. Cerebral cortex expansion and folding: what have we learned? EMBO J 35, 1021–1044. https://doi.org/10.15252/embj.201593701

Fischl, B., Rajendran, N., Busa, E., Augustinack, J., Hinds, O., Yeo, B.T.T., Mohlberg, H., Amunts, K., Zilles, K., 2008. Cortical Folding Patterns and Predicting Cytoarchitecture. Cerebral Cortex 18, 1973–1980. https://doi.org/10.1093/cercor/bhm225

Fischl, B., 2012. FreeSurfer. NeuroImage 62, 774–781. https://doi.org/10.1016/j.neuroimage.2012.01.021

Fish, A.M., Cachia, A., Fischer, C., Mankiw, C., Reardon, P.K., Clasen, L.S., Blumenthal, J.D., Greenstein, D., Giedd, J.N., Mangin, J.-F., Raznahan, A., 2016. Influences of Brain Size, Sex, and Sex Chromosome Complement on the Architecture of Human Cortical Folding. Cereb. Cortex cercor;bhw323v1. https://doi.org/10.1093/cercor/bhw323

Fornito, A., Yücel, M., Wood, S.J., Stuart, G., Buchanan, J.-A., Proffitt, T., Anderson, V., Velakoulis, D., Pantelis, C., 2004. Individual Differences in Anterior Cingulate/Paracingulate Morphology Are Related to Executive Functions in Healthy Males. Cerebral Cortex 14, 424–431. https://doi.org/10.1093/cercor/bhh004

Fornito, A., Wood, S.J., Whittle, S., Fuller, J., Adamson, C., Saling, M.M., Velakoulis, D., Pantelis, C., Yücel, M., 2008. Variability of the paracingulate sulcus and morphometry of the medial frontal cortex: Associations with cortical thickness, surface area, volume, and sulcal

depth. Hum. Brain Mapp. 29, 222–236. https://doi.org/10.1002/hbm.20381

Foubet, O., Trejo, M., Toro, R., 2019. Mechanical morphogenesis and the development of neocortical organisation. Cortex 118, 315–326. https://doi.org/10.1016/j.cortex.2018.03.005

Frey, B.J., Dueck, D., 2007. Clustering by passing messages between data points. Science

315, 972–976.

Friedrich, P., Forkel, S.J., Amiez, C., Balsters, J.H., Coulon, O., Fan, L., Goulas, A., Hadj-Bouziane, F., Hecht, E.E., Heuer, K., Jiang, T., Latzman, R.D., Liu, X., Loh, K.K., Patil, K.R., Lopez-Persem, A., Procyk, E., Sallet, J., Toro, R., Vickery, S., Weis, S., Wilson, C.R.E., Xu, T., Zerbi, V., Eickoff, S.B., Margulies, D.S., Mars, R.B., Thiebaut de Schotten, M., 2021. Imaging evolution of the primate brain: the next frontier? NeuroImage 228, 117685. https://doi.org/10.1016/j.neuroimage.2020.117685

Frost, M.A., Goebel, R., 2012. Measuring structural–functional correspondence: Spatial variability of specialised brain regions after macro-anatomical alignment. NeuroImage 59, 1369–1381. https://doi.org/10.1016/j.neuroimage.2011.08.035

Garcia, K.E., Kroenke, C.D., Bayly, P.V., 2018. Mechanics of cortical folding: stress, growth and stability. Phil. Trans. R. Soc. B 373, 20170321. https://doi.org/10.1098/rstb.2017.0321

Garel, C., Chantrel, E., Brisse, H., Elmaleh, M., Luton, D., Oury, J.-F., Sebag, G., Hassan, M., 2001. Fetal Cerebral Cortex: Normal Gestational Landmarks Identified Using Prenatal MR Imaging 6.

Gay, O., Plaze, M., Oppenheim, C., Gaillard, R., Olié, J.-P., Krebs, M.-O., Cachia, A., 2017. Cognitive control deficit in patients with first-episode schizophrenia is associated with complex deviations of early brain development. JPN 42, 87–94. https://doi.org/10.1503/jpn.150267

Germanaud, D., Lefèvre, J., Toro, R., Fischer, C., Dubois, J., Hertz-Pannier, L., Mangin, J.-F., 2012. Larger is twistier: Spectral analysis of gyrification (SPANGY) applied to adult brain size polymorphism. NeuroImage 63, 1257–1272. https://doi.org/10.1016/j.neuroimage.2012.07.053

Germann, J., Robbins, S., Halsband, U., Petrides, M., 2005. Precentral sulcal complex of the human brain: Morphology and statistical probability maps. J. Comp. Neurol. 493, 334–356. https://doi.org/10.1002/cne.20820

Germann, J., Chakravarty, M.M., Collins, L.D., Petrides, M., 2019. Tight Coupling between Morphological Features of the Central Sulcus and Somatomotor Body Representations: A Combined Anatomical and Functional MRI Study. Cerebral Cortex bhz208. https://doi.org/10.1093/cercor/bhz208

Gholipour, A., Estroff, J.A., Barnewolt, C.E., Connolly, S.A., Warfield, S.K., 2011. Fetal brain volumetry through MRI volumetric reconstruction and segmentation. Int J CARS 6, 329–339. https://doi.org/10.1007/s11548-010-0512-x

Ginsberg, Y., Ganor-Ariav, O., Hussein, H., Adam, D., Khatib, N., Weiner, Z., Beloosesky, R., Goldstein, I., 2021. Quantification of Fetal Gyrogenesis in the Third Trimester. A Novel Algorithm for Evaluating Fetal Sulci Development. Journal of Neuroimaging 31, 372–378. https://doi.org/10.1111/jon.12817

Glasel, H., Leroy, F., Dubois, J., Hertz-Pannier, L., Mangin, J.F., Dehaene-Lambertz, G., 2011. A robust cerebral asymmetry in the infant brain: The rightward superior temporal sulcus. NeuroImage 58, 716–723. https://doi.org/10.1016/j.neuroimage.2011.06.016

Gratiolet, P., 1854. Mémoire sur les plis cérébraux de l'homme et des primates. A. Bertrand, Paris. *In French*

Gui, L., Lisowski, R., Faundez, T., Hüppi, P.S., Lazeyras, F., Kocher, M., 2012. Morphology-driven automatic segmentation of MR images of the neonatal brain. Medical Image Analysis 16, 1565–1579. https://doi.org/10.1016/j.media.2012.07.006

Habas, P.A., Kim, K., Corbett-Detig, J.M., Rousseau, F., Glenn, O.A., Barkovich, A.J., Studholme, C., 2010. A spatiotemporal atlas of MR intensity, tissue probability and shape of the fetal brain with application to segmentation. NeuroImage 53, 460–470. https://doi.org/10.1016/j.neuroimage.2010.06.054

Habas, P.A., Scott, J.A., Roosta, A., Rajagopalan, V., Kim, K., Rousseau, F., Barkovich, A.J., Glenn, O.A., Studholme, C., 2012. Early Folding

Patterns and Asymmetries of the Normal Human Brain Detected from in Utero MRI. Cerebral Cortex 22, 13–25. https://doi.org/10.1093/cercor/bhr053

Hansen, P., Ballesteros, M., Soila, K., Garcia, L., Howard, J.M., 1993. MR Imaging of the Developing Human Brain. RadioGraphics 13, 21–36.

Heuer, K., Toro, R., 2019. Role of mechanical morphogenesis in the development and evolution of the neocortex. Physics of Life Reviews 31, 233–239. https://doi.org/10.1016/j.plrev.2019.01.012

Hill, J., Inder, T., Neil, J., Dierker, D., Harwell, J., Van Essen, D., 2010. Similar patterns of cortical expansion during human development and evolution. Proceedings of the National Academy of Sciences 107, 13135–13140. https://doi.org/10.1073/pnas.1001229107

Hopkins, W.D., Meguerditchian, A., Coulon, O., Bogart, S., Mangin, J.-F., Sherwood, C.C., Grabowski, M.W., Bennett, A.J., Pierre, P.J., Fears, S., Woods, R., Hof, P.R., Vauclair, J., 2014. Evolution of the Central Sulcus Morphology in Primates. Brain Behav Evol 84, 19–30. https://doi.org/10.1159/000362431

Hopkins, W.D., Procyk, E., Petrides, M., Schapiro, S.J., Mareno, M.C., Amiez, C., 2021. Sulcal Morphology in Cingulate Cortex is Associated with Voluntary Oro-Facial Motor Control and Gestural Communication in Chimpanzees (*Pan troglodytes*). Cerebral Cortex 31, 2845–2854. https://doi.org/10.1093/cercor/bhaa392

Hotier, S., Leroy, F., Boisgontier, J., Laidi, C., Mangin, J.-F., Delorme, R., Bolognani, F., Czech, C., Bouquet, C., Toledano, E., Bouvard, M., Petit, J., Mishchenko, M., d'Albis, M.-A., Gras, D., Gaman, A., Scheid, I., Leboyer, M., Zalla, T., Houenou, J., 2017. Social cognition in autism is associated with the neurodevelopment of the posterior superior temporal sulcus. Acta Psychiatrica Scandinavica 136, 517–525. https://doi.org/10.1111/acps.12814

Hou, L., Xiang, L., Crow, T.J., Leroy, F., Rivière, D., Mangin, J.-F., Roberts, N., 2019. Measurement of Sylvian Fissure asymmetry and occipital bending in humans and Pan troglodytes. NeuroImage 184, 855–870. https://doi.org/10.1016/j.neuroimage.2018.08.045

Huntgeburth, S.C., Petrides, M., 2008. Morphological relation of the lingual sulcus to the Posterior parahippocampal region in the human brain. Ann Gen Psychiatry 7, S308, 1744-859X-7-S1–S308. https://doi.org/10.1186/1744-859X-7-S1-S308

Huntgeburth, S.C., Petrides, M., 2012. Morphological patterns of the collateral sulcus in the human brain: Morphology of the collateral sulcus. European Journal of Neuroscience 35, 1295–1311. https://doi.org/10.1111/j.1460-9568.2012.08031.x

Huntgeburth, S.C., Petrides, M., 2016. Three-dimensional probability maps of the rhinal and the collateral sulci in the human brain. Brain Struct Funct 221, 4235–4255. https://doi.org/10.1007/s00429-016-1189-x

Iaria, G., Petrides, M., 2007. Occipital sulci of the human brain: Variability and probability maps. J. Comp. Neurol. 501, 243–259. https://doi.org/10.1002/cne.21254

Iaria, G., Robbins, S., Petrides, M., 2008. Three-dimensional probabilistic maps of the occipital sulci of the human brain in standardized stereotaxic space. Neuroscience 151, 174–185. https://doi.org/10.1016/j.neuroscience.2007.09.050

Im, K., Lee, J.-M., Lyttelton, O., Kim, S.H., Evans, A.C., Kim, S.I., 2008. Brain Size and Cortical Structure in the Adult Human Brain. Cerebral Cortex 18, 2181–2191. https://doi.org/10.1093/cercor/bhm244

Im, K., Jo, H.J., Mangin, J.-F., Evans, A.C., Kim, S.I., Lee, J.-M., 2010. Spatial distribution of deep sulcal landmarks and hemispherical asymmetry on the cortical surface. Cereb Cortex 20, 602–611. https://doi.org/10.1093/cercor/bhp127

Im, K., Pienaar, R., Lee, J.-M., Seong, J.-K., Choi, Y.Y., Lee, K.H., Grant, P.E., 2011. Quantitative comparison and analysis of sulcal patterns using sulcal graph matching: A twin study. NeuroImage 57, 1077–1086. https://doi.org/10.1016/j.neuroimage.2011.04.062

Im, K., Grant, P.E., 2019. Sulcal pits and patterns in developing human brains. NeuroImage 185, 881–890. https://doi.org/10.1016/j.neuroimage.2018.03.057

Išgum, I., Benders, M.J.N.L., Avants, B., Cardoso, M.J., Counsell, S.J., Gomez, E.F., Gui, L., Hűppi, P.S., Kersbergen, K.J., Makropoulos, A.,

Melbourne, A., Moeskops, P., Mol, C.P., Kuklisova-Murgasova, M., Rueckert, D., Schnabel, J.A., Srhoj-Egekher, V., Wu, J., Wang, S., de Vries, L.S., Viergever, M.A., 2015. Evaluation of automatic neonatal brain segmentation algorithms: The NeoBrainS12 challenge. Medical Image Analysis 20, 135–151. https://doi.org/10.1016/j.media.2014.11.001

Jiang, X., Zhang, T., Zhang, S., Kendrick, K.M., Liu, T., 2021. Fundamental functional differences between gyri and sulci: implications for brain function, cognition, and behavior. Psychoradiology 1, 23–41. https://doi.org/10.1093/psyrad/kkab002

Jouvent, E., Sun, Z.Y., De Guio, F., Duchesnay, E., Duering, M., Ropele, S., Dichgans, M., Mangin, J.-F., Chabriat, H., 2016. Shape of the Central Sulcus and Disability After Subcortical Stroke: A Motor Reserve Hypothesis. Stroke 47, 1023–1029. https://doi.org/10.1161/STROKEAHA.115.012562

Kersbergen, K.J., Leroy, F., Išgum, I., Groenendaal, F., de Vries, L.S., Claessens, N.H.P., van Haastert, I.C., Moeskops, P., Fischer, C., Mangin, J.-F., Viergever, M.A., Dubois, J., Benders, M.J.N.L., 2016. Relation between clinical risk factors, early cortical changes, and neurodevelopmental outcome in preterm infants. NeuroImage 142, 301–310. https://doi.org/10.1016/j.neuroimage.2016.07.010

Kim, S.H., Lyu, I., Fonov, V.S., Vachet, C., Hazlett, H.C., Smith, R.G., Piven, J., Dager, S.R., Mckinstry, R.C., Pruett, J.R., Evans, A.C., Collins, D.L., Botteron, K.N., Schultz, R.T., Gerig, G., Styner, M.A., 2016a. Development of cortical shape in the human brain from 6 to 24months of age via a novel measure of shape complexity. NeuroImage 135, 163–176. https://doi.org/10.1016/j.neuroimage.2016.04.053

Kim, H., Lepage, C., Maheshwary, R., Jeon, S., Evans, A.C., Hess, C.P., Barkovich, A.J., Xu, D., 2016b. NEOCIVET: Towards accurate morphometry of neonatal gyrification and clinical applications in preterm newborns. NeuroImage 138, 28–42. https://doi.org/10.1016/j.neuroimage.2016.05.034

Kim, S.Y., Liu, M., Hong, S.-J., Toga, A.W., Barkovich, A.J., Xu, D., Kim, H., 2020. Disruption and Compensation of Sulcation-based Covariance Networks in Neonatal Brain Growth after Perinatal Injury. Cerebral Cortex bhaa181. https://doi.org/10.1093/cercor/bhaa181

Kochunov, P., Mangin, J.-F., Coyle, T., Lancaster, J., Thompson, P., Rivière, D., Cointepas, Y., Régis, J., Schlosser, A., Royall, D.R., Zilles, K., Mazziotta, J., Toga, A., Fox, P.T., 2005. Age-related morphology trends of cortical sulci. Human Brain Mapping 26, 210–220. https://doi.org/10.1002/hbm.20198

Koenderink, J.J., van Doorn, A.J., 1992. Surface shape and curvature scales. Image and Vision Computing 10, 557–564. https://doi.org/10.1016/0262-8856(92)90076-F

Kostović, I., Sedmak, G., Judaš, M., 2019. Neural histology and neurogenesis of the human fetal and infant brain. NeuroImage 188, 743–773. https://doi.org/10.1016/j.neuroimage.2018.12.043

Kroenke, C.D., Bayly, P.V., 2018. How Forces Fold the Cerebral Cortex. J. Neurosci. 38, 767–775. https://doi.org/10.1523/JNEUROSCI.1105-17.2017

Kuklisova-Murgasova, M., Aljabar, P., Srinivasan, L., Counsell, S.J., Doria, V., Serag, A., Gousias, I.S., Boardman, J.P., Rutherford, M.A., Edwards, A.D., Hajnal, J.V., Rueckert, D., 2011. A dynamic 4D probabilistic atlas of the developing brain. NeuroImage 54, 2750–2763. https://doi.org/10.1016/j.neuroimage.2010.10.019

Kuklisova-Murgasova, M., Quaghebeur, G., Rutherford, M.A., Hajnal, J.V., Schnabel, J.A., 2012. Reconstruction of fetal brain MRI with intensity matching and complete outlier removal. Medical Image Analysis 16, 1550–1564. https://doi.org/10.1016/j.media.2012.07.004

Lebenberg, J., Labit, M., Auzias, G., Mohlberg, H., Fischer, C., Rivière, D., Duchesnay, E., Kabdebon, C., Leroy, F., Labra, N., Poupon, F., Dickscheid, T., Hertz-Pannier, L., Poupon, C., Dehaene-Lambertz, G., Hüppi, P., Amunts, K., Dubois, J., Mangin, J.-F., 2018. A framework based on sulcal constraints to align preterm, infant and adult human brain images acquired in vivo and post mortem. Brain Struct Funct 223, 4153–4168. https://doi.org/10.1007/s00429-018-1735-9

Le Guen, Y., Leroy, F., Auzias, G., Riviere, D., Grigis, A., Mangin, J.-F., Coulon, O., Dehaene-Lambertz, G., Frouin, V., 2018. The chaotic morphology of the left superior temporal sulcus is genetically constrained. NeuroImage 174, 297–307. https://doi.org/10.1016/j.neuroimage.2018.03.046

Le Guen, Y., Leroy, F., Philippe, C., IMAGEN consortium, Mangin, J.-F., Dehaene-Lambertz, G., Frouin, V., 2019. Enhancer locus in ch14q23.1 modulates brain asymmetric temporal regions involved in language processing. Neuroscience. https://doi.org/10.1101/539189

Lefèvre, J., Mangin, J.-F., 2010. A Reaction-Diffusion Model of Human Brain Development. PLoS Comput Biol 6, e1000749. https://doi.org/10.1371/journal.pcbi.1000749

Lefèvre, J., Germanaud, D., Dubois, J., Rousseau, F., de Macedo Santos, I., Angleys, H., Mangin, J.-F., Hüppi, P.S., Girard, N., De Guio, F., 2016. Are Developmental Trajectories of Cortical Folding Comparable Between Cross-sectional Datasets of Fetuses and Preterm Newborns? Cereb. Cortex 26, 3023–3035. https://doi.org/10.1093/cercor/bhv123

Leiberg, K., Papasavvas, C., Wang, Y., 2021. Local Morphological Measures Confirm that Folding Within Small Partitions of the Human Cortex Follows Universal Scaling Law, in: de Bruijne, M., Cattin, P.C., Cotin, S., Padoy, N., Speidel, S., Zheng, Y., Essert, C. (Eds.), Medical Image Computing and Computer Assisted Intervention – MICCAI 2021, Lecture Notes in Computer Science. Springer International Publishing, Cham, pp. 691–700. https://doi.org/10.1007/978-3-030-87234-2_65

Leroy, F., Mangin, J.-F., Rousseau, F., Glasel, H., Hertz-Pannier, L., Dubois, J., Dehaene-Lambertz, G., 2011. Atlas-Free Surface Reconstruction of the Cortical Grey-White Interface in Infants. PLoS ONE 6, e27128. https://doi.org/10.1371/journal.pone.0027128

Leroy, F., Cai, Q., Bogart, S.L., Dubois, J., Coulon, O., Monzalvo, K., Fischer, C., Glasel, H., Van der Haegen, L., Bénézit, A., Lin, C.-P., Kennedy, D.N., Ihara, A.S., Hertz-Pannier, L., Moutard, M.-L., Poupon, C., Brysbaert, M., Roberts, N., Hopkins, W.D., Mangin, J.-F., Dehaene-Lambertz, G., 2015. New human-specific brain landmark: The depth asymmetry of superior temporal sulcus. Proc Natl Acad Sci USA 112, 1208–1213. https://doi.org/10.1073/pnas.1412389112

Lewitus, E., Kelava, I., Huttner, W.B., 2013. Conical expansion of the outer subventricular zone and the role of neocortical folding in evolution and development. Front. Hum. Neurosci. 7. https://doi.org/10.3389/fnhum.2013.00424

Li, G., Wang, L., Shi, F., Lyall, A.E., Lin, W., Gilmore, J.H., Shen, D., 2014. Mapping Longitudinal Development of Local Cortical Gyrification in Infants from Birth to 2 Years of Age. Journal of Neuroscience 34, 4228–4238. https://doi.org/10.1523/JNEUROSCI.3976-13.2014

Li, G., Wang, L., Yap, P.-T., Wang, F., Wu, Z., Meng, Y., Dong, P., Kim, J., Shi, F., Rekik, I., Lin, W., Shen, D., 2019. Computational neuroanatomy of baby brains: A review. NeuroImage 185, 906–925. https://doi.org/10.1016/j.neuroimage.2018.03.042

Liu, M., Kitsch, A., Miller, S., Chau, V., Poskitt, K., Rousseau, F., Shaw, D., Studholme, C., 2016. Patch-based augmentation of Expectation–Maximization for brain MRI tissue segmentation at arbitrary age after premature birth. NeuroImage 127, 387–408. https://doi.org/10.1016/j.neuroimage.2015.12.009

Llinares-Benadero, C., Borrell, V., 2019. Deconstructing cortical folding: genetic, cellular and mechanical determinants. Nat Rev Neurosci 20, 161–176. https://doi.org/10.1038/s41583-018-0112-2

Lohmann, G., von Cramon, D.Y., Colchester, A.C.F., 2008. Deep Sulcal Landmarks Provide an Organizing Framework for Human Cortical Folding. Cerebral Cortex 18, 1415–1420. https://doi.org/10.1093/cercor/bhm174

Lombaert, H., J. Sporring, and K. Siddiqi. 2013. Diffeomorphic spectral matching of cortical surfaces. Inform. Process. Med. Imaging 7917:376–389.

Lopez-Persem, A., Verhagen, L., Amiez, C., Petrides, M., Sallet, J., 2019. The Human Ventromedial Prefrontal Cortex: Sulcal Morphology and Its Influence on Functional Organization. J. Neurosci. 39, 3627–3639. https://doi.org/10.1523/JNEUROSCI.2060-18.2019

Luders, E., Thompson, P.M., Narr, K.L., Toga, A.W., Jancke, L., Gaser, C., 2006. A curvature-based approach to estimate local gyrification on the cortical surface. NeuroImage 29, 1224–1230. https://doi.org/10.1016/j.neuroimage.2005.08.049

Lyttelton, O., Boucher, M., Robbins, S., Evans, A., 2007. An unbiased iterative group registration template for cortical surface analysis. NeuroImage 34, 1535–1544. https://doi.org/10.1016/j.neuroimage.2006.10.041

MacDonald, D., Avis, D., Evans, A.C., 1994. Multiple surface identification and matching in magnetic resonance images, in: Robb, R.A. (Ed.), . Presented at the Visualization in Biomedical Computing 1994, Rochester, MN, pp. 160–169. https://doi.org/10.1117/12.185176

Makropoulos, A., Gousias, I.S., Ledig, C., Aljabar, P., Serag, A., Hajnal, J.V., Edwards, A.D., Counsell, S.J., Rueckert, D., 2014. Automatic Whole Brain MRI Segmentation of the Developing Neonatal Brain. IEEE Trans. Med. Imaging 33, 1818–1831. https://doi.org/10.1109/TMI.2014.2322280

Makropoulos, A., Robinson, E.C., Schuh, A., Wright, R., Fitzgibbon, S., Bozek, J., Counsell, S.J., Steinweg, J., Vecchiato, K., Passerat-Palmbach, J., Lenz, G., Mortari, F., Tenev, T., Duff, E.P., Bastiani, M., Cordero-Grande, L., Hughes, E., Tusor, N., Tournier, J.-D., Hutter, J., Price, A.N., Teixeira, R.P.A.G., Murgasova, M., Victor, S., Kelly, C., Rutherford, M.A., Smith, S.M., Edwards, A.D., Hajnal, J.V., Jenkinson, M., Rueckert, D., 2018a. The developing human connectome project: A minimal processing pipeline for neonatal cortical surface reconstruction. NeuroImage 173, 88–112. https://doi.org/10.1016/j.neuroimage.2018.01.054

Makropoulos, A., Counsell, S.J., Rueckert, D., 2018b. A review on automatic fetal and neonatal brain MRI segmentation. NeuroImage 170, 231–248. https://doi.org/10.1016/j.neuroimage.2017.06.074

Mallela, A.N., Deng, H., Brisbin, A.K., Bush, A., Goldschmidt, E., 2020. Sylvian fissure development is linked to differential genetic expression in the pre-folded brain. Sci Rep 10, 14489. https://doi.org/10.1038/s41598-020-71535-4

Mangin, J.-F., Riviere, D., Cachia, A., Duchesnay, E., Cointepas, Y., Papadopoulos-Orfanos, D., Collins, D.L., Evans, A.C., Regis, J., 2004a. Object-Based Morphometry of the Cerebral Cortex. IEEE Trans. Med. Imaging 23, 968–982. https://doi.org/10.1109/TMI.2004.831204

Mangin, J., Poupon, F., Duchesnay, E., Riviere, D., Cachia, A., Collins, D., Evans, A., Regis, J., 2004b. Brain morphometry using 3D moment invariants. Medical Image Analysis 8, 187–196. https://doi.org/10.1016/j.media.2004.06.016

Mangin, J.-F., Jouvent, E., Cachia, A., 2010. In vivo measurement of cortical morphology: means and meanings: Current Opinion in Neurology 1. https://doi.org/10.1097/WCO.0b013e32833a0afc

Mangin, J.-F., Auzias, G., Coulon, O., Sun, Z.Y., Rivière, D., Régis, J., 2015a. Sulci as Landmarks, in: Brain Mapping. Elsevier, pp. 45–52. https://doi.org/10.1016/B978-0-12-397025-1.00198-6

Mangin, J.-F., Perrot, M., Operto, G., Cachia, A., Fischer, C., Lefèvre, J., Rivière, D., 2015b. Sulcus Identification and labelling, in: Brain Mapping. Elsevier, pp. 365–371. https://doi.org/10.1016/B978-0-12-397025-1.00307-9

Mangin, J.-F., Lebenberg, J., Lefranc, S., Labra, N., Auzias, G., Labit, M., Guevara, M., Mohlberg, H., Roca, P., Guevara, P., Dubois, J., Leroy, F., Dehaene-Lambertz, G., Cachia, A., Dickscheid, T., Coulon, O., Poupon, C., Rivière, D., Amunts, K., Sun, Z.Y., 2016. Spatial normalization of brain images and beyond. Medical Image Analysis 33, 127–133. https://doi.org/10.1016/j.media.2016.06.008

Mangin, J.-F., Rivière, D., Duchesnay, E., Cointepas, Y., Gaura, V., Verny, C., Damier, P., Krystkowiak, P., Bachoud-Lévi, A.-C., Hantraye, P., Remy, P., Douaud, G., 2020. Neocortical morphometry in Huntington's disease: Indication of the coexistence of abnormal neurodevelopmental and neurodegenerative processes. NeuroImage: Clinical 26, 102211. https://doi.org/10.1016/j.nicl.2020.102211

Margiotoudi, K., Marie, D., Claidière, N., Coulon, O., Roth, M., Nazarian, B., Lacoste, R., Hopkins, W.D., Molesti, S., Fresnais, P., Anton, J.-L., Meguerditchian, A., 2019. Handedness in monkeys reflects hemispheric specialization within the central sulcus. An in vivo MRI study in right- and left-handed olive baboons. Cortex 118, 203–211. https://doi.org/10.1016/j.cortex.2019.01.001

Mellerio, C., Roca, P., Chassoux, F., Danière, F., Cachia, A., Lion, S., Naggara, O., Devaux, B., Meder, J.-F., Oppenheim, C., 2015. The Power Button Sign: A Newly Described Central Sulcal Pattern on Surface Rendering MR Images of Type 2 Focal Cortical Dysplasia. Radiology 274, 500–507. https://doi.org/10.1148/radiol.14140773

Meng, Y., Li, G., Lin, W., Gilmore, J.H., Shen, D., 2014. Spatial distribution and longitudinal development of deep cortical sulcal landmarks in infants. NeuroImage 100, 206–218. https://doi.org/10.1016/j.neuroimage.2014.06.004

Meng, Y., Li, G., Wang, L., Lin, W., Gilmore, J.H., Shen, D., 2018. Discovering cortical sulcal folding patterns in neonates using large-scale dataset. Hum. Brain Mapp. 39, 3625–3635. https://doi.org/10.1002/hbm.24199

Moeskops, P., Benders, M.J.N.L., Kersbergen, K.J., Groenendaal, F., de Vries, L.S., Viergever, M.A., Išgum, I., 2015. Development of Cortical Morphology Evaluated with Longitudinal MR Brain Images of Preterm Infants. PLoS ONE 10, e0131552. https://doi.org/10.1371/journal.pone.0131552

Molko, N., Cachia, A., Rivière, D., Mangin, J.-F., Bruandet, M., Le Bihan, D., Cohen, L., Dehaene, S., 2003. Functional and Structural Alterations of the Intraparietal Sulcus in a Developmental Dyscalculia of Genetic Origin. Neuron 40, 847–858. https://doi.org/10.1016/S0896-6273(03)00670-6

Moorhead, T.W.J., Harris, J.M., Stanfield, A.C., Job, D.E., Best, J.J.K., Johnstone, E.C., Lawrie, S.M., 2006. Automated computation of the Gyrification Index in prefrontal lobes: Methods and comparison with manual implementation. NeuroImage 31, 1560–1566. https://doi.org/10.1016/j.neuroimage.2006.02.025

Ono, M., Kubik, S., & Abernathey, C. D. (1990). *Atlas of the cerebral sulci*. Thieme Medical Publishers.

Orasanu, E., Melbourne, A., Cardoso, M.J., Lomabert, H., Kendall, G.S., Robertson, N.J., Marlow, N., Ourselin, S., 2016. Cortical folding of the preterm brain: a longitudinal analysis of extremely preterm born neonates using spectral matching. Brain Behav 6, e00488. https://doi.org/10.1002/brb3.488

Padilla, N., Alexandrou, G., Blennow, M., Lagercrantz, H., Ådén, U., 2015. Brain Growth Gains and Losses in Extremely Preterm Infants at Term. Cerebral Cortex 25, 1897–1905. https://doi.org/10.1093/cercor/bht431

Parent, A., 2014. Louis Pierre Gratiolet (1815-1865) and His Contribution to the Study of Cerebral Convolutions in Primates. NM 05, 1–8. https://doi.org/10.4236/nm.2014.51001

Paus, T., Tomaiuolo, F., Otaky, N., MacDonald, D., Petrides, M., Atlas, J., Morris, R., Evans, A.C., 1996. Human Cingulate and Paracingulate Sulci: Pattern, Variability, Asymmetry, and Probabilistic Map. Cereb Cortex 6, 207–214. https://doi.org/10.1093/cercor/6.2.207

Payette, K., de Dumast, P., Kebiri, H., Ezhov, I., Paetzold, J.C., Shit, S., Iqbal, A., Khan, R., Kottke, R., Grehten, P., Ji, H., Lanczi, L., Nagy, M., Beresova, M., Nguyen, T.D., Natalucci, G., Karayannis, T., Menze, B., Bach Cuadra, M., Jakab, A., 2021. An automatic multi-tissue human fetal brain segmentation benchmark using the Fetal Tissue Annotation Dataset. Sci Data 8, 167. https://doi.org/10.1038/s41597-021-00946-3

Petrides, M., 2019. Atlas of the morphology of the human cerebral cortex on the average MNI brain. Academic Press, New York

Piao, X., Hill, R.S., Bodell, A., Chang, B.S., Basel-Vanagaite, L., Straussberg, R., Dobyns, W.B., Qasrawi, B., Winter, R.M., Innes, A.M., Voit, T., Ross, M.E., Michaud, J.L., Déscarie, J.-C., Barkovich, A.J., Walsh, C.A., 2004. G Protein-Coupled Receptor-Dependent Development of Human Frontal Cortex. Science 303, 2033–2036. https://doi.org/10.1126/science.1092780

Pizzagalli, F., Auzias, G., Yang, Q., Mathias, S.R., Faskowitz, J., Boyd, J.D., Amini, A., Rivière, D., McMahon, K.L., de Zubicaray, G.I., Martin, N.G., Mangin, J.-F., Glahn, D.C., Blangero, J., Wright, M.J., Thompson, P.M., Kochunov, P., Jahanshad, N., 2020. The reliability and heritability of cortical folds and their genetic correlations across hemispheres. Commun Biol 3, 510. https://doi.org/10.1038/s42003-020-01163-1

Plaze, M., Paillere-Martinot, M.-L., Penttila, J., Januel, D., de Beaurepaire, R., Bellivier, F., Andoh, J., Galinowski, A., Gallarda, T., Artiges, E., Olie, J.-P., Mangin, J.-F., Martinot, J.-L., Cachia, A., 2011. "Where Do Auditory Hallucinations Come From?"--A Brain Morphometry Study of Schizophrenia Patients With Inner or Outer Space Hallucinations. Schizophrenia Bulletin 37, 212–221. https://doi.org/10.1093/schbul/sbp081

Prastawa, M., Gilmore, J.H., Lin, W., Gerig, G., 2005. Automatic segmentation of MR images of the developing newborn brain. Medical Image Analysis 9, 457–466. https://doi.org/10.1016/j.media.2005.05.007

Rakic, P., 1988. Specification of cerebral cortical areas. Science 241, 170–176. https://doi.org/10.1126/science.3291116

Rana, S., Shishegar, R., Quezada, S., Johnston, L., Walker, D.W., Tolcos, M., 2019. The Subplate: A Potential Driver of Cortical Folding? Cerebral Cortex 29, 4697–4708. https://doi.org/10.1093/cercor/bhz003

Régis, J., Mangin, J.-F., Ochiai, T., Frouin, V., Riviére, D., Cachia, A., Tamura, M., Samson, Y., 2005. "Sulcal Root" Generic Model: a Hypothesis to Overcome the Variability of the Human Cortex Folding Patterns. Neurol. Med. Chir.(Tokyo) 45, 1–17. https://doi.org/10.2176/nmc.45.1

Régis, J., Tamura, M., Park, M.C., McGonigal, A., Rivière, D., Coulon, O., Bartolomei, F., Girard, N., Figarella-Branger, D., Chauvel, P., Mangin, J.-F., 2011. Subclinical abnormal gyration pattern, a potential anatomic marker of epileptogenic zone in patients with magnetic resonance imaging-negative frontal lobe epilepsy. Neurosurgery 69, 80–93; discussion 93-94. https://doi.org/10.1227/NEU.0b013e318212bb1a

Rekik, I., Li, G., Lin, W., Shen, D., 2018. Do Baby Brain Cortices that Look Alike at Birth Grow Alike During the First Year of Postnatal Development?, in: Frangi, A.F., Schnabel, J.A., Davatzikos, C., Alberola-López, C., Fichtinger, G. (Eds.), Medical Image Computing and Computer Assisted Intervention – MICCAI 2018. Springer International Publishing, Cham, pp. 566–574. https://doi.org/10.1007/978-3-030-00931-1_65

Rettmann, M.E., Han, X., Xu, C., Prince, J.L., 2002. Automated Sulcal Segmentation Using Watersheds on the Cortical Surface. NeuroImage 15, 329–344. https://doi.org/10.1006/nimg.2001.0975

Rivière, D., Mangin, J.-F., Papadopoulos-Orfanos, D., Martinez, J.-M., Frouin, V., Régis, J., 2002. Automatic recognition of cortical sulci of the human brain using a congregation of neural networks. Medical

Image Analysis 6, 77–92. https://doi.org/10.1016/S1361-8415(02)00052-X

Rockel, A.J., Hiorns, R.W., Powell, T.P.S., 1980. The basic uniformity in structure of the neocortex. Brain 103, 221–244. https://doi.org/10.1093/brain/103.2.221

Robinson, E.C., Jbabdi, S., Glasser, M.F., Andersson, J., Burgess, G.C., Harms, M.P., Smith, S.M., Van Essen, D.C., Jenkinson, M., 2014. MSM: A new flexible framework for Multimodal Surface Matching. NeuroImage 100, 414–426. https://doi.org/10.1016/j.neuroimage.2014.05.069

Robinson, E.C., Garcia, K., Glasser, M.F., Chen, Z., Coalson, T.S., Makropoulos, A., Bozek, J., Wright, R., Schuh, A., Webster, M., Hutter, J., Price, A., Cordero Grande, L., Hughes, E., Tusor, N., Bayly, P.V., Van Essen, D.C., Smith, S.M., Edwards, A.D., Hajnal, J., Jenkinson, M., Glocker, B., Rueckert, D., 2018. Multimodal surface matching with higher-order smoothness constraints. NeuroImage 167, 453–465. https://doi.org/10.1016/j.neuroimage.2017.10.037

Ronan, L., Fletcher, P.C., 2015. From genes to folds: a review of cortical gyrification theory. Brain Struct Funct 220, 2475–2483. https://doi.org/10.1007/s00429-014-0961-z

Rousseau, F., Glenn, O.A., Iordanova, B., Rodriguez-Carranza, C., Vigneron, D.B., Barkovich, J.A., Studholme, C., 2006. Registration-Based Approach for Reconstruction of High-Resolution In Utero Fetal MR Brain Images. Academic Radiology 13, 1072–1081. https://doi.org/10.1016/j.acra.2006.05.003

Rousseau, F., Oubel, E., Pontabry, J., Schweitzer, M., Studholme, C., Koob, M., Dietemann, J.-L., 2013. BTK: An open-source toolkit for fetal brain MR image processing. Computer Methods and Programs in Biomedicine 109, 65–73. https://doi.org/10.1016/j.cmpb.2012.08.007

Sarrazin, S., Cachia, A., Hozer, F., McDonald, C., Emsell, L., Cannon, D.M., Wessa, M., Linke, J., Versace, A., Hamdani, N., D'Albis, M.-A., Delavest, M., Phillips, M.L., Brambilla, P., Bellani, M., Polosan, M., Favre, P., Leboyer, M., Mangin, J.-F., Houenou, J., 2018. Neurodevelopmental subtypes of bipolar disorder are related to cortical folding patterns: An

international multicenter study. Bipolar Disord 20, 721–732. https://doi.org/10.1111/bdi.12664

Schaer, M., Cuadra, M.B., Tamarit, L., Lazeyras, F., Eliez, S., Thiran, J.-P., 2008. A Surface-Based Approach to Quantify Local Cortical Gyrification. IEEE Trans. Med. Imaging 27, 161–170. https://doi.org/10.1109/TMI.2007.903576

Segal, E., Petrides, M., 2012. The morphology and variability of the caudal rami of the superior temporal sulcus: Caudal rami of the STS. European Journal of Neuroscience 36, 2035–2053. https://doi.org/10.1111/j.1460-9568.2012.08109.x

Segal, E., Petrides, M., 2013. Functional activation during reading in relation to the sulci of the angular gyrus region. Eur J Neurosci 38, 2793–2801. https://doi.org/10.1111/ejn.12277

Shi, F., Fan, Y., Tang, S., Gilmore, J.H., Lin, W., Shen, D., 2010. Neonatal brain image segmentation in longitudinal MRI studies. NeuroImage 49, 391–400. https://doi.org/10.1016/j.neuroimage.2009.07.066

Shimony, J.S., Smyser, C.D., Wideman, G., Alexopoulos, D., Hill, J., Harwell, J., Dierker, D., Van Essen, D.C., Inder, T.E., Neil, J.J., 2016. Comparison of cortical folding measures for evaluation of developing human brain. NeuroImage 125, 780–790. https://doi.org/10.1016/j.neuroimage.2015.11.001

Snyder, W., Patti, M., Troiani, V., 2019. An evaluation of automated tracing for orbitofrontal cortex sulcogyral pattern typing. Journal of Neuroscience Methods 326, 108386. https://doi.org/10.1016/j.jneumeth.2019.108386

Sowell, E.R., Thompson, P.M., Rex, D., Kornsand, D., Tessner, K.D., Jernigan, T.L., Toga, A.W., 2002. Mapping Sulcal Pattern Asymmetry and Local Cortical Surface Gray Matter Distribution In Vivo: Maturation in Perisylvian Cortices. Cerebral Cortex 12, 17–26. https://doi.org/10.1093/cercor/12.1.17

Sprung-Much, T., Petrides, M., 2018. Morphological patterns and spatial probability maps of two defining sulci of the posterior ventrolateral frontal cortex of the human brain: the sulcus diagonalis and

the anterior ascending ramus of the lateral fissure. Brain Struct Funct 223, 4125–4152. https://doi.org/10.1007/s00429-018-1733-y

Steinmetz, H., 1990. Sulcus topography of the parietal opercular region: An anatomic and MR study*1. Brain and Language 38, 515–533. https://doi.org/10.1016/0093-934X(90)90135-4

Studholme, C., 2015. Mapping the developing human brain in utero using quantitative MR imaging techniques. Seminars in Perinatology 39, 105–112. https://doi.org/10.1053/j.semperi.2015.01.003

Sun, Z.Y., Rivière, D., Poupon, F., Régis, J., Mangin, J.-F., 2007. Automatic Inference of Sulcus Patterns Using 3D Moment Invariants, in: Ayache, N., Ourselin, S., Maeder, A. (Eds.), Medical Image Computing and Computer-Assisted Intervention – MICCAI 2007, Lecture Notes in Computer Science. Springer Berlin Heidelberg, Berlin, Heidelberg, pp. 515–522. https://doi.org/10.1007/978-3-540-75757-3_63

Sun, Z.Y., Perrot, M., Tucholka, A., Rivière, D., Mangin, J.-F., 2009. Constructing a Dictionary of Human Brain Folding Patterns. Lecture Notes in Computer Science 5762, 117–124.

Sun, Z.Y., Klöppel, S., Rivière, D., Perrot, M., Frackowiak, R., Siebner, H., Mangin, J.-F., 2012. The effect of handedness on the shape of the central sulcus. NeuroImage 60, 332–339. https://doi.org/10.1016/j.neuroimage.2011.12.050

Sun, Z.Y., Pinel, P., Rivière, D., Moreno, A., Dehaene, S., Mangin, J.-F., 2016. Linking morphological and functional variability in hand movement and silent reading. Brain Struct Funct 221, 3361–3371. https://doi.org/10.1007/s00429-015-1106-8

Sun, Z.Y., Cachia, A., Rivière, D., Fischer, C., Makin, T., Mangin, J.-F., 2017. Congenital

unilateral upper limb absence flattens the contralateral hand-knob. Organization for Human

Brain Mapping Meeting (OHBM 2017), Vancouver, Canada. ⟨hal-02876124⟩

Sur, M., Rubenstein, J.L.R., 2005. Patterning and Plasticity of the Cerebral Cortex. Science 310, 805–810. https://doi.org/10.1126/science.1112070

Takerkart, S., Auzias, G., Brun, L., Coulon, O., 2017. Structural graph-based morphometry: A multiscale searchlight framework based on sulcal pits. Medical Image Analysis 35, 32–45. https://doi.org/10.1016/j.media.2016.04.011

Tallinen, T., Chung, J.Y., Biggins, J.S., Mahadevan, L., 2014. Gyrification from constrained cortical expansion. Proceedings of the National Academy of Sciences 111, 12667–12672. https://doi.org/10.1073/pnas.1406015111

Tallinen, T., Chung, J.Y., Rousseau, F., Girard, N., Lefèvre, J., Mahadevan, L., 2016. On the growth and form of cortical convolutions. Nature Phys 12, 588–593. https://doi.org/10.1038/nphys3632

Tenenbaum, J.B., 2000. A Global Geometric Framework for Nonlinear Dimensionality Reduction. Science 290, 2319–2323. https://doi.org/10.1126/science.290.5500.2319

Tissier, C., Linzarini, A., Allaire-Duquette, G., Mevel, K., Poirel, N., Dollfus, S., Etard, O., Orliac, F., Peyrin, C., Charron, S., Raznahan, A., Houdé, O., Borst, G., Cachia, A., 2018. Sulcal Polymorphisms of the IFC and ACC Contribute to Inhibitory Control Variability in Children and Adults. eNeuro 5, ENEURO.0197-17.2018. https://doi.org/10.1523/ENEURO.0197-17.2018

Toro, R., Burnod, Y., 2005. A Morphogenetic Model for the Development of Cortical Convolutions. Cerebral Cortex 15, 1900–1913. https://doi.org/10.1093/cercor/bhi068

van der Knaap, M.S., van Wezel-Meijler, G., Barth, P.G., Barkhof, F., Adèr, H.J., Valk, J., 1996. Normal Gyration and Sulcation in Preterm and Term Neonates: Appearance on MR Images. Radiology. https://doi.org/10.1148/radiology.200.2.8685331

Van Essen, D.C., 1997. A tension-based theory of morphogenesis and compact wiring in the central nervous system. Nature 385, 313–318. https://doi.org/10.1038/385313a0

Van Essen, D.C., Donahue, C.J., Coalson, T.S., Kennedy, H., Hayashi, T., Glasser, M.F., 2019. Cerebral cortical folding, parcellation, and connectivity in humans, nonhuman primates, and mice. Proc Natl Acad Sci USA 116, 26173–26180. https://doi.org/10.1073/pnas.1902299116

Vasung, L., Rollins, C.K., Yun, H.J., Velasco-Annis, C., Zhang, J., Wagstyl, K., Evans, A., Warfield, S.K., Feldman, H.A., Grant, P.E., Gholipour, A., 2019. Quantitative In vivo MRI Assessment of Structural Asymmetries and Sexual Dimorphism of Transient Fetal Compartments in the Human Brain. Cerebral Cortex bhz200. https://doi.org/10.1093/cercor/bhz200

Vogt, C., Vogt, O., 1911. Nouvelle contribution à l'étude de la myéloarchitecture de l'écorce cérébrale. XX. *In French*. Congres des médecins aliénistes et neurologistes de France, Brüssel

Voorhies, W.I., Miller, J.A., Yao, J.K., Bunge, S.A., Weiner, K.S., 2021. Cognitive insights from tertiary sulci in prefrontal cortex. Nat Commun 12, 5122. https://doi.org/10.1038/s41467-021-25162-w

Wang, L., Shi, F., Lin, W., Gilmore, J.H., Shen, D., 2011. Automatic segmentation of neonatal images using convex optimization and coupled level sets. NeuroImage 58, 805–817. https://doi.org/10.1016/j.neuroimage.2011.06.064

Wang, L., Gao, Y., Shi, F., Li, G., Gilmore, J.H., Lin, W., Shen, D., 2015. LINKS: Learning-based multi-source IntegratioN frameworK for Segmentation of infant brain images. NeuroImage 108, 160–172. https://doi.org/10.1016/j.neuroimage.2014.12.042

Wang, L., Yao, J., Hu, N., 2019. A mechanical method of cerebral cortical folding development based on thermal expansion. Sci Rep 9, 1914. https://doi.org/10.1038/s41598-018-37461-2

Wang, X., Lefèvre, J., Bohi, A., Harrach, M.A., Dinomais, M., Rousseau, F., 2021. The influence of biophysical parameters in a biomechanical model of cortical folding patterns. Sci Rep 11, 7686. https://doi.org/10.1038/s41598-021-87124-y

Welker, W., 1990. Why Does Cerebral Cortex Fissure and Fold?, in: Cerebral Cortex. pp. 3–137.

Wright, R., Kyriakopoulou, V., Ledig, C., Rutherford, M.A., Hajnal, J.V., Rueckert, D., Aljabar, P., 2014. Automatic quantification of normal cortical folding patterns from fetal brain MRI. NeuroImage 91, 21–32. https://doi.org/10.1016/j.neuroimage.2014.01.034

Wright, R., Makropoulos, A., Kyriakopoulou, V., Patkee, P.A., Koch, L.M., Rutherford, M.A., Hajnal, J.V., Rueckert, D., Aljabar, P., 2015.

Construction of a fetal spatio-temporal cortical surface atlas from in utero MRI: Application of spectral surface matching. NeuroImage 120, 467–480. https://doi.org/10.1016/j.neuroimage.2015.05.087

Wu, J., Sun, T., Yu, B., Li, Z., Wu, Q., Wang, Y., Qian, Z., Zhang, Y., Jiang, L., & Wei, H. (2021). Age-specific structural fetal brain atlases construction and cortical development quantification for chinese population. *NeuroImage*, *241*, 118412. https://doi.org/10.1016/j.neuroimage.2021.118412

Wysiadecki, G., Mazurek, A., Walocha, J., Majos, A., Tubbs, R.S., Iwanaga, J., Żytkowski, A., Radek, M., 2021. Revisiting the Morphology and Classification of the Paracingulate Gyrus with Commentaries on Ambiguous Cases. Brain Sciences 11, 872. https://doi.org/10.3390/brainsci11070872

Xu, G., Knutsen, A.K., Dikranian, K., Kroenke, C.D., Bayly, P.V., Taber, L.A., 2010. Axons Pull on the Brain, But Tension Does Not Drive Cortical Folding. Journal of Biomechanical Engineering 132, 071013. https://doi.org/10.1115/1.4001683

Yang, F., Kruggel, F., 2009. A graph matching approach for labelling brain sulci using location, orientation, and shape. Neurocomputing 73, 179–190. https://doi.org/10.1016/j.neucom.2008.09.031

Yang, J., Wang, D., Rollins, C., Leming, M., Liò, P., Suckling, J., Murray, G., Garrison, J., Cachia, A., 2019. Volumetric Segmentation and Characterisation of the Paracingulate Sulcus on MRI Scans (preprint). Bioinformatics. https://doi.org/10.1101/859496

Yousry, T., 1997. Localization of the motor hand area to a knob on the precentral gyrus. A new landmark. Brain 120, 141–157. https://doi.org/10.1093/brain/120.1.141

Yun, H.J., Chung, A.W., Vasung, L., Yang, E., Tarui, T., Rollins, C.K., Ortinau, C.M., Grant, P.E., Im, K., 2019. Automatic labelling of cortical sulci for the human fetal brain based on spatio-temporal information of gyrification. NeuroImage 188, 473–482. https://doi.org/10.1016/j.neuroimage.2018.12.023

Zilles, K., Armstrong, E., Schleicher, A., Kretschmann, H.-J., 1988. The human pattern of gyrification in the cerebral cortex. Anat Embryol 179, 173–179. https://doi.org/10.1007/BF00304699

Zilles, K., Palomero-Gallagher, N., Amunts, K., 2013. Development of cortical folding during evolution and ontogeny. Trends in Neurosciences 36, 275–284. https://doi.org/10.1016/j.tins.2013.01.006

Zlatkina, V., Petrides, M., 2010. Morphological patterns of the postcentral sulcus in the human brain. J. Comp. Neurol. 518, 3701–3724. https://doi.org/10.1002/cne.22418

Zlatkina, V., Amiez, C., Petrides, M., 2016. The postcentral sulcal complex and the transverse postcentral sulcus and their relation to sensorimotor functional organization. Eur J Neurosci 43, 1268–1283. https://doi.org/10.1111/ejn.13049

7.3 TRANSITION

This article gives a general overview of the current understanding on sulcal pattern development, and an interesting picture of the interdisciplinarity required to investigate it. We can notice that the corpus of sulcal pattern studies per se is not very dense. As can be understood from the review, this field is relatively recent, mostly emerging in the 21st century with advances in MRI. Moreover, the technology enabling sulcal studies in the developing brain was also lacking in the past, greatly hindering the possibilities of early folding pattern investigation. Yet, the increasing understanding of relationships between sulcation and function, be it in health or in pathology, calls for a specific effort to explore its developmental dynamics.

This effort has been remarkably undertaken by seeking answers to a series of questions, which I would summarize as why, when and how does the human cerebral cortex fold. Out of those three questions, the "when" is the best solved: post mortem pre-MRI fetal studies already provided valuable observations on the chronology of folding (Cunningham, 1892; Chi et al., 1977a), which have since then been refined in typically developing newborns and in the context of premature birth. Yet, it should be noticed that this chronology is assessed in terms of apparition of the sulci and not in terms of pattern encoding. This induces a currently poor understanding of the timings at which specific shape characteristics emerge. The "why" has inspired multiple hypotheses from different domains, which, combined together, pave the way for an integrative theory of cortical folding, combining genetic, cellular and biomechanical processes.

The "how", however, is still vastly unexplored. Some common features within groups of infants have been reported, such as early length asymmetries in the sylvian fissure and depth asymmetries in the temporal sulcus. In parallel, hypotheses justifying the common pattern have been proposed, such as the sulcal roots theory and joint sulcal pits model, and seem to be supported by experimental data. Yet, studies assessing the variability of folding patterns, and even more so in the very young brain, are scarce. They are nonetheless fundamental both for a better understanding of the ins and outs of adult sulcal

pattern, and for potential early interventions if we can infer neurodevelopmental adversities from sulcal development.

In this context, I have oriented my PhD mostly to address this third question: How does the sulcal pattern emerges? through the observation of developing sulci in a cohort of longitudinally scanned preterm infants. The context of my PhD will be exposed in the following Chapter II.

8 CHAPTER II: CONTEXTUALIZATION OF THE SULCAL PATTERN STUDIES AND PRESENTATION OF THE COHORT

My PhD subject is born from my supervisors' collaboration in the CEA NeuroSpin neuroimaging center: Dr. Jean-François Mangin and Dr. Denis Rivière are specialized in adult sulcal studies, while Dr. Jessica Dubois is specialized in neurodevelopment. A previous collaboration between Dr. Jessica Dubois and the team of Pr. Manon Benders (Wilhelmina's Children Hospital, University Medical Center, in Utrecht, Netherlands) led to an investigation exploring basic sulcal measures, such as length or depth, in a longitudinally acquired preterm cohort, and relating them to later functional outcome (Kersbergen et al., 2016). This study inspired my supervisors about the potential of this setting for more in-depth sulcal pattern exploration, and led them to the proposition of a PhD project on the dynamics of cortical folding pattern and to the renewal of the collaboration with Pr. Manon Benders, based on the preterm dataset they acquired and shared with us.

Thus, at the start of my PhD, I had access to MRI images fully preprocessed for sulcal studies of a longitudinally-acquired preterm cohort. Moreover, I was introduced to the in-house brain anatomy software, BrainVISA (https://brainvisa.info), essential for sulcal analysis. To contextualise the different contributions of my PhD, in this chapter I aim to present the data and methods which were anterior to my contribution, which are at the basis of both of my original research articles, along with some specific adjustments I had to foresee to.

8.1 PRESENTATION OF THE COHORT

The cohort that I have studied during my PhD is composed of 71 infants born extremely preterm (51% males), between 24 and 28 weeks of gestational age (w GA), and recruited at the Wilhelmina's Children Hospital, University Medical Center, Utrecht, between 2008 and 2012. Perinatal clinical data was recorded in these infants, and a longitudinal follow-up allowed the team to assess their motor and cognitive outcome at around 2 years of age with the Bayley Scales of Infant and

Toddler Development, third edition (BSITD-III), and their motor performances at 5 years of age through the movement Assessment Battery for Children, 2nd edition, Dutch version (MABC-2-NL), as well as their handedness. The perinatal clinical characteristics and fine motor follow-up of the study participants at 5 are detailed in Table 1.

Table 1: Perinatal clinical characteristics and fine motor follow-up of the study participants (n=71)

Characteristics	*Mean ± Standard deviation (range) or N (percentage)*
Perinatal clinical characteristics	
Sex, male	36 (51%)
Gestational age at birth (weeks)	26.5 ± 1.0 (24.4 – 27.9)
Birth-weight z-score	0.4 ± 0.8 (-2.5 – 1.8)
Presence of severe IVH (grade 3 or 4): number of infants	8 (11%)
Presence of broncho-pulmonary dysplasia: number of infants	20 (39%)
Age at MRI scans	
PMA at early acquisition (weeks)	30.7 ± 0.9 (28.7 – 32.7)
PMA at term-equivalent age acquisition (weeks)	41.2 ± 0.6 (40.0 – 42.7)
Fine motor follow-up at 5-years	
Manual lateralization	
Handedness: number of infants (left / ambidextrous / right) (n=70)	18 / 2 / 50 (26 / 3 / 71%)
Corrected handedness*: number of infants (left / right) (n=57)	7 / 50 (12 / 88%)
Fine motor assessment (n=66)	
Age at mABC	5 years 9 months ± 4 months (4y 6m – 6y 7m)
mABC manual dexterity standardized score	7.7 ± 2.4 (3 – 14)
mABC manual dexterity outcome: number of infants (poor/borderline/good)	15 / 16 / 35 (23 / 24 / 53%)

IVH: intra-ventricular hemorrhage. PMA: post-menstrual age. *Corrected handedness excludes ambidextrous and left-handed children having both parents right-handed. mABC: Movement Assessment Battery for Children.

During their initial stay at the hospital, these preterm infants were scanned twice with MRI: once around 30 weeks of post-menstrual age (w PMA) (28.7 − 32.7w, mean: 30.7 ± 0.9w) and again around term equivalent age (TEA) (40.0 − 42.7w, mean: 41.2 ± 0.6w). For each scan, MR imaging was performed on a 3-Tesla MR system (Achieva, Philips Medical Systems, Best, The Netherlands). The protocol included T2-weighted imaging with a turbo-spin echo sequence in the coronal plane (at early MRI: repetition time (TR) 10.085 ms; echo time (TE) 120 ms; slice thickness 2 mm, in-plane spatial resolution 0.35 × 0.35 mm; at TEA: TR 4847 ms; TE 150 ms; slice thickness 1.2 mm, in-plane spatial resolution 0.35 × 0.35 mm).

8.2 PREPROCESSING OF THE DATA

A major part of the data processing performed on the resulting MRI images was operated by the previous team working on this data, as detailed in Kersbergen et al., 2016, and as summarized in the "preprocessing of brain images" section of my contribution on the central sulcus (Chapter III).

Extract from Kerbergen et al., 2016:

"In order to assess the folding stage and measure changes in cortical sulci, a dedicated approach was implemented by taking benefit of the complementarity of three previously validated methods that enable 1) reliable brain tissue segmentation of preterm images (Moeskops et al., 2015), 2) relevant 3D reconstructions of inner cortical surfaces in infants (Leroy et al., 2011), and 3) sulci identification in the adult brain (Fischer et al., 2012). First, T2-weighted images were segmented with a recently developed automatic segmentation method, defining masks of the cortical grey matter, unmyelinated white matter and cerebrospinal fluid in the extracerebral space (Moeskops et al., 2015). In short, this method uses supervised voxel classification on T2-weighted images in three subsequent stages. In the first stage, voxels that can be easily assigned to one of the three tissue types are labelled. In the second stage, dedicated analysis of the remaining voxels is performed. The third stage is used to resolve possible inconsistencies resulting from the first two tissue-specific segmentation stages by performing multi-class classification (Moeskops et al., 2015). Before the segmentation, a brain

mask was automatically generated based on the T2-weighted image using the Brain Extraction Tool (BET) from the FMRIB Software Library (FSL) (Smith, 2002). For both early and TEA segmentations, the same set of features was used.

This method has been evaluated on images of preterm infants acquired at both early and term equivalent age, and has been validated by comparison with several manually segmented scans, as described in detail in Moeskops et al. (2015). The probabilistic segmentations resulting from the second stage were used to subsequently reconstruct inner cortical surfaces of both hemispheres, by adapting the anatomical pipelines of the BrainvVISA® software (Baby and Morphologist pipelines) (Leroy et al., 2011; Mangin et al., 2004). Probability maps for the tissues of interest (cortical grey matter, unmyelinated white matter and cerebrospinal fluid) (Moeskops et al., 2015) were combined within a single feature map to maximize the contrast between grey and white matter. This optimized feature field was used in the stage of homotopic deformation of coupled surfaces (Leroy et al., 2011), which computes a mask of white matter with homotopic properties and reconstructs 3D meshes of inner cortical surfaces. While this method is already robust to partial volume effects and loss of tissue contrast due to maturation up to six months after birth (Leroy et al., 2011), we further increased its performance by using probability maps as an extra feature. Where necessary, the resulting automatic segmentations and meshes were manually corrected to obtain biologically relevant surfaces. Corrections were performed by two of the authors (KJK and NHPC), with one author (KJK) judging all the final segmentations and meshes. For these corrections the result of the automatic segmentation, the cortex mesh and the MR image with maximum tissue contrast were compared. Errors were detected onto the 3D mesh, carefully checked using the MR image and corrected in the segmentation image using the software editing tool. Training sessions with both authors took place to secure correction was done the same way, and repartition of segmentations was done in a random way, preventing systematic bias. Segmentation correction occurred during a relatively short period, which prevents risk of significant drift in segmentation rating. From the final meshes, sulcal objects were automatically detected in the places where folding was sufficiently pronounced (i.e. no sulci was identified at the level of small

dimples) (Fischer et al., 2012).”

After segmentation of the brain images and delimitation of the inner cortical surface using the BrainVISA suite combining the Baby (unreleased) and morphologist pipelines, the sulci were defined as the set of voxels equidistant to the walls of two neighbouring gyri, with the brain hull (defined as the morphological closing of the outer cortical surface) as upper bound (Mangin et al., 1995). Even though a first sulcal extraction had been performed for the previous study, I noticed the need for more sensitivity in this step because of dimples not being captured as sulci and the limited sylvian fissure extraction in brains in an early opercularization stage. Together with my colleague Clara Fischer, we then tuned the sulcal extraction parameters, in order to increase the morphological closing of the brain hull, and to allow very small sulci to be detected by lowering the minimal sulcal size threshold (which was initially set to discard artefacts in the adult brain). The increase of the morphological closure of the brain hull ensured a stricter closing of “open regions”, either for small dimples with very light slopes, or for the insular region, to ensure a consistent capture of the sylvian fissure in brains at different opercularization stages. We then applied an automatic sulcal recognition pipeline developed for the adult (Perrot et al., 2011) to the resulting sulci, and I performed manual corrections to the resulting sulcal labelization on the entire cohort (2 acquisitions × 71 brains), after having received appropriate training. The resulting whole-brain labelization was discussed with Dr. Denis Rivière and Dr. Jean-François Mangin who are experts on sulcal labelization. We were particularly careful on the definition of the central sulcus and sylvian fissure to identify homologous items between individuals, and also tried to ensure a global validity of labelization across the whole brain for further analyses.

After their labelization, the different sulci relevant for my studies were extracted, after registering the brains to the Talairach space, in order to normalize the brains’ size before comparing their sulci, in order to remove the scaling factor due to difference in brain size throughout the cohort. The registration to the Talairach space, which is a referential intended for adults, could be discussed in regard to models developed for the neonate, but the general purpose of the brain normalization was fulfilled through the affine Talairach registration (i.e. adjusting the

brains to a common coordinate system) so I did not pursue the task of refining the registration to infant templates.

8.3 PRE-EXISTING SHAPE CHARACTERIZATION PIPELINE

In order to quantify the shape variability of the different sulcal elements that I have investigated, I was given access to the shape characterization pipeline previously developed by my team and used in adult sulcal studies (Sun et al., 2012; Sun et al., 2016). The pipeline has been re-developed during my PhD in order to make it more flexible and ergonomic. Consequently, the results from Chapter III were generated using the original version of the pipeline, while the results from Chapter IV were obtained from the new version. The pipeline is detailed in each original research article, with adjustments specific to each sub-studies, which will be detailed in the corresponding chapters.

The global framework of the shape characterization pipeline is as follows: sulcal objects are extracted, then right objects are mirror flipped in order to match their left counterparts. Then, the dissimilarity between every pair of sulcal object is computed by capturing the residual distance after rigid pairwise registration. This was originally entirely managed by the Iterative Closest Point algorithm (ICP; Besl & McKay, 1992), but using the ICP distance as a post-registration metric induced strong biases in the case ofimportant size differences between objects, which was an issue in my setting since the 30w PMA sulcal items were significantly smaller than their 40w PMA counterparts. Therefore, I propose to adapt the pipeline to register each pair of sulci using the ICP algorithm, and to replace the ICP distance by the Wasserstein distance, an optimal transport metric which did not carry the same bias. The resulting dissimilarity metrics were stored in a square matrix of size Nitems×Nitems with Nitems the number of sulcal objects considered. For each pair of sulci, 2 registrations were computed (sulcus 1 to sulcus 2 and sulcus 2 to sulcus 1), resulting in two measures. The matrix was symmetrised to keep only the minimum value out of the two distances, therefore capturing the dissimilarity metric of the best registration. Such a matrix captures the global shape variability of the sulcal objects, but is of too high dimension for interpretation. We therefore operated a dimensionality reduction using the Isomap algorithm (Tenenbaum, 1999), which has been

demonstrated to efficiently discriminate sulcal shape (Sun et al., 2009). This algorithm can be tuned by two parameters, k, the number of nearest neighbours to build the neighbourhood graph before applying the dimension reduction through multi-dimensional scaling, and d, the number of dimensions on which to project the data. With no previously recommended selection technique for these parameters applicable to infants' data, I had to devise a methodology with the help of a mathematician colleague and friend of mine from Cambridge University, Marin Ballu, to infer the optimal parameter choice from the data, which I have detailed in Annex 1 of the Chapter III original research article.

Resulting from this processing, we obtained a set of d-dimensional coordinates for each sulcal object. By projecting the objects on each dimension, we obtained d dimensions positioning sulcal objects according to their main shape variability. These raw Isomap results were used for visualisation, as they ensured to capture the most variability and therefore to gain interpretability, but all statistical analyses were led after correcting the Isomap results for age at acquisition: through Pearson correlations, we noticed that the discrepancy of PMA at acquisition had some effect on Isomap positioning. We therefore considered the residuals of Isomap positions after correction for PMA, obtained by solving the linear model:

$$d_{n,i}(subj, hemisphere) = \alpha_{n,i} \times PMA_i(subj) + \beta_{n,i} + r_{n,i}(subj, hemisphere)$$

with $d_{n,i}$ the raw position of the sulci from the i-week acquisition (i= 30 or 40) on the n^{th} dimension of the Isomap, PMA_i the post-menstrual age at the i-week acquisition, $\alpha_{n,i}$ and $\beta_{n,i}$ constants estimated by the model, and $r_{n,i}$ the sulci's residual position on the nth dimension after correction for PMA at the i-week acquisition.

We thereafter defined the Isomap positions corrected for PMA as follows:

$$R_{n,i}(subj, hemisphere) = r_{n,i}(subj, hemisphere) + < d_{n,i} >$$

with $<d_{n,i}>$ the mean position of the sulci from the i-week acquisition (i= 30 or 40) on the n^{th} dimension of the Isomap.

These Isomap positions corrected for PMA were thereafter used to compare group-wise positioning on the different dimensions, through Spearman correlations and Wilcoxon signed-rank tests.

For visualization, the easiest option is to project each sulcal object on its coordinate and to visualize the shape variability encoded on the dimension by simply looking at the sulcal objects. Nevertheless, this option is not suitable for our context because of their number and shape variability. I therefore used the Moving Average (MA) method from Sun et al., 2016, which did not need specific adaptation in the context of my studies. For a given Isomap dimension, ten equidistant coordinates are computed iteratively to span as much of the dimension as possible while setting a minimum requisite number of sulci closest to the extrema coordinates to prevent from too few sparse sulci to shape the extreme MAs. These ten coordinates are the coordinates of the MAs, which are computed by weighting the sulcal objects (represented as point clouds) depending on their distance to the moving average's coordinate, then summing them, then convolving the sum with a 3D Gaussian, and finally thresholding the result. The resulting MAs capture the average shape of sulcal objects surrounding their coordinates, allowing a substantially clearer interpretability of the shape features encoded by each dimension.

The pre-existing preprocessed dataset, neuroimaging software for image analysis, and shape characterization pipeline, offered me a turnkey start to sulcal shape characterization in the developing brain. In return, I had to stay very attentive to the ins and outs of every step of the pipeline, both to ensure my correct understanding of the methods that I did not conceive, and to identify potential shortcomings of the adult-oriented method when applied to the developing brain. My technical contributions to the shape characterization pipeline used in the following chapters were the following: with the assistance of Clara Fischer, the better detection of small and shallow sulci from the segmented images; relying on the advice of my supervisors, the manual correction of automatic sulcal labelization; with the help of Marin Ballu, the switch of residual distance after ICP pairwise registration, and the choice of optimal parameters for the Isomap algorithm based on the data; following another advice from my supervisors, the correction for discrepancy of

age at acquisition before statistical modeling. Additionally, I contributed to the testing of the new implementation of the shape characterization pipeline, which is still undergoing development upgrades (https://github.com/neurospin/point-cloud-pattern-mining).

My additional PhD contributions resided in the application of this shape characterization pipeline and the interpretation of the results, which are presented in the following chapters, through two original research articles and a general discussion about their potential implications in links to the state of the art presented in Chapter I.

9 CHAPTER III: SHAPE VARIABILITY OF THE CENTRAL SULCUS IN THE DEVELOPING BRAIN: A LONGITUDINAL DESCRIPTIVE AND PREDICTIVE STUDY IN PRETERM INFANTS. *(FULL-LENGTH ARTICLE 2)*

9.1 CONTEXTUALIZATION

The central sulcus was my first candidate for sulcal shape investigation, for multiple reasons. First, it is an early developing primary sulcus already relevant to extract at 30w PMA, enabling me to consider dynamic folding pattern through longitudinal analyses at 30 and 40w PMA. Second, its main shape feature's variability has already been assessed in the adult (Sun et al., 2012; Sun et al., 2016), using almost the same methodology as the one I aimed to apply in this study. This allowed me to gain insight from a previous study, and motivated my early works through questions that I have subsequently tried to answer: can we find the main adult variability in the developing brain? Is the asymmetrical shape feature captured in the adult already encoded at birth or does it develop later on? Third, a specific research effort on the maturation of the sensory-motor area in the developing brain was led by my supervisor Dr. Jessica Dubois, and by looking into the central sulcus, which is central to this area, I could both contribute to the team's neuroscientific questions and benefit from state-of-the-art inputs to understand and discuss the implications of my study. Fourth, it is a well-defined sulcus with generally no branching or interruptions (except in some cases which were not represented in the current cohort), therefore, compared to other sulci such as the superior temporalor the lateral occipito-temporal sulci which can show a variety of complex configurations, the chances of mislabelling and comparing anatomically incompatible objects in this sulcus were very low.

The main purpose of my research on the central sulcus was to qualify and quantify its shape variability, and to assess its longitudinal pattern development and interhemispheric asymmetries. This work was iterative in terms of algorithmic refinements, and led to a first poster presentation at the Organisation for Human Brain Mapping (OHBM)

international conference in Rome, Italy, in 2019 (using the minimal ICP distance for the pre-dimension reduction shape variability matrix, which induced bias because of the variability in size between the sulci), then to a poster, a proceedings article and a selected oral presentation at the Perinatal, Preterm and Paediatric Image Analysis (PIPPI) workshop of the Medical Image Computing and Computer Assisted Intervention Society (MICCAI) conference in Shenzhen, China, in 2020 (using the maximal ICP distance to counter the shape discrepancy bias, but increasing the potential imperfect registration bias). I was incidentally awarded the "Best Presentation Award" at this occasion. I implemented the method for Isomap parameter selection and the use of the Wasserstein distance after these first two works, thus reaching the methodological refinement stage of the presented article.

In order to complement the sulcal shape analysis, I was offered to investigate its links to motor outcome thanks to the longitudinal follow-up of the infants from this cohort, operated by Pr. Benders's team, who granted me access to follow up scores of handedness and motor outcome based on the movement Assessment Battery for Children (mABC), 2nd edition, Dutch version (mABC-II-NL). This led me to the conceptualisation of a method to interrogate sulcal pattern relevance in fine motor outcome at 5 years of age.

These works led to an invited oral presentation at the Néobrain 2 conference, in Reims, France, in 2021, and to the following full-length original research article, which published in the NeuroImage journal.

9.2 FULL-LENGTH ARTICLE

9.2.1 Header

9.2.1.1 Title

Shape variability of the central sulcus in the developing brain: a longitudinal descriptive and predictive study in preterm infants.

9.2.1.2 Authors

de Vareilles H[1], Rivière D[1], Sun Z[1], Fischer C[1], Leroy F[1,2], Neumane S[3,4], Stopar N[5], Eijsermans R[5], Ballu M[6], Tataranno ML[5], Benders MJNL[5], Mangin JF[1]*, Dubois J[3,4]*

9.2.1.3 Affiliations

1: Université Paris-Saclay, NeuroSpin-BAOBAB, CEA, Gif-sur-Yvette, France
2: Université Paris-Saclay, NeuroSpin-UNICOG, Inserm, CEA, Gif-sur-Yvette, France
3: Université de Paris, NeuroDiderot, Inserm, Paris, France
4: Université Paris-Saclay, NeuroSpin-UNIACT, CEA, Gif-sur-Yvette, France
5: Utrecht University, University Medical Center Utrecht, Department of Neonatology, Utrecht, the Netherlands
6: Department of Pure Mathematics and Mathematical Statistics, University of Cambridge, Cambridge, United Kingdom
* co-last authors

9.2.1.4 Funding

The project was supported by the Médisite Foundation and the IdEx Université de Paris (ANR-18-IDEX-0001), the European Union's Horizon 2020 Research and Innovation Programme through Grant Agreement No. 785907 \& 945539 (HBP SGA2 \& SGA3), by the FRM through grant DIC20161236445, the ANR through the grants ANR-19-CE45-0022-01 IFOPASUBA , the ANR-14-CE30-0014-02 APEX the ANR-20-CHIA-0027-01 FOLDDICO

This work includes infants participating in the Neobrain study (LSHM-CT-2006-036534), and infants from a study funded by the Wilhelmina Research Fund (10-427).

9.2.1.5 Acknowledgements

The authors thank Y. Leprince, H. Peyre, L. Perus, L. Guillon and W. Shu-Quartier-Dit-Maire for their participation in discussions about this study.

9.2.2 Abstract

Despite growing evidence of links between sulcation and function in the adult brain, the folding dynamics, occurring mostly before normal-term-birth, is vastly unknown. Looking into the development of cortical sulci in infants can give us keys to address fundamental questions: what is the sulcal shape variability in the developing brain? When are the shape features encoded? How are these morphological parameters related to further functional development?

In this study, we aimed to investigate the shape variability of the developing central sulcus, which is the frontier between the primary somatosensory and motor cortices. We studied a cohort of 71 extremely preterm infants scanned twice using MRI – once around 30 weeks post-menstrual age (w PMA) and once at term-equivalent age, around 40w PMA –, in order to quantify the sulcus's shape variability using manifold learning, regardless of age-group or hemisphere. We then used these shape descriptors to evaluate the sulcus's variability at both ages and to assess hemispheric and age-group specificities. This led us to propose a description of ten shape features capturing the variability in the central sulcus of preterm infants. Our results suggested that most of these features (8/10) are encoded as early as 30w PMA. We unprecedentedly observed hemispheric asymmetries at both ages, and the one captured at term-equivalent age seems to correspond with the asymmetry pattern previously reported in adults. We further trained classifiers in order to explore the predictive value of these shape features on manual performance at 5 years of age (handedness and fine motor outcome). The central sulcus's shape alone showed a limited but relevant predictive capacity in both cases. The study of sulcal shape features during early neurodevelopment may

participate to a better comprehension of the complex links between morphological and functional organization of the developing brain.

9.2.3 Introduction

The folding of the brain is highly complex: it shows similar patterns within all humans, yet it is unique for each individual. Even though its general aspect has been studied and described centuries ago (Cunningham, 1892), the inter-individual variability in sulcation has historically been eluded due to its complexity. More recently, this topic has made its appearance in literature, but in the vast majority of cases, this variability was addressed as a problem for group studies and the purpose was to dim it out (Fox et al., 1985). In the last few decades, we have witnessed the emergence of studies focusing on the description of sulcal pattern variability (Ono et al., 1990; Welker, 1990; Mangin et al., 2015). This new trend can be explained by multiple advances, among which the ones in magnetic resonance imaging (MRI), allowing non-invasive imaging of the brain of both pathological and healthy subjects, and the advances in machine learning, which enables the scientific community to address complex questions which used to be out of the reach of human comprehension.

Different observations have suggested that the shape of sulci can be linked to function, both in healthy and pathological cases. The most obvious examples reside in pathologies with strong sulcal malformation, such as lissencephaly (resulting in a flat brain with no sulci) or polymicrogyria (resulting in supernumerary unusually small convolutions). In less obviously sulcation-linked pathologies, a vast quantity of studies have investigated basic shape markers such as sulcal length or depth, easily quantifiable (Cachia et al., 2008). Subtle alterations in folding have also been highlighted based on complex shape variability, embedded in the pattern of folds in some neurological and psychiatric diseases, such as epilepsy or schizophrenia (Plaze et al., 2011; Mellerio et al., 2015). Variations in sulcal patterns linked to function have also been observed in healthy populations. For instance, the sulcal pattern of the anterior cingulate cortex has been reported to predict cognitive control performance across lifespan, and the favorable pattern for cognitive control has been reported to be the opposite in the monolingual and bilingual

populations (Cachia et al., 2017).

These different elements give us keys to address fundamental questions about sulcation: can we differentiate a healthy variability in the folding pattern of the brain versus a pathological one? What are the functional implications of this variability?

To explore these questions, we focused this study on a single sulcus, to characterize its folding pattern during development and to look into its relationships with clinical and functional outcomes. The central sulcus was an excellent candidate for this purpose. First of all, it is a primary fold that appears as early as 20 weeks of GA during development (Chi et al., 1977), with potential long-lasting developmental alterations in cases of early disturbance during gestation or perinatal period (e.g. early brain injury, preterm birth). Moreover, it appears to be very stable across individuals, which makes it easy to identify even in very young preterm infants. Secondly, the central sulcus represents the anatomical border between two highly specialized cortical regions: the primary motor and somatosensory cortices. A detailed functional organization has been described into both areas (i.e. somatotopic motor and sensory maps) in adults (Penfield and Rasmussen, 1950; Germann et al., 2019), such that we can identify precise correspondent subregions of the central sulcus related to specific body parts. Some studies have already shown strong relationships between the central sulcus shape and some functional characteristics in adults (Sun et al., 2012; Sun et al., 2016; Germann et al., 2019; Mangin et al., 2019). For example, the location and shape of the upper knob of the central sulcus, commonly referred to as the "hand-knob", has been related to the functional hand region (Yousry et al., 1997; Sastre-Janer et al., 1998; Sun et al., 2016), with differences observed between left and right-handers (Sun et al., 2012).

It should be noted that during the third trimester of pregnancy, the brain undergoes drastic changes, on both the macroscopic and microscopic scales. Many concurrent events occur, key to the development of the brain structure and function, among which the development of sulcation, with the brain progressively switching from the state of slightly dimpled to a well-folded state (Dubois et al., 2019; Kostović et al., 2019). At full-term birth, the brain of an infant roughly

resembles that of an adult in terms of complexity and advancement of folding, and even though the shape of the sulci keeps on evolving throughout infancy and lifetime, the changes remain subtle compared to the ones observed during late gestation. Therefore, since sulcation is well developed at full-term birth, one can wonder when the general sulcal patterns emerge. In order to look into this question in normal development, it would seem sensible to study sulcal development in healthy fetuses. Yet, longitudinal studies of sulcation on healthy fetuses are currently highly challenging because of the difficulties encountered in acquisition and processing of fetal images at a sufficient resolution to study subtle shape variations in folding. Moreover, it has been reported that birth affects the shape and folding of the brain (Lefèvre et al., 2016), which makes it even more challenging to consider longitudinal studies comparing pre- and post-natal images. Therefore, an interesting alternative is to study the shape of sulci in preterm neonates before full-term equivalent age, even though their sulcation is somehow altered by prematurity (Bouyssi-Kobar et al., 2016; Dubois et al., 2019).

Studying the sulcation at different time-points in infants born preterm allows us to investigate longitudinally the dynamics of early sulcation, and to explore the effects of early brain adversities on these mechanisms. Very preterm infants are at risk of a wide variety of neurodevelopmental disorders, including motor disabilities and cerebral palsy (Korzeniewski et al., 2018; Pascal et al., 2018). The sensorimotor cortex is already well developed and connected at full-term birth, while it is still vastly developing in the case of very preterm births. Extreme prematurity therefore exposes the sensorimotor cortex to adversities when it is most vulnerable, and still growing, which could have parallel effects on function and sulcation (Yamada et al., 2016).

In a previous study, we assessed the relationship between early cortical changes and neurodevelopmental outcome in extremely preterm infants, using basic shape markers (sulcal surface area and mean depth) (Kersbergen et al., 2016). This study reported some links between sulcation and outcome, particularly between the inferior frontal sulcus and receptive language score at 2 years of age. But no links were captured between the central sulcus and the motor outcome, suggesting that basic shape markers might not be sufficient

to capture relevant folding variability for the motor outcome. Regarding the sensorimotor region, early developmental disturbances have long-term consequences on brain morphology. For example, congenital one-hander adult participants showed a significantly flatter central sulcus in the contralateral hemisphere compared to both individuals with acquired upper-limb amputation and control subjects (Sun et al., 2017). This suggested that the mature sulcus's shape is influenced by early sensorimotor activity and by the development of brain connectivity. This led us to the hypothesis that some specific folding variability observed in the central sulcus of preterm infants, resulting from premature birth and strong differences in ex utero perceptions, movements and environment, might be characteristic of deviations in normal brain development impacting their functional outcome. Therefore, quantifying the links between the early central sulcus's shape and the infant's motor outcome at a later age could allow both a better understanding of the early functional implications of shape variability and the identification of early informative biomarkers for earlier diagnosis and accurate follow-up of these at-risk infants.

In this study, our aim was therefore to capture the early central sulcus's shape variability from a longitudinal cohort of extremely preterm infants, and to link it to their fine motor outcome at 5 years of age. In order to do so, we used longitudinally acquired MRI data at two specific ages: one at around 30 weeks of post-menstrual age (w PMA), when the central sulcus is already present but at an early stage of development, and one around term-equivalent age (TEA, at around 40w PMA), when the central sulcus is well developed. We then characterized the shape variability of the central sulcus in this cohort, explored the relationships between its shape at 30w PMA and at 40w PMA, and investigated the shape predictive capacity on the motor development of children evaluated at around 5 years of age.

9.2.4 Materials and methods

9.2.4.1 Subjects and preprocessing of brain images

9.2.4.1.1 Cohort and collection of clinical and outcome data

The study was carried out on a retrospective longitudinal cohort of extremely preterm infants (Kersbergen et al., 2016). Permission from the medical ethics review committee was obtained for this study. A total of 71 subjects (51% males) from the Wilhelmina's Children Hospital, University Medical Center, Utrecht, born between 24 and 28 weeks of gestational age were included.

In agreement with our previous study (Kersbergen et al., 2016), the perinatal clinical factors of interest retained for the analyses were the gestational age at birth (GA), the birth-weight z-score (BWZ) computed according to the Dutch Perinatal registry reference data (Visser et al., 2009), and the presence of an intra-ventricular hemorrhage (IVH, dichotomized between absent or mild (no IVH or IVH of grades 1 - 2 according to the Papile scale) and severe (grades 3 - 4)). We also recorded the presence of broncho-pulmonar dysplasia (BPD).

Around five years of age (age range: 4 years and 6 months – 6 years and 7 months, mean: 5 years and 9 months ± 4 months), the children's handedness was assessed by a trained pediatric physical therapist who asked them first either to write their name or draw a picture, and secondly to pick up a coin placed at the center of the table. If the two tasks were done using the same hand, the hand preference was set to either left or right, otherwise it was reported as mixed. The parents were then asked if this hand preference matched that observed at home while writing or drawing. If the parents disagreed, the hand preference was set to mixed. At the same age, 66 out of the 71 children underwent the Movement Assessment Battery for Children, 2nd edition, Dutch version (MABC-2-NL). The scores were corrected for age at evaluation. The assessment included tests for balance, aiming/catching and manual dexterity. See Sup. Info., Table 1 for the description of these clinical factors and outcome scores.

9.2.4.1.2 MRI data acquisition

The infants were scanned twice soon after birth: once around 30w PMA (28.7 − 32.7w, mean: 30.7 ± 0.9w) and again around term equivalent age (TEA) (40.0 − 42.7w, mean: 41.2 ± 0.6w). For each scan, MR imaging was performed on a 3-Tesla MR system (Achieva, Philips Medical Systems, Best, The Netherlands). The protocol included T2-weighted imaging with a turbo-spin echo sequence in the coronal plane (at early MRI: repetition time (TR) 10.085 ms; echo time (TE) 120 ms; slice thickness 2 mm, in-plane spatial resolution 0.35 × 0.35 mm; at TEA: TR 4847 ms; TE 150 ms; slice thickness 1.2 mm, in-plane spatial resolution 0.35 × 0.35 mm).

9.2.4.1.3 Preprocessing of brain images

The preprocessing of MRI images was performed following the methodology already described in a previous study (Kersbergen et al., 2016): after generating a brain mask, T2-weighted images were segmented into three classes (grey matter, unmyelinated white matter and cerebrospinal fluid) using supervised voxel classification (Moeskops et al., 2015). By adapting the BabySeg and Morphologist anatomical pipelines of the BrainVISA software (BrainVISA suite, https://brainvisa.info), these segmentations allowed a reconstruction of the inner cortical surfaces of both hemispheres, and the extraction of objects depicting the sulci. A summary of the pipeline and the resulting 3D visualizations of the left hemisphere of a subject are presented in Figure 1.

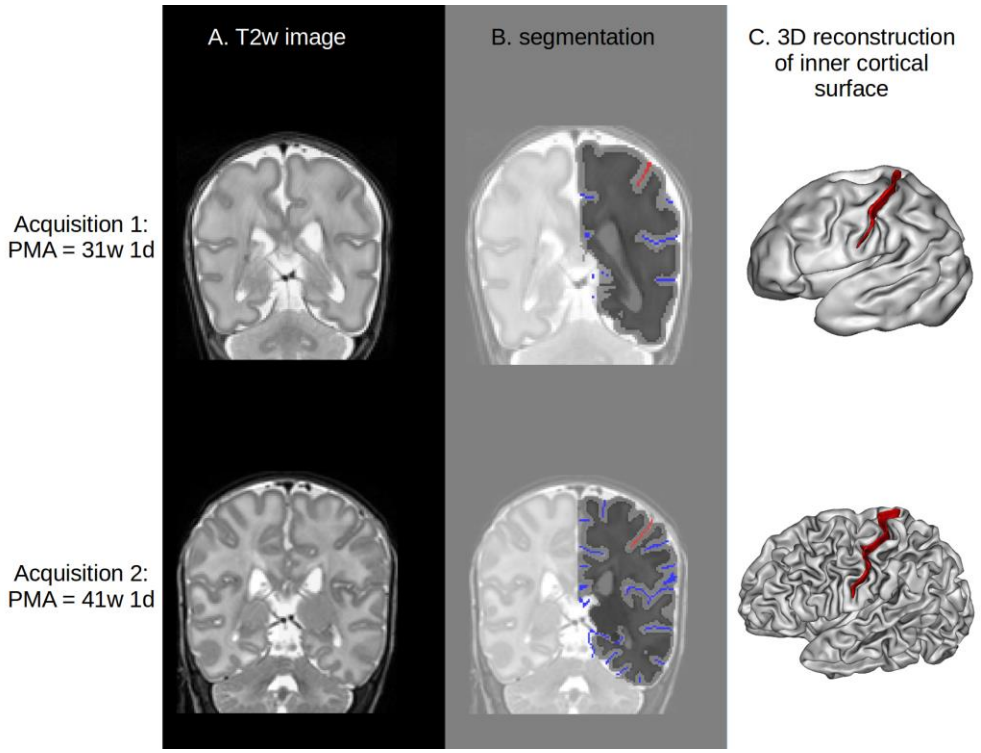

Figure 1. Summary of pipeline for sulcal extraction. A: sample T2-weighted coronal MRI. B: corresponding segmentation of the left hemisphere, showing the boundary between white (dark grey) and grey (light grey) matter. The sulci are represented in blue, except for the central sulcus, in red. C: 3D representation of the reconstructed surface of the white matter. Red ribbon: central sulcus.

9.2.4.2 Characterization of the central sulcus's shape

9.2.4.2.1 Purpose of shape characterization

The purpose of shape characterization on the central sulcus is first to identify the shape features covering the main variability across infants (descriptive approach), and second to quantify the individual specificities relative to these shape features (comparative approach). The method used for shape characterization is inspired by a method already deployed on adults (Sun et al., 2016). A previous study in this cohort (Kersbergen et al., 2016) already addressed the link between sulcation (including the central sulcus) and clinical outcome, but using

simpler metrics to quantify sulcal shape, such as surface area or depth. The added value of the current study is to improve the accuracy of sulcal shape assessment.

9.2.4.2.2 Sulci extraction

First, all the cortical folds were extracted using the Morphologist toolbox of the BrainVISA software in the two serial images of each subject. Each fold was materialized by the skeleton of the volume of its cerebrospinal fluid, namely a set of voxels sampling a surface equidistant to the walls of the two adjacent gyri (Mangin et al., 1995). Each sulcus of the anatomical nomenclature corresponds to a set of the elementary folds extracted during this initial stage. The sulci labels were then identified automatically using a Bayesian pattern recognition strategy (Perrot et al., 2011). Finally, the central sulci labels were manually checked and corrected when necessary by one of the authors (HV). In order to dim out the important variability in cerebral size and shape, particularly between the two sessions of investigation (early at ~30w PMA, vs TEA at ~40w PMA), the obtained central sulci representations were transformed to the Talairach space using an affine transformation. The right sulci were finally mirrored relative to the interhemispheric plane in order to facilitate the comparison with the left ones.

9.2.4.2.3 Sulci co-registration

The previous step led to the extraction of 284 central sulci (71 subjects x 2 hemispheres x 2 acquisitions). The dissimilarity between any two given sulci was then computed in the following way: sulcus A was registered to sulcus B using a rigid transformation, using the Iterative Closest Point algorithm (ICP) (Besl & McKay, 1992), and the residual distance $d_{A \rightarrow B}$ between the two sulci after registration was captured using the Wasserstein distance (Dobrushin, 1970). This choice of distance differed from the original approach (Sun et al., 2016) where the residual distance was captured using directly the distance from the ICP algorithm. In this study, this was a problem due to the fact that we were manipulating sulci of different size, in spite of the affine normalization to the Talairach space. Indeed, the length of the central sulcus relative to the brain size differs between the two time steps.

Hence, using the ICP method, to register sulcus A on sulcus B, each point of sulcus A was matched to a point of sulcus B, but not every point of sulcus B was assured to have a match from sulcus A (as some points from sulcus B have been ignored for the registration). The residual distance minimized by the ICP registration was the sum of distances between the points in sulcus A and their match from sulcus B. This was satisfactory for the registration, but not to capture the dissimilarity between the two sulci, because it would have underestimated the distance when registering a small sulcus to a big one (e.g. if only the lower half of sulcus B exactly matched the point cloud from a shorter sulcus A, the upper half of sulcus B would have been completely ignored and the resulting distance would have been zero, even though sulcus A and B actually differed geometrically). The Wasserstein distance solved this problem by capturing the distance between the whole set of points from both sulci. Thus, we used the ICP algorithm for registration and then captured the resulting Wasserstein distance as the dissimilarity metric using the POT python toolbox (Flamary & Courty, 2017). After aligning sulcus A to sulcus B and capturing $d_{A \to B}$, sulcus B was registered to sulcus A using the same method, resulting in the residual distance $d_{B \to A}$. To mitigate the effect of a potential poor registration, the resulting dissimilarity metric was chosen as $d_{A,B} = \min(d_{A \to B}, d_{B \to A})$.

9.2.4.2.4 Use of distance matrix as shape descriptor for the whole cohort

This allowed us to build a 284x284 dissimilarity matrix, capturing the shape variability of the central sulci over the whole cohort through pairwise distances between sulci. In order to capture the main shape features of the whole cohort, we chose to operate a non-linear dimension reduction algorithm, the Isomap (Tenenbaum, 2000), which is detailed in the next section.

These first steps are summarized on Figure 2.

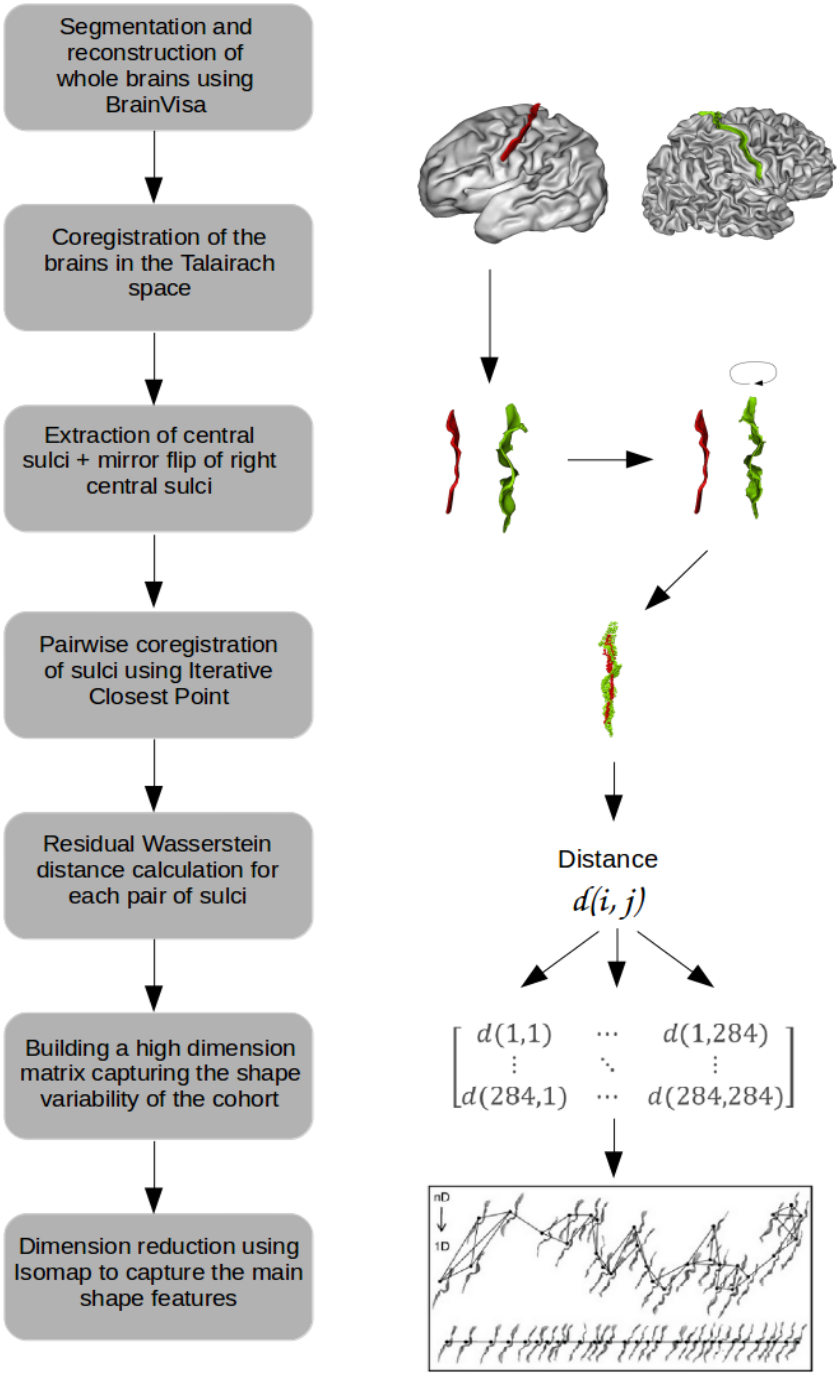

Figure 2. Summary of the preparatory steps for shape characterization.

9.2.4.2.5 Choice of parameters for the Isomap algorithm

The Isomap algorithm builds a matrix of geodesic pairwise distances using an input dissimilarity matrix, by constructing a graph linking each sulcus to its *k* nearest neighbors, with *k* an adjustable parameter. The geodesic distance between any pair of sulci is then defined as the sum of the distances traveled by following the shortest path in the graph. A Multi-Dimensional Scaling algorithm is then applied to this geodesic distance matrix, to project the input data (the sulci) on a lower-dimension space of dimension *d*. Practically, the output consists of the coordinates of each sulcus on *d* axes representative of each dimension.

This algorithm requires two parameters: the number of nearest neighbors *k* used to build the neighborhood graph, and the number of dimensions *d* on which to project the geodesic distance matrix. The methods used to choose the *k* and *d* parameters are detailed in Annex 1, and resulted in the choice of $k = 11$ and $d = 10$.

9.2.4.2.6 Visualization of the shape characteristics (descriptive approach)

To help interpreting the shape characteristics encoded by each selected Isomap dimension computed from the whole cohort, we used moving averages of the embedded sulci. In order to maximize the readability of these moving averages, we separated the sulci at 30w PMA from those at 40w PMA. This was necessary since the 30w PMA sulci are less developed than the 40w ones, and averaging both age-groups together for visualization would thus mix flatter and curvier sulci, making the shape interpretation complex. After separating the groups, the first step was to project the sulci on an axis, based on their Isomap coordinates for each dimension, after a rigid alignment of each sulcus to the most neutral one, namely the sulcus minimizing the average distance to the whole set. This resulted in *d* axes with the sulci ordered by shape characteristics. As this visualization was difficult to interpret, we used moving averages computed for a set of ten regularly spaced coordinates to help us identify the shapes encoded for each dimension. First, the range for the moving averages' coordinates was defined iteratively, in order to cover as wide a span as possible for each dimension while ensuring that at least 10% of the sulci at each time point (n=14) could be closest to the extreme coordinates, in order to

prevent from building moving averages from very few sparse sulci on the borders of the dimensions. After computing the ten resulting moving averages' coordinates, each moving average was constructed by weighting the sulci (represented as point clouds) depending on their distance to the moving average's coordinate, then summing them, then convolving the sum with a 3D Gaussian, and finally thresholding the result. The resulting shape was an average of the sulci's shape in close vicinity to its location. Once the moving averages were generated at both ages, we used the 40w PMA moving averages to interpret the shape characteristics encoded on each dimension. A reading key for shape description and a dimension description resulting from this method is illustrated on Figure 3.

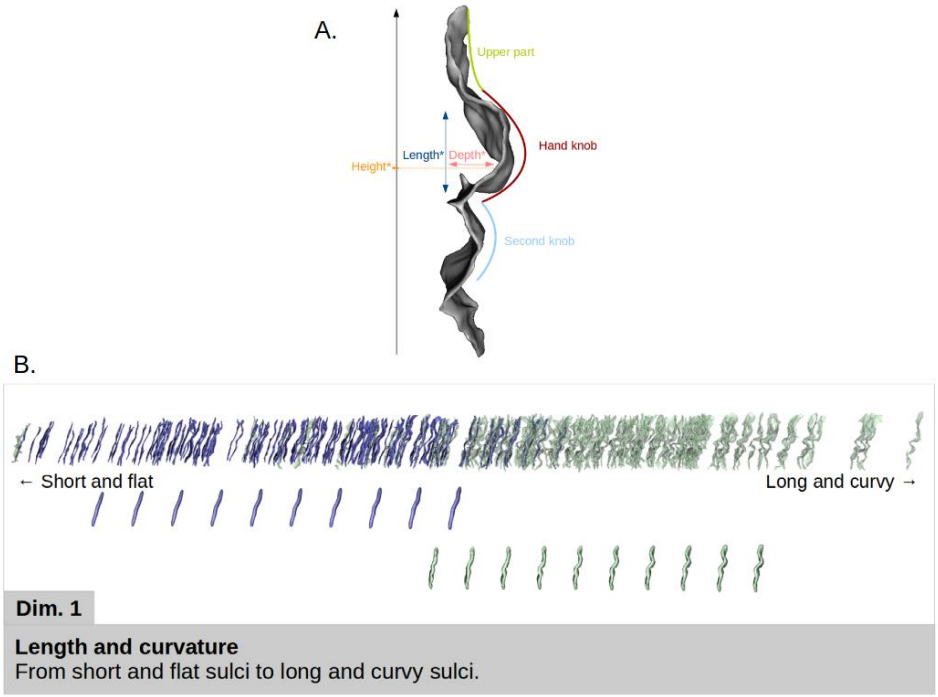

Figure 3. A: Reading key for shape description of the central sulcus with a two-knob configuration. The height of the hand-knob is defined as the vertical distance from the bottom of the sulcus to the deepest region of the hand-knob. B: Representation of the first Isomap dimension. In blue (resp. green): 30w PMA (resp. 40w PMA) sulci and moving averages. Top: sulcal projection. Middle: 30w PMA moving averages. Bottom: 40w PMA moving averages. Simple shape descriptors are given under the sulcal projection, more detailed descriptors are given in the lower box.

9.2.4.3 Analyses of the developmental evolution (comparative approach for the two age-groups)

9.2.4.3.1 Correction for age discrepancy at MRI acquisition

We hypothesized that the PMA variability around each MRI acquisition time-point could bias the shape characteristics. Therefore, we tested if the coordinates for any Isomap dimension correlated with PMA at acquisition, independently for each age-group but together for left and right sulci (see Sup. Info., Table 2). The resultant correlations (going up to 0.30 for dimension 1 at 30w PMA) confirmed the importance of correcting the dimension coordinates for PMA at MRI acquisition in each group, before conducting further analyses.

For this purpose, we decided to perform the quantitative analyses on the Isomap dimensions after correction for PMA in each group: instead of using the raw Isomap coordinates for each dimension as the input for the subsequent analyses, we used their residuals after correction for PMA (that we centered on the age-group mean position on the Isomap in order to restore the information about inter-age-group positioning). The residuals were computed by solving, independently for each age-group, the linear model:

$$d_{n,i}(subj, hemisphere) = \alpha_{n,i} \times PMA_i(subj) + \beta_{n,i} + r_{n,i}(subj, hemisphere)$$

with $d_{n,i}$ the raw position of the sulci from the i-week acquisition (i= 30 or 40) on the n^{th} dimension of the Isomap, PMA_i the post-menstrual age at the i-week acquisition, $\alpha_{n,i}$ and $\beta_{n,i}$ constants estimated by the model, and $r_{n,i}$ the sulci's residual position on the n^{th} dimension after correction for PMA at the i-week acquisition.

Therefore, the shape characteristics considered in the following analyses, and which we refer to as Isomap positions corrected for PMA, were defined as:

$$R_{n,i}(subj, hemisphere) = r_{n,i}(subj, hemisphere) + \langle d_{n,i} \rangle$$

with <dn,i> the mean position of the sulci from the I-week acquisition (i= 30 or 40) on the n^{th} dimension of the Isomap.

9.2.4.3.2 Comparison of the subjects' positioning on the different dimensions

In the following, individual sulci from the two age-groups (i.e. 30w and 40w acquisitions) were considered separately, as well as left (L) and right (R) sulci. For each Isomap dimension, we investigated the relative positioning of the subgroups using two tests: a Wilcoxon signed-rank test to investigate whether the two age- or hemisphere-groups differed in positioning on a specific dimension (suggesting a difference in the shape of the sulci throughout development or between hemispheres), and a Spearman correlation to assess whether the two age- or hemisphere-groups showed correlated shape features (suggesting early and stable shape patterns throughout development or between the hemispheres). We conducted these tests between ages for each hemisphere (L30 vs L40, R30 vs R40), and between hemispheres at each age (L30 vs R30, L40 vs R40). Applying a correction for multiple comparisons with the Bonferroni approach would have led to a statistical threshold at 0.00125 for an alpha level at 0.05 because of the 40 tests performed (4 age-and-hemisphere-specific tests x 10 dimensions tested). However, as the Bonferroni method may be considered as too restrictive, we focused on results with p-values under the threshold computed for each age-and-hemisphere-specific test, thus only compensating for the number of dimensions, resulting in a statistical threshold at 0.005. Only the results with p-values below or in the same range as this corrected threshold are described in the Results section. The whole test results are available in Sup. Info., Table 3 for Wilcoxon signed rank tests and Table 4 for Spearman correlations.

9.2.4.4 Handedness and fine motor outcome predictability

9.2.4.4.1 Purpose of prediction of handedness and fine motor outcome

We aimed to predict the children's handedness and fine motor outcome (manual dexterity score from the mABC scale) assessed at 5 years of age, based on the early shape of the central sulcus, with a cross-sectional approach. We therefore performed two different analyses, aiming to classify either left versus right handers, or children with poor

versus good fine motor outcome, using three sets of features: 1) a selection of early clinical factors (without sulcal considerations), 2) the shape features of the central sulci (without clinical considerations), encoded by the Isomap positions corrected for PMA, and 3) the combination of both. The purpose of using these three sets of features was to be able to compare the predictive capacity of these different features, and more specifically to assess whether sulcal shape is a better predictor for motor development than early clinical factors, and whether the combination of both outperforms the two previous classifiers, suggesting a complementary influence of early morphological and clinical features on the long-term motor development.

9.2.4.4.2 Dichotomization of the motor classes

The cohort was dichotomized for each motor characteristic: right versus left handedness, and poor versus good fine motor outcome (manual dexterity).

Children born preterm display a significantly higher occurrence of non-right handedness than full-term children (odds ratio 2.12) according to a meta-analysis (Domellöf et al., 2011). Studying handedness in preterm children may be a potentially important index reflecting hemispheric organization and sensorimotor functions ensuing neurodevelopmental disturbances. Thus, we hypothesised that among the left-handed children in our cohort, some would be "natural" left-handers while the others may express a non-right-hand preference following a disruption in the lateralized early brain organization associated with premature birth. Since a previous study reported links between handedness and the shape of the central sulcus on healthy adults (Sun et al., 2012), we decided to focus on typical handedness by maximizing the proportion of "natural" left-handers (n=7 left-handers with at least one left-handed parent (Bryden et al., 1997), subsequently referred to as "left-handers") to compare with right-handed (n=50) children. We thus excluded children with missing data (n=1), ambidextrous children (n=2) and left-handers for whom both parents were right-handers (n=11). Compared to the whole cohort, the first prediction study thus focused on infants supposed to be representative of the normal population in terms of handedness.

In terms of fine motor assessment provided by the mABC score, we focused on the manual dexterity subscore, which assessed three tasks: posting coins, threading beads, and drawing a trail. We chose to focus on this score because links between functional activation of the hand and the shape of the central sulcus (more specifically the height of the hand-knob) have already been reported in adults (Sun et al., 2016), and we therefore suspected that, compared to the other two mABC subtests – aiming/catching and balance – it was the subtest with the most direct link to the central sulcus's shape.

We dichotomized the children group according to their poor and good fine motor outcome, removing children with borderline results from the classification. For the mABC total score, a score inferior or equal to the 5th percentile indicates definite motor problems; between the 6th and 15th percentiles indicates borderline performance; and strictly above the 15th percentile indicates normal motor development (van Heerwaarde et al., 2020). Since for the manual dexterity subscore no percentile cut-offs have been assessed, we used the same cut-offs in our study population, with the corresponding standard scores for each percentile range: children whose standard score ranked between 1 and 5 were assigned to the poor fine motor outcome group (n=15), children who ranked strictly above 7 were assigned to the good fine motor outcome group (n=35), and children ranking 6 or 7 (n=16) were considered as borderline and were not included in the classification analyses. Compared to the whole cohort, the second prediction study thus focused on a mixed group of infants with either healthy or pathological motor development.

9.2.4.4.3 Subgroup differentiation and feature choice

In terms of clinical factors, the retained variables were the following: gestational age at birth, the birth-weight z-score, the presence of a severe intra-ventricular hemorrhage, and the presence of broncho-pulmonar dysplasia. All the continuous variables were normalized, and the categorical variables were binary, encoded as 0 or 1.

In terms of shape features of the central sulcus, the features retained were the Isomap positions corrected for PMA at scan, on the 10 relevant Isomap dimensions. We once again considered separately the

L30, R30, L40 and R40 subgroups, because of the high variability in sulcal shapes at both ages, and because we expected that inter-hemispheric asymmetries in shape might play a role on handedness and fine motor outcome.

The classifiers were trained once per age and hemisphere subgroup, except for the classifiers using the clinical factors as only features, since the clinical factors considered are neither age nor hemisphere dependent.

9.2.4.4.4 Cross-validated training of subgroup-specific classifiers

We used a linear Support Vector Classifier (SVC) to assess the predictive capacity of the shape and clinical features on the handedness and fine motor outcome. We parametrized the SVC to take into account the imbalance between classes (either 7 vs 50 or 15 vs 35) by weighting the regularization parameter by the inverse of class frequency in the input data. Due to the small size of the groups (either 57 or 50 sulci for handedness or fine motor outcome respectively), we took two precautions to limit the chances of overfitting our model: we used the predetermined regularization value (C=1), and we used a Stratified Shuffled Cross-Validation (number of folds: 5, number of repeats: 10) to evaluate the performance of the algorithm. We then evaluated the balanced accuracy (the average of correctly predicted samples for both classes) and Area Under the Receiving Operator Curve (ROC AUC). For the best classifier using only sulcal shape for prediction, we plotted the ROC and Precision-Recall (PR) curves, next to the ROC and PR curves obtained for the clinical factors alone for comparison. In order to assess the predictive value of these classifiers, we added to the ROC curves the mean ROC and 95% confidence interval obtained after performing 1000 chance models on the data.

9.2.4.4.5 Observation of most-weighted features

For the classifiers using only sulcal shape which showed the best performance, we were interested in the most relevant shape features in the training of the classifiers. Therefore, during the cross-validation, we stored the coefficients attributed to each Isomap dimension. After the cross-validation, we looked into the consistency of coefficient

attribution depending on the training/testing set using a box plot picturing the coefficient attributed to each Isomap dimension for every iteration of the cross-validation. More importantly, we assessed which shape features were the most discriminative for each outcome. The dimensions corresponding to these specific shape features were described in more detail.

9.2.5 Results

9.2.5.1 Characterization of the central sulcus' shape

9.2.5.1.1 Visual Isomap results

For brevity concerns, we only present, in the following sections, the visual representations of the dimensions relevant in the performed analyses. The detailed descriptions for all 10 dimensions (not corrected for age, to improve interpretation) are shown in Annex 2.

9.2.5.1.2 Age dependency of Isomap positioning

The Pearson correlation coefficients between age at MRI acquisition and raw Isomap position (not corrected for age) are reported for the 30w PMA and 40w PMA sulci separately in Sup. Info., Table 2. The highest correlation observed was r=0.30 for the first Isomap dimension at 30w PMA, the dimension coding for length and global curvature of the sulci. Along with the other coefficients observed, the correlations suggested that the Isomap position of sulci is somewhat affected by PMA, which justified our decision to correct for it in subsequent analyses.

9.2.5.1.3 Hemispheric comparisons for each age-group

The Wilcoxon signed-rank test results obtained by comparing the PMA-corrected positioning of left and right sulci on each Isomap dimension, for each 30w and 40w PMA group, highlighted in Sup. Info., Table 3.A. two dimensions (one per age-group) with significant hemispheric asymmetry (Sup. Info., Table 3.A, Figure 4). At 30w PMA, dimension 3 (coding for the curvature of the hand-knob at fixed height) suggested that left central sulci were roughly flatter than the right ones. At 40w PMA, dimension 8 (coding for the switch from a single to a double-knob configuration) also showed some asymmetry, with

more left central sulci in the double knob configuration and more right central sulci in the single knob configuration.

In terms of Spearman correlations (Sup. Info., Table 4.A), four dimensions showed a significant correlation between the left and right central sulci: dimension 1 at both ages, dimension 5 and 2 at 30w PMA, and dimension 3 at 40w PMA. These results suggest that at 30w PMA, left and right central sulci show a coherent encoding of length, curvature (dimension 1), wrapping around (dimension 5) and height (dimension 2) of the hand-knob, and depth of the second knob (dimension 2). At 40w PMA, left and right central sulci seem to show consistent sulcal length (dimension 1) and depth of the hand-knob at low fixed height (dimension 3).

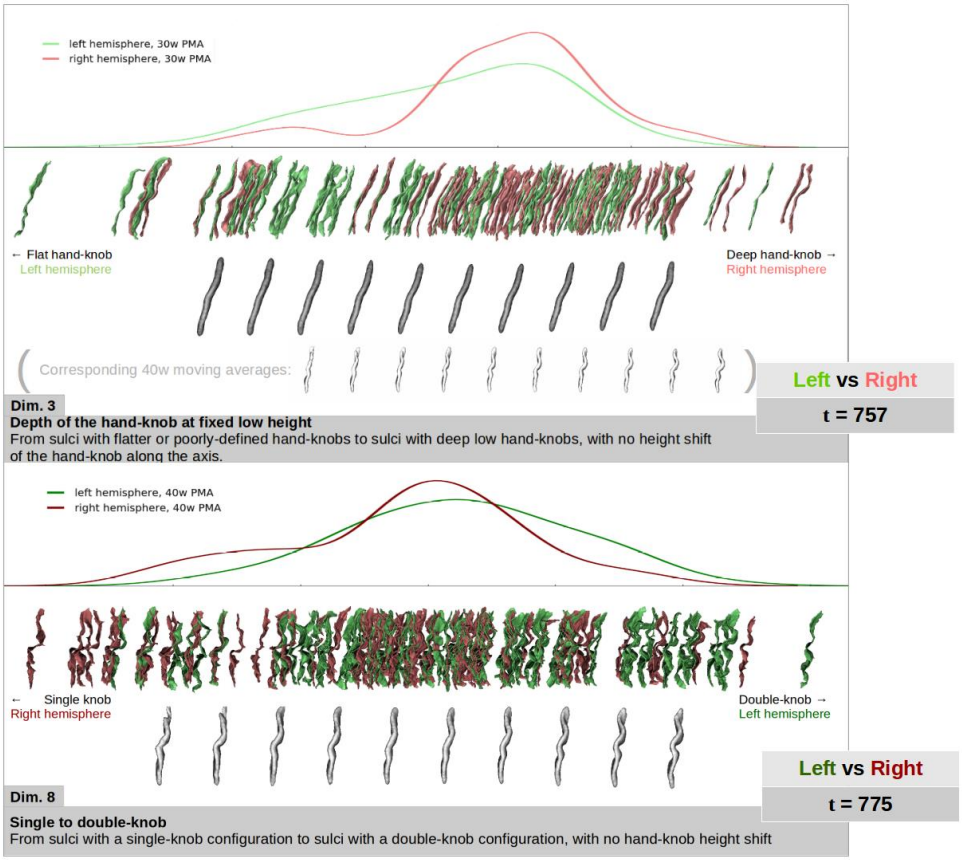

Figure 4. Representation of left (green) versus right (red) central sulci distribution on the two dimensions showing statistically significant hemispheric asymmetries (Dim. 3 and 8), with t the Wilcoxon signed-rank test statistic. Upper rows: density plot of sulcal distribution along the dimension. Lower rows: sulcal projection and corresponding moving averages (in grey). On the 30w PMA representation of Dim. 3, the 40w moving averages (in white) are shown for shape interpretation purposes.

9.2.5.1.4 Age-group comparisons of the hemisphere-specific shape characteristics

Wilcoxon signed-rank tests performed to compare PMA central sulci characteristics (Sup. Info., Table 3.B) identified several dimensions with different positions at 30 versus 40w (Sup. Info., Table 3.B). Two dimensions (1 and 5) were highlighted on both hemispheres, suggesting that sulci on both hemispheres are roughly shorter, flatter, and show a

more wrapped-around hand-knob at 30w PMA compared to 40w PMA. Two other dimensions were relevant only for one hemisphere: dimension 4 for the left hemisphere, with shallower and lower hand-knob at 40w than at 30w, and dimension 2 for the right hemisphere, with a higher hand-knob and a deeper second knob at 40w PMA compared to 30w PMA.

Out of the 10 dimensions of interest, we observed relevant trends in Spearman correlation between the PMA-corrected Isomap positioning at 30w and 40w PMA on 8 dimensions (Sup. Info., Table 4.B). The three dimensions showing the strongest correlations between both ages are presented in Figure 5. Dimension 4 was observed on both hemispheres and encoded a variation of height and depth of the hand-knob, as well as the presence and depth of the second knob (i.e. from double-knobbed sulci with deeper and higher hand-knobs, to sulci with a single, lower, and shallower hand-knob). On the left hemisphere, dimension 2 showed correlations between 30w and 40w PMA in the height of the hand-knob and the depth of the second knob. On the right hemisphere, the highest correlation was observed on dimension 8, correlating the sulci depending on their single-knob or double-knob configurations, with no height shift of the hand-knob. This suggested that between 30 and 40w PMA, most of the early morphological characteristics (8 dimensions over 10) tend to evolve into a more complex but consistent encoding (i.e. a sulcus with a single, low and shallow hand-knob at 30w will most often show the same characteristics at 40w, rather than a double-knob configuration).

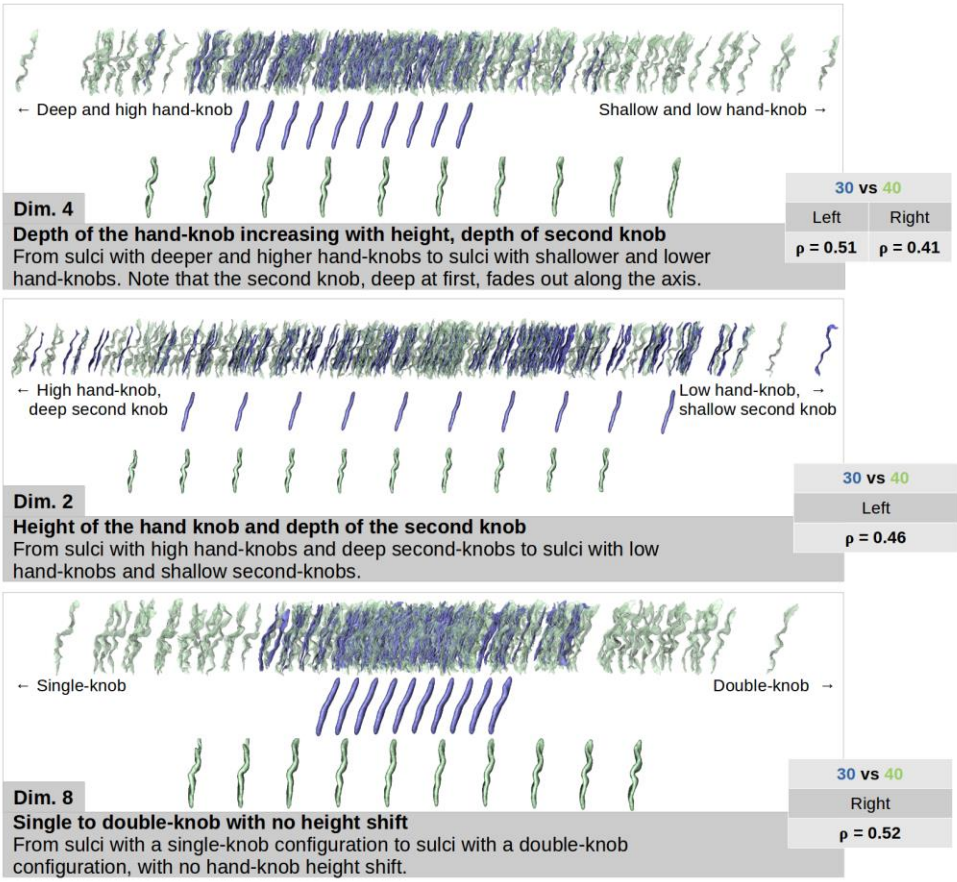

Figure 5. Representation of the three dimensions showing the strongest correlations between 30w (blue) and 40w (green) PMA central sulci, with ρ the Spearman correlation coefficient. For each dimension, the sulcal projections were represented in the upper rows, and the age-specific moving averages on the lower rows.

9.2.5.2 Classification of handedness and fine motor score based on sulcal shape features

9.2.5.2.1 Discrimination by shape for left- vs right-handers: classifiers' performance

The support vector classifiers were trained to differentiate right-handers (n=50) from left-handers (n=7). The cross-validated scores of the classifiers considering either clinical factors, age- or hemisphere-specific shape features (corrected for PMA) or both, are shown in Table 1.

Table 1. Cross-validated scores for handedness classification. Scores obtained using 1) clinical factors; 2) sulcal shape features (positions corrected for PMA on the 10 dimensions), for each age and hemisphere subgroup; and 3) combination of both (clinical factors and sulcal shape features), for the handedness discrimination at 5 years of age. The bold values are the ones equal or superior to the baseline, i. e. the values obtained for the clinical factors alone.

	Subgroup	Balanced accuracy	ROC AUC
1) Clinical factors (baseline)		0.55	0.59
2) Sulcal shape	L30	**0.57**	**0.61**
	R30	0.38	0.35
	L40	0.44	0.49
	R40	0.43	0.33
3) Combination of clinical factors and sulcal shape	L30	0.53	**0.65**
	R30	**0.64**	**0.65**
	L40	0.48	0.57
	R40	0.43	0.37

ROC AUC: Area Under the Receiving Operator Curve. L: left hemisphere; R: right hemisphere. 30: 30w PMA; 40: 40w PMA.

The best classifier (highest balanced accuracy and ROC AUC) was obtained using the combination of clinical factors and sulcal shape features at 30w PMA on the right hemisphere. Yet, the performances obtained with these shape features alone were quite low. In contrast, the best classifier using only shape features was the one obtained at 30w PMA on the left hemisphere, and it exceeded the performance of the classifier using only clinical factors, while adding the clinical factors to these shape features also provided a quite relevant classifier. That is why we further focused on the classifier obtained with shape features of left sulci at 30w PMA alone. The ROC and PR curves of this classifier (and correspondent curves obtained for clinical factors alone as a comparison) are shown in Figure 6.

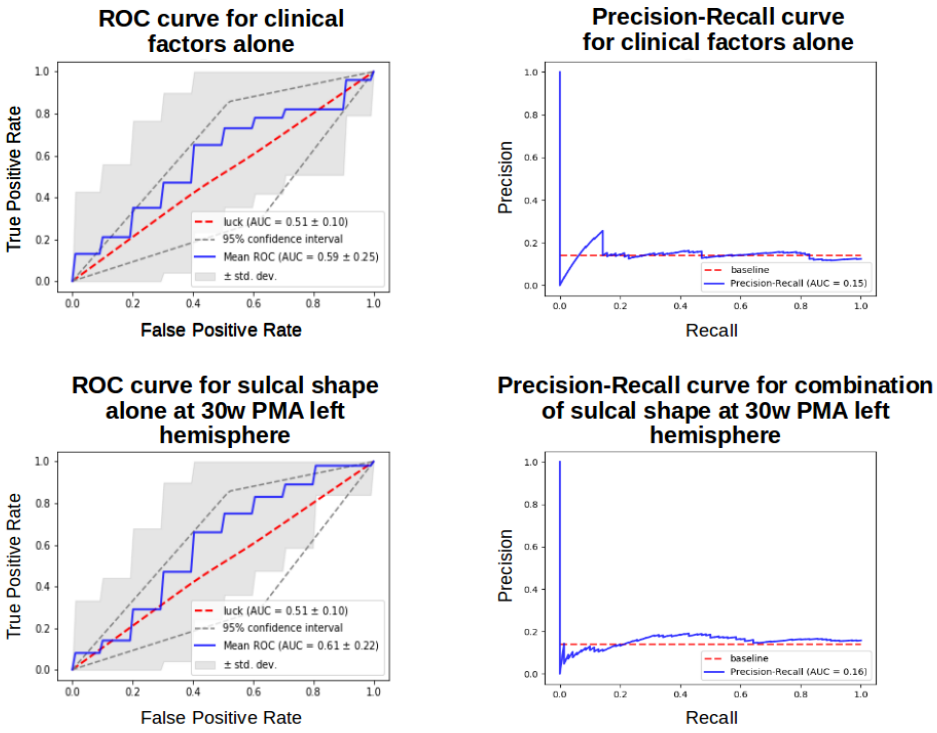

Figure 6. ROC and PR curves obtained for clinical factors alone and sulcal shape factors alone at 30w PMA on the left hemisphere. Target: handedness

For this classifier, we further wondered which shape features were considered relevant in differentiating left-handers and right-handers. Using the different folds of the repeated stratified cross-correlation, we

aggregated the coefficients attributed to each Isomap dimension and generated the box plot presented in Figure 7.

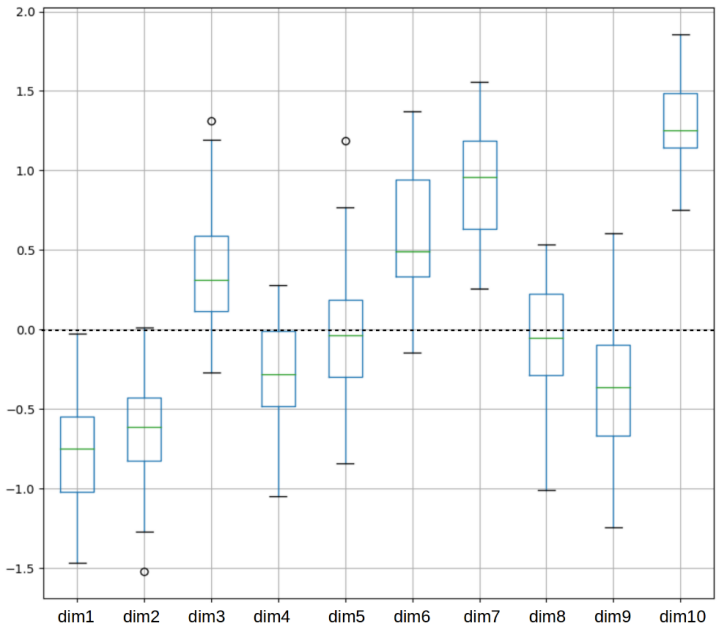

Figure 7. Box plot of the coefficients attributed to each Isomap dimension during the cross validation for the handedness classification with sulcal shape factors alone at 30w PMA on the left hemisphere. Coefficients for the dimensions were obtained for each iteration of a 5-fold 10-times repeated stratified cross-validation training of the SVC for handedness. Dimension 10 weighted generally more than the other dimensions throughout this cross-validation.

Most Isomap dimensions were reasonably consistent in weight through the cross-validation. The 10th dimension was clearly and almost systematically the most informative. The visual interpretation of this dimension (Figure 8) suggested that the most discriminative traits for handedness were the length of the hand-knob and the orientation of its upper part. Compared to right-handers, the left-handers tended to have a left central sulcus at 30w PMA with a longer hand-knob, with its upper part bending backwards.

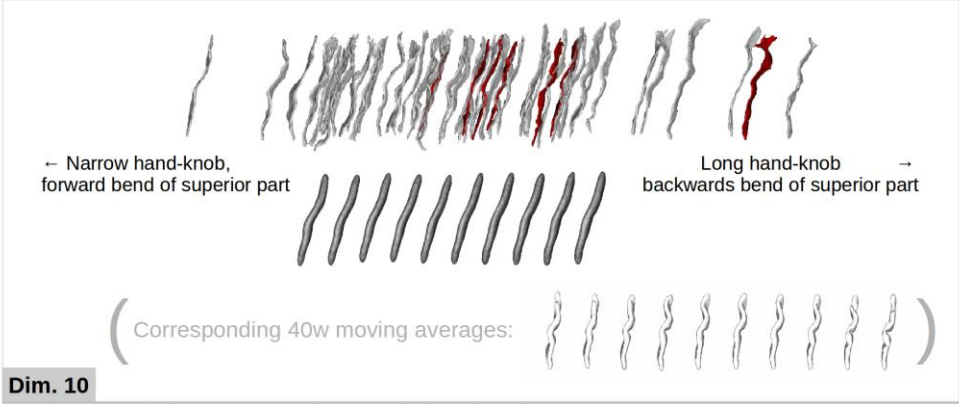

Figure 8. Representation of the dimension weighting the most for handedness classification using sulcal features at 30w PMA in the left hemisphere. The sulcal projections of the subjects used in the classification were represented (right handers in grey and left handers in red), as well as the age-specific moving averages (in dark grey). The 40w PMA moving averages (in white) are also shown for shape interpretation purposes.

9.2.5.2.2 Discrimination by shape for the fine motor outcome: classifiers' performances

The support vector classifiers were trained to differentiate subjects with poor fine motor outcome (n=15) from subjects with good motor outcome (n=35), again considering either clinical factors, age-and-hemisphere specific shape features (corrected for PMA) or both. The cross-validated scores of the classifiers are shown in Table 2.

Table 2. Cross-validated scores for fine motor outcome classification.
Scores obtained using 1) clinical factors; 2) sulcal shape features (positions corrected for PMA on the 10 dimensions), for each age and hemisphere subgroup; and 3) combination of both (clinical factors and sulcal shape features), for the fine motor outcome discrimination at 5 years of age. The bold values are the ones equal or superior to the baseline, i. e. the values obtained for the clinical factors alone.

	Subgroup	Balanced accuracy	ROC AUC
1) Clinical factors (baseline)		0.58	0.59
2) Sulcal shape alone	L30	**0.62**	**0.66**
	R30	0.45	0.44
	L40	0.40	0.38
	R40	**0.62**	**0.66**
3) Combination of clinical factors and sulcal shape	L30	**0.59**	**0.61**
	R30	0.48	0.50
	L40	0.46	0.41
	R40	0.57	**0.64**

ROC AUC: Area Under the Receiving Operator Curve. L: left hemisphere; R: right hemisphere. 30: 30w PMA; 40: 40w PMA.

Two classifiers scored a tie for balanced accuracy and ROC AUC, using the sulcal shape features alone: the left hemisphere at 30w PMA and the right hemisphere at 40w PMA. We chose to focus on the one with the best recall (proportion of correctly identified poor fine motor outcome, the most interesting clinical issue), which was the one for the right hemisphere at 40w PMA (recall = 0.61 against recall = 0.53 for 30w PMA left hemisphere). For this classifier, the ROC and PR curves are shown in Figure 9. The results for the classifier obtained at 30w PMA on the left hemisphere using only the sulcal shape features are presented in Annex 3.

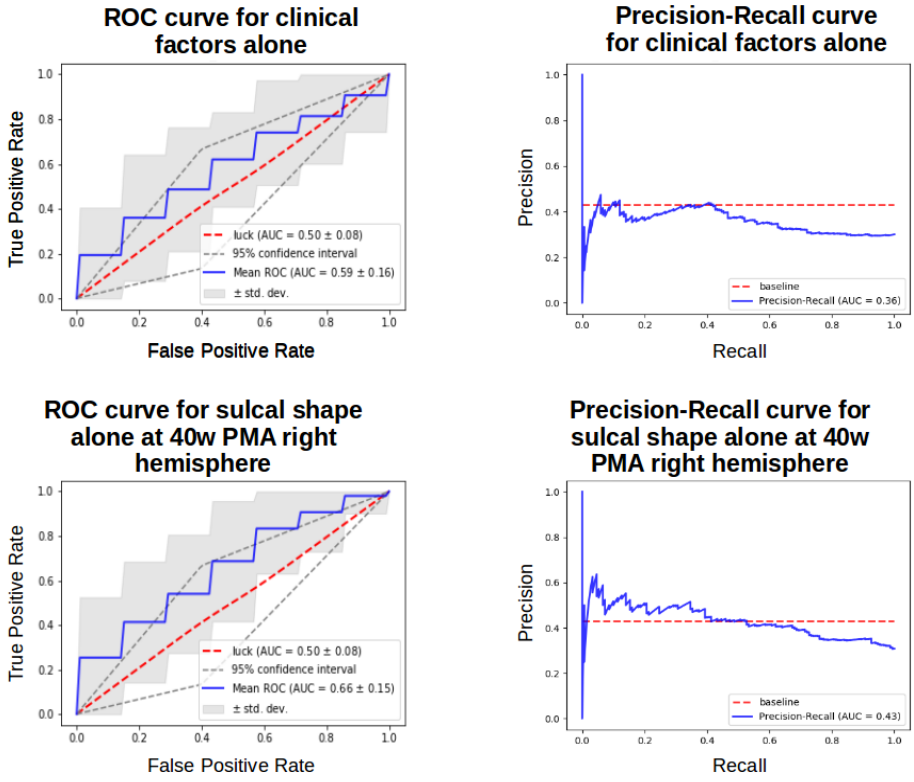

Figure 9. ROC and PR curves obtained for clinical factors alone and sulcal shape factors alone at 40w PMA on the right hemisphere. Target: fine motor outcome.

This latter resulting classifier performed better than a random classifier, and again we addressed the question of the relevance of the different shape features in the classification.

Using the different folds of the repeated stratified cross-correlation, we aggregated the coefficients attributed to each feature and generated the box plot presented in Figure 10.

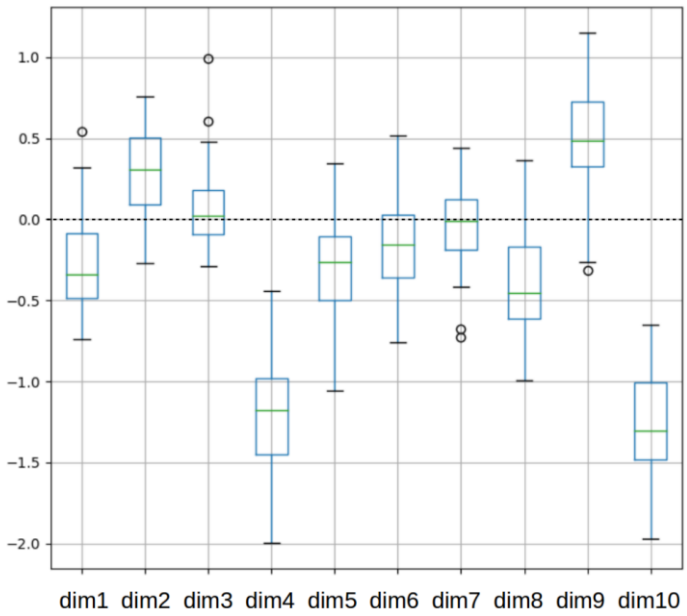

Figure 10. Box plot of the coefficients attributed to each Isomap dimension during the cross validation for the fine motor outcome classification with sulcal shape factors alone at 40w PMA on the right hemisphere. Coefficients for the dimensions were obtained for each iteration of a 5-fold 10-times repeated stratified cross-validation training of the SVC for fine motor outcome. Dimensions 4 and 10 weighted generally more than the other dimensions throughout this cross-validation.

Once again, the dimensions were rather consistent in weight through the cross-validation. Dimension 10 was the most relevant dimension, but dimension 4 seemed to have a comparable role in the classification, so we considered both dimensions for the shape description (Figure 11). The visual interpretation of these dimensions suggested that children presenting a poor fine motor outcome at 5 years of age tend to have a right central sulci at 40w PMA with a shorter but higher and deeper hand-knob, with a superior sulcal part leaning frontally.

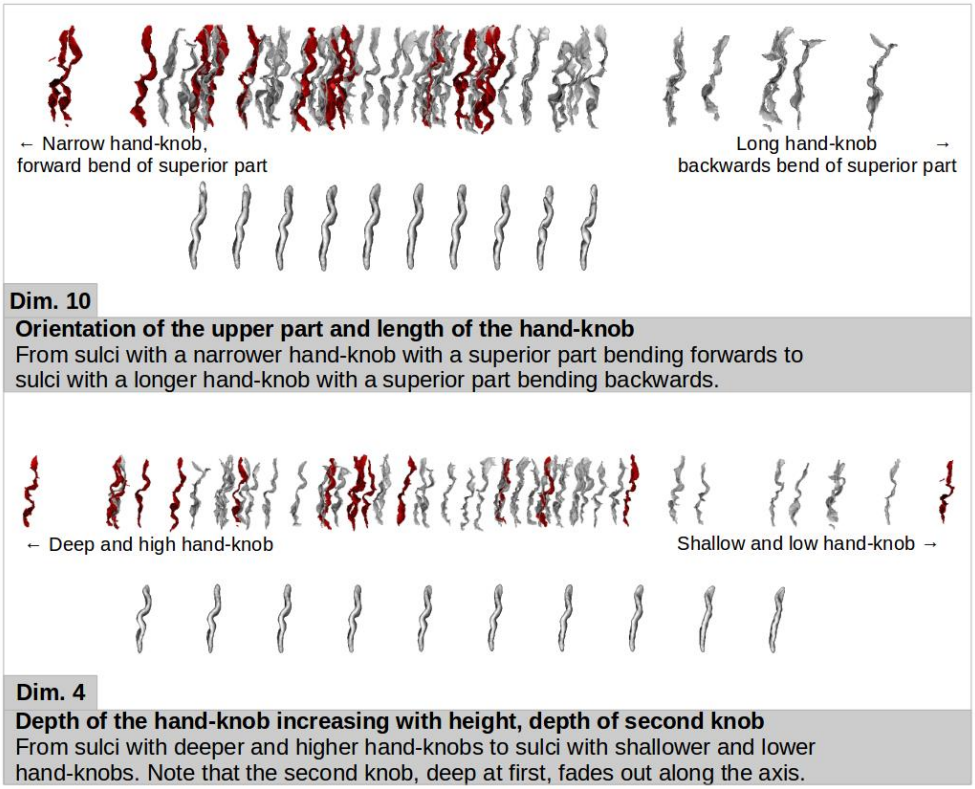

Figure 11. Representation of the two dimensions weighting the most for fine motor outcome in the classification at 40w PMA in the right hemisphere. For each dimension, the sulcal projections of the subjects used in the classification were represented (good outcome in grey, poor outcome in red), as well as the age-specific moving averages (lower row, in light grey).

9.2.6 Discussion

This study 1) longitudinally described the shape characteristics and variability of the central sulcus in extremely preterm infants at 30 and 40w PMA; 2) brought to light hemispheric asymmetries at each age; 3) showed a close developmental relationship between the sulcal shape at both postnatal ages; and 4) unraveled links between the perinatal shape of the central sulcus and the later handedness and fine motor outcome in this cohort of children born extremely preterm.

9.2.6.1 How to study cortical folding

Different approaches have been developed and used to study the *complexity and implications of cortical folding*, but few have described its variability, and even fewer specifically in the developing brain. Sulcal information has been collected through various means and for multiple purposes. The simpler sulcal information includes basic geometric measures, such as length, surface area or mean depth after sulcal extraction, as proxies for shape (Kersbergen et al., 2016). More sophisticated ones include the use of mean depth profiles (Gajawelli et al., 2021), the calculation of local or global gyrification indices (Cachia et al., 2008) or focus on sulcal pits (Régis et al., 2005; Im & Grant, 2019). Such studies addressed general brain development issues, such as normal development in the fetus (Vasung et al., 2019) or in the preterm newborn (Moeskops et al., 2015; Orasanu et al., 2016; Garcia et al., 2018), and more specific adversarial development questions, such as early neurodevelopmental events linked to pathological outcomes (Mellerio et al., 2015). Compared with previous studies, the approach developed in this article additionally describes and quantifies the inter-individual sulcal variability.

In relation to this issue of inter-subject variability, the historical method relied on visual examination and description of sulcal morphology (Ono et al., 1990) but implied long, subjective and potentially biased examination processes, and resulted in small sample sizes. Newer methods have been developed to automate both sulcal extraction and shape characterization. They can either use a clustering approach or a continuous approach. Clustering methods try to identify a finite number of shape patterns to characterize a given sulcus. This approach seems appropriate for structures presenting great variability, such as the sulci from the anterior cingulate cortex (Del Maschio et al., 2019), or the gyri from different regions using multi-view curvature features (Duan et al., 2019). These clustering approaches are hardly suited for the study of the central sulcus because of the simplicity of its configuration: generally uninterrupted and without branches, except for a few individual exceptions (Mangin et al., 2019). Moreover, the clustering methodology is not suited for a longitudinal comparison of shape. Therefore, we opted for a continuous approach in our study. Some continuous approaches of sulcal shape description have relied

on morphologic landmarks, such as the superior temporal asymmetrical pit in the superior temporal sulcus (Leroy et al., 2015), or the occipital bending of the Sylvian fissure (Hou et al., 2019). Both of these studies used these landmarks to quantify the difference in sulcation between humans and chimpanzees in order to highlight human specificities, and therefore did not focus on intra-species variability. Another continuous approach was the one previously used to study the central sulcal shape in adults (Sun et al., 2012; Sun et al., 2016). We chose to adapt this method to the developmental context of our study, in order to obtain a detailed characterization of the central sulcus's shape, requiring neither prior assumptions about distinct clusters nor the definition of anatomical landmarks, as well as allowing multiple-age comparison.

The method retained, using pairwise coregistration of sulci to capture the shape dissimilarity within the cohort, allowed us to explore multiple shape characteristics of the central sulcus and therefore to capture its variability with unprecedented precision, leading to the observation of new specificities of this sulcus. In particular, the previous study assessing sulcal specificities on the same cohort using basic shape features reported a single significant hemispheric asymmetry in the central sulcus at 30w PMA – involving depth of the central sulcus but not surface area – and none at 40w PMA (Kersbergen et al., 2016). Our method, capturing multiple shape features, allowed us to reveal hemispheric asymmetries both at 30 and 40w PMA.

9.2.6.2 How does preterm birth affect cortical folding around the central sulcus

In order to capture the early folding dynamics of the developing brain, it would be ideal to study longitudinal data from fetal period to full-term birth, but using a mix of fetal and post-natal data is slippery because birth *per se* seems to affect the shape and folding of the brain (Lefèvre et al., 2016). Therefore, we chose to longitudinally study sulcal features in extremely preterm infants in order to investigate early brain development. Yet, prematurity has been reported to provoke alterations in sulcation: compared to term-born neonates, very preterm infants at term-equivalent age showed decreased sulcation index and folding power specifically in primary sulci (Shimony et al., 2016; Dubois

et al., 2019), confirming that a very preterm population may not reflect perfectly typical folding of the central sulcus.

In this context, different studies have focused on the sulcation variability in the neonate. In particular, recent studies described the major sulcal or gyral patterns of cortical folding in newborns – including the central sulcus – using clustering approaches based either on deep sulcal pits (Meng et al., 2018) or on multi-view curvature features (Duan et al., 2019). Yet, to the best of our knowledge, the present study is the first to describe qualitatively and quantitatively the shape variability of the central sulcus in the preterm neonate, and more importantly to address the question of longitudinal shape evolution between early folding and the resulting sulcation pattern at term-equivalent-age.

In terms of qualitative morphological description of the central sulci, we presented a visual representation of the shape variability through 10 dimensions, and we concurrently suggested corresponding shape descriptions (see Annex 2). The scope of this work has yet to be explored in future studies: to what extent does the shape variability reported in this study describe globally the neonate population (including fetal and term-born populations)? What fraction of this variability is specifically associated either to prematurity or to related early pathological events? Since this first approach was exploratory, we decided to analyze the whole cohort regardless of clinical characteristics which can impact brain development (e.g. low gestational age, being a twin) (Dubois et al., 2008; Kersbergen et al., 2016) or other factors which might have a slight influence on our sulcal asymmetry observations (e.g. the positioning of the infant in the scanner: on the side at 30w PMA versus on the back at 40w PMA). To investigate the question further, it would be interesting to compare the difference in shape of the central sulcus between a preterm population at term-equivalent-age and healthy term-born subjects, in order to differentiate prematurity-related variability from typical variability. It would also be informative to investigate the effects of clinical conditions on early sulcation by differentiating subgroups of patients. Nevertheless, our cohort was too small to provide reliable results on this question. The application of our approach to other large databases, such as the developing Human Connectome Project (dHCP) (Makropoulos et al. 2018), is therefore an interesting prospect, but was beyond the scope of the current study.

In terms of quantitative shape description, we reported an early encoding of most shape features, with eight out of ten dimensions showing a statistically relevant correlation between 30 and 40w PMA. The fact that the early shape of the central sulcus remained mostly consistent despite the later development of secondary sulci – which mostly happens between 30w and 40w PMA (Dubois et al., 2019) – was informative about the interactions between folding waves. The secondary folding wave does not seem to drastically affect the central sulcus's characteristics. To illustrate this, we could have suspected that the wrapping around the hand-knob (illustrated by dimension 5) might be affected by the secondary folding of the superior frontal sulcus (which might constraint the gyrus adjacent to the superior part of the central sulcus to retract dorsally and "push back" the upper part of the central sulcus, "unwrapping" the hand-knob). Yet, the correspondent Spearman correlation coefficients (0.38 and 0.32 for left and right hemisphere respectively) indicated that this feature evolved consistently between its 30w and 40w PMA encoding. The only two features showing low ($\rho = 0.19$) or very low ($|\rho| < 0.1$) correlations between the two age-groups on both hemispheres were dimensions 7 and 10, namely the height of the hand-knob at fixed depth and the orientation of the upper part and length of the hand-knob. These two specific features may have a delayed developmental dynamic or may present significant morphological changes between the two ages, which would explain why the 30w PMA encoding of these features did not foreshadow their 40w PMA counterparts. The knob height and the upper part orientation may depend on a shorter or longer period of elongation of the top of the central sulcus, which occurs between 30w and 40w PMA (Mangin et al., 2019).

Looking into the correlations between hemispheres, we also investigated hemispheric asymmetries in the central sulcus. A previous study on the same cohort reported solely a rightwards sulcal depth asymmetry at 30w PMA, and no hemispheric asymmetries in terms of surface area in the central sulcus, at both ages (Kersbergen et al., 2016). In this study, using more complex shape characterization techniques, we identified one dimension per age-group showing a statistically significant asymmetry. At 30w PMA, right central sulci showed a generally

deeper hand-knob than left ones (dimension 3). This could be explained by the earlier maturation of the right hemisphere compared to the left one (Chiron et al., 1997), and by the earlier sulci formation in the right hemisphere (Chi et al., 1977; Dubois et al., 2008; Habas et al., 2012). Yet, with an earlier maturation of the right central sulci, we could have expected a length asymmetry, which would have been encoded on dimension 1 – which did not show a significant asymmetry. An interpretation would be that at 30w PMA the left central sulci have caught up to the right ones in terms of length, and the relative maturational advance of the right central sulci is therefore expressed in terms of depth of the hand knob rather than length of the sulcus. At 40w PMA, the left central sulci favoured a "double-knob" configuration (versus "single-knob" configuration for the right ones) (dimension 8). This finding is consistent with a previous study on adults, which reported a visually similar main shape variability (from single to double-knob configuration with hand-knob height increase), and asymmetry (Sun et al., 2012). After evaluating hemispheric asymmetries, we chose not to assess the relative positioning of ipsi- versus contralateral sulci on the isomap dimensions, for two reasons. First, the results would have been redundant because of the low proportion of left-handers in this cohort leading to a significant overlap between contralateral (vs. ipsilateral) and left (vs. right) hemispheres. Secondly, we would have had to limit the study to the subjects with a suspected "natural" lateralization, implying both handedness hypotheses and a loss in statistical power.

9.2.6.3 To what extent s the central sulcal shape relevant to predict handedness and fine motor outcome?

A number of recent studies have investigated the predictability of adversarial developmental outcomes linked to prematurity. The purpose is to identify biomarkers in order to set up appropriate subject-specific interventions to counter or reduce the effects of neurodevelopmental afflictions. Several studies have focused on term-equivalent-age neuroimaging in order to evaluate the predictive capacity of either anatomical (Woodward et al., 2006), diffusion (Spittle et al., 2011) or functional imaging (Della Rosa et al., 2021) on motor and cognitive outcomes. A few studies have also investigated data acquired earlier than term-equivalent-age, and checked which has a better predictive power

between early, term-equivalent, or the difference between them in case of longitudinal studies. Examples of such studies included motor outcome prediction, using volumetric measures relative to whole brain volumes (Gui et al., 2019), diffusion tensor parameters (Roze et al., 2015), or computing anatomical features such as cortical surface area or gyrification indices (Moeskops et al., 2017). All these studies focused on whole brain analysis to predict outcome. Yet, because of important methodology discrepancies, the results we obtained are hardly comparable.

We chose to investigate the *predictive ability of the central sulcus' shape on motor development*, in the continuity of our shape characterization and description approach, in order to interrogate its functional relevance. In particular, we observed that the best shape feature to discriminate handedness was the length and backwards bend of the hand-knob of the left central sulcus at 30w PMA, and that a poor fine motor outcome at 5 years was mostly linked to a higher, deeper, but shorter right hand-knob, with the sulcal upper part bending forwards, at 40w PMA. To the best of our knowledge, we are the very first to assess the predictive capacity of sulcal shape during early development. We decided to use a classifier trained on the clinical factors that have been reported as relevant for motor outcome prediction in previous studies (Anderson et al., 2006; Kersbergen et al., 2016) as a benchmark to evaluate whether some shape features were relevant in classifying motor outcome, but other clinical factors might have been relevant to include, such as white matter injuries or venous infarctions. By extension we aimed to assess if motor neurodevelopmental adversities showed a signature in the central sulcus. In this "proof-of-concept" study, no classifier showed a strictly significant performance when compared to the 95% confidence interval of a chance prediction. Yet, the ROC curves of the best classifiers were close to the upper boundary of this 95% confidence interval, and the standard deviation of the cross-validation showed that multiple folds actually showed a better performance, leading us to stipulate that a few early sulcal features, in some hemisphere- and age-specific groups, contain functional information. Still, the results were not strictly significant and, moreover, approximately half of the results reported showed a ROC

AUC inferior to 0.5 (indicating a classifier performing worse than random). This can be due to an absence of relevant data to predict motor outcome in the shape of the central sulcus on specific groups, or to a methodological choice taken in this article: the predictors are probably under-fitted. Because of the size of the cohort and the small proportion of either left-handers or poor-manual-dexterity-outcomes, the decision was taken to prevent from operating feature selection or algorithmic tuning such as regularization in order to prevent from overfitting. We can also question the way we decided to dichotomize outcomes.

A limitation to our classification is that the data is globally preprocessed before entering the K-Fold cross-validation process (i.e. the Isomap dimensions are computed using the whole cohort before the classification process). This is discouraged as it induces bias in the classification. The recommended method would be to produce new Isomap dimensions at each fold, using only the training set. Yet, we chose to pursue the first method nonetheless, to enable interpretation: if we generated new Isomap dimensions at each fold, we would be unable to associate a given feature to each dimension, and dimensions would risk swapping within different folds. This would have prevented us from grasping the relevant shape features.

In terms of *handedness*, we observed that the left hemisphere was more informative than the right one, and the only relevant classifier using only shape features was obtained at 30w PMA, where left-handers tend towards a backwards bend of the superior part of the left central sulcus and a longer hand-knob (dimension 10). The result concerning the length of the hand-knob could suggest that, while the shape of the hand-knob is mostly driven by the hand area in the dominant hemisphere, the bulk of the hand-knob in the non-dominant hemisphere could be influenced by the adjacent functional areas (such as the immediate upper portion corresponding to the arm), justifying its wider sprawl. On the right hemisphere, it is surprising to observe that at 30w PMA, the right hemisphere combined with clinical factors performed well whereas the right hemisphere alone showed a very poor performance. This seems to suggest that the 30w PMA right central sulcus was only predictive in light of the clinical factors. This observation, in addition to the fact that the best classifier scores were

obtained by combining sulcal shape and clinical factors, probably indicates that we did not succeed in retaining only "natural" left-handers (i.e. subjects who were most likely to present this handedness independently from the pathological implications of extreme prematurity). As indicated in the Methods section, for the analysis we considered as left-handers only the left-handed children who had at least one left-handed parent (taking into account a genetic factor was an attempt to retain as much "natural" left-handers as possible). Interestingly, the number of left-handers obtained with this criterion corresponds to the range usually observed in the general population (7/71: 9.9%). Nevertheless, it has been reported that additive genetic effects only accounts for a quarter of the variance in handedness (Medland et al., 2009), therefore this left-hander-selection-choice is somewhat arbitrary. However, recent studies reported that paternal non-right-handedness was significantly related to left-hand preference in children (van Heerwaarde et al., 2020; Fagard et al., 2021). In our study, all the selected left-handers happened to have a left-handed father, comforting our criteria choice. Still, there is no way to confirm that the 7 left-handers that we studied for the laterality analysis are "natural" left-handers. To look into this, we observed a condition which can alter lateralization towards left-handedness: left-hemisphere IVH. The excluded left-handers showed a higher prevalence of left-sided IVH than the selected left-handers (see Sup. Info., Table 5), suggesting that our criteria for selection was relevant to an extent. Yet, the selected left-handers showed a higher prevalence of left-sided IVH than the right-handers, as well as a globally worse MRI anomaly classification using the Kidokoro scale (Kidokoro et al., 2013) (see Sup. Info., Table 5). Therefore, we might not have succeeded in filtering adversarial left-handedness. In order to dim out pathological variability, further studies should focus on cohort selection, either by selecting preterms depending on clinical factors, or by looking into predictability of handedness through the central sulcus's shape on term-born neonates.

In terms of *motor outcome prediction*, we observed relevant sulcal signatures at both ages. We aimed to investigate fine motor outcome (and not global motor score) in order to focus on the development of manual dexterity, as we were interested on the central sulcus' shape

that is highly characterized by the hand-knob, whose shape is associated with hand activation (Sun et al., 2016; Germann et al., 2019; Mangin et al., 2019). We should highlight that in the mABC-II, the subscores have not been thoroughly tested for psychometric relevance, contrarily to the global score (Hirata et al., 2018). They still have been reported to be acceptably relevant in different studies, especially for the manual dexterity and balance subscores (Ellinoudis et al., 2011). It is for all these reasons that we specifically chose to focus only on the manual dexterity subscore. Before addressing the shape features relevant to predict this outcome, we can notice that the most predictive hemisphere switches between 30 and 40w PMA, with the left hemisphere scoring better at 30w PMA and the right one at 40w PMA. This is surprising when shape features were observed to evolve consistently between the two ages. We can highlight the fact that both classifiers' most weighted shape feature is dimension 10, which specifically shows very low correlations between 30 and 40w PMA on both hemispheres, and therefore does not seem to evolve consistently during this period. Moreover, we can hypothesize that at 30w PMA, not enough time has passed since birth for the anatomical adversarial consequences of *ex utero* development after premature birth to have formed (this hypothesis should be mitigated by the fact that we do not know the cause of premature birth, and that alterations could have started before birth). Then, according to a previous review on lateralization in fetuses (Hepper, 2013), 90% of the subjects would be supposed to be genetically right-handers, which would explain why the left hemisphere (supposedly dominant for 90% of the group) was observed as the most predictive of motor outcome. If the adversities from preterm birth then develop anomalies in sensorimotor development which induce "pathological" left-handedness, then the proportion of right-handers would decrease. In fact, in the poor fine motor outcome group, 7 subjects were left-handed and 8 right-handed, and therefore the left hemisphere could no longer be considered as dominant at 40w PMA, with the "pathological" left-handers pulling the results towards the right hemisphere. In terms of shape interpretation, the most weighted shape feature for fine motor outcome (dimension 10) was observed at 40w PMA on the right hemisphere, suggesting a narrower hand-knob corresponding to the left hand in infants with poor fine motor outcome. This could suggest a compensation for a less functional right hand for

right-handers, and an abnormal development of the dominant hemisphere for left-handers, but this hypothesis needs to be investigated more thoroughly, especially since we had a mix of left- and right-handers for the fine motor outcome classification. Interestingly, this same 10th dimension was the most weighted for the handedness on the left 30w PMA central sulcus (tendency to a longer hand-knob and an upper part of the sulcus bending backwards in left handers). This might suggest a less precise location of the right-hand region at 30w PMA. Although relevant for both motor classifications, this 10th dimension shows no significant correlation between 30 and 40w PMA sulci: the early 30w shape encoded in the sulcus does not evolve to the corresponding shape at 40w PMA. A recent study refined the somatomotor mapping of the central sulcus and differentiated the central sulcus in 5 segments (Germann et al., 2019). Here, the upper part of the sulcus, bending forwards to backwards along the dimension, fits the first segment reported in that study, and the second segment corresponds to the hand area and comprises the hand-knob area. Segments one and two are reported to be separated by a narrow gyral passage linking the precentral and postcentral gyrus. It is possible that this buried gyrus develops mostly between 30 and 40w PMA and would justify the discordant expression of this feature at 30 and 40w PMA.

To sum up, this study, based on an original method for sulcal investigation, allowed us to describe the central sulcus' shape variability and consistency at 30w and 40w PMA in a cohort of infants born extremely preterm and to make exploratory investigations of the functional relevance of these features. To complement our study, it would be relevant to compare the central sulcal shape of preterm infants at TEA with that of term-born newborns imaged right after birth, in order to assess whether prematurity-induced patterns are captured by our method. It is interesting to note that both for handedness and fine motor outcome, the left central sulcus at 30w PMA seemed to carry relevant information, which suggests that these functional aspects are already partially encoded at this early age. This opens perspectives about the possibility to target subjects at risk of abnormal motor development very early on and to mitigate this risk through early interventions.

9.2.7 References

Anderson, P.J., Doyle, L.W., 2006. Neurodevelopmental Outcome of Bronchopulmonary Dysplasia. Seminars in Perinatology 30, 227–232. https://doi.org/10.1053/j.semperi.2006.05.010

Besl, P.J., McKay, N., 1992. A method for registration of 3-D shapes. IEEE Transactions on Pattern Analysis and Machine Intelligence 14, 239–256. https://doi.org/10.1109/34.121791

Bouyssi-Kobar, M., Murnick, J., Tinkleman, L., Robertson, R.L., Limperopoulos, C., 2016. Third Trimester Brain Growth in Preterm Infants Compared With In Utero Healthy Fetuses 138, 13.

Bryden, M.P., Roy, E.A., Manus, I.C., Mc Bulman-Fleming, M.B., 1997. On the Genetics and Measurement of Human Handedness, Laterality, 2:3-4, 317-336, DOI: 10.1080/713754269

Cachia, A., Paillère-Martinot, M.-L., Galinowski, A., Januel, D., de Beaurepaire, R., Bellivier, F., Artiges, E., Andoh, J., Bartrés-Faz, D., Duchesnay, E., Rivière, D., Plaze, M., Mangin, J.-F., Martinot, J.-L., 2008. Cortical folding abnormalities in schizophrenia patients with resistant auditory hallucinations. NeuroImage 39, 927–935. https://doi.org/10.1016/j.neuroimage.2007.08.049

Cachia, A., Del Maschio, N., Borst, G., Della Rosa, P.A., Pallier, C., Costa, A., Houdé, O., Abutalebi, J., 2017. Anterior cingulate cortex sulcation and its differential effects on conflict monitoring in bilinguals and monolinguals. Brain and Language 175, 57–63. https://doi.org/10.1016/j.bandl.2017.09.005

Chi, J.G., Dooling, E.C., Gilles, F.H., 1977. Gyral development of the human brain. Ann Neurol. 1, 86–93. https://doi.org/10.1002/ana.410010109

Chiron, C., Jambaque, I., Nabbout, R., Lounes, R., Syrota, A., Dulac, O., 1997. The right brain hemisphere is dominant in human infants. Brain 120, 1057–1065. https://doi.org/10.1093/brain/120.6.1057

Cunningham, D.J., 1892. Cunningham Memoirs - Contribution to the surface anatomy of the cerebral hemispheres by D.J. Cunningham with a chapter upon cranio-cerebral topography by Victor Horsley.

Del Maschio, N., Sulpizio, S., Fedeli, D., Ramanujan, K., Ding, G., Weekes, B.S., Cachia, A., Abutalebi, J., 2019. ACC Sulcal Patterns and Their Modulation on Cognitive Control Efficiency Across Lifespan: A Neuroanatomical Study on Bilinguals and Monolinguals. Cerebral Cortex 29, 3091–3101. https://doi.org/10.1093/cercor/bhy175

Della Rosa, P.A., Canini, M., Marchetta, E., Cirillo, S., Pontesilli, S., Scotti, R., Natali Sora, M.G., Poloniato, A., Barera, G., Falini, A., Scifo, P., Baldoli, C., 2021. The effects of the functional interplay between the Default Mode and Executive Control Resting State Networks on cognitive outcome in preterm born infants at 6 months of age. Brain and Cognition 147, 105669. https://doi.org/10.1016/j.bandc.2020.105669

Dobrushin, R.L., 1970. Definition of a system of random variables by conditional distributions. Teor. Verojatnost. i Primenen., 15, 469–497 (In Russian)

Domellöf, E., Johansson, A.-M., Rönnqvist, L., 2011. Handedness in preterm born children: A systematic review and a meta-analysis. Neuropsychologia 49, 2299–2310. https://doi.org/10.1016/j.neuropsychologia.2011.04.033

Duan, D., Xia, S., Rekik, I., Meng, Y., Wu, Z., Wang, L., Lin, W., Gilmore, J.H., Shen, D., Li, G., 2019. Exploring folding patterns of infant cerebral cortex based on multi-view curvature features: Methods and applications. NeuroImage 185, 575–592. https://doi.org/10.1016/j.neuroimage.2018.08.041

Dubois, J., Benders, M., Cachia, A., Lazeyras, F., Ha-Vinh Leuchter, R., Sizonenko, S.V., Borradori-Tolsa, C., Mangin, J.F., Huppi, P.S., 2008. Mapping the Early Cortical Folding Process in the Preterm Newborn Brain. Cerebral Cortex 18, 1444–1454. https://doi.org/10.1093/cercor/bhm180

Dubois, J., Lefèvre, J., Angleys, H., Leroy, F., Fischer, C., Lebenberg, J., Dehaene-Lambertz, G., Borradori-Tolsa, C., Lazeyras, F., Hertz-Pannier, L., Mangin, J.-F., Hüppi, P.S., Germanaud, D., 2019. The dynamics of cortical folding waves and prematurity-related deviations revealed by spatial and spectral analysis of gyrification. NeuroImage 185, 934–946. https://doi.org/10.1016/j.neuroimage.2018.03.005

Ellinoudis, T., Evaggelinou, C., Kourtessis, T., Konstantinidou, Z., Venetsanou, F., Kambas, A., 2011. Reliability and validity of age band 1 of the Movement Assessment Battery for Children – Second Edition. Research in Developmental Disabilities 32, 1046–1051. https://doi.org/10.1016/j.ridd.2011.01.035

Fagard, J., De Agostini, M., Huet, V., Granjon, L., Heude, B., 2021. Is Handedness at Five Associated with Prenatal Factors? IJERPH 18, 3529. https://doi.org/10.3390/ijerph18073529

Flamary, R. and Courty, N. POT Python Optimal Transport library, <https://pythonot.github.io/> , 2017 (accessed 17.01.20)

Fox, P., Perlmutter, J., Raichle, M., 1985. A stereotactic method of anatomical localization for PET. J. Comput. Assist. Tomogr. 9, 141 – 153.

Gajawelli, N., Deoni, S.C.L., Ramsy, N., Dean, D.C., O'Muircheartaigh, J., Nelson, M.D., Lepore, N., Coulon, O., 2021. Developmental changes of the central sulcus morphology in young children. Brain Struct Funct 226, 1841–1853. https://doi.org/10.1007/s00429-021-02292-x

Garcia, K.E., Robinson, E.C., Alexopoulos, D., Dierker, D.L., Glasser, M.F., Coalson, T.S., Ortinau, C.M., Rueckert, D., Taber, L.A., Van Essen, D.C., Rogers, C.E., Smyser, C.D., Bayly, P.V., 2018. Dynamic patterns of cortical expansion during folding of the preterm human brain. Proc Natl Acad Sci USA 115, 3156–3161. https://doi.org/10.1073/pnas.1715451115

Germann, J., Chakravarty, M.M., Collins, L.D., Petrides, M., 2019. Tight Coupling between Morphological Features of the Central Sulcus and Somatomotor Body Representations: A Combined Anatomical and

Functional MRI Study. Cerebral Cortex bhz208. https://doi.org/10.1093/cercor/bhz208

Gui, L., Loukas, S., Lazeyras, F., Hüppi, P.S., Meskaldji, D.E., Borradori Tolsa, C., 2019. Longitudinal study of neonatal brain tissue volumes in preterm infants and their ability to predict neurodevelopmental outcome. NeuroImage 185, 728–741. https://doi.org/10.1016/j.neuroimage.2018.06.034

Habas, P.A., Scott, J.A., Roosta, A., Rajagopalan, V., Kim, K., Rousseau, F., Barkovich, A.J., Glenn, O.A., Studholme, C., 2012. Early Folding Patterns and Asymmetries of the Normal Human Brain Detected from in Utero MRI. Cerebral Cortex 22, 13–25. https://doi.org/10.1093/cercor/bhr053

Hepper, P.G., 2013. The developmental origins of laterality: Fetal handedness: Fetal Handedness. Dev Psychobiol 55, 588–595. https://doi.org/10.1002/dev.21119

Hirata, S., Kita, Y., Yasunaga, M., Suzuki, K., Okumura, Y., Okuzumi, H., Hosobuchi, T., Kokubun, M., Inagaki, M., Nakai, A., 2018. Applicability of the Movement Assessment Battery for Children-Second Edition (MABC-2) for Japanese Children Aged 3–6 Years: A Preliminary Investigation Emphasizing Internal Consistency and Factorial Validity. Front. Psychol. 9, 1452. https://doi.org/10.3389/fpsyg.2018.01452

Hou, L., Xiang, L., Crow, T.J., Leroy, F., Rivière, D., Mangin, J.-F., Roberts, N., 2019. Measurement of Sylvian Fissure asymmetry and occipital bending in humans and Pan troglodytes. NeuroImage 184, 855–870. https://doi.org/10.1016/j.neuroimage.2018.08.045

Im, K., Grant, P.E., 2019. Sulcal pits and patterns in developing human brains. NeuroImage 185, 881–890. https://doi.org/10.1016/j.neuroimage.2018.03.057

Kersbergen, K.J., Leroy, F., Išgum, I., Groenendaal, F., de Vries, L.S., Claessens, N.H.P., van Haastert, I.C., Moeskops, P., Fischer, C., Mangin, J.-F., Viergever, M.A., Dubois, J., Benders, M.J.N.L., 2016. Rela-

tion between clinical risk factors, early cortical changes, and neurodevelopmental outcome in preterm infants. NeuroImage 142, 301–310. https://doi.org/10.1016/j.neuroimage.2016.07.010

Kidokoro, H., Neil, J.J., Inder, T.E., 2013. New MR Imaging Assessment Tool to Define Brain Abnormalities in Very Preterm Infants at Term. AJNR Am J Neuroradiol 34, 2208–2214. https://doi.org/10.3174/ajnr.A3521

Korzeniewski, S.J., Slaughter, J., Lenski, M., Haak, P., Paneth, N., 2018. The complex aetiology of cerebral palsy. Nat Rev Neurol 14, 528–543. https://doi.org/10.1038/s41582-018-0043-6

Kostović, I., Sedmak, G., Judaš, M., 2019. Neural histology and neurogenesis of the human fetal and infant brain. NeuroImage 188, 743–773. https://doi.org/10.1016/j.neuroimage.2018.12.043

Lefèvre, J., Germanaud, D., Dubois, J., Rousseau, F., de Macedo Santos, I., Angleys, H., Mangin, J.-F., Hüppi, P.S., Girard, N., De Guio, F., 2016. Are Developmental Trajectories of Cortical Folding Comparable Between Cross-sectional Datasets of Fetuses and Preterm Newborns? Cereb. Cortex 26, 3023–3035. https://doi.org/10.1093/cercor/bhv123

Leroy, F., Cai, Q., Bogart, S.L., Dubois, J., Coulon, O., Monzalvo, K., Fischer, C., Glasel, H., Van der Haegen, L., Bénézit, A., Lin, C.-P., Kennedy, D.N., Ihara, A.S., Hertz-Pannier, L., Moutard, M.-L., Poupon, C., Brysbaert, M., Roberts, N., Hopkins, W.D., Mangin, J.-F., Dehaene-Lambertz, G., 2015. New human-specific brain landmark: The depth asymmetry of superior temporal sulcus. Proc Natl Acad Sci USA 112, 1208–1213. https://doi.org/10.1073/pnas.1412389112

Makropoulos, A., Robinson, E.C., Schuh, A., Wright, R., Fitzgibbon, S., Bozek, J., Counsell, S.J., Steinweg, J., Vecchiato, K., Passerat-Palmbach, J., Lenz, G., Mortari, F., Tenev, T., Duff, E.P., Bastiani, M., Cordero-Grande, L., Hughes, E., Tusor, N., Tournier, J.-D., Hutter, J., Price, A.N., Teixeira, R.P.A.G., Murgasova, M., Victor, S., Kelly, C., Rutherford, M.A., Smith, S.M., Edwards, A.D., Hajnal, J.V., Jenkinson, M., Rueckert, D., 2018. The developing human connectome project: A minimal processing pipeline for neonatal cortical surface reconstruction. NeuroImage 173, 88–112.

https://doi.org/10.1016/j.neuroimage.2018.01.054

Mangin, J.-F., Frouin, V., Bloch, I., Régis, J., López-Krahe, J., 1995. From 3D magnetic resonance images to structural representations of the cortex topography using topology preserving deformations. J Math Imaging Vis 5, 297–318. https://doi.org/10.1007/BF01250286

Mangin, J.-F., Auzias, G., Coulon, O., Sun, Z.Y., Rivière, D., Régis, J., 2015. Sulci as Landmarks, in: Brain Mapping. Elsevier, pp. 45–52. https://doi.org/10.1016/B978-0-12-397025-1.00198-6

Mangin, J.-F., Le Guen, Y., Labra, N., Grigis, A., Frouin, V., Guevara, M., Fischer, C., Rivière, D., Hopkins, W.D., Régis, J., Sun, Z.Y., 2019. "Plis de passage" Deserve a Role in Models of the Cortical Folding Process. Brain Topogr 32, 1035–1048. https://doi.org/10.1007/s10548-019-00734-8

Medland, S.E., Duffy, D.L., Wright, M.J., Geffen, G.M., Hay, D.A., Levy, F., van-Beijsterveldt, C.E.M., Willemsen, G., Townsend, G.C., White, V., Hewitt, A.W., Mackey, D.A., Bailey, J.M., Slutske, W.S., Nyholt, D.R., Treloar, S.A., Martin, N.G., Boomsma, D.I., 2009. Genetic influences on handedness: Data from 25,732 Australian and Dutch twin families. Neuropsychologia 47, 330–337. https://doi.org/10.1016/j.neuropsychologia.2008.09.005

Mellerio, C., Roca, P., Chassoux, F., Danière, F., Cachia, A., Lion, S., Naggara, O., Devaux, B., Meder, J.-F., Oppenheim, C., 2015. The Power Button Sign: A Newly Described Central Sulcal Pattern on Surface Rendering MR Images of Type 2 Focal Cortical Dysplasia. Radiology 274, 500–507. https://doi.org/10.1148/radiol.14140773

Meng, Y., Li, G., Wang, L., Lin, W., Gilmore, J.H., Shen, D., 2018. Discovering cortical sulcal folding patterns in neonates using large-scale dataset. Hum. Brain Mapp. 39, 3625–3635. https://doi.org/10.1002/hbm.24199

Moeskops, P., Benders, M.J.N.L., Kersbergen, K.J., Groenendaal, F., de Vries, L.S., Viergever, M.A., Išgum, I., 2015. Development of Cor-

tical Morphology Evaluated with Longitudinal MR Brain Images of Preterm Infants. PLoS ONE 10, e0131552. https://doi.org/10.1371/journal.,pone.0131552

Moeskops, P., Išgum, I., Keunen, K., Claessens, N.H.P., van Haastert, I.C., Groenendaal, F., de Vries, L.S., Viergever, M.A., Benders, M.J.N.L., 2017. Prediction of cognitive and motor outcome of preterm infants based on automatic quantitative descriptors from neonatal MR brain images. Sci Rep 7, 2163. https://doi.org/10.1038/s41598-017-02307-w

Ono M., Kubik S., Abarnathey C.D., 1990. Atlas of the cerebral sulci. Georg Thieme, New York

Orasanu, E., Melbourne, A., Cardoso, M.J., Lomabert, H., Kendall, G.S., Robertson, N.J., Marlow, N., Ourselin, S., 2016. Cortical folding of the preterm brain: a longitudinal analysis of extremely preterm born neonates using spectral matching. Brain Behav 6, e00488. https://doi.org/10.1002/brb3.488

Pascal, A., Govaert, P., Oostra, A., Naulaers, G., Ortibus, E., Van den Broeck, C., 2018. Neurodevelopmental outcome in very preterm and very-low-birthweight infants born over the past decade: a meta-analytic review. Dev Med Child Neurol 60, 342–355. https://doi.org/10.1111/dmcn.13675

Penfield, W., & Rasmussen, T., 1950. *The cerebral cortex of man; a clinical study of localization of function*. Macmillan.

Perrot, M., Rivière, D., Mangin, J.-F., 2011. Cortical sulci recognition and spatial normalization. Medical Image Analysis 15, 529–550. https://doi.org/10.1016/j.media.2011.02.008

Plaze, M., Paillere-Martinot, M.-L., Penttila, J., Januel, D., de Beaurepaire, R., Bellivier, F., Andoh, J., Galinowski, A., Gallarda, T., Artiges, E., Olie, J.-P., Mangin, J.-F., Martinot, J.-L., Cachia, A., 2011. "Where Do Auditory Hallucinations Come From?"--A Brain Morphometry Study of Schizophrenia Patients With Inner or Outer Space Hallucinations. Schizophrenia Bulletin 37, 212–221. https://doi.org/10.1093/schbul/sbp081

Régis, J., Mangin, J.-F., Ochiai, T., Frouin, V., Riviére, D., Cachia, A., Tamura, M., Samson, Y., 2005. "Sulcal Root" Generic Model: a Hypothesis to Overcome the Variability of the Human Cortex Folding Patterns. Neurol. Med. Chir.(Tokyo) 45, 1–17. https://doi.org/10.2176/nmc.45.1

Roze, E., Benders, M.J., Kersbergen, K.J., van der Aa, N.E., Groenendaal, F., van Haastert, I.C., Leemans, A., de Vries, L.S., 2015. Neonatal DTI early after birth predicts motor outcome in preterm infants with periventricular hemorrhagic infarction. Pediatr Res 78, 298–303. https://doi.org/10.1038/pr.2015.94

Sastre-Janer, F.A., Régis, J., Belin, P., Mangin, J.F., Dormont, D., Masure, M.C., Remy, P.,

Frouin, V., Samson, Y., 1998. Three-dimensional reconstruction of the human central

sulcus reveals a morphological correlate of the hand area. Cereb. Cortex 8, 641–647.

Shimony, J.S., Smyser, C.D., Wideman, G., Alexopoulos, D., Hill, J., Harwell, J., Dierker, D., Van Essen, D.C., Inder, T.E., Neil, J.J., 2016. Comparison of cortical folding measures for evaluation of developing human brain. NeuroImage 125, 780–790. https://doi.org/10.1016/j.neuroimage.2015.11.001

Spittle, A.J., Cheong, J., Doyle, L.W., Roberts, G., Lee, K.J., Lim, J., Hunt, R.W., Inder, T.E., Anderson, P.J., 2011. Neonatal white matter abnormality predicts childhood motor impairment in very preterm children: White Matter Abnormalities and Motor Impairment. Developmental Medicine & Child Neurology 53, 1000–1006. https://doi.org/10.1111/j.1469-8749.2011.04095.x

Sun, Z.Y., Klöppel, S., Rivière, D., Perrot, M., Frackowiak, R., Siebner, H., Mangin, J.-F., 2012. The effect of handedness on the shape of the central sulcus. NeuroImage 60, 332–339. https://doi.org/10.1016/j.neuroimage.2011.12.050

Sun, Z.Y., Pinel, P., Rivière, D., Moreno, A., Dehaene, S., Mangin, J.-F., 2016. Linking morphological and functional variability in hand movement and silent reading. Brain Struct Funct 221, 3361–3371. https://doi.org/10.1007/s00429-015-1106-8

Sun, Z.Y., Cachia, A., Rivière, D., Fischer, C., Makin, T., Mangin, J.-F., n.d. Congenital unilateral upper limb absence flattens the contralateral hand-knob. 2017 Organization for Human Brain Mapping Meeting (OHBM 2017), Organization for Human Brain Mapping, Jun 2017, Vancouver, Canada. ⟨hal-02876124⟩

Tenenbaum, J.B., 2000. A Global Geometric Framework for Nonlinear Dimensionality Reduction. Science 290, 2319–2323. https://doi.org/10.1126/science.290.5500.2319

van Heerwaarde, A.A., van der Kamp, L.T., van der Aa, N.E., de Vries, L.S., Groenendaal, F., Jongmans, M.J., Eijsermans, R.J.C., Koopman-Esseboom, C., van Haastert, I.-L.C., Benders, M.J.N.L., Dudink, J., 2020. Non-right-handedness in children born extremely preterm: Relation to early neuroimaging and long-term neurodevelopment. PLoS ONE 15, e0235311. https://doi.org/10.1371/journal.pone.0235311

Vasung, L., Rollins, C.K., Yun, H.J., Velasco-Annis, C., Zhang, J., Wagstyl, K., Evans, A., Warfield, S.K., Feldman, H.A., Grant, P.E., Gholipour, A., 2019. Quantitative In vivo MRI Assessment of Structural Asymmetries and Sexual Dimorphism of Transient Fetal Compartments in the Human Brain. Cerebral Cortex bhz200. https://doi.org/10.1093/cercor/bhz200

Visser, G.H., Eilers, P.H., Elferink-Stinkens, P.M., Merkus, H.M., Wit, J.M., 2009. New Dutch reference curves for birthweight by gestational age. Early Hum. Dev. 85, 737–744.

Welker, W., 1990. Why Does Cerebral Cortex Fissure and Fold?, in: Cerebral Cortex. pp. 3–137.

Woodward, L.J., Anderson, P.J., Austin, N.C., Howard, K., Inder, T.E., 2006. Neonatal MRI to Predict Neurodevelopmental Outcomes in

Preterm Infants. N Engl J Med 355, 685–694. https://doi.org/10.1056/NEJMoa053792

Yamada, Y., Kanazawa, H., Iwasaki, S., Tsukahara, Y., Iwata, O., Yamada, S., Kuniyoshi, Y., 2016. An Embodied Brain Model of the Human Foetus. Sci Rep 6, 27893. https://doi.org/10.1038/srep27893

Yousry, T.A., Schmid, U.D., Alkadhi, H., Schmidt, D., Peraud, A., Buettner, A., Winkler, P.,

1997. Localization of the motor hand area to a knob on the precentral gyrus. A new landmark. Brain 120, 141–157.

9.2.8 Supplementary information

Supplementary Table 1: Perinatal clinical characteristics and fine motor follow-up of the study participants (n=71)

Characteristics	*Mean ± Standard deviation (range) or N (percentage)*
Perinatal clinical characteristics	
Sex, male	36 (51%)
Gestational age at birth (weeks)	26.5 ± 1.0 (24.4 – 27.9)
Birth-weight z-score	0.4 ± 0.8 (-2.5 – 1.8)
Presence of severe IVH (grade 3 or 4): number of infants	8 (11%)
Presence of broncho-pulmonary dysplasia: number of infants	20 (39%)
Age at MRI scans	
PMA at early acquisition (weeks)	30.7 ± 0.9 (28.7 – 32.7)
PMA at term-equivalent age acquisition (weeks)	41.2 ± 0.6 (40.0 – 42.7)
Fine motor follow-up at 5-years	
Manual lateralization	
Handedness: number of infants (left / ambidextrous / right) (n=70)	18 / 2 / 50 (26 / 3 / 71%)
Corrected handedness*: number of infants (left / right) (n=57)	7 / 50 (12 / 88%)
Fine motor assessment (n=66)	
Age at mABC	5 years 9 months ± 4 months (4y 6m – 6y 7m)
mABC manual dexterity standardized score	7.7 ± 2.4 (3 – 14)
mABC manual dexterity outcome: number of infants (poor/borderline/good)	15 / 16 / 35 (23 / 24 / 53%)

IVH: intra-ventricular hemorrhage. PMA: post-menstrual age. *Corrected handedness excludes ambidextrous and left-handed children having both parents right-handed. mABC: Movement Assessment Battery for Children

Supplementary Table 2: Pearson correlations between Isomap positions and PMA at MRI acquisition (n=71)

	r	
	At 30w PMA	At 40w PMA
Dimension 1	0.30	0.13
Dimension 2	-0.01	-0.08
Dimension 3	-0.13	0.15
Dimension 4	0.11	-0.05
Dimension 5	-0.13	-0.14
Dimension 6	0.24	-0.04
Dimension 7	0.04	0.19
Dimension 8	0.15	0.14
Dimension 9	-0.01	0.16
Dimension 10	0.22	0.13

Supplementary Table 3: Wilcoxon signed-rank tests between either left / right hemisphere (A.) or 30w / 40w PMA (B.), for Isomap PMA-corrected positions (n=71)

	Wilcoxon signed-rank test: t (p-value)			
	A. Hemispheric comparison		B. Age-group comparison	
	L30 vs R30	L40 vs R40	L30 vs L40	R30 vs R40
Dimension 1	959 (0.068)	1022 (0.142)	**3.0 (3.10^{-13})**	**0.0 (2.10^{-13})**
Dimension 2	1044 (0.180)	1276 (0.991)	882.0 (0.023)	**774.0 (0.004)**
Dimension 3	**757 (0.003)**	1110 (0.336)	903.0 (0.032)	978.0 (0.086)
Dimension 4	941 (0.053)	1113 (0.344)	**627.0 (2.10^{-4})**	1129.0 (0.393)
Dimension 5	878 (0.022)	1137 (0.419)	**606.0 (1.10^{-4})**	**686.0 (7.10^{-4})**
Dimension 6	1133 (0.406)	1152 (0.470)	1165.0 (0.517)	1178.0 (0.567)
Dimension 7	1169 (0.532)	947 (0.058)	986.0 (0.094)	849.0 (0.014)
Dimension 8	1242 (0.837)	**775 (0.004)**	804.0 (0.007)	1138.0 (0.422)
Dimension 9	1208 (0.689)	1254 (0.891)	1099.0 (0.305)	1212.0 (0.705)
Dimension 10	1132 (0.403)	881 (0.023)	871.0 (0.020)	1066.0 (0.224)

Bold values verify p-value<0.005. L: left hemisphere; R: right hemisphere. 30: 30w PMA (early scan); 40: 40w PMA (term-equivalent-age scan).

Supplementary Table 4: Spearman correlations between either left / right hemisphere (A.) or 30w / 40w PMA (B.), for Isomap PMA-corrected positions (n=71).

	Spearman correlation: ρ (p-value)			
	A. Hemispheric comparison		B. Age-group comparison	
	L30 vs R30	L40 vs R40	L30 vs L40	R30 vs R40
Dimension 1	**0.607 (2.10^{-8})**	**0.385 (9.10^{-4})**	0.232 (0.051)	**0.428 (2.10^{-4})**
Dimension 2	**0.407 (4.10^{-4})**	0.232 (0.051)	**0.458 (6.10^{-5})**	0.329 (0.005)
Dimension 3	0.222 (0.063)	**0.351 (0.003)**	0.307 (0.009)	**0.353 (0.003)**
Dimension 4	0.254 (0.032)	0.283 (0.017)	**0.512 (5.10^{-6})**	**0.414 (3.10^{-4})**
Dimension 5	**0.411 (3.10^{-4})**	0.327 (0.005)	**0.376 (0.001)**	0.317 (0.007)
Dimension 6	0.216 (0.070)	0.150 (0.213)	0.284 (0.017)	**0.383 (0.001)**
Dimension 7	0.188 (0.116)	0.249 (0.036)	0.081 (0.500)	0.191 (0.111)
Dimension 8	0.212 (0.076)	0.186 (0.120)	0.246 (0.039)	**0.522 (3.10^{-6})**
Dimension 9	0.157 (0.190)	0.123 (0.308)	0.294 (0.013)	**0.334 (0.004)**
Dimension 10	0.158 (0.189)	0.264 (0.026)	-0.024 (0.842)	-0.063 (0.599)

Bold values verify p-value<0.005. L: left hemisphere; R: right hemisphere. 30: 30w PMA (early scan); 40: 40w PMA (term-equivalent-age scan).

Supplementary Table 5: Additional perinatal characteristics reported for right-handers, selected left-handers and excluded left-handers (based on parental handedness) (n=68)

Characteristics	N (percentage)		
Handedness class	Right-handers (n=50)	Selected left-handers (n=7)	Excluded left-handers (n=11)
Presence of left IVH (any grade): number of in-fants	12 (24%)	2 (29%)	4 (36%)
Kidokoro classes			
Normal	25 (50%)	1 (14%)	3 (27%)
Mild	20 (40%)	6 (86%)	7 (64%)
Moderate	4 (8%)	0 (0%)	1 (9%)
Severe	1 (2%)	0 (0%)	0 (0%)

IVH: intra-ventricular hemorrhage

9.2.9 Annex 1 : Parameter selection for the Isomap algorithm

Method to choose the intrinsic dimensionality of the manifold d_{opt} for a given k

Let M_{dist} be the input distance matrix. A distance matrix of D-dimensional Gaussian vectors was computed, with the same average square distance as M_{dist}, which we called M_{rand}. Using a loop, we computed the reconstruction error e_{dist} of the Isomap fitted on M_{dist} and the reconstruction error e_{rand} of the Isomap fitted on M_{rand} for the whole range of possible number of components for the Isomap, so for $d \in [1, dim(M_{dist})]$. We then considered the number of components maximizing the ratio e_{rand} / e_{dist} as the intrinsic dimensionality of the manifold (see Supplementary Figure 1.1.A).

Method to choose the number of nearest neighbors k

Using the previous method, we computed the intrinsic dimensionality of the manifold for each possible k in our study, so for $k \in [1, 283]$. The choice of k was based on the following considerations:

1. In order to prevent short-circuits in the manifold, k should be rather small.

2. The smallest value to consider for k is the smallest value allowing the nearest neighbors graph to be connected $\Rightarrow k_{\min} = 2$.

3. Such a small k is not suited for our study since we wish to interconnect 30w sulci with 40w sulci and reciprocally. The number of inter-age-subgroup connections grows with k (see Supplementary Figure 1.1.B).

4. Our purpose was to choose a k small enough to prevent short-circuits in the manifold, but high enough to capture accurately the complexity of the dataset. In order to get an idea of the range of k which corresponds to this criterion, we have plotted the graph of reconstruction error depending on k (see Supplementary Figure 1.1.C).

We observed an interesting reconstruction error drop between k=5 and k=20, so this is the scope we focused on.

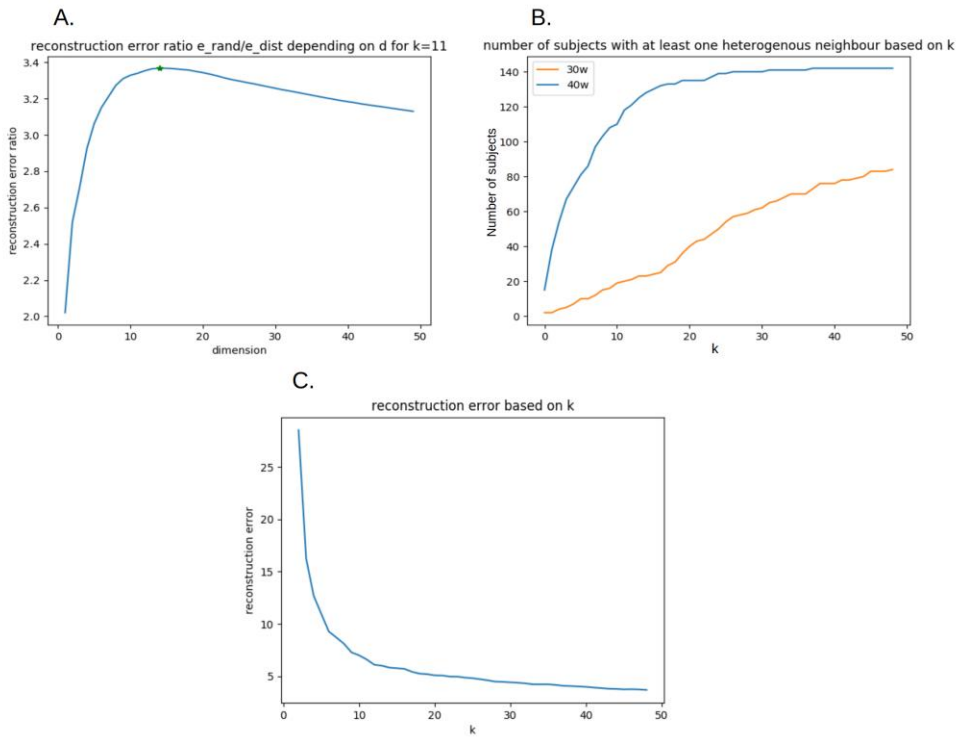

Supplementary Figure 1.1. A. Reconstruction error ratio depending on dimension *d* for a fixed *k* (here, *k*=11, leading to an intrinsic dimensionality of 14). B. Number of sulci with at least one nearest neighbor of the other age-group depending on *k*. Orange: 30w sulci, blue: 40w sulci. C. Reconstruction error based on *k*.

5. In this scope, we have observed that the Isomap results did not differ drastically, as can be seen using the correlation matrices for the Isomap projections using different values for *k*, as shown in Supplementary Figure 1.2.

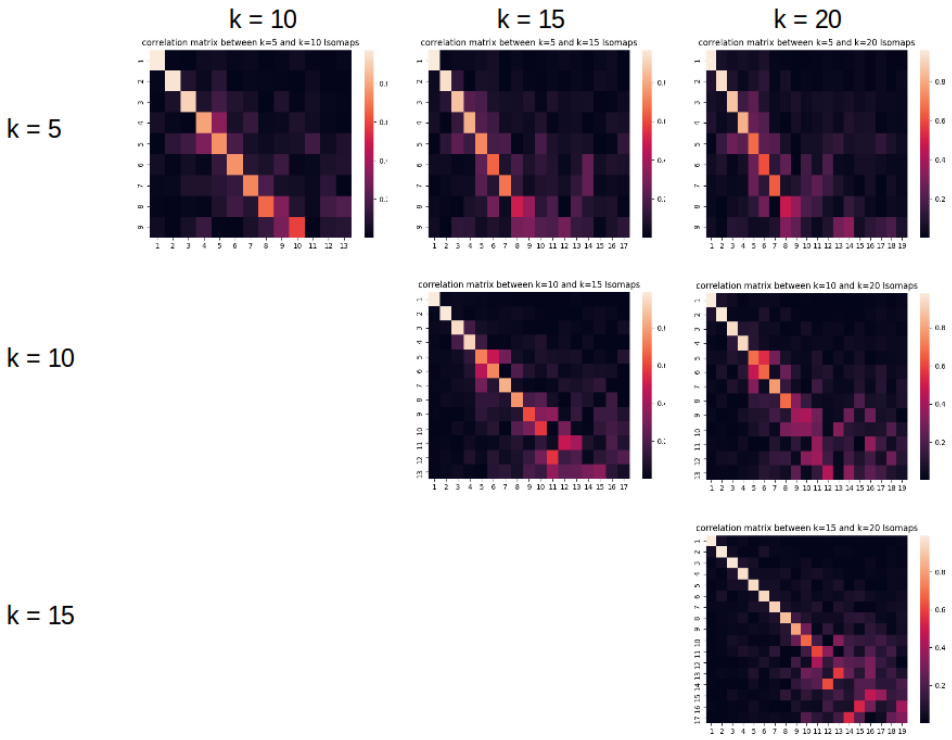

Supplementary Figure 1.2. Correlation matrices between the positioning of the sulci on the dimensions obtained using *k*∈{5,10,15,20}. The correlation values suggest that most dimensions are not drastically altered by different choices of *k* in this scope.

6. In order to select a specific *k* within this range, we looked into the residual variance graph based on k, as shown in Supplementary Figure 1.3.

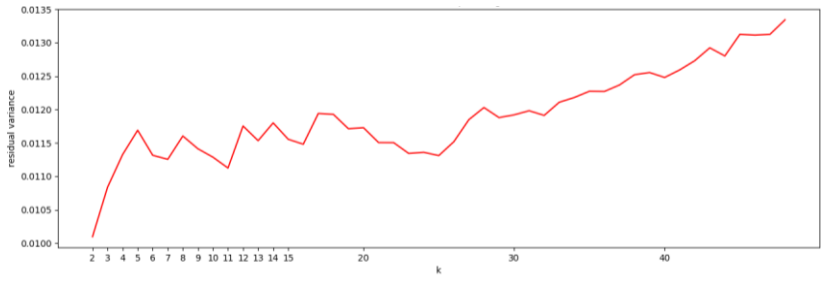

Supplementary Figure 1.3. Residual variance depending on *k*.

We observed a local minimum for $k=11$ and therefore chose this value.

Method to choose the relevant number of dimensions for our study

According to Supplementary Figure 1.1.A, the intrinsic dimensionality for k=11 was 14. Looking back into this figure, we observed that the reconstruction error ratio reached a plateau. The fact that e_{rand}/e_{dist} did not change around this plateau suggested that the additional data gained on the input distance matrix was not significantly higher than the random distance matrix. Therefore, in order to capture the most relevant dimensionality reduction in the data, we considered that even though the intrinsic dimensionality of the manifold was the one maximizing this ratio, the relevant dimensionality to consider in this study was the first d for which the curve stopped growing significantly. Here, by looking at the derivative from figure Supplementary Figure 1.4, we considered the relevant dimensionality d=10:

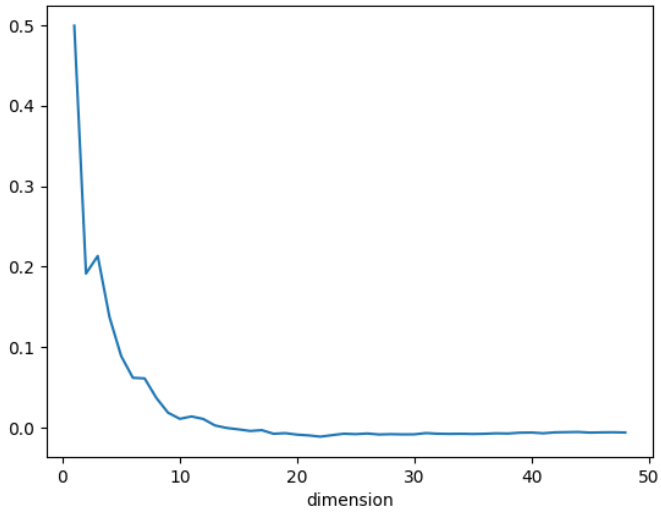

Supplementary Figure 1.4. Derivative of the reconstruction error ratio for *k*=11 depending on *d*

Confirmation that the observations for k=11 (and d=10) are stable for neighboring values of k

To confirm that this decision is not inducing too much bias in our observations, we computed the correlation matrices for the Isomap projections using k=10 and k=12 to compare with k=11, represented on Supplementary Figure 1.5.

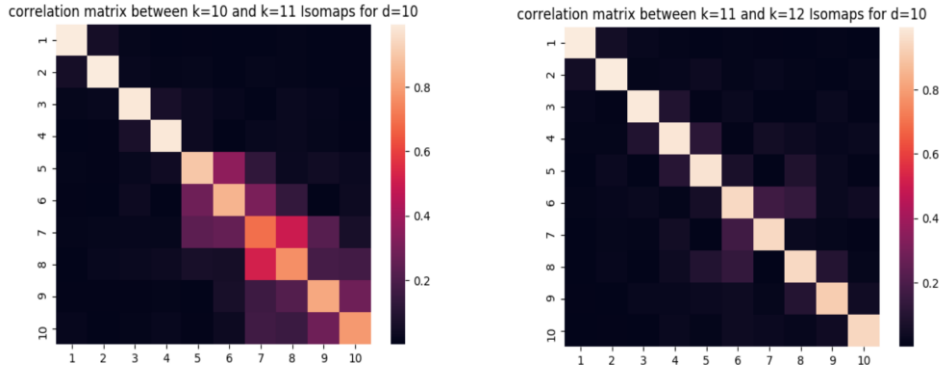

Supplementary Figure 1.5. Correlation matrices between the positioning of the sulci on the dimensions obtained using *k*=10 and *k*=11 (left), and *k*=11 and *k*=12 (right).

These correlations matrices confirmed that the choice of parameter *k*=11 does not excessively affect the projection results.

9.2.10 Annex 2 : Representation of the 10 Isomap dimensions

For each dimension, the sulcal projections were represented as well as the age-specific moving averages (blue = 30w PMA, green = 40w PMA). A description for the shape feature captured is suggested for each dimension. Additionally, the information about statistical tests for each dimension (Wilcoxon signed-rank test and Spearman correlation for L30, R30, L40 and R40) is summarized in the table next to it (✓for a p-value < 0.005, ~ for a p-value between 0.05 and 0.005, and x for a p-value > 0.05).

The reading key for shape description (Figure 3.A) is reminded on Supplementary Figure 2.1.

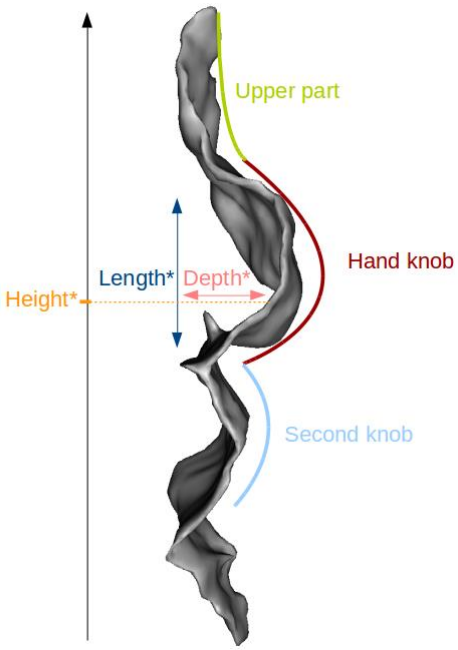

Supplementary Figure 2.1. Reading key for shape description of the central sulcus with a two-knob configuration. The height of the hand-knob is defined as the vertical distance from the bottom of the sulcus to the deepest region of the hand-knob. *Measures relative to the hand-knob.

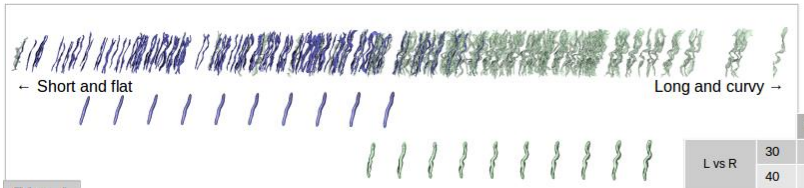

		Wilcoxon	Spearman
L vs R	30	x	✓
	40	x	✓
30 vs 40	L	✓	x
	R	✓	✓

Dim. 1

Length and curvature
From short and flat sulci to long and curvy sulci.

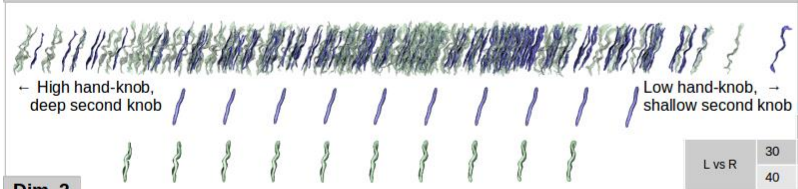

		Wilcoxon	Spearman
L vs R	30	x	✓
	40	x	x
30 vs 40	L	~	✓
	R	✓	~

Dim. 2

Height of the hand knob and depth of the second knob
From sulci with high hand-knobs and deep second-knobs to sulci with low hand-knobs and shallow second-knobs.

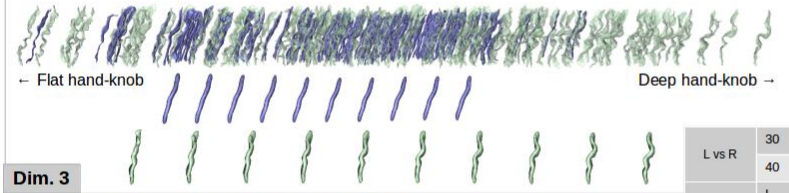

		Wilcoxon	Spearman
L vs R	30	✓	x
	40	x	✓
30 vs 40	L	~	~
	R	x	✓

Dim. 3

Depth of the hand-knob at fixed low height
From sulci with flatter or poorly-defined hand-knobs to sulci with deep low hand-knobs, with no height shift of the hand-knob along the axis.

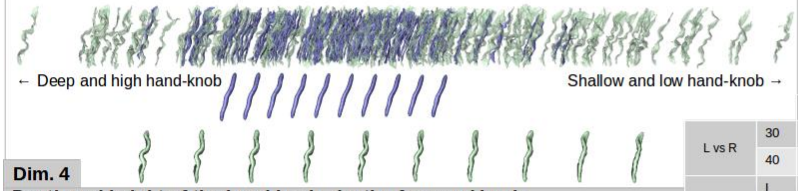

		Wilcoxon	Spearman
L vs R	30	x	~
	40	x	~
30 vs 40	L	✓	✓
	R	x	✓

Dim. 4

Depth and height of the hand knob, depth of second knob
From sulci with deeper and higher hand-knobs to sulci with shallower and lower hand-knobs. Note that the second knob, deep at first, fades out along the axis.

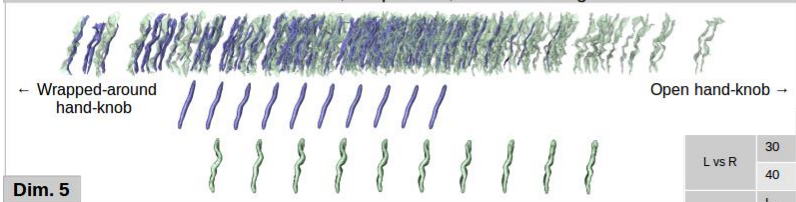

		Wilcoxon	Spearman
L vs R	30	x	~
	40	x	~
30 vs 40	L	✓	✓
	R	x	✓

Dim. 5

Wrapping around the hand-knob
From sulci with wrapped-around hand-knobs to sulci with open hand-knobs.

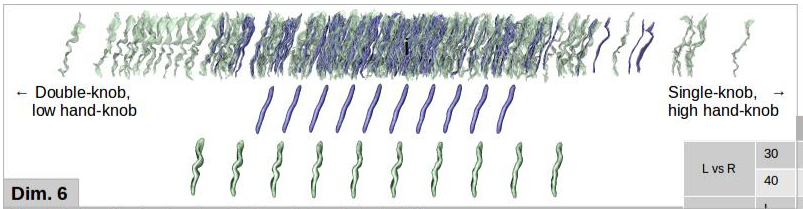

Dim. 6

Double to single-knob with hand-knob height increase

From sulci with two knobs and a lower hand-knob to sulci with a single-knob configuration, with a higher hand-knob.

		Wilcoxon	Spearman
L vs R	30	x	x
	40	x	x
30 vs 40	L	x	~
	R	x	✓

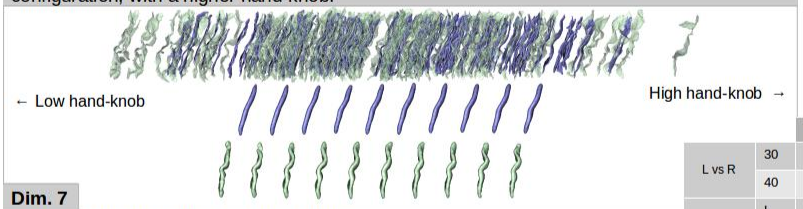

Dim. 7

Height of the hand-knob at fixed depth

From sulci with a lower hand knob to sulci with a higher hand knob, at fixed depth.

		Wilcoxon	Spearman
L vs R	30	x	x
	40	x	~
30 vs 40	L	x	x
	R	~	x

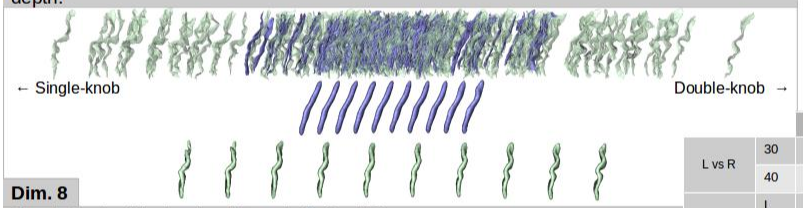

Dim. 8

Single to double-knob with no height shift

From sulci with a single-knob configuration to sulci with a double-knob configuration, with no hand-knob height shift.

		Wilcoxon	Spearman
L vs R	30	x	x
	40	✓	~
30 vs 40	L	~	x
	R	x	x

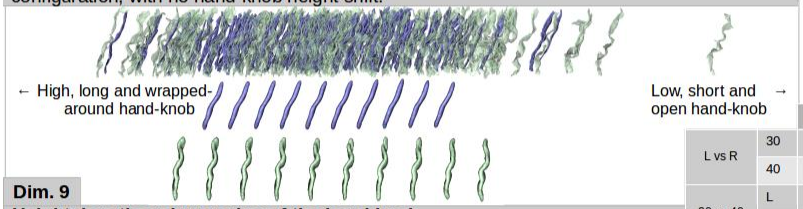

Dim. 9

Height, length and wrapping of the hand knob

From sulci with a higher, longer and more wrapped-around hand knob to sulci with a lower, shorter and less wrapped-around hand knob.

		Wilcoxon	Spearman
L vs R	30	x	x
	40	x	x
30 vs 40	L	x	~
	R	x	✓

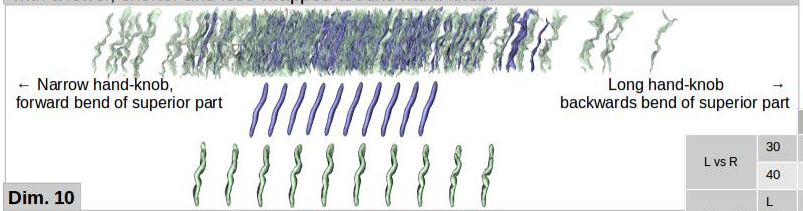

Dim. 10

Orientation of the upper part and length of the hand-knob

From sulci with a narrower hand-knob with a superior part bending forwards to sulci with a longer hand-knob with a superior part bending backwards.

		Wilcoxon	Spearman
L vs R	30	x	x
	40	~	~
30 vs 40	L	~	x
	R	x	x

9.2.11 Annex 3 : Analysis of the second-best mABC fine motor outcome classifier obtained at 30w PMA on the left hemisphere using sulcal shape features alone.

Two classifiers using sulcal shape features alone scored a tie in terms of ROC AUC for fine motor outcome classification. The one with the highest recall (right hemisphere, 40w PMA) was presented in the main section. Here is presented the analysis of the other classifier, obained at 30w PMA on the left hemisphere.

In order to address the best-scoring classifiers for fine motor outcome, the comparison for ROC and PR curves between the baseline classifier and the left hemisphere 30w PMA sulcal shape features' classifier is presented here.

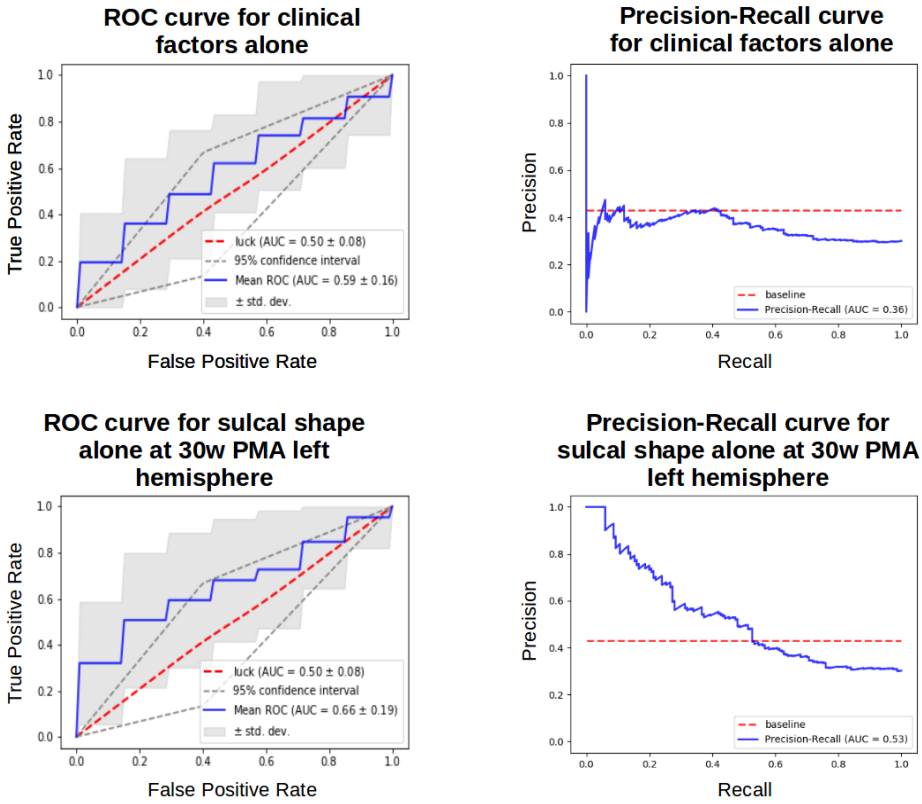

Supplementary Figure 3.1. ROC and PR curves obtained for clinical factors alone and sulcal shape factors alone at 30w PMA on the left hemisphere. Target: fine motor outcome

Using the different folds of the repeated stratified cross-correlation, we aggregated the coefficients attributed to each feature and generated the box-plot (Supplementary Figure 3.2).

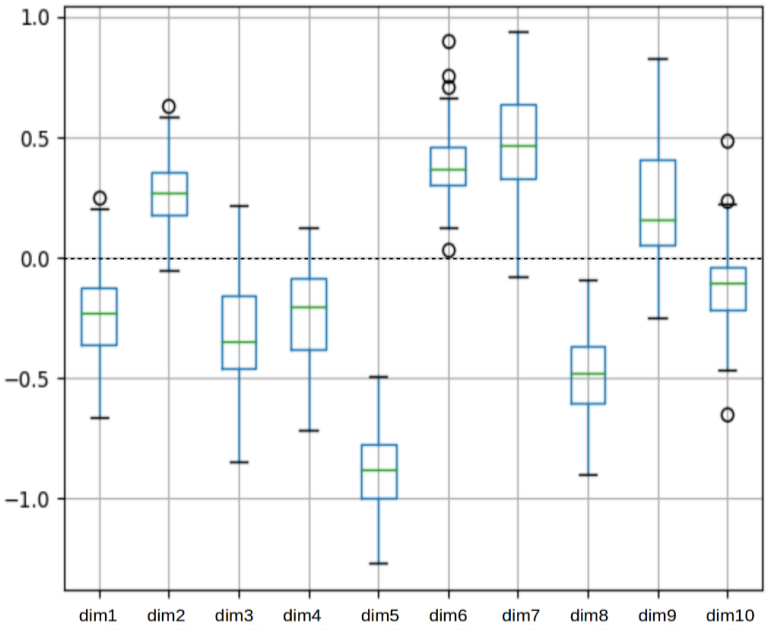

Supplementary Figure 3.2. Box plot of the coefficients attributed to each Isomap dimension during the cross validation for the fine motor outcome classification with sulcal shape factors alone at 30w PMA on the left hemisphere. Coefficients for the dimensions were obtained for each iteration of a 5-fold 10-times repeated stratified cross-validation training of the SVC for fine motor outcome. Dimension 5 weighted generally more than the other dimensions throughout this cross-validation.

The most weighted feature appeared to be dimension 5, represented in Supplementary Figure 3.3. Compared to right-handers, the 30w PMA left central sulcus of left-handers tended to have a more wrapped-around hand-knob.

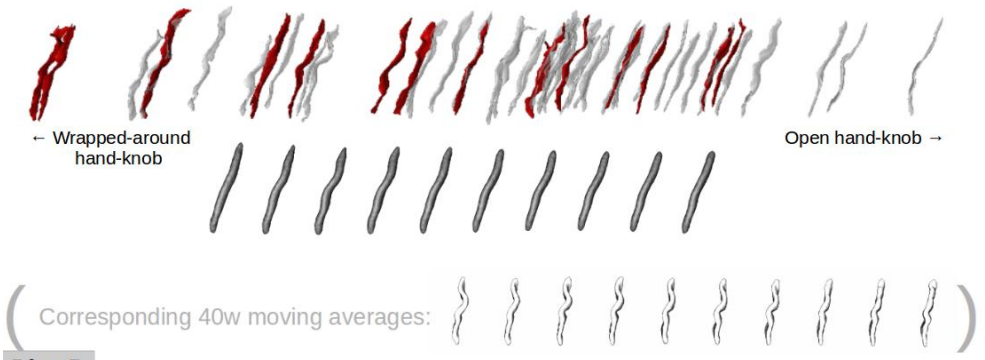

Supplementary Figure 3.3. Representation of the dimension weighting the most for fine motor outcome classification using sulcal features at 30w PMA in the left hemisphere. The sulcal projections of the subjects used in the classification were represented (good outcome in grey, poor outcome in red), as well as the age-specific moving averages (in dark grey). The 40w PMA moving averages (in white) are shown for shape interpretation purposes.

9.3 TRANSITION

This article stems from the adaptation of an originally adult-oriented shape characterization pipeline for the application to a longitudinal developmental context. As a result, ten different shape features representative of the cohort's variability of the central sulcus have been identified, and they have additionally been tested for consistency of inter-age shape evolution, inter-hemispheric asymmetries and predictive ability on fine motor outcome at 5 years of age. We characterized the sulcal shape variability at 30 and 40w PMA, we observed relevant trends in the shape encoding of 8 out of the ten shape features at both ages, and we captured one asymmetrically expressed shape feature by age-group. This led to a specific investigation of the traits uncorrelated between ages, and to speculate on developmental events inducing a loss of asymmetry between 30 and 40w PMA on the dimension which only captured asymmetry at 30w PMA and inducing later-than-30w-PMA-encoding of the specific shape features which showed low correlations between the two ages.

I was the first investigator of this original research article, and my contributions to the adaptation of the originally adult-oriented shape characterization pipeline have been detailed in Chapter II. I have thereafter led the design and application of the prediction, with the valuable support of different team-members and collaborators from Utrecht. My supervisors monitored the advance of the experimental design. Discussions with machine-learning colleagues from my team helped me devise a rigorous approach to prevent from overfitting my data (special thanks to Louise Guillon, Clément Poiret and WenQi Shu-Quartier-Dit-Maire), and very importantly, discussions with clinical experts both from my team and from Utrecht allowed me to manipulate the data in a clinically relevant manner (special thanks to Sara Neumane, Hugo Peyre, Maria-Luisa Tataranno and Nuša Stopar). This was essential since I have no clinical formation and both the choice of relevant outcome measures, and the choice of clinical parameters were challenging in the absence of sufficiently similar previous studies to orient my decision. Besides, the 95% chance interval of the classifiers was added to my study thanks to a comment from one of its reviewers. I was delighted by this comment as the

reviewer not only signalled his doubt on the validity of my classifiers (which I also considered as not very convincing and addressed as such in the initial version) but also suggested a general idea on how to assess this chance interval. This required some additional thinking and implementation, but I am grateful to have had the opportunity to quantify the general relevance of these classifiers.

During the article, I argued that because of the small number of individuals in the cohort, I prevented from adjusting any parameter and that the resulting classifiers were therefore underfitted. This statement is erroneous: even though adjusting the parameters to optimize the classifiers' performances would have led to overfitting the data, it is incorrect to conclude that the data is underfitted because the parameter was left to default. It is probably underfitted, yet this should be confirmed by observing the behaviour of the classifier by varying the regularisation parameter.

In the end, although these classifiers did not yield sufficient results to be categorical on the matter of early sulcal encoding of later neurodevelopmental outcomes and adversities, they still suggested some relevance of sulcal pattern on the subject, which is a first step in the direction of using sulci as biomarkers in the developing brain. These classifications concluded my studies on the central sulcus, after which I chose to investigate another early developing fold of the human cerebral cortex: the Sylvian Fissure.

10 CHAPTER IV: EXPLORING THE EMERGENCE OF MORPHOLOGICAL ASYMMETRIES AROUND THE BRAIN'S SYLVIAN FISSURE: A LONGITUDINAL STUDY OF SHAPE VARIABILITY IN PRETERM INFANTS. *(FULL-LENGTH ARTICLE 3)*

10.1 CONTEXTUALIZATION

After the in-depth study of the central sulcus's shape, the sylvian fissure was an excellent second candidate to study the development of cortical folding pattern. Once again, it is an early encoded fold which is already sufficiently developed at 30w PMA to consider a longitudinal shape assessment. Contrarily to the central sulcus, the sylvian fissure may display branches, which makes it slightly more complex to define a labelling permitting rigorous inter-subject comparison, but it still is a fold with little labelization error margins compared to many others. Additionally, some of its variability in shape has been previously reported through its inter-hemispheric asymmetries at different ages, including in the preterm (Dubois et al., 2010; Kersbergen et al., 2016), inciting me to quantify its shape variability in more details. Moreover, looking into the sylvian fissure allowed me to complement my first study about a fold fathered by the sulcation process (the central sulcus) with a fold fathered by the opercularization process (the sylvian fissure).

The shape characterization of the sylvian fissure at 30 and 40w PMA, following the same methodology as the central sulcus, led to a fist poster presentation at the OHBM 2020 virtual conference. The important asymmetries captured in this first step led me to question the patterning implications of opercularization on the perisylvian region. In parallel, I was appealed by exploring the relevance of the shape characterization pipeline on more complex sulcal objects than single, mostly mono-branched folds. This led me to conceptualize a sulcal extraction method which would allow me to assess consistent region-wise inter-individual variability in pattern around the sylvian fissure rather than classical sulcus-wise pattern variability, at 40w PMA.

Already by studying the sylvian fissure, and even more so when assessing the asymmetries around it, I joined the research efforts to characterize anatomical asymmetries of regions functionally linked to language. After validating the region-wise approach on sulcal elements from the general vicinity of the sylvian fissure and defined as the perisylvian region, I therefore decided to adapt this new method to assess the region-wise variability of sulci around the functionally-defined Broca's area, by looking into sulcal objects from the inferior frontal region.

The combination of pattern asymmetry considerations in the sylvian fissure, perisylvian region, and inferior frontal region, led to the redaction of the following full-length original research article, intended for submission to the Cerebral Cortex journal.

10.2 Full-length article

10.2.1 Header

10.2.1.1 Title

Exploring the emergence of morphological asymmetries around the brain's sylvian fissure: a longitudinal study of shape variability in preterm infants.

10.2.1.2 Authors

de Vareilles H[1], Rivière D[1], Pascucci M[1], Sun Z[1], Fischer C[1], Leroy F[1,2], Tataranno ML[3], Benders MJNL[3], Dubois J[4,5]*, Mangin JF[1]*

10.2.1.3 Affiliations

1: Université Paris-Saclay, NeuroSpin-BAOBAB, CEA, Gif-sur-Yvette, France
2: Université Paris-Saclay, NeuroSpin-UNICOG, Inserm, CEA, Gif-sur-Yvette, France
3: Utrecht University, University Medical Center Utrecht, Department of Neonatology, Utrecht, the Netherlands
4: Université de Paris, NeuroDiderot, Inserm, Paris, France
5: Université Paris-Saclay, NeuroSpin-UNIACT, CEA, Gif-sur-Yvette, France
* co-last authors

10.2.1.4 Funding

The project was supported by the Médisite Foundation and the IdEx Université de Paris (ANR-18-IDEX-0001), the European Union's Horizon 2020 Research and Innovation Programme through Grant Agreement No. 785907 \& 945539 (HBP SGA2 \& SGA3), by the FRM through grant DIC20161236445, the ANR through the grants ANR-19-CE45-0022-01 IFOPASUBA , the ANR-14-CE30-0014-02 APEX the ANR-20-CHIA-0027-01 FOLDDICO

10.2.1.5 Acknowledgements

The authors thank Y. Leprince, L. Perus, L. Guillon and W. Shu-Quartier-Dit-Maire for their participation in discussions about this study.

10.2.2 Abstract

Brain folding patterns vary within the human species, but some folding properties seem to be common across individuals. Among them, the previously-reported asymmetry of the sylvian fissure between hemispheres may be related to the leftward functional lateralization for language processing. Contrarily to the other folds of the brain (sulci), the sylvian fissure develops through the process of opercularization, with the frontal, parietal and temporal lobes growing over the insular lobe. In this study, we investigated refined shape features of the sylvian fissure and their longitudinal development in 71 extremely preterm infants (mean gestational age at birth: 26.5 weeks) imaged once before and once at term-equivalent age (TEA). We additionally assessed asymmetrical sulcal patterns at TEA in two regions neighbor to the sylvian fissure: the perisylvian and inferior frontal regions. While reproducing state-of-the-art observations of strong asymmetries, our results suggested an early encoding of its main asymmetrical shape features. Regarding the perisylvian and inferior frontal regions, the asymmetrical global shape features that we observed seemed representative of a left-hemisphere advance in opercularization, contrasting with the previously-reported right-hemisphere advance in sulcation. This added novel insights about the processes governing early-life brain folding mechanisms, potentially linked to the development of language-related capacities.

10.2.3 Introduction

Compared to other species, one of the specificities of the human brain lies in its anatomical asymmetries, implying a different macroscopic configuration of the left and right hemispheres. Not all asymmetries which have been reported in the human are human-specific (Amiez et al., 2021), yet a consensus is reached on some of them, including the Yakovlevian torque (Hou et al., 2019; frontal forward warping of the right hemisphere and dorsal backwards warping of the left hemisphere), asymmetries in the Sylvian Fissure's shape (Hou et al., 2019), and a depth asymmetry in the superior temporal sulcus (STS) (Leroy et al., 2015).

These human-specific asymmetries have been described through the

study of cortical folds (including fissures and sulci) since these objects can be reliably identified for comparisons within and between individuals. In particular, in the adult, the Sylvian Fissure has been reported to be shorter and more anteriorly bending in the right hemisphere than the left one (Lyttleton et al., 2009), and right-hemisphere STS have been reported to be deeper than left ones in their middle part, under Heschl's gyrus (Leroy et al., 2015), with specific relationships to genetic constraints (Le Guen et al., 2019). These asymmetries are considered to be linked to the functional lateralization of brain networks.

The most renown functional lateralization of the human brain is the one observed for language processing, which can be roughly dissociated between a ventral stream for speech perception and a dorsal stream for speech production (Hickok and Poeppel, 2007), both involving the perisylvian regions (brain regions located around the Sylvian Fissure). The primary auditory cortex is located in Heschl's gyrus, within the temporal wall of the Sylvian Fissure. Just behind, the *planum temporale* ensures the spectrotemporal analysis of sounds. Posterior to the *planum temporale* is Wernicke's area, responsible for speech comprehension. Also involved in speech production are Broca's area, located in the inferior frontal gyrus of the left hemisphere, and the parieto-temporal region, just along the posterior extremity of the Sylvian Fissure, which ensures the transformation of sensory encoding of sounds for the motor system. The language ventral stream has been reported to show mostly bilateral activations across hemispheres, while the dorsal stream presents a strong leftward functional asymmetry (Hickok and Poeppel, 2007): about 90% of the general population processes word generation through the left hemisphere (Knecht et al., 2000). The relationship between this strong functional lateralization and the anatomical asymmetries of the perisylvian structures are still under investigation (Sprung-Much et al., 2021).

In parallel, correlations between functional specialization and anatomical properties have already been demonstrated using sulcal pattern as an anatomical landmark (Mangin et al., 2015; Jiang et al., 2021), with recent studies showing interesting population-wise tendencies. For example, an asymmetrical configuration of either the anterior cingulate cortex (inducing a more prominent paracingulate

sulcus in the left hemisphere than in the right), or the inferior frontal sulcus's pattern (with one continuous and one interrupted, interdependently of the hemisphere) seem to be related to a better inhibitory control in children and adults (Tissier et al., 2019). The central sulcus has been reported to show shape asymmetries related to handedness including height considerations about the "hand-knob" (a specific bump of the central sulcus; Sun et al., 2012), and the height of this "hand-knob" seems intertwined with the height of the hand functional activation (Sun et al., 2016). This same study demonstrated anatomo-functional links between sulcal patterns around the Sylvian Fissure and a task related to language: the location and size of functional activations induced by silent reading are linked to the pattern of sulci in the precentral gyrus, and along the superior temporal sulcus, depending on the pattern of the neighboring sulci. This leads us to consider that shape asymmetry of folds around the Sylvian Fissure might carry out valuable links to function and should be investigated further, including by getting a finer understanding of its early-life development.

This leads us, in a first time, to clarify the developmental phenomenons leading to the formation of the Sylvian Fissure and its neighboring sulci. The Sylvian Fissure forms through the process of opercularization: differential growth of the frontal, parietal and temporal cortices and underlying white matter, compared to the insular cortex, which induces the growth of these regions over the insula (Kostović et al., 2019). On the reverse, sulci surrounding the Sylvian Fissure form through the classical sulcation process, supposed to rely on several mechanisms among which the larger expansion of cortical grey matter compared to white matter (Llinares-Benadero et al., 2019). In terms of relative chronology, opercularization starts earlier than sulcation, as the start of invagination of the insula happens as soon as 14 to 16 weeks of gestational age (w GA), while the first sulci to form first emerge around 22w GA in fetuses (Habas et al., 2012). In terms of anatomical asymmetries throughout development, the right hemisphere shows an advance in sulcation, with an approximate two weeks lag with the left hemisphere (Dubois et al., 2008, Habas et al., 2012).

Going back to language-related perisylvian regions, the Sylvian

Fissure's asymmetries reported in the adult have been observed as being already present in childhood from 7 years of age and adolescence, and to increase with age (Sowell et al., 2002). Asymmetries both in the Sylvian Fissure and the STS have been accounted for in the infant brain (Hill et al., 2010; Glasel et al., 2011), and to a certain extent in the preterm (Dubois et al., 2008; Dubois et al., 2010; Kersbergen et al., 2016) and fetal brain (Habas et al., 2012). This raises questions on how these asymmetries emerge in the very young brain. Studying folding mechanisms in the preterm is then particularly interesting as it allows for longitudinal analyses including developmental stages happening before normal-term birth without being impacted by brain modifications induced by birthing (Lefèvre et al., 2016). It should still be noted that prematurity has been linked to altered gyrification (Bouyssi-Kobar et al., 2016; Dubois et al., 2019).

In this context, the purpose of this study was to investigate developmental asymmetries of the Sylvian Fissure and regions around it, through MRI acquisitions of a cohort of infants born extremely premature and imaged longitudinally at two ages, once before full-term birth and once at term-equivalent age. To explore regions that anatomically match the aforementioned language-related regions, we decided to focus on three folding pattern proxies, focused on the Sylvian Fissure, the perisylvian region, and the inferior frontal region. The Sylvian Fissure and perisylvian region proxies (defined as the congregation of sulci from the inferior frontal, inferior parietal and superior temporal lobes neighboring the Sylvian Fissure, belonging to a series of different functional regions) have been included in our study in particular to investigate the process of opercularization which modulates the whole folding patterns surrounding the Sylvian Fissure. Additionally, we included the inferior frontal region (selecting sulci from the inferior frontal gyrus) because of its anatomical correspondence to Broca's region in the left hemisphere and thus its specific relevance in language lateralization.

10.2.4 Material and methods

10.2.4.1 Cohort

The present study was conducted on a longitudinal retrospective cohort of 71 infants born extremely preterm (gestational age at birth: 26.5 ± 1.0 weeks, range: 24.4 – 27.9 weeks) admitted in the intensive care unit of the Wilhelmina Children's Hospital in Utrecht (the Netherlands) between June 2008 and March 2013 (Kersbergen et al., 2016). Clinical specificities about this cohort are detailed in Table 1. Approval for this study was granted by the medical ethics committee.

Table 1. Perinatal clinical characteristics of the study participants

Characteristics	*Mean ± Standard deviation (range) or N (percentage)*
Perinatal clinical characteristics	
Sex, male	36 (51%)
Gestational age at birth (weeks)	26.5 ± 1.0 (24.4 – 27.9)
Birth-weight z-score	0.4 ± 0.8 (-2.5 – 1.8)
Presence of severe IVH (grade 3 or 4): number of infants	8 (11%)
Presence of broncho-pulmonary dysplasia: number of infants	20 (39%)
Age at MRI scans	
PMA at early acquisition (weeks)	30.7 ± 0.9 (28.7 – 32.7)
PMA at term-equivalent age acquisition (weeks)	41.2 ± 0.6 (40.0 – 42.7)

10.2.4.2 MRI acquisitions

Each subject underwent two MRI acquisitions, one around 30 weeks of post-menstrual age (w PMA) (30.7 ± 0.9, range: 28.7 - 32.7) and one around 40w PMA (41.2 ± 0.6, range: 40.0 - 42.7) corresponding to term equivalent age (TEA). The images were acquired on a 3-Tesla MR system (Achieva, Philips Medical Systems, Best, The Netherlands). The protocol included T2-weighted imaging with a turbo-spin echo sequence in the coronal plane (MRI at ~30w PMA: repetition time (TR) 10,085 ms; echo time (TE) 120 ms; slice thickness 2 mm, in-plane spatial resolution 0.35 × 0.35 mm; MRI at ~40w PMA: TR 4847 ms; TE 150 ms; slice thickness 1.2 mm, in-plane spatial resolution 0.35 × 0.35 mm).

10.2.4.3 Image preprocessing

The MRI brain images underwent preprocessing in order to reconstruct the 3D volumes of the brain as described in (Kersbergen et al., 2016, de Vareilles et al., 2022). The T2-weighted images were first of all segmented in three classes: cerebrospinal fluid, unmyelinated white matter and grey matter using supervised voxel classification (Moeskops et al., 2015). Using the BrainVISA software (https://brainvisa.info) and combining the Morphologist (publicly available) and BabySeg (internal toolbox adapted for infant brain segmentation) toolboxes, we were able to reconstruct the inner cortical surface of both hemispheres and extract items depicting the sulci. A summary of the segmentation pipeline for sulcal extraction is presented Figure 1.

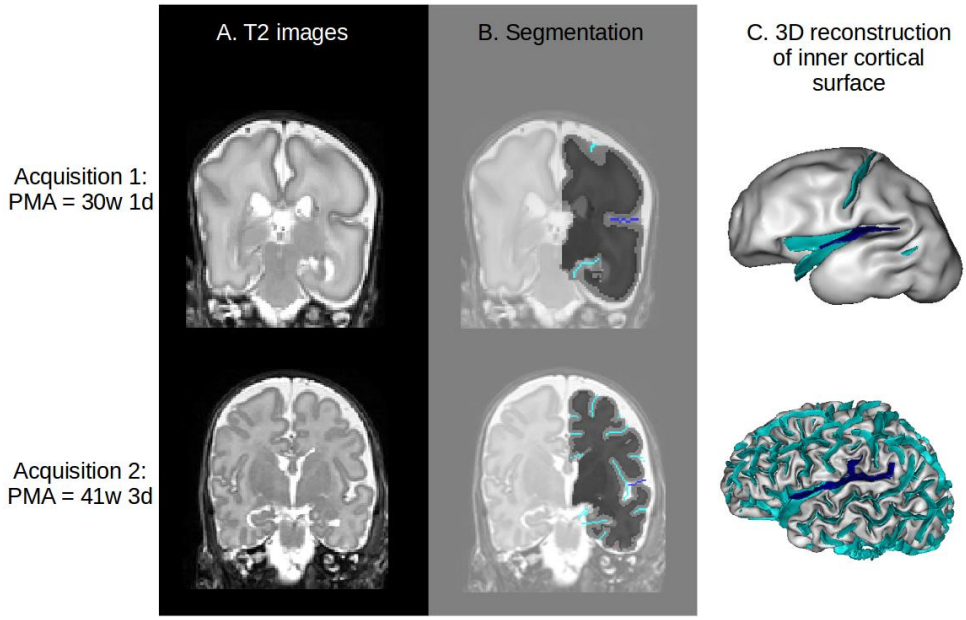

Figure 1. Illustration of the segmentation pipeline. A: Sample T2-weighted coronal MRI. B: Corresponding segmentation on the left hemisphere, showing the boundary between white (dark grey) and grey (light grey) matter. The sulci are represented in cyan, except for the Sylvian Fissure, in deep blue. C: Resulting reconstruction of inner cortical surface. Deep blue ribbon: Sylvian Fissure (main branches), cyan ribbons: other sulci.

10.2.4.4 Sulcal extraction and labelization

Based on the white matter segmentation and the resulting reconstruction of the inner cortical surface, sulci were materialized as the surface created by the set of voxels equidistant to the walls of two adjacent gyri (Mangin et al., 1995). Once extracted, the sulci were automatically labeled using a Bayesian pattern recognition strategy (Perrot et al., 2011). Finally, the labelling was manually checked and corrected when necessary by one of the authors (HV) using open access software Anatomist (Rivière et al., 2022). In particular and as detailed below, we focused on the labelling of the 1) Sylvian Fissure and its branches, 2) sulci of the perisylvian region, and 3) sulci of the infero-posterior region of the frontal lobe (supposed to correspond, at the anatomical level, to Broca's region defined functionally).

10.2.4.4.1 Selection of anatomical landmarks for the Sylvian Fissure

In order to study the development of the Sylvian Fissure longitudinally, our aim in the selection of its anatomical landmarks was to capture comparable proxies at 30 and 40w PMA. For this reason, we excluded the anterior part of the Sylvian Fissure, which was not reliably extracted from 30w PMA brain reconstructions. Then, we selected the Sylvian fissure's landmarks to include: 1) the main part of the fissure, ascending from the insula, which was given a specific label, 2) the branches stemming from this main part that appear posteriorly to the central sulcus, under the condition that they are anchored at mid-depth or deeper of the main path of the fissure and that they reach the surface of the brain to create a visible sulcus, and 3) ramifications of the main part of the fissure appearing posteriorly to the postcentral gyrus, either on the parietal or temporal lobe. The other branches of the Sylvian Fissure which do not meet the criteria (such as the anterior branches diving in the inferior frontal gyrus, the sulci buried in the insula, and the buried sulcus in the planum temporale) were labeled and considered independently from the Sylvian Fissure in this study. These criteria were chosen to capture analogous proxies for the Sylvian Fissure at 30 and 40w PMA since the excluded sulci were absent from 30w PMA images, while early post-central ramifications were occasionally captured. Figure 2 illustrates our choice of Sylvian Fissure proxy definition in preterm infants at 40w PMA.

10.2.4.4.2 Selection of anatomical landmarks for the perisylvian region

In order to study the sulcal specificities around the Sylvian Fissure, we first considered selecting all sulci neighboring the sylvian fissure, but this approach was problematic because a number of sulci neighboring the sylvian fissure reach farther than the perisylvian region (such as the precentral, central and post-central sulci for example). Moreover, the sulcal pattern variability sometimes led sulci which do not usually neighbor the sylvian fissure to extend up to the perisylvian region. We therefore chose to include sulcal items based on their distance to the

sylvian fissure, by opting for an inclusion of probabilistically pruned point clouds of neighboring sulci, with the pruning weighted by the distance to the Sylvian Fissure. First of all, to extract sulcal elements defining the perisylvian region, we defined a list of labels which can be assigned to any sulcus susceptible to neighbor the Sylvian Fissure (e.g. inferior frontal sulcus, intraparietal sulcus, superior temporal sulcus; see the complete list of sulci labels in Annex 1). The subsequent steps were carried out independently for each individual and each hemisphere, after affinely registering the brains to the Talairach space.

First, we extracted the sulci corresponding to the predetermined list as a point cloud. We computed a 3-D distance map capturing the Euclidean distance to the Sylvian Fissure's main part (even though we had excluded the Sylvian Fissure from the point cloud of selected sulci). We used a binomial draw on each of the cloud points, using a Gaussian probability *p* based on its distance to the Sylvian Fissure's main part. Let X be a point from the point cloud, p(X) its probability of being selected and d(X) its distance to the Sylvian Fissure. We defined p(X) as:

$$p(X) = \exp(\frac{1}{2\sigma^2} * d(X)^2)$$

with σ^2 the variance (i.e. σ the standard deviation), an adjustable constant to constraint the size of the region selected. The σ^2 parameter was adjusted visually, after examination of the point cloud resulting of a range of different values on two given subjects, with considerations about the ratio of relevant versus irrelevant sulci captured, and validated by visual examination of the resulting point clouds of the whole cohort.

In the perisylvian study, it resulted in $\sigma^2=80mm^2$ ($\sigma=8.94mm$).

This resulted in a point cloud sampling the sulci neighboring the Sylvian Fissure based on their distance to its main part. These steps are summarized on Figure 2. This pipeline was only applied to 40w PMA brain reconstructions because of insufficient sulcation at 30w PMA.

10.2.4.4.3 Selection of anatomical landmarks for the inferior frontal region

The method to focus more specifically on the inferior frontal region was similar to that used for the perisylvian region, but was operated separately and differed on two aspects. First, the initial sulcus list was centered around the area, therefore including the anterior branches of

the Sylvian Fissure (horizontal ramus, ascending ramus, diagonal sulcus), the inferior frontal sulcus and the inferior and intermediary part of the precentral sulcus. These are classically considered as the anatomical landmarks of Broca's area, delineating the pars orbitalis, the pars triangularis, and the pars opercularis. Secondly, the sampling of the point cloud was based on the most anterior point of the posterior Sylvian Fissure, as it is the junction of its anterior branches in most classical configurations (this point was automatically within the points of the Sylvian Fissure based on their spatial coordinates), rather than the whole main part. Once again we selected σ^2 by hand after visual examination, resulting in $\sigma^2=240mm^2$ ($\sigma=15.49mm$). These steps are illustrated on Figure 2. Once again, this pipeline was only applied to 40w PMA brain reconstructions because of insufficient sulcation at 30w PMA.

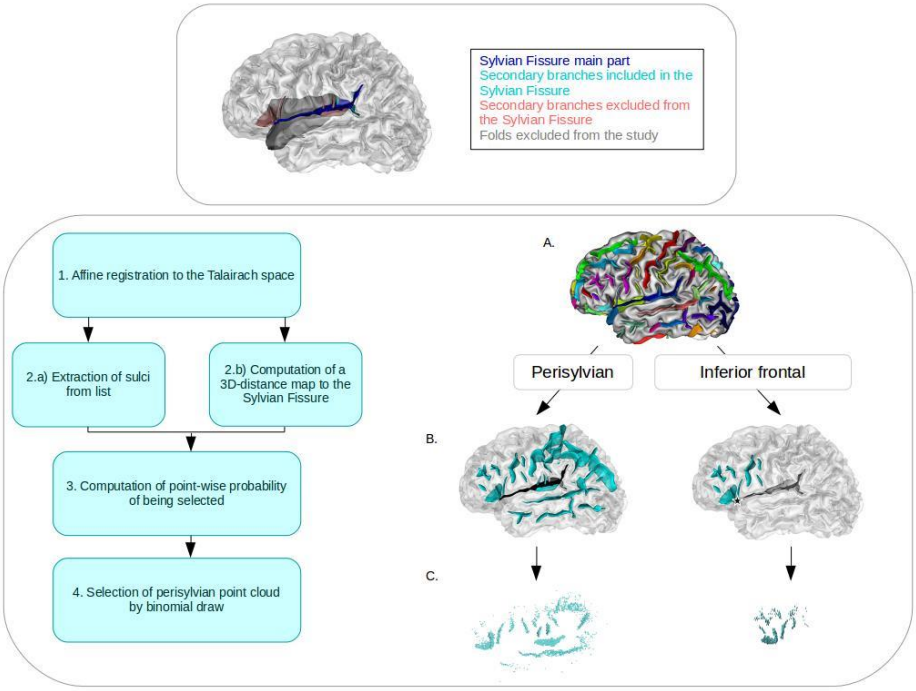

Figure 2. Illustration of the different proxies studied on the left hemisphere of a preterm infant at 40w PMA. Top: Definition of the sulcal elements included and excluded from the Sylvian Fissure proxy. Deep blue: main part, cyan: included secondary branches, pink: excluded secondary branches, grey: folds excluded from the study. Bottom: Description of the method for selection of perisylvian and inferior frontal region proxies. Left: Summary of steps to generate the point cloud of a subject on a given hemisphere. Right: Illustration on an infant's left hemisphere: A. Full hemisphere with labeled sulci, B. Sulci retained based on inclusion list. Cyan: sulci included, black (sulcal element or star): element of the Sylvian Fissure used to create the distance map, white: elements of the Sylvian Fissure ignored for the distance map computation, C. Resulting point cloud and probabilistic selection of points based on their distance to the relevant Sylvian Fissure element.

10.2.4.5 Pipeline for shape characterization

For each sulcal proxy of this study (even the complex ones relying on point clouds), we used a similar methodology for shape characterization as the one used in a previous study of infants' central sulci (de Vareilles et al., 2021), derived from a method previously applied to adults (Sun et al., 2016). As detailed below, this included the following steps: folding pattern proxies registration, computation of shape dissimilarity matrix and dimensionality reduction.

First, every subjects' brain was affinely aligned into the Talairach space, and after extracting the relevant folding pattern proxies from both hemispheres (referred to as proxies in the following), the right ones were mirror-flipped to be comparable to the left ones. In order to capture the shape variability from the whole cohort, a pairwise coregistration using the Iterative Closest Point (Besl & McKay, 1992) was applied to every pair of proxies.

For the perisylvian and inferior frontal region, the retained proxies presented too much shape variability for simple pairwise registration to ensure anatomical consistency: without further anatomical anchoring, proxies extracted from very dissimilar brains could achieve optimal registration while matching together incompatible sulci. Therefore, we chose to add items derived from the main part of the Sylvian Fissure exclusively for the registration step. For that matter, in the analysis of perisylvian region, we added the whole Sylvian Fissure in the point clouds for the registration steps. In the analysis of inferior frontal region, including the whole Sylvian Fissure would have driven the registration based on its posterior part (which is very large compared to the inferior frontal region proxy), while we were interested in matching the anterior parts of the Sylvian Fissure between subjects. We therefore included only an anterior subpart of the Sylvian Fissure, which we selected with the same method as the original point cloud, but with σ^2=480mm^2 (σ=21.91mm), in order to ensure that this bigger sulcal element would be consistently registered between subjects. As a result, the registrations were computed with point clouds obtained by including at least a part of the Sylvian Fissure in addition to the sulci list be-

fore sampling, and the corresponding transformations were then applied to the original point clouds, which did not include the Sylvian Fissure (see Sup. Fig S1).

After this step, anatomically consistent pairwise registrations of the initial proxies were achieved, which allowed us to compute the residual Wasserstein distances after coregistration and to store them in a matrix. The resulting matrix therefore captured the shape dissimilarity of the cohort but was of high dimension $N_{items} \times N_{items}$ with N_{items} the number of proxies considered (N_{items}= 71 subjects × 2 hemispheres × number of acquisitions). As the Sylvian Fissure folds very early on during brain development, its shape was characterized longitudinally, including the proxies from both 30 and 40w PMA acquisitions (N_{items} = 71 subjects × 2 hemispheres × 2 acquisitions = 284). On the contrary, folding patterns of the perisylvian and inferior frontal regions are almost not visible at 30w PMA, so the shape of the corresponding proxies was investigated exclusively at 40w PMA (N_{items}= 71 subjects × 2 hemispheres = 142).

The Isomap algorithm (Tenenbaum et al., 2000) was then applied for dimension reduction, resulting in N_{dim} dimensions capturing the main shape variability from this matrix. This pipeline is summarized in Figure 3. The relevant number of dimensions *d* as well as the number of nearest neighbors *k* retained for the Isomap algorithm were determined according to the methodology developed for the central sulcus in infants (see de Vareilles et al., 2021, Annex 1). For the Sylvian Fissure, the resulting parameters were $d = 6$ and $k = 7$, for the perisylvian region, they were $d = 10$ and $k = 7$, and for the inferior frontal region, $d = 8$ and $k = 7$.

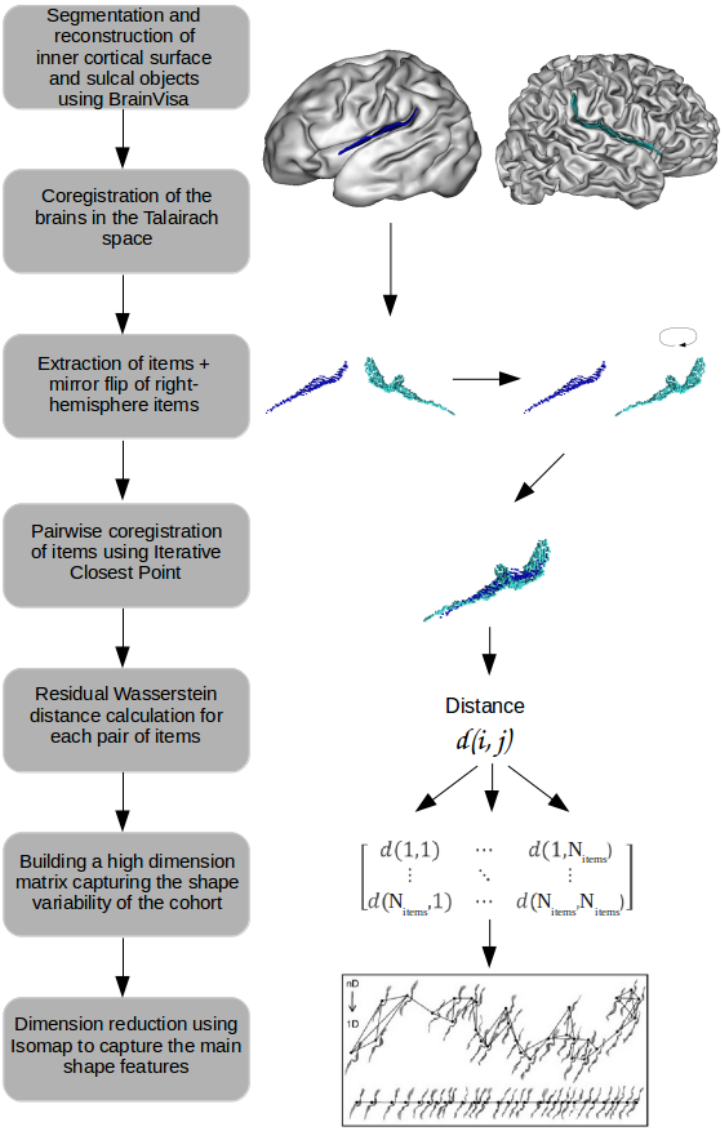

Figure 3. Summary of the general pipeline for shape characterization, illustrated on a left hemisphere 30w PMA Sylvian Fissure proxy (deep blue) and a right hemisphere 40w PMA Sylvian Fissure proxy (cyan).

10.2.4.6 Correction for discrepancies in age at MRI

Even though the subjects were aimed to be imaged at the same age (either around 30w or 40w PMA), there was some age differences between the subjects (up to 4 weeks), which might have an impact on the folding shape given the considered periods of development. Therefore, before any additional analysis, we tested if some of the shape variability we captured was linked to the infant's age by computing the Pearson correlations between positions of each folding pattern proxy on the isomap dimensions and the infants' age at MRI, combining left and right folding pattern proxies, as presented in Sup. Table S1 (for the Sylvian Fissure, this test was conducted separately for the 30w and 40w PMA groups).

To prevent from considering effects which could be due to this age difference as intrinsic shape variability, we corrected all of the positions on isomap dimensions for age at MRI by considering the residual positions r_n as the shape characteristics of interest in the following numerical – but not visual – analyses (referred to as Isomap positions corrected for PMA). Such corrected positions r_n were computed by solving the following linear model, for the 30 and 40w PMA groups independently:

$$d_n(subj, hemisphere) = \alpha_n \times PMA(subj) + \beta_n + r_n(subj, hemisphere)$$

with d_n the raw position of the folding pattern proxies on the n^{th} dimension of the Isomap, *PMA* the post-menstrual age at MRI, α_n and β_n constants estimated by the model.

We did not apply this correction to the visualization results, since they were intended to enable us to decipher the overall shape variability captured by the isomap algorithm (even if some of that variability was relayed by age differences).

10.2.4.7 Analyses and visualization of inter-hemispheric asymmetries

As the main aim of this study was to characterize the inter-hemispheric asymmetries of folding patterns, for each proxy, we focused on the dimensions discriminating left and right hemispheres, out of the N_{dim} dimensions capturing the shape variability. Only dimensions showing a statistically significant Wilcoxon signed-rank test between left and right folding pattern proxies (after Bonferonni correction) are detailed.

For the analysis of the Sylvian Fissure (1), the Wilcoxon signed-rank tests were applied separately to the 30w and 40w PMA proxies; we additionally tested for Spearman correlations between the positions of 30w PMA and 40w PMA proxies on the dimensions that appeared to be asymmetric at either 30 or 40w PMA.

Once the asymmetrical dimensions from the Isomap algorithm were identified, the visualization of the resulting shape features were obtained through the means of moving averages, which capture the local average shape of sulci at ten equidistant locations along the dimension (for details on their construction, see de Vareilles et al., 2021). For the longitudinal study of the Sylvian Fissure (1), for visualization purposes, moving averages were generated independently for 30w and 40w PMA proxies even though the Isomap dimension of interest was computed considering the two ages together. Moreover, to highlight the difference of distribution between left and right sulcal items, we computed graphs of left versus right hemisphere distribution along the dimension, through the means of kernel density estimates. An example of sulcal projection with corresponding moving averages at both ages is presented on Figure 4 for the Sylvian Fissure, with a sample of left versus right hemisphere distribution graph at 40w PMA. In the following, only moving averages and distribution graphs (either for the left and right hemisphere proxies or for the 30w and 40w PMA proxies) will be presented to describe the isomap dimensions.

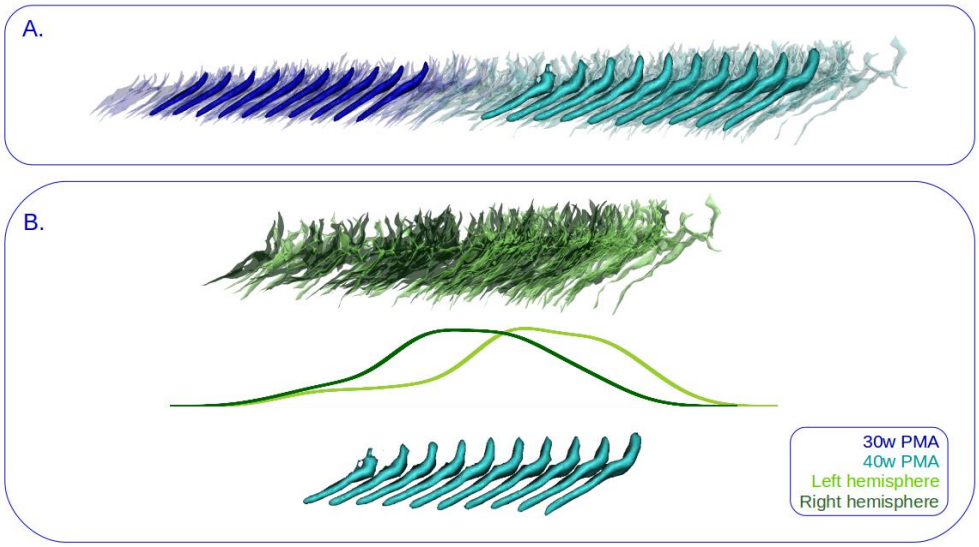

Figure 4. Example of folding pattern proxies and isomap representations. A) Visualization of the first isomap dimension of the Sylvian Fissure. Transparent: sulcal projections. Opaque: corresponding moving averages. B) At 40w PMA, representation of the left versus right hemisphere proxies distribution. Top: sulcal projection, Middle: left versus right hemisphere distribution graph, Bottom: moving averages. Deep blue: 30w PMA, cyan: 40w PMA, light green: left hemisphere, Dark green: right hemisphere.

10.2.4.8 Analysis of inter-region shape correlations

In order to assess whether the proxies' patterns captured in the different sulcal regions tended to match, we computed the Spearman correlations between the Isomap positions of the 40w PMA sylvian fissure, the perisylvian region proxy, and the inferior frontal region proxy. The p-values obtained were corrected according to the Bonferroni method.

10.2.5 Results

10.2.5.1 Longitudinal analysis of the Sylvian Fissure shape characteristics

The Sylvian Fissure's shape variability was investigated by considering the 30 and 40w PMA proxies together. Out of the 6 dimensions of interest, 3 showed asymmetries at both ages, and the 3 others showed asymmetries only at one age (cf. Sup. Table S2.A). Actually, the 3 dimensions showing consistent asymmetries across development showed significant correlations between the positioning of the 30 and

the 40w PMA proxies on both hemispheres (cf. Sup. Table S3). A reading key for the shape description of the Sylvian Fissure is presented on Figure 5, and the 6 isomap dimensions obtained on the Sylvian Fissure are represented on Figure 6. At both ages, left Sylvian Fissures tend to be longer, flatter or even bending backwards, and to branch more than right Sylvian Fissures. Additionally, compared to the right Fissures, the left Sylvian Fissures at 30w PMA showed a narrower knob in the posterior part and a shorter anterior part relatively to the posterior part. At 40w PMA exclusively, the left Sylvian Fissures showed a deeper knob than their right hemisphere counterparts.

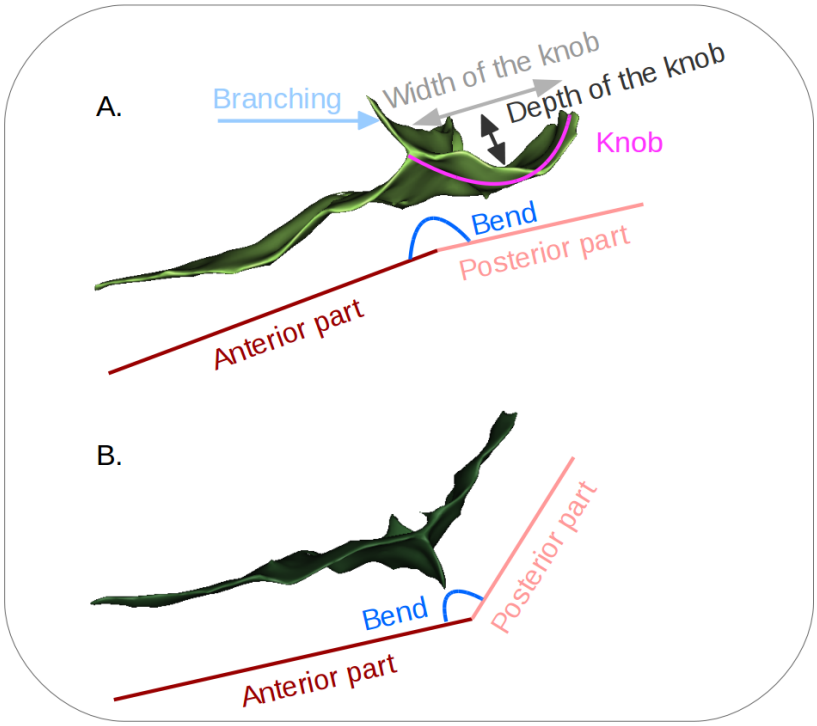

Figure 5. Reading keys for the shape of the Sylvian Fissure, presented on A. a 40w PMA left Sylvian Fissure and on B. a 40w PMA right Sylvian Fissure after mirror-flip. The posterior part may (as in A.) or may not (as in B.) contain a knob, which itself may occupy all of the posterior part (as in A.) or only part of it (not represented). In B. no knob is observed, thus the width and depth of the knob would be null.

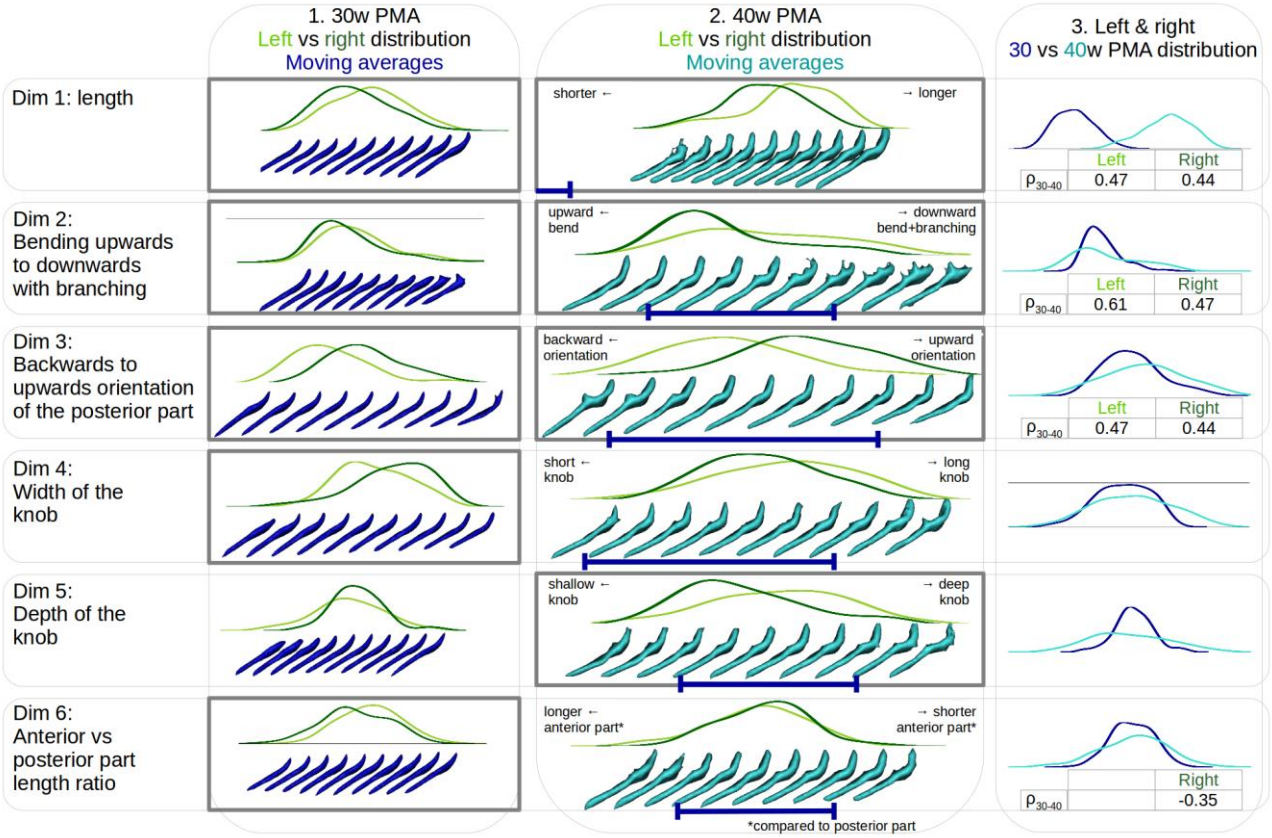

Figure 6. Description of each of the 6 isomap dimensions obtained on the Sylvian Fissure. Left versus right hemisphere distribution plots of the Sylvian Fissure are represented at 30w PMA (1) and 40w PMA (2), along with the respective moving averages. On the 40w PMA column (2), a deep blue interval was indicated under the 40w PMA moving averages to locate the span of the corresponding 30w PMA moving averages. 30w versus 40w PMA distribution plots are further superposed for the Sylvian Fissures, combining left and right proxies (3). In each column, bold contours indicate dimensions showing a statistically significant left vs right hemisphere proxies' positioning (for 1 and 2, see Sup. Table S2). When significant, the hemisphere-specific Spearman correlation ($\rho_{30\text{-}40}$) is indicated under the 30w versus 40w PMA position comparisons (3, see Sup. Table S3). Deep blue: relative to 30w PMA proxies, cyan: relative to 40w PMA proxies, dark green: relative to right hemisphere proxies, light green: relative to left hemisphere proxies.

10.2.5.2 Shape asymmetries of the perisylvian region at term-equivalent age

Out of the 10 dimensions relevant to describe the shape characteristics of the perisylvian region, only the first one was asymmetric, but very significantly (cf Sup. Table S2.B). This dimension is represented on Figure 7 (Fig 7.A), as well as a reading key for the perisylvian region (Fig 7.B). On this dimension, 1) left proxies show a higher density of sulci in the inferior frontal region than right ones, 2) left proxies have a narrower gap between the frontal and temporal lobes than right proxies, and 3) the temporo-parietal region of left proxies is less curvy than that of right ones. Incidentally, right perisylvian region proxies seem to have been drawn from hemispheres with curvier Sylvian Fissures while left ones from hemispheres with flatter Sylvian Fissures. This suspicion was visually confirmed by projecting the individual Sylvian Fissures on this perisylvian region's isomap dimension and generating the resulting moving averages (Fig 7.C): the dimension seems to capture a shift from an upward to a backward orientation of the Sylvian Fissure.

This was also confirmed by the significant negative correlation (cf Sup. Table S4) between the perisylvian region's dimension and the 40w PMA sylvian fissure's 1st (length), 3rd (backwards to upwards orientation of the posterior part), and 5th (depth of the supra-marginal knob) dimensions. The highest correlation was captured on the 3rd dimension.

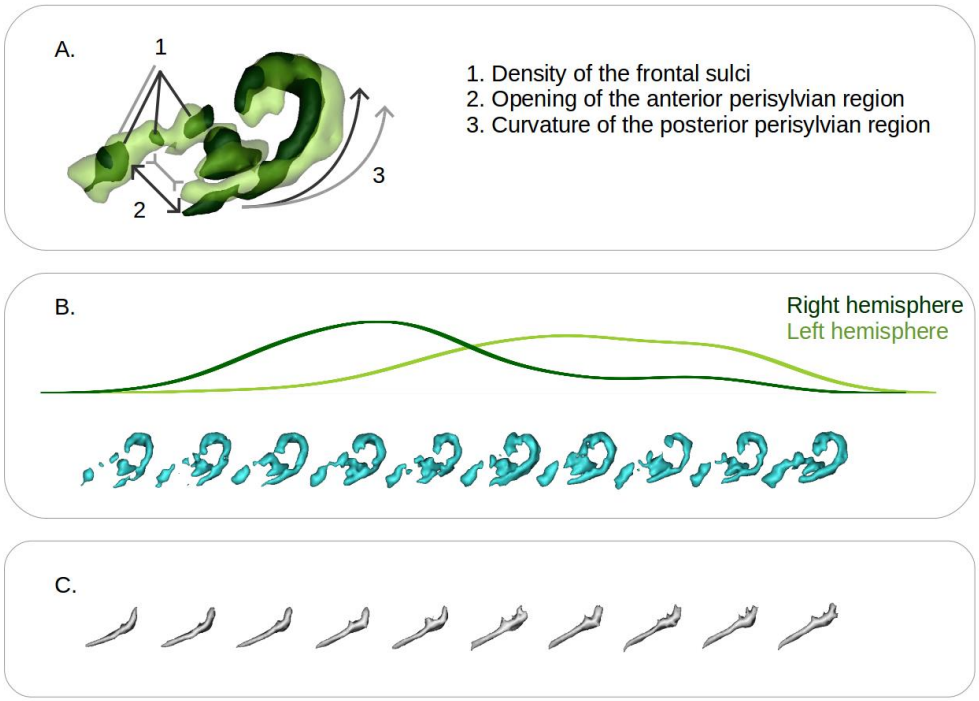

Figure 7. Representation of the first isomap dimension obtained for the perisylvian region at 40w PMA. A. Reading key for the perisylvian region, based on the projection of the two extreme moving averages (representative of the right hemisphere: dark green; representative of left hemisphere: light green) and illustration of their main differences, illustrative of the shape features captured (dark grey, representative of the right hemisphere, light grey, representative of the left hemisphere). B. Left (light green) versus right (dark green) hemisphere distribution plot of the perisylvian folding pattern proxies along with the corresponding moving averages (cyan). C. Moving averages obtained by projecting the Sylvian Fissures on the perisylvian region isomap dimension.

10.2.5.3 Shape asymmetries of the inferior frontal region at term-equivalent age

Again, out of the 8 dimensions highlighted in the analysis of the inferior frontal region shape characteristics, only the first dimension showed a statistically highly significant hemispheric asymmetry (cf Sup. Table S2.C), represented on Figure 8.

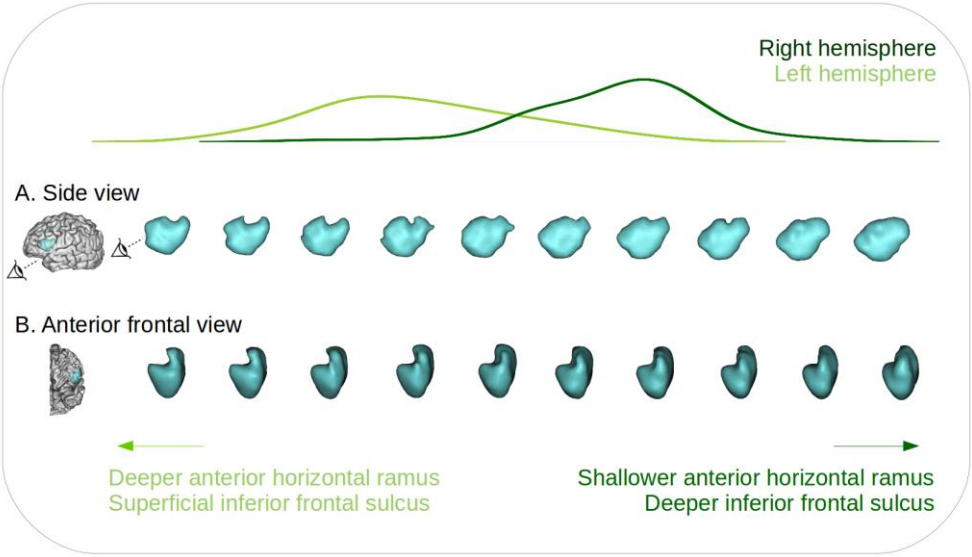

Figure 8. Representation of the first isomap dimension obtained for the inferior frontal region at 40w PMA. Left (light green) versus right (dark green) hemisphere distribution plot of the distribution of the inferior frontal region proxies, along with the corresponding moving averages, from a sideways view (A) and an anterior front-side view (B). Two eye indicators are represented in (A) to illustrate the orientation of the anterior frontal view (B).

The shape characteristics of this isomap dimension was quite complex to interpret probably because of the high inter-individual variability. Nevertheless, on the side view of this dimension, we observed a hole in the superior part of the moving averages which was predominant in the left hemisphere compared to the right. More importantly, on the anterior frontal view, we observed that the left hemisphere proxies presented a deeper inferior part of the moving average – capturing the anterior horizontal ramus – and a thinner upper part – capturing the anterior part of the inferior frontal sulcus – than their right counterpart, along with a different angle between the inferior and upper part of the moving averages, switching from acute on the left hemisphere to perpendicular or even slightly obtuse on the right one.

By correlating the inferior frontal region's Isomap dimension with the sylvian fissure's and perisylvian region's Isomap dimensions, we found statistically significant links with 4 dimensions of the sylvian fissure (the

1st, 2nd, 3rd and 5th; cf Sup. Table S4), the strongest one being with the 3rd dimension once again, encoding for the backward to upward orientation of the posterior part of the fissure. It showed a significant negative correlation with the perisylvian region dimension (ρ = -0.47, p-value = 5.10^{-9}).

10.2.6 Discussion

In this study, we investigated the early shape asymmetries of the Sylvian Fissure, the perisylvian region, and the inferior frontal region, in a cohort of extremely preterm infants. The Sylvian Fissure was investigated in a longitudinal manner, enabling us to qualify and quantify its early shape at 30w PMA and to evaluate the shape evolution dynamic until the age of normal-term birth. We then captured asymmetries in multiple interpretable shape features, and we could assess how early and how linearly they develop between 30w and 40w PMA. Around term-equivalent age, the analysis of the perisylvian region unveiled an important shape asymmetry between the hemispheres, which we suggest is due to an advance in opercularization on the left hemisphere compared to the right. Focusing on the inferior frontal region, we captured a novel strong hemispheric asymmetry that would deserve interest to better understand the development of functional lateralization for language processing.

10.2.6.1 Methodological considerations

Before detailing the different findings of this study and their implications, we will discuss some methodological choices. The scientific opportunity of studying the early development of the 30w PMA sylvian fissure led us to necessary arrangements for the definition of its proxy. We had to exclude the anterior part of the sylvian fissure (posterior to the precentral gyrus) and the circular sulcus of the insula because the limited progress of opercularization at 30w PMA prevented us from a reliable segmentation for longitudinal comparison.

We kept this focus in mind when choosing the sulci to preselect for the perisylvian region proxy at around TEA. We selected all the sulci neighboring the Sylvian Fissure from the frontal, parietal and temporal lobes, except for the sulci from the extreme anterior frontal and temporal cortices, then excluding the orbitofrontal sulci and the polar temporal

sulcus, in order to focus on the lateral view of the perisylvian region, and to focus on objects neighboring the Sylvian Fissure proxy, which did not extend anteriorly. Because of the variability of sulcal configurations represented in this cohort, we preferred to preselect a list of sulci and weight their inclusion by their distance to the sylvian fissure rather than including them whole. This allowed us to ensure that even in chaotic circumstances, we would efficiently capture the relevant sulci (close to the Sylvian Fissure), and that irrelevant sulcal elements would be sufficiently weighted out to be negligible. The same method was applied to select a relevant proxy for the inferior frontal region.

In addition to the list of sulci preselected before weighting their inclusion in the study, two choices impacted our final perisylvian and inferior frontal proxies selection: the Sylvian Fissure-derived items selected to weight the inclusion of sulci (the sylvian fissure's main branch for the perisylvian region, and the most anterior point of the sylvian fissure for the inferior frontal region), and the choice of σ. For the perisylvian region, we chose to retain only the main part of the Sylvian Fissure - and not the branch posterior to the central sulcus for example- in order to select an anatomical object with the lowest inter-individual variability. In the inferior frontal region, using only the most anterior point of the Sylvian Fissure proxy was optimal to capture gyri specifically around this marker, allowing for the inferior parts of the precentral gyrus and the relevant part of the inferior frontal sulcus to both be included, and with a similar weight.

In terms of σ^2, its manual selection was decided in order to ensure that each selected region would capture relevant landmarks: neither too few nor too many sulci selected, which would either result in an incomplete or a too broad depiction of the two regions assessed. For example, in the perisylvian region, we aimed at selecting only the parts of the superior and inferior temporal sulci which were adjacent to the Sylvian Fissure. These kinds of consideration led to a value of σ^2 which could be fine tuned within a range corresponding to this type of criterion. Yet, we argue that small variations of σ^2 would have led to very similar proxies and therefore equivalent results, and that big variations of σ^2 would change the specific focus of the study.

10.2.6.2 Asymmetries linked to the Sylvian Fissure's shape

Taking into consideration these methodological decisions, let us focus now on the findings we have reported. First of all, multiple shape features with hemispheric asymmetries were observed in the Sylvian Fissure, at 30w and 40w PMA. Three shape features captured asymmetries at both ages: the left Sylvian Fissure tends to be longer, flatter or curved backwards, and to branch more than their right counterparts, as soon as 30w PMA and ongoing at 40w PMA. Additionally, at 30w PMA only, the ratio between the lengths of the anterior part and the superior part of the fissure was smaller on the left than on the right side. And at 40w PMA only, the left Sylvian Fissure presented a deeper supra-marginal knob than the right one. The length asymmetry of the Sylvian Fissure (along with an asymmetry in surface area which we did not quantify here) has already been reported in multiple studies, either directly through the Sylvian Fissure (in the adult: Lyttleton et al., 2009; comparatively in the child, adolescent and adult: Sowell et al., 2002; in the preterm newborn: Kersbergen et al., 2016), or, for its posterior extent, through the length asymmetry of the *planum temporale*, an adjacent gyral structure (in the adult: Lyttleton et al., 2009; in the full-term newborn: Glasel et al., 2011; in the preterm newborn: Dubois et al., 2010). This length asymmetry is reported to be due to the left Sylvian Fissure extending both more anteriorly and more posteriorly than its right counterpart (Dubois et al., 2010), and to increase with age (Sowell et al., 2002). The curvature asymmetry has also previously been reported in the adult (Lyttleton et al., 2009; the posterior ascending ramus being more anterior in the right hemisphere), comparatively in the child, adolescent and adult (Sowell et al., 2002), in the full-term newborn (Glasel et al., 2011), and in the fetus (Habas et al., 2012; the posterior temporal operculum being more concave in the right hemisphere). To the best of our knowledge, the tendency of the left Sylvian Fissure to bend backwards and to branch more than the right one is previously unreported, all the more so in the developing brain. Nevertheless, the backward bend might be paralleled with a pattern-oriented study of the parietal opercular region (Steinmetz et al., 1990), which reported a configuration of the posterior part of the Sylvian Fissure – only observed in the left hemisphere – without a posterior ascending ramus, suggesting a flat or bending backwards Sylvian Fissure.

Interestingly, it should be noted that these three shape features capturing asymmetries at both 30 and 40w PMA are the only ones that showed significant positive correlations between the two ages, suggesting an early asymmetry encoding and a development according to the early shape predisposition.

We further observed two asymmetries encoded only at 30w PMA: the width of the knob, and the ratio between the anterior part of the Sylvian Fissure and its posterior part. These seem to encode transient shape encoding differences and we suggest that they might reflect differences in developmental trajectories between left and right hemisphere sylvian fissures. At 40w PMA only, an asymmetry was captured in the depth of the knob of the posterior part of the Sylvian Fissure. This knob is located under the supramarginal gyrus, and its deepening in the left hemisphere is most likely due to a bigger supramarginal gyrus in the left hemisphere, which has been reported repeatedly in the adult (Lyttleton et al., 2009; Kong et al., 2018) and infant (Li et al., 2014). Interestingly, this observation is consistent with the fact that, in the nomenclature we use, the only sulcus which is not defined bilaterally but only in the left hemisphere is specific to the supramarginal gyrus (Perrot et al., 2011; Borne et al., 2020). Not capturing this asymmetry at 30w PMA suggests that the differential development of the supramarginal gyrus between the two hemispheres is progressing between 30w and 40w PMA.

Visually, the shape asymmetries of the Sylvian Fissure in terms of curvature and length in its posterior region seem to have overlapped on those captured in the perisylvian region: right Sylvian Fissures are more curvy and shorter than their left counterparts, and these same curvature and posterior extension seem to be captured in the perisylvian region. This was confirmed by the significant correlations captured between the perisylvian and three of the sylvian fissure Isomap dimensions. This might rely on the fact that the opercularization process, leading to the Sylvian Fissure formation, also displaces all the surrounding folding regions. This mix between a less curved and more posteriorly extended left perisylvian region is compatible with a previous study which reported increased distances in the left hemisphere between the bottom point of the central sulcus and both of the pos-

terior extremities of the Sylvian Fissure and the superior temporal sulcus in the full-term infant (Glasel et al, 2011). While we could visually expect the perisylvian dimension to correlate with the sylvian fissure's shape, it was not specifically the case for the inferior frontal region, whose pattern should *a priori* not be specifically impacted by the shape of the sylvian fissure. Yet, we observed significant correlations with 4 of its dimensions, which happened to be the 4 sylvian fissure dimensions showing asymmetrical configurations at 40w PMA, as well as with the perisylvian region isomap dimension. This suggested a consistent encoding of asymmetrical shape features in these three regions.

10.2.6.3 Opercularization is more advanced in the left hemisphere

In the perisylvian region, apart from the previous asymmetric shape features derived from the Sylvian Fissure, two additional characteristics were captured: the size of the gap between the frontal and anterior temporal sulci (smaller on the left), and the density of sulci in the frontal region (higher on the left). The volume of the part corresponding to the superior temporal sulcus appeared to be greater on the configurations corresponding to left rather than right hemispheres, even though the trend was not linear along the axis. These characteristics pointed towards an advance in opercularization in the left hemisphere compared to the right one, since an advance in opercularization means bringing closer together the frontal and temporal lobes and consequently bringing closer to the Sylvian Fissure both the superior temporal sulcus and the sulci of the inferior frontal lobe. With the retained methodology, this would have induced a greater inclusion of inferior frontal and superior temporal sulci, matching the trends captured in the perisylvian region moving averages. Incidentally, we interpreted the greater consistency in capturing more sulci in the frontal lobe, relative to temporal lobe, as being due to the organization of inferior frontal sulci, globally perpendicular to the Sylvian Fissure, while the superior temporal sulcus is globally parallel to the Sylvian Fissure. Therefore, using our methodology, even a small advance of the inferior frontal lobe towards the insula would have induced more sulcal elements to be captured, while a small advance of the temporal lobe would have led to weight slightly more the inclusion of the superior temporal sulcus but not to capture additional sulcal elements. These

suggestions were supported by the fact that the sulcation developmental asynchrony globally favors the right hemisphere (Chi et al., 1977; Dubois et al., 2008a; Habas et al., 2012).

Therefore, the observation of asymmetries in the perisylvian proxy support the hypothesis of an advanced or more pronounced operecularization process in the left hemisphere, which would contrast with a more advanced folding process on the right side.

The asymmetry captured in the inferior frontal region proxy is relatively coherent with these findings as it seems to capture a more prominent anterior part in the left compared with the right hemisphere, corresponding to the horizontal ramus of the Sylvian Fissure being buried deeper in the frontal cortex in the anterior frontal view. We interpreted the thinner superior part in the left hemisphere, corresponding to a shallower anterior part of the inferior frontal sulcus, as being related to the advance in sulcation of the right hemisphere. The encoded asymmetry may therefore relay concurrent expressions of two different mechanisms, with opercularization favouring the left hemisphere and sulcation favouring the right hemisphere. Surprisingly, contrarily to the perisylvian proxy, the inferior frontal region moving averages did not specifically capture more inferior frontal sulci on the left hemisphere. This may have been due to the difference in σ between the two regions, inducing a more comprehensive capture of inferior frontal sulci in the inferior frontal region proxy, which might have limited the additional capture of inferior frontal sulci due to a small displacement of the frontal lobe, or to the parameters retained to threshold the moving average, which may have pruned out this variability. Nevertheless, the shape asymmetry captured in the inferior frontal gyrus proxy, suggesting more deeply buried anterior rami of the sylvian fissure, was supported by the observation that the anterior region of the sylvian fissure (bordering the inferior frontal gyrus) seemed larger on the left hemisphere using voxel-based analyses on preterm infants between 24 and 36w PMA (Dubois et al., 2010). Our method proved the presence of a leftward asymmetry in this region which was previously inconsistently reported (Sprung-Much et al., 2021). This asymmetry could be fundamental for the development of language lateralization since it is the anatomical region corresponding to Broca's area.

10.2.6.4 Perspectives

This opercularization advance was foreshadowed by previous studies. The study reporting a more extended anterior and posterior sylvian fissure in the left hemisphere in the preterm suggested that it might either capture a developmental asynchrony or an intrinsically different structural morphology between left and right sylvian fissure development (Dubois et al., 2010). Both seemed to be the case in the present study. In a study comparing maturation indices hemisphere-wise along a set of sulci around the sylvian fissure, the most leftward asymmetries were captured in the anterior precentral cortex and in the pars opercularis, and may have captured a maturational advance linked to opercularization, even though they did not reach statistical significance (Leroy et al., 2011). Studying the maturation of opercular cortices in larger cohorts might therefore capture maturational asymmetries. Microstructural investigations show more consistent leftward asymmetry tendency in the inferior frontal region corresponding to Broca's area than macroscopical investigations (Sprung-Much et al., 2021). Moreover, based on a human fetal brain atlas between 21 and 38w GA, a recent study demonstrated the link between differential genetic expression in the opercular cortices compared to the insular cortex, suggesting an important genetic control over opercularization (Mallela et al., 2020). The asynchronous development of opercularization could therefore be linked to an asymmetrical genetic regulation of opercularization. Therefore, microstructural and genetic investigations should be undertaken in the context of opercularization in order to quantify its specificities, since its dynamics seem different from those of sulcation.

Alternatively, the current study focused on preterm infants to investigate early folding development, yet the observations at 40w PMA could and should be reproduced on term-born neonates to assess normal folding development, since extreme prematurity is associated to pathology and atypical cortical development, including in sulcation (Shimony et al., 2016; Dubois et al., 2019). In the preterm, the relationship between opercularization dynamics, prematurity, and anatomo-functional links to language should also be investigated further, as prematurity has been reported to affect both the lateralization of language (in neonates: Kwon et al., 2015; in adolescents: Scheinost et al.,

2015; in adults: Tseng et al., 2019) and language scores (in children: Barnes-Davis et al., 2020; in adolescents: Scheinost et al., 2015; in adults: Tseng et al., 2019). In these studies, the only reported link to anatomy was not related to altered brain folding, but to a significant decrease in callosal connectivity accompanied by an increase in non-callosal connectivity; this non-callosal connectivity was positively correlated to language assessments in children born preterm but not in controls (Barnes-Davis et al., 2020). Language scores were additionally reported to correlate with language lateralization specifically in the population which was born very preterm (Scheinost et al., 2015), suggesting developmental adversities affecting jointly lateralization and efficiency of language networks. To assess links between folding development and language scores, an analysis between numerous sulcal metrics in the Sylvian Fissure and superior temporal sulcus (area, depth, and sulcal index) in the present cohort reported significant correlations to receptive language outcome assessed at around 2 years of age (Kersbergen et al., 2016).

Therefore, to complement our study, it would be most informative to investigate further the specificities of opercularization, either through the observation of pattern dynamics at more time-points, through maturational or microstructural considerations, or through the evaluation of asymmetrical genetic regulation. Our method should further be applied to control term-born neonates to quantify the extent to which observations of early asymmetries in perisylvian regions in preterm infants correspond to a normal variability. A functional investigation would also be informative to assess whether the fine shape of any of the three proxies that we have investigated relates to later language outcomes.

10.2.7 References

Amiez, C., Sallet, J., Novek, J., Hadj-Bouziane, F., Giacometti, C., Andersson, J., Hopkins, W.D., Petrides, M., 2021. Chimpanzee histology and functional brain imaging show that the paracingulate sulcus is not human-specific. Commun Biol 4, 54. https://doi.org/10.1038/s42003-020-01571-3

Barnes-Davis, M.E., Williamson, B.J., Merhar, S.L., Holland, S.K., Kadis, D.S., 2020. Rewiring the extremely preterm brain: Altered structural connectivity relates to language function. NeuroImage: Clinical 25, 102194. https://doi.org/10.1016/j.nicl.2020.102194

Besl, P.J., McKay, N., 1992. A method for registration of 3-D shapes. IEEE Transactions on Pattern Analysis and Machine Intelligence 14, 239–256. https://doi.org/10.1109/34.121791

Borne, L., 2019. Design of a top-down computer vision algorithm dedicated to the recognition of cortical sulci. PhD thesis, Université Paris-Saclay.

Borne, L., Rivière, D., Mancip, M., Mangin, J.-F., 2020. Automatic labeling of cortical sulci using patch- or CNN-based segmentation techniques combined with bottom-up geometric constraints. Medical Image Analysis 62, 101651. https://doi.org/10.1016/j.media.2020.101651

Bouyssi-Kobar, M., Murnick, J., Tinkleman, L., Robertson, R.L., Limperopoulos, C., 2016. Third Trimester Brain Growth in Preterm Infants Compared With In Utero Healthy Fetuses 138, 13.

Chi, J.G., Dooling, E.C., Gilles, F.H., 1977. Gyral development of the human brain. Ann Neurol. 1, 86–93. https://doi.org/10.1002/ana.410010109

de Vareilles, H., Rivière, D., Sun, Z., Fischer, C., Leroy, F., Neumane, S., Stopar, N., Eijsermans, R., Ballu, M., Tataranno, M., Benders, M., Mangin, J., Dubois, J., 2022. Shape variability of the central sulcus in the developing brain: a longitudinal descriptive and predictive study

in preterm infants. NeuroImage 118837. https://doi.org/10.1016/j.neuroimage.2021.118837

Dubois, J., Benders, M., Cachia, A., Lazeyras, F., Ha-Vinh Leuchter, R., Sizonenko, S.V., Borradori-Tolsa, C., Mangin, J.F., Huppi, P.S., 2008. Mapping the Early Cortical Folding Process in the Preterm Newborn Brain. Cerebral Cortex 18, 1444–1454. https://doi.org/10.1093/cercor/bhm180

Dubois, J., Benders, M., Lazeyras, F., Borradori-Tolsa, C., Leuchter, R.H.-V., Mangin, J.F., Hüppi, P.S., 2010. Structural asymmetries of perisylvian regions in the preterm newborn. NeuroImage 52, 32–42. https://doi.org/10.1016/j.neuroimage.2010.03.054

Dubois, J., Lefèvre, J., Angleys, H., Leroy, F., Fischer, C., Lebenberg, J., Dehaene-Lambertz, G., Borradori-Tolsa, C., Lazeyras, F., Hertz-Pannier, L., Mangin, J.-F., Hüppi, P.S., Germanaud, D., 2019. The dynamics of cortical folding waves and prematurity-related deviations revealed by spatial and spectral analysis of gyrification. NeuroImage 185, 934–946. https://doi.org/10.1016/j.neuroimage.2018.03.005

Glasel, H., Leroy, F., Dubois, J., Hertz-Pannier, L., Mangin, J.F., Dehaene-Lambertz, G., 2011. A robust cerebral asymmetry in the infant brain: The rightward superior temporal sulcus. NeuroImage 58, 716–723. https://doi.org/10.1016/j.neuroimage.2011.06.016

Habas, P.A., Scott, J.A., Roosta, A., Rajagopalan, V., Kim, K., Rousseau, F., Barkovich, A.J., Glenn, O.A., Studholme, C., 2012. Early Folding Patterns and Asymmetries of the Normal Human Brain Detected from in Utero MRI. Cerebral Cortex 22, 13–25. https://doi.org/10.1093/cercor/bhr053

Hickok, G., Poeppel, D., 2007. The cortical organization of speech processing. Nat Rev Neurosci 8, 393–402. https://doi.org/10.1038/nrn2113

Hill, J., Dierker, D., Neil, J., Inder, T., Knutsen, A., Harwell, J., Coalson, T., Van Essen, D., 2010. A Surface-Based Analysis of Hemi-

spheric Asymmetries and Folding of Cerebral Cortex in Term-Born Human Infants. Journal of Neuroscience 30, 2268–2276. https://doi.org/10.1523/JNEUROSCI.4682-09.2010

Hou, L., Xiang, L., Crow, T.J., Leroy, F., Rivière, D., Mangin, J.-F., Roberts, N., 2019. Measurement of Sylvian Fissure asymmetry and occipital bending in humans and Pan troglodytes. NeuroImage 184, 855–870. https://doi.org/10.1016/j.neuroimage.2018.08.045

Jiang, X., Zhang, T., Zhang, S., Kendrick, K.M., Liu, T., 2021. Fundamental functional differences between gyri and sulci: implications for brain function, cognition, and behavior. Psychoradiology 1, 23–41. https://doi.org/10.1093/psyrad/kkab002

Kersbergen, K.J., Leroy, F., Išgum, I., Groenendaal, F., de Vries, L.S., Claessens, N.H.P., van Haastert, I.C., Moeskops, P., Fischer, C., Mangin, J.-F., Viergever, M.A., Dubois, J., Benders, M.J.N.L., 2016. Relation between clinical risk factors, early cortical changes, and neurodevelopmental outcome in preterm infants. NeuroImage 142, 301–310. https://doi.org/10.1016/j.neuroimage.2016.07.010

Knecht, S., Dräger, B., Deppe, M., Bobe, L., Lohmann, H., Flöel, A., Ringelstein, E.-B., Henningsen, H., 2000. Handedness and hemispheric language dominance in healthy humans. Brain 123, 2512–2518. https://doi.org/10.1093/brain/123.12.2512

Kong, X.-Z., Mathias, S.R., Guadalupe, T., ENIGMA Laterality Working Group, Glahn, D.C., Franke, B., Crivello, F., Tzourio-Mazoyer, N., Fisher, S.E., Thompson, P.M., Francks, C., 2018. Mapping cortical brain asymmetry in 17,141 healthy individuals worldwide via the ENIGMA Consortium. Proc Natl Acad Sci USA 115, E5154–E5163. https://doi.org/10.1073/pnas.1718418115

Kong, X.-Z., Mathias, S.R., Guadalupe, T., ENIGMA Laterality Working Group, Glahn, D.C., Franke, B., Crivello, F., Tzourio-Mazoyer, N., Fisher, S.E., Thompson, P.M., Francks, C., 2018. Mapping cortical brain asymmetry in 17,141 healthy individuals worldwide via the ENIGMA Consortium. Proc Natl Acad Sci USA 115, E5154–E5163. https://doi.org/10.1073/pnas.1718418115

Kostović, I., Sedmak, G., Judaš, M., 2019. Neural histology and neurogenesis of the human fetal and infant brain. NeuroImage 188, 743–773. https://doi.org/10.1016/j.neuroimage.2018.12.043

Kwon, S.H., Scheinost, D., Lacadie, C., Sze, G., Schneider, K.C., Dai, F., Constable, R.T., Ment, L.R., 2015. Adaptive mechanisms of developing brain: Cerebral lateralization in the prematurely-born. NeuroImage 108, 144–150. https://doi.org/10.1016/j.neuroimage.2014.12.032

Le Guen, Y., Leroy, F., Philippe, C., IMAGEN consortium, Mangin, J.-F., Dehaene-Lambertz, G., Frouin, V., 2019. Enhancer locus in ch14q23.1 modulates brain asymmetric temporal regions involved in language processing (preprint). Neuroscience. https://doi.org/10.1101/539189

Lefèvre, J., Germanaud, D., Dubois, J., Rousseau, F., de Macedo Santos, I., Angleys, H., Mangin, J.-F., Hüppi, P.S., Girard, N., De Guio, F., 2016. Are Developmental Trajectories of Cortical Folding Comparable Between Cross-sectional Datasets of Fetuses and Preterm Newborns? Cereb. Cortex 26, 3023–3035. https://doi.org/10.1093/cercor/bhv123

Leroy, F., Glasel, H., Dubois, J., Hertz-Pannier, L., Thirion, B., Mangin, J.-F., Dehaene-Lambertz, G., 2011. Early Maturation of the Linguistic Dorsal Pathway in Human Infants. Journal of Neuroscience 31, 1500–1506. https://doi.org/10.1523/JNEUROSCI.4141-10.2011

Leroy, F., Cai, Q., Bogart, S.L., Dubois, J., Coulon, O., Monzalvo, K., Fischer, C., Glasel, H., Van der Haegen, L., Bénézit, A., Lin, C.-P., Kennedy, D.N., Ihara, A.S., Hertz-Pannier, L., Moutard, M.-L., Poupon, C., Brysbaert, M., Roberts, N., Hopkins, W.D., Mangin, J.-F., Dehaene-Lambertz, G., 2015. New human-specific brain landmark: The depth asymmetry of superior temporal sulcus. Proc Natl Acad Sci USA 112, 1208–1213. https://doi.org/10.1073/pnas.1412389112

Li, G., Wang, L., Shi, F., Lyall, A.E., Lin, W., Gilmore, J.H., Shen, D., 2014. Mapping Longitudinal Development of Local Cortical Gyrification in Infants from Birth to 2 Years of Age. Journal of Neuroscience 34, 4228–4238. https://doi.org/10.1523/JNEUROSCI.3976-13.2014

Llinares-Benadero, C., Borrell, V., 2019. Deconstructing cortical folding: genetic, cellular and mechanical determinants. Nat Rev Neurosci 20, 161–176. https://doi.org/10.1038/s41583-018-0112-2

Lyttelton, O.C., Karama, S., Ad-Dab'bagh, Y., Zatorre, R.J., Carbonell, F., Worsley, K., Evans, A.C., 2009. Positional and surface area asymmetry of the human cerebral cortex. NeuroImage 46, 895–903. https://doi.org/10.1016/j.neuroimage.2009.03.063

Mallela, A.N., Deng, H., Brisbin, A.K., Bush, A., Goldschmidt, E., 2020. Sylvian fissure development is linked to differential genetic expression in the pre-folded brain. Sci Rep 10, 14489. https://doi.org/10.1038/s41598-020-71535-4

Mangin, J.-F., Frouin, V., Bloch, I., Régis, J., López-Krahe, J., 1995. From 3D magnetic resonance images to structural representations of the cortex topography using topology preserving deformations. J Math Imaging Vis 5, 297–318. https://doi.org/10.1007/BF01250286

Mangin, J.-F., Auzias, G., Coulon, O., Sun, Z.Y., Rivière, D., Régis, J., 2015. Sulci as Landmarks, in: Brain Mapping. Elsevier, pp. 45–52. https://doi.org/10.1016/B978-0-12-397025-1.00198-6

Moeskops, P., Benders, M.J.N.L., Kersbergen, K.J., Groenendaal, F., de Vries, L.S., Viergever, M.A., Išgum, I., 2015. Development of Cortical Morphology Evaluated with Longitudinal MR Brain Images of Preterm Infants. PLoS ONE 10, e0131552. https://doi.org/10.1371/journal.pone.0131552

Perrot, M., Rivière, D., Mangin, J.-F., 2011. Cortical sulci recognition and spatial normalization. Medical Image Analysis 15, 529–550. https://doi.org/10.1016/j.media.2011.02.008

Rivière, D., Leprince, Y., Labra, N., Vindas, N., Foubet, O., Cagna, B., Loh, K.K., Hopkins, W., Balzeau, A., Mancip, M., Lebenberg, J., Cointepas, Y., Coulon, O., Mangin, J.-F., 2022. Browsing Multiple Subjects When the Atlas Adaptation Cannot Be Achieved via a Warping Strategy. Front. Neuroinform. 16, 803934. https://doi.org/10.3389/fninf.2022.803934

Scheinost, D., Lacadie, C., Vohr, B.R., Schneider, K.C., Papademetris, X., Constable, R.T., Ment, L.R., 2015. Cerebral Lateralization is Protective in the Very Prematurely Born. Cerebral Cortex 25, 1858–1866. https://doi.org/10.1093/cercor/bht430

Shimony, J.S., Smyser, C.D., Wideman, G., Alexopoulos, D., Hill, J., Harwell, J., Dierker, D., Van Essen, D.C., Inder, T.E., Neil, J.J., 2016. Comparison of cortical folding measures for evaluation of developing human brain. NeuroImage 125, 780–790. https://doi.org/10.1016/j.neuroimage.2015.11.001

Sowell, E.R., Thompson, P.M., Rex, D., Kornsand, D., Tessner, K.D., Jernigan, T.L., Toga, A.W., 2002. Mapping Sulcal Pattern Asymmetry and Local Cortical Surface Gray Matter Distribution In Vivo: Maturation in Perisylvian Cortices. Cerebral Cortex 12, 17–26. https://doi.org/10.1093/cercor/12.1.17

Sprung-Much, T., Eichert, N., Nolan, E., Petrides, M., 2021. Broca's area and the search for anatomical asymmetry: commentary and perspectives. Brain Struct Funct 227, 441–449. https://doi.org/10.1007/s00429-021-02357-x

Steinmetz, H., 1990. Sulcus topography of the parietal opercular region: An anatomic and MR study. Brain and Language 38, 515–533. https://doi.org/10.1016/0093-934X(90)90135-4

Sun, Z.Y., Klöppel, S., Rivière, D., Perrot, M., Frackowiak, R., Siebner, H., Mangin, J.-F., 2012. The effect of handedness on the shape of the central sulcus. NeuroImage 60, 332–339. https://doi.org/10.1016/j.neuroimage.2011.12.050

Sun, Z.Y., Pinel, P., Rivière, D., Moreno, A., Dehaene, S., Mangin, J.-F., 2016. Linking morphological and functional variability in hand movement and silent reading. Brain Struct Funct 221, 3361–3371. https://doi.org/10.1007/s00429-015-1106-8

Tenenbaum, J.B., 2000. A Global Geometric Framework for Nonlinear Dimensionality Reduction. Science 290, 2319–2323. https://doi.org/10.1126/science.290.5500.2319

Tissier, C., Linzarini, A., Allaire-Duquette, G., Mevel, K., Poirel, N., Dollfus, S., Etard, O., Orliac, F., Peyrin, C., Charron, S., Raznahan, A., Houdé, O., Borst, G., Cachia, A., 2018. Sulcal Polymorphisms of the IFC and ACC Contribute to Inhibitory Control Variability in Children and Adults. eNeuro 5, ENEURO.0197-17.2018. https://doi.org/10.1523/ENEURO.0197-17.2018

Tseng, C.-E.J., Froudist-Walsh, S., Kroll, J., Karolis, V., Brittain, P.J., Palamin, N., Clifton, H., Counsell, S.J., Williams, S.C.R., Murray, R.M., Nosarti, C., 2019. Verbal Fluency Is Affected by Altered Brain Lateralization in Adults Who Were Born Very Preterm. eNeuro 6, ENEURO.0274-18.2018. https://doi.org/10.1523/ENEURO.0274-18.2018

10.2.8 Annex 1 : List of sulci preselected for the perisylvian region, ordered by lobe (except for the Sylvian fissure)

Frontal lobe:
Inferior frontal sulcus
Inferior and intermediary parts of the precentral sulcus
Central sulcus*
Parietal lobe:
Inferior part of the post-central sulcus
Intraparietal sulcus (including ramifications)
Sulcus of the supra-marginal gyrus
Temporal lobe:
Superior temporal sulcus (including ramifications)
Inferior temporal sulcus
Polar temporal sulcus
Sylvian Fissure Area: (Sylvian Fissure branches excluded from the Sylvian Fissure proxy)
Planum temporale sulcus
Transverse retrocentral ramus
Posterior sub-central ramus
Anterior sub-central ramus
Ascending ramus
Diagonal sulcus
Horizontal ramus

*Any item which did not fit any sulci label was labeled as unknown. The unkown labeled items were included in the preselected list. *sulci between lobes were affected arbitrarily to one of its neighboring lobes*

10.2.9 Supplementary materials

Sup. Table S1. Pearson correlations between Isomap positions and PMA at MRI for the three studies (n=71)

	r			
	Sylvian Fissure		*Perisylvian region*	*Inferior frontal region*
	At 30w PMA	At 40w PMA	At 40w PMA	At 40w PMA
Dimension 1	0.38	0.12	-0.14	-0.01
Dimension 2	0.04	-0.21	0.07	0.00
Dimension 3	0.02	-0.13	-0.02	0.03
Dimension 4	-0.14	0.00	0.06	0.14
Dimension 5	-0.15	-0.03	0.03	0.07
Dimension 6	0.16	0.02	0.02	-0.15
Dimension 7	-	-	-0.06	-0.10
Dimension 8	-	-	0.00	0.00
Dimension 9	-	-	0.20	-
Dimension 10	-	-	0.06	-

Sup. Table S2. Wilcoxon singed-rank test statistics and Bonferonni corrected p-value applied to the left versus right hemisphere isomap positions corrected for PMA

	Stat (corrected p-value)			
	A. Sylvian Fissure		*B. Perisylvian region*	*C. Inferior frontal region*
	30w PMA	40w PMA	40w PMA	40w PMA
Dimension 1	**558 (2.10^{-4})**	**390 (2.10^{-6})**	**224 (2.10^{-8})**	**75 (4.10^{-11})**
Dimension 2	**772 (0.02)**	**629 (1.10^{-3})**	1177 (5.63)	913 (0.29)
Dimension 3	**400 (3.10^{-6})**	**258 (3.10^{-8})**	1203 (6.68)	1111 (2.71)
Dimension 4	**596 (6.10^{-4})**	834 (0.07)	993 (1.02)	1098 (2.42)
Dimension 5	995 (0.62)	**693 (4.10^{-3})**	964 (0.72)	939 (0.42)
Dimension 6	**725 (9.10^{-3})**	1131 (2.40)	1202 (6.63)	1090 (2.25)
Dimension 7	-	-	1247 (8.59)	1140 (3.43)
Dimension 8	-	-	1113 (3.44)	1116 (2.83)
Dimension 9	-	-	1205(6.76)	-
Dimension 10	-	-	1163 (5.10)	-

Bold values verify corrected p-value<0.05

Sup. Table S3. Spearman correlations (statistics and Bonferonni corrected p-value) between the 30 and 40w PMA isomap positions corrected for PMA, for the Sylvian Fissure analysis

	ρ (corrected p-value)	
	Left hemisphere	Right hemisphere
Dimension 1	**0.47 (2.10^{-4})**	**0.44 (8.10^{-4})**
Dimension 2	**0.61 (1.10^{-7})**	**0.47 (2.10^{-4})**
Dimension 3	**0.75 (2.10^{-13})**	**0.59 (5.10^{-7})**
Dimension 4	0.17 (1.01)	0.29 (0.08)
Dimension 5	0.01 (5.65)	0.13 (1.76)
Dimension 6	-0.23 (0.34)	**-0.35 (0.02)**

Bold values verify corrected p-value<0.05

Sup. Table S4. Spearman correlations (statistics and Bonferonni corrected p-value) of the 40w PMA Isomap positions corrected for PMA between the sylvian fissure, perisylvian region, and inferior frontal region proxies

Sylvian fissure	Perisylvian region	Inferior frontal region
Dimension 1	**0.37 (4.10^{-5})**	**-0.27 (0.006)**
Dimension 2	**0.30 (0.002)**	**-0.27 (0.007)**
Dimension 3	**-0.42 (1.10^{-6})**	**0.41 (3.10^{-6})**
Dimension 4	0.04 (3.92)	-0.18 (0.17)
Dimension 5	0.20 (0.12)	-0.16 (0.38)
Dimension 6	-0.15 (0.49)	0.13 (0.64)

Bold values verify corrected p-value<0.05

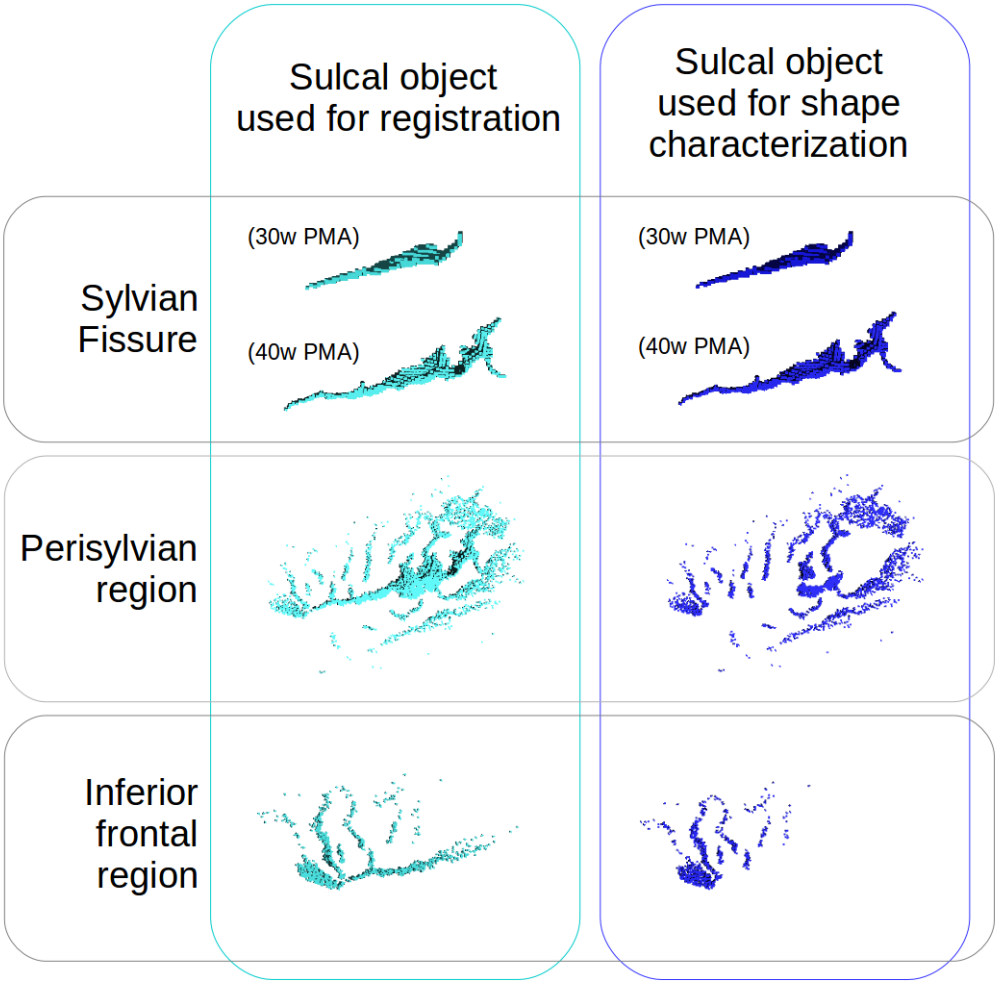

Supplementary Figure S1. Representation of the sulcal items used for registration (left panel) and for the analyses of shape characterization (right panel). For the Sylvian Fissure, one sulcus per age-group was represented and the corresponding age-group was specified. Note that the dark blue point clouds are included in their cyan counterparts.

10.3 TRANSITION

This contribution precisely described the developing shape variability of the sylvian fissure at 30 and 40w PMA, and described its asymmetries at both ages, along with the asymmetries of the perisylvian and inferior frontal regions at 40w PMA. While the results on the sylvian fissure were concordant with previous literature and proposed a more comprehensive characterization of its asymmetrical shape features, the results on the perisylvian and inferior frontal regions were new by construction. The combination of these three sub-studies at 40w PMA led to the observation that the opercularization process seemed to affect these regions differentially depending on the hemisphere, and we inferred that the opercularization process seems to show an advance in the left hemisphere both at 30 and 40w PMA.

Since this contribution relied mostly on methods which had already been developed and adapted for the developing longitudinal setting of my PhD studies on the central sulcus, the most demanding methodological developments for this contribution were, first, the definition of a sulcal extraction method ensuring inter-individual anatomical consistency of compared objects, along with the conceptual assessment of the potential biases of the approach, and secondly, the tuning of the moving averages to capture interpretable shapes for the studies of the perisylvian and Broca regions. This second aspect highlighted the limits of the moving averages approach, which best represent the shape variability along one direction when it can be encoded in a mix of 3D features. This was especially tricky in more complex objects such as regional folding objects as presented in this contribution.

While conceptualizing this contribution and as proposed in the study by Kersbergen et al., 2016, I originally intended to link these results to language outcomes in the cohort, which were assessed at the age of 2 or 2.5 years old. Yet, because fewer subjects had a later-assessed language outcome (n=34) than those having a later-assessed motor outcome (mABC: n=66; handedness: n=70), the prediction approach developed in the central sulcus's context was not applicable. I also did not assess links to language because of a lack of time at the end of my

PhD, but I intend to assess basic correlations between language outcome and perisylvian pattern for the relevant subset of subjects, before submitting the article for publication.

This original research article concluded my PhD original research contributions, with interesting insights on the opercularization process, complementing my first contribution which investigated dynamics linked to the sulcation process.

11 CHAPTER V: GENERAL DISCUSSION

During my PhD, I was offered the opportunity to enter the worlds of the developing human brain and cortical folding pattern. Both of these domains are in their youth because of previous technical difficulties, among which feasibility of data acquisition, and computational limitations. Multiple breakthroughs in different domains, such as the MRI technology and its successive improvements, or the development of computational power and machine learning, have opened up possibilities to explore new horizons, even on questions which could seem already well explored such as the brain's macroscopical anatomy. The recent discoveries on a number of implications of sulcal pattern consecrates the importance of better understanding its development. While considerable efforts have been devoted to the investigation of its underlying mechanisms, not enough attention has been accorded to the pattern of the developing sulci. The different articles presented in this thesis have tried to contribute to a better understanding of the development of cortical folding patterns.

11.1 STUDYING CORTICAL FOLDING PATTERN

The study of cortical folding pattern was initially constrained to be purely descriptive, based on post mortem specimens in which functional correlates could only be hypothetical (in the adult: Cunningham, 1892; during development: Chi et al., 1977a). These studies relied on small numbers of subjects which limited the possibility to capture the complex variability within the human species, and post mortem fetal studies allowed for a physio-pathological description of cortical folding, only representative of normal cortical folding in a limited extent (Chi et al., 1977a; Hansen et al., 1993). The breakthrough of in vivo non-invasive brain imaging, through MRI among others, paved the way for large cohort studies of normal variability in brain folding patterns. This remained a challenging task because of the important inter-individual variability, which often makes it complex to identify with certainty corresponding items in different brains. The first efforts were therefore oriented towards the most securely identified sulci on a strictly anatomical point of view, therefore favouring primary sulci, and those neighbouring regions with

well-defined functional implications (such as the sylvian fissure: Sowell et al., 2002; or the central sulcus: Sun et al., 2012). The same principles, with the added value that previous studies on mature brains had been led, have motivated my choice of folds in the developing brain. Nevertheless, both in the developing and developed brains, the pattern of many other sulci should be investigated, as they represent an interesting window into early neurodevelopment (Cachia et al., 2018; Del Maschio et al., 2019).

The central sulcus is a very interesting candidate for sulcal pattern investigation: its position and pattern are very stable across the general population, making it easy to identify, and its two neighbouring gyri (primary motor and somatosensory) show a somatotopic representation, offering a unique functional interpretability of regional shape specificities (Germann et al., 2019). In the adult, its main pattern variability feature was identified as switching from a single-knob to a double knob configuration (Sun et al., 2012; Sun et al., 2016), and in the neonate, three possible configurations were proposed on the basis of sulcal pits using a clustering approach, with either two or three sulcal basins, compatible with the single-to-double knob observed in the adult (Meng et al., 2018). When characterizing the shape of the central sulcus in the preterm infant at 30 and 40w PMA using a continuous approach, we managed to describe not one but 10 variability features representative of its main shape variability within this time-window. The shape variability features globally concerned the length of the sulcus, the height, depth, length, and wrapping around of the hand-knob, the presence of a second knob, and the orientation of the central sulcus's upper part. A striking resemblance was observed between the 8th dimension of the current study and the 1st dimension captured in the adult (Sun et al., 2012; Sun et al., 2016), and both seemed consistent with the observations in the neonate (Meng et al., 2018), suggesting that the main adult variability trait is already encoded at TEA, but that other early shape features take the lead for traducing shape variability in the developing brain. It should still be reminded that post-birth sulcal pattern evolution has been reported (through parametrized sulcal depth) between 12 and 60 months of age (Gajawelli et al., 2021), and that even though we considered TEA acquisitions as representative of an almost mature cortex, minor

pattern evolutions still take place after birth.

Regarding the sylvian fissure, the length and orientation of posterior part in relation to the planum temporale are its most frequently reported shape variability features, notably between the two brain hemispheres (post mortem: Chi et al., 1977a; in the foetus: Habas et al., 2012; in the preterm: Dubois et al., 2010; Kersbergen et al., 2016; in the term-born neonate: Hill et al., 2010; Glasel et al., 2011; in the child, adolescent and adult: Sowell et al., 2002). In the contribution presented in this thesis, the shape variability features captured concerned the length of the fissure, the general orientation of its posterior part, its branching, the width and depth of the supra-marginal knob, and the relative length of its inferior and posterior parts. The two first features were therefore concordant with existing literature, as well as the width and depth of the supra-marginal knob (indirectly, through the observation of the volume of the supra-marginal gyrus; Lyttleton et al., 2009) while the relative length of its anterior and posterior parts were previously unreported. These previously unreported shape features may reflect 1) the fact that the sylvian fissure's shape variability has never been captured in such detail, 2) the fact that the sylvian fissure's shape variability has mostly been explored in the light of its asymmetries, while two of our novel findings did not show hemispheric asymmetries at TEA, and 3) the fact that the cohort studied is based on extremely preterm infants which still can't be considered as typical subjects.

11.2 How relevant is our methodological approach ?

As detailed in the state of the art section, different methods have been developed to study sulcal pattern, either for the assessment of variability within a given sulcus or for regional considerations. During my PhD, I have chosen to use and adapt the continuous shape characterization pipeline previously validated in the adult brain, in which the captured shape features happened to relate to functional observations, as a proof of relevance (Sun et al., 2012; Sun et al., 2016). The continuity of pattern expression appeared as a model closer to reality concerning the central sulcus and sylvian fissure, and I argue that in clustering (and therefore discontinuous) configurations (Meng et al., 2018; Duan et al., 2019), a continuity can be found between the

different proposed clusters, and that in-between configurations are bound to happen. Our continuous approach prevented us from assuming that we could differentiate clusters in the sulcal pattern of the central sulcus and sylvian fissure, but with the counterpart of making shape description more challenging. Compared to parametrized approaches, the Isomap-based shape characterization derived the main shape variability from the studied cohort, while a parametrized method would have required to choose a shape feature to investigate; therefore, we preferred this method in the context of our exploratory studies.

The previous adult studies using the same core methodology limited its analyses to the first Isomap dimension, which was sufficiently relevant to pursue meaningful sulcal studies (Sun et al., 2012; Sun et al., 2016; Sun et al., 2017). In the case of our longitudinal developmental studies, the first Isomap dimension tended not to be very informative since it captured length variability in both cases, even though the affine Talairach registration compensated the brain size difference. This variability was both due to the PMA difference at each acquisition and to the age-gap between the two groups. Therefore, I had to rethink the scope of applicability of the Isomap dimensionality reduction and find a reliable way to assess the number of dimensions relevant to each of my studies. This allowed me to project the data on multiple dimensions and to capture a number of shape features in each case, resulting in unprecedented exhaustiveness of pattern description.

A limit of Isomap algorithm method, which first creates a neighbourhood graph from the data and then projects the data based on the geodesic distances extracted from this neighbourhood graph, is that it is not perfectly suited for projection of new elements on an existing dimension. *A posteriori* projection of a new element on an existing dimension is feasible based on nearest neighbour considerations, yet the new element would not be included in the topology of the original manifold. Therefore, only the shape features captured using the original dataset would be assessed in the new element – even if this new element expressed another shape feature previously uncaptured. Therefore, in order to capture the same shape features in the 30 and 40w PMA central sulci using this method, while

accurately capturing the shape variability from both subgroups, I had no other choice but to compute the shape variability by including both ages. As a result, the shape variability features observed with this method captured the shape variability from the two regrouped age-groups. Therefore, the order of the Isomap dimensions – which, in addition, cannot be described in terms of explained variance because of the non-linearity of the Isomap algorithm – are representative of the whole group shape variability and should not be extrapolated at either 30 or 40w PMA. To illustrate this, while length is the most variable feature within the 30 and 40w PMA central sulci (thus identified as the first dimension when the analysis was run on both groups together), an early run of the shape characterization pipeline on the 40w PMA central sulci alone did not capture length as the first Isomap dimension.

Nevertheless, the shape variability captured by investigating 30 and 40w PMA sulci together was relevant to capture their global shape variability also within each group. Because of the greater complexity of 40w PMA sulci, it is likely that the Isomap dimensions were mostly driven by them, and thanks to the global resemblance between 30 and 40w PMA central sulci or sylvian fissures, the shape features encoded in each subgroup were relevant to the other subgroup, which justified our methodological choice. A further assessment of sulcal shape variability in the age-specific subgroups in addition to the combined age-groups would have been redundant and not very informative, and we rapidly discarded this option.

Independently from the algorithmic choice, a noteworthy experimental decision was to base our studies on extremely preterm infants, including infants with neurological adversities such as intra-ventricular hemorrhage (N= 8 over 71 with grade 3 and 4 IVH). Independently of their clinical condition,the preterm infants at TEA have been reported to have, compared to the term-born neonate, a specific lesser depth of the insula as well as pre- and post-central sulci (Engelhardt et al., 2015), all of which are neighbours to the sulci and fissures explored during my PhD. Therefore, the sulcal shape variability captured in this cohort of extremely premature infants might reflect some atypical folding patterns, yet, both for the central sulcus and sylvian fissure, it is the most detailed shape characterization in the very young infant,

including a time point before normal-term birth. This was both an opportunity for an approximation of folding dynamics during this period of intense folding, and for prematurity-oriented analyses of neurodevelopmental adversities impacting the sulcal pattern, specifically in the context of fine motor outcome at 5 years of age in relation to the central sulcus shape (Chapter III).

In the context of outcome prediction, even though identifying a reliable sulcal biomarker for motor outcome would have a great impact on preterm well-being as it could justify early interventions, the assessment presented in the central sulcus article had little clinical ambition and was very exploratory. Because of the limits of projecting a new element to the Isomap dimensions, the generalization of the classifiers using the previously captured Isomap dimensions for fine motor outcome prediction would have been hazardous. This motivated me to make methodological choices which did not maximise the classifiers' performances, since my main objective was to obtain as unbiased observations as possible on the potential relevance of sulcal shape for motor outcome. As a result, while some sulcal shape-based predictors performed better than the one trained on clinical factors (which I chose as a baseline), both for handedness and fine motor outcome, none performed strictly above a 95% chance interval, but they still seemed to be a relevant trend suggesting a relationship.

Both the cohort-specific property of the Isomap method and the voluntary absence of fitting of the outcome classifiers were justified in an exploratory approach. In the event of the capturing of shape features which would seem relevant to explore in a broader context and with new subjects, I recommend the identification of the shape feature through the Isomap method, and, if possible, the generalization of the feature's identification on a broader cohort based on a parametrization approach, as proposed in the central sulcus, for example (Cykowski et al., 2008). In the meantime, the approach retained allowed not only to describe the shape features encoded, but also to quantify the features captured, allowing for quantitative analyses to be led to explore their longitudinal development and interhemispheric asymmetries.

11.3 EARLY SULCAL DEVELOPMENT

Early sulcal development has been reported through the relative chronology of appearance of different sulci (Chi et al., 1977a; Hansen et al., 1993; Garel et al., 2001; Dubois et al., 2008a; Habas et al., 2012). Fewer studies have assessed the post-appearance dynamics of cortical folding by looking into the evolution of specific sulci. In the foetus, the evolution of the mean curvature of specific sulci within the 20-28w GA age range has been reported (Habas et al., 2012), and the evolution of volumes around the sylvian fissure were dynamically explored on the basis of a fetal atlas covering the 21 to 38w GA time window (Mallela et al., 2020). In the preterm, the evolution of the length and surface area of a set of sulci was assessed in a longitudinal setting between 30 and 40w PMA (Kersbergen et al., 2016). Yet, the longitudinal assessment of sulcal pattern (more complex than length or surface area) was previously unexplored in the time-window before normal-term birth.

Our quantitative shape characterization method allowed me to investigate this topic. When testing the correlations between the 30 and 40w PMA central sulci and sylvian fissures, most were significant or showed relevant trends, suggesting that a majority of the shape features present at TEA are already encoded at 30w PMA, during early sulcal pattern development. This contributed to a better understanding of the chronology of folding pattern, as we demonstrated through these two examples that the development of secondary sulci and to a lesser extent of tertiary sulci (developing respectively starting from 32 and 38w GA) affect in a minor extent the general pattern of primary folds.

In the central sulcus, 8 out of 10 shape features showed relevant trends in shape encoding across age groups on both hemispheres. They suggested an overall consistent development of its length, combined size and height of the hand-knob, wrapping around the hand knob, and presence of a second knob. In the sylvian fissure, only 3 out of 6 shape features showed relevant and interpretable correlations between groups, suggesting more later-than-30w-PMA encoding of shape features than in the central sulcus. The consistently evolving shape features concern length and orientation of its posterior part,

which match the generally reported asymmetries, and strengthen the idea that these are encoded early and evolving accordingly.

In addition to identifying the sulcal features which developed consistently between the two ages, our analyses revealed additional features which appeared within this time window. In the central sulcus, these were the length and size-independant-height of the hand knob, as well as the orientation of its superior part. The later encoding of these shape features seems consistent with a delayed elongation of the upper part of the central sulcus (Cunningham, 1892). In the sylvian fissure, the 4th dimension (left hemisphere) and the 5th dimension (bilaterally) showed a rather low correlation between age groups, while the 6th dimension showed trends towards a negative correlation, which we failed to interpret. These quantified the length and depth of what I name the supra-marginal knob, and which seems to gain in amplitude independently from its 30w PMA encoding.

A question that arose was whether the process governing the most posterior part of the sylvian fissure, within the parietal cortex rather than marking the limitation between the temporal and parietal cortices, and posterior to the planum temporale as defined in Altarelli et al., 2014, was linked to opercularization or to sulcation. We suggested that it may be closer to sulcation, as the 4th dimension, encoding the length of the supra-marginal knob, showed a higher (and almost significant) correlation in the right hemisphere compared to the left one. This could be interpreted as related to the prenatal sulcation advance of the right hemisphere, leading to an already encoded length of the intra-parietal part of the sylvian fissure on the right but not on the left hemisphere at 30w PMA. This type of consideration was induced by our findings in the sylvian fissure, perisylvian and inferior frontal regions, which seemed to indicate different dynamics in opercularization compared to sulcation.

11.4 Different dynamics between the opercularization and sulcation processes

The process of opercularization has not yet been thoroughly investigated. The sylvian fissure's shape is a proxy for it, but the assessment of its asymmetries has globally been treated as being similar to that of sulci. Yet, the early appearance of importantly

asymmetric shape features, highly reproducible throughout the population, yet specific to the humankind (when compared to one of our closest phylogenetic cousin, the chimpanzee; Hou et al., 2019), tends to suggest a more important genetic control on the sylvian fissure than classical sulci. Genetic factors specifically linked to opercularization have recently been explored using a 23w GA fetal atlas, along with the relative expansion of perisylvian regions on an atlas spanning from 21 to 38w GA (Mallela et al., 2020). This study did not assess interhemispheric asymmetries in opercularization, which would have been very informative since our study on the perisylvian regions suggested a leftward advance in this process, which would probably be apparent in its genetic encoding.

Our hypothesis on different dynamics of opercularization and sulcation spawned from observations in the perisylvian and inferior frontal regions, after the first hints were captured through the sylvian fissure's early developmental dynamics. Both regions showed a single asymmetrical shape feature which was very pronounced and captured as the first dimension. The asymmetry in the perisylvian region captured a reduced gap between inferior frontal and superior temporal sulci in the left hemisphere compared with the right, with ventral inferior frontal sulci closer to the sylvian fissure, as well as a flatter posterior temporoparietal configuration. In the inferior frontal region, the asymmetry seemed to capture a deeper anterior horizontal ramus and a shallower ventral extremity of the inferior frontal sulcus in the left hemisphere. Apart from the shallower ventral inferior frontal sulcus, which may be due to the right-hemisphere advance in sulcation, we interpreted these shape features as representative of a differentially expressed and a more advanced opercularization process in the left hemisphere than in the right, inducing a greater overgrowth of the frontal and temporal lobes over the insula.

The fact that strong shape asymmetries were captured in the 40w PMA sylvian fissure, perisylvian region, and inferior frontal region made us question the inter-object correlations. Significant correlations were found between these three objects, specifically between the asymmetrical dimensions. At first, the correlations between the inferior frontal region and the sylvian fissure could seem unexplainable because of the a priori absence of relation between the shape of the

posterior sylvian fissure and the depth of the ventral sulci from the inferior frontal region. Yet, the three objects' combined evidence seem to link the differential expression of left versus right opercularization to combined effects in the burying of the anterior horizontal ramus, the convergence of inferior frontal sulcus and the anterior part of the superior temporal sulcus, and the length and orientation of the posterior sylvian fissure along with the depth of its supramarginal knob.

This led us to question the differences between asymmetries in terms of opercularization and sulcation. Directly linked to the opercularization process, asymmetries in the insular region are reported as soon as 23w GA, with a more convex frontoparietal operculum and a more concave posterior temporal operculum on the right hemisphere (Habas et al., 2012). The most important asymmetries of the developing brain are along the sylvian fissure (Chi et al., 1977a; Chi et al., 1977b; Dubois et al., 2010; Hill et al., 2010; Glasel et al., 2011; Habas et al., 2012; Kersbergen et al., 2016) and in the superior temporal sulcus's depth (Dubois et al., 2008; Glasel et al., 2011; Habas et al., 2012; Leroy et al., 2015), yet these two asymmetries have been reported to be uncorrelated (Glasel et al., 2011). This could have been due to a different genetic control in these two areas, especially since asymmetrically expressed genes have been identified specifically in the perisylvian cortices (Sun et al., 2005), and linked to the asymmetry of the planum temporale (Carrion-Castillo et al., 2020). This was supported by the observation that the gene expression profile of the pre-folded brain was significantly different in the developing opercular cortex (corresponding to the future frontal, parietal and temporal lobes) compared to the insular cortex (Mallela et al., 2020).

An asymmetrical genetic expression has also been related to the superior temporal sulcus's asymmetry in adults (Le Guen et al., 2018), in a similar location as in the infant (Leroy et al., 2015). With the absence of correlation between the rightward superior temporal sulcus's asymmetry and the leftward asymmetry of the posterior part of the sylvian fissure (Glasel et al., 2011), we hypothesized that different genetic cues lead these two asymmetries, which would be consistent with different dynamics of opercularization and sulcation in the left and right hemisphere, which are themselves coherent with the left

advance we observed in opercularization and previously-reported right advance in sulcation.

We therefore suggested that opercularization and sulcation may be orchestrated by an overall different genetic, cellular and biomechanical agenda, which could explain the different dynamics of these two processes, with opercularization showing a left-hemisphere advance and strong, early encoded leftward asymmetries, while sulcation would show a right-hemisphere advance and early rightward asymmetries (Habas et al., 2012).

11.5 BRAIN ASYMMETRIES AND FUNDTIONAL LATERALIZATION

Asymmetries in cortical folding have been reported as soon as 22w GA in the fetal brain (Habas et al., 2012), and the two most reported ones are in the sylvian fissure (leftward asymmetry of local folding appearing as soon as 22w GA) and in the superior temporal sulcus (rightward asymmetry appearing at 26w GA). Both of these asymmetries are consistently reported in the developing brain (sylvian fissure: Chi et al., 1977a; Chi et al., 1977b; Dubois et al., 2010; Hill et al., 2010; Glasel et al., 2011; Habas et al., 2012; Kersbergen et al., 2016; superior temporal sulcus: Chi et al., 1977b; Dubois et al., 2008a; Glasel et al., 2011; Duan et al., 2019) as well as in the more mature human brain (sylvian fissure: Sowell et al., 2002; superior temporal sulcus: Leroy et al., 2015) and therefore seem to be encoded early and durably during development. Asides from the opercularization-linked asymmetries addressed in the previous section, additional asymmetries have been reported in the very young brain: in the cingulate sulcal complex, and in the central sulcus. The cingulate sulcus was reported to show pattern configuration asymmetries in the neonate (Duan et al., 2019), which were similarly reported at later ages and have been functionally related to cognitive control efficiency (Del Maschio et al., 2019). In this thesis, the pattern of the central sulcus was reported to be asymmetric to some extent in the TEA preterm infant, which was similarly reported at a later age and functionally linked to handedness and hand activation (Sun et al., 2012; Sun et al., 2016).

Reciprocally, lateralized functional activations are observed in these asymmetrical anatomical regions. The sylvian fissure, inferior frontal

region, superior temporal sulcus, and more generally the perisylvian region have been demonstrated to participate, among others, in the dorsal stream of language for speech production, which was reported to show a strong leftward functional lateralization (Hickok and Poeppel, 2007): about 90% of the general population processes word generation through the left hemisphere (Knecht et al., 2000). The central sulcus is adjacent to the primary motor regions, which are lateralized in adults (with roughly 90% of the population being right-handed). It has also been shown that the anterior cingulate cortex, for its part, is the place of lateralized activations in the context of response inhibition (Serrien et al., 2013), but this functional lateralization is less clearly defined and understood than those of language and handedness.

These anatomo-functional laterality considerations made me wonder whether early sulcal shape pattern could be predictive of later functional lateralization. This question was previously investigated by correlating simple sulcal metrics and functional outcome at 2 years of age, which revealed a link between receptive language performance and the bilateral sylvian fissure, bilateral superior temporal sulcus, and left insula at TEA (Kersergen et al., 2016). We additionally investigated the anatomo-functional lateralization in the central sulcus, regarding handedness assessed at 5 years of age, through the training of classifiers using hemisphere and age-specific Isomap dimensions. The best and only relevant classifier based on sulcal shape alone was obtained using the 30w PMA left central sulcus and its most weighted shape feature suggested a combination of a longer hand-knob and a backwards bend of its superior part for left-handers, which we found challenging to interpret functionally. While the classifier's score was better than that obtained with clinical factors alone, it did not show a strictly above-chance performance; additionally, despite our best efforts, we seem to have captured left-handedness related to preterm pathology, since the best performances were achieved by classifiers trained with both clinical factors and sulcal shape features.

This raised additional questions about the representativeness of the cohort studied compared to a control folding situation: prematurity has been related to altered lateralization, both in terms of handedness (for meta-analysis, see Domellöf et al., 2011) and language (in

neonates: Kwon et al., 2015; in adolescents: Scheinost et al., 2015; in adults: Tseng et al., 2019). Moreover, white matter injuries in prematurity have also been related to altered motor and language outcomes (Guo et al., 2017). We have nonetheless chosen to include all the subjects to capture shape variability because excluding these subjects would have . Therefore, in the absence of evidenced causal relationships between prematurity, structural development and functional outcomes, early sulcal shape investigations based on preterm cohorts should be interpreted carefully and considered as exploratory towards the understanding of normal development.

11.6 Conclusion and perspectives

The cortical folding pattern in the human has received increasing attention as a signature for early neurodevelopmental trajectories. A finer understanding of its developmental dynamics would therefore be valuable both for its general understanding and to uncover and investigate abnormal folding situations and their functional correlates. Throughout this thesis that was based on a longitudinally scanned cohort of extremely premature infants, I have contributed to a finer description of the folding variability of the central sulcus and sylvian fissure at early ages, and to the demonstration of early encoded shape features and asymmetries in these objects. I have also tested whether early sulcal pattern was predictive for later outcome, and additionally captured region-wise asymmetries in the perisylvian region revealing a difference in dynamics between the process of sulcation and opercularization.

As detailed in the previous sections, sulcal pattern exploration is a beautiful way to address early neurodevelopment, especially since it mostly develops in utero and stays globally stable throughout lifespan. In order to gain a better understanding of both normal and pathological variability in brain folding, and their implications on brain functions, multiple directions might be investigated in the future.

A better general understanding of the variability of cortical folding pattern both in the developing and mature brain is a necessary starting block, and numerous efforts are under-way in that direction. International efforts are converging towards a more precise definition and observation of sulcal specificities, including their relation to

underlying white matter. A recent call was issued to address the specific question of "plis de passage", which are gyri buried within a given sulcus, and which may contribute to a better understanding of sulcal variability (Mangin et al., 2019). In parallel, many new functional correlates of pattern variability are to be discovered, which could lead us to useful findings in terms of general understanding of brain function and clinical applications. In particular, sulcal pattern has already been proven to be relevant to psychiatry and neurology, and we can hope that their further investigation will lead to improvement in diagnosis and general patient care.

To gain a better understanding on normal development of cortical folding pattern, my contributions should be complemented by sulcal or fissure shape analysis in term-born control neonates, to better grasp the extent of sulcal variability linked to adversarial events in links with prematurity that were captured in my studies. This is already possible thanks to the deployment of rich open-source neonatal datasets such as the Developing Human Connectome Project (http://www.developingconnectome.org/), but I did not have the time to pursue this investigation during my PhD. Moreover, investigating the relationship between cortical folding pattern and related white matter and cortical maturation would bring additional insights to cerebral anatomy. If ethically approved, and thanks to the remarkable efforts in fetal image processing, reproducing a similar methodology on fetal brains scanned longitudinally would bring additional insights on normal sulcal development during the preterm period but in "real typical" subjects compared to premature infants.

On the reverse, to identify early markers of prematurity-induced neurodevelopmental adversities, considering larger preterm cohorts is required to account for the important inter-individual variability and assess the predictive ability of sulcal pattern on functional outcomes in a more refined manner than proposed on the central sulcus. Indeed, having more subjects would allow to tune the classifiers and proceed to feature selection, as well as including both left and right sulci together as an input, which would most likely bring a more convincing predictive capacity and a more interpretable outcome than what we did …

On another note, the question of the difference between sulcation and

opercularization should be investigated further. Previous studies reporting leftward asymmetries in the sylvian fissure foreshadowed a different developmental agenda and the contributions of this thesis reported additional evidence. Genetic assessments have already been undertaken to investigate opercularization (Mallela et al.,2020), but additional endeavours should be considered to pinpoint the mechanisms behind its asymmetrical development. A finer understanding of the process of opercularization could additionally benefit the biomechanical modelling of cortical folding. Microstructural investigation could also contribute to a better understanding of this phenomenon. The variability in opercularization and early asymmetries of perisylvian regions should also further be interrogated in the light of receptive language lateralization and outcome, as it might yield relevant neurodevelopmental information.

To conclude, sulcal variability is present in every fold of the brain, and to this date, only a few have been thoroughly investigated as only a few teams worldwide are interested in this question. Our methods are extendible to the rest of the brain, maybe requiring some methodological adaptation depending on the sulcus. Nevertheless, as outlined during this thesis, different approaches can be proposed solutions to adapt the methodology to challenging questions. So far, the patterning of secondary and tertiary sulci have received little attention, while they may carry valuable functional information (Miller et al., 2021). Current efforts should therefore be sustained in order to achieve a global comprehension of the implications of the variability of cortical folding pattern.

12 RESUME DES TRAVAUX DE THESE

12.1 LISTE DES ABBREVIATIONS

AET : âge équivalent du terme de la grossesse

APM (s APM) : âge post-menstruel (semaines d'âge post-menstruel)

IRM : imagerie par résonnance magnétique

SVC : classifieur à support vectoriel

12.2 INTRODUCTION

Le plissement du cerveau, qui fait apparaître en surface des creux (sillons) et des bosses (gyri), est un phénomène complexe qui donne lieu à la fois à une certaine homogénéité sur l'ensemble du cerveau dans l'espèce humaine, et à une variabilité inter-individuelle encore peu explorée. La question de la variabilité en forme du plissement du cerveau a longtemps été éludée à cause de sa complexité et de son observation exclusivement post mortem, qui limitait l'interprétabilité des potentielles relations entre anatomie sulcale (liée aux sillons) et fonctionnement cérébral.

Récemment, les avancées technologiques permises par l'avènement de l'imagerie cérébrale non invasive et essentielles aux neurosciences ont permis de réaborder cette question in vivo. Notamment l'imagerie par résonance magnétique (IRM), à la fois anatomique et fonctionnelle, a permis d'envisager des études à grande échelle nécessaires pour la quantification de la variabilité globale de la forme des sillons chez l'humain. Par ailleurs, les avancées technologiques en termes de puissance de calcul et d'algorithmie computationnelle ont ouvert la voie à des études avancées de la forme des sillons, permettant entre autres de mettre en évidence des relations entre certains motifs de plissement et certaines spécificités fonctionnelles.

Dans ce contexte, il est souhaitable et pertinent d'envisager une meilleure compréhension du développement de la forme des sillons, lequel prend majoritairement place in utero pendant le troisième trimestre de grossesse et reste globalement stable après la naissance.

Au cours de ma thèse, j'ai étudié le développement de différents plis ou régions du cerveau à l'aide de données d'imagerie par IRM acquises longitudinalement auprès d'une cohorte de 71 nourrissons nés prématurés extrêmes (nés entre 24 et 28 semaines d'âge gestationnel) et imagés aux alentours de 30 semaines d'âge post-menstruel (s APM) et de 40s APM, qui correspond à l'âge équivalent du terme (AET) d'une grossesse typique (9 mois). Ces travaux ont donné lieu à trois articles (deux études expérimentales, dont une parue et une à soumettre, et un article de revue de la littérature à soumettre) qui seront présentés dans les sections suivantes.

12.3 ETAT DE L'ART

Afin de contextualiser mes travaux au vu des connaissances actuelles dans les différents domaines en liens avec ma thèse, j'ai tout d'abord proposé un article d'état de l'art portant sur l'investigation des motifs de plissement, et qui s'articule autour de deux sections : la première partie porte sur l'étude de la variabilité sulcale dans le cerveau mature, et la deuxième partie sur le plissement au cours du développement.

Dans la première section portant sur le plissement dans le cerveau mature, j'ai tout d'abord détaillé les différentes raisons pour lesquelles il est pertinent de s'intéresser à la variabilité du plissement. Cet intérêt se justifie à la fois à des fins purement descriptives, mais aussi dans le contexte de recalages inter-individuels (pour lesquels la prise en compte de la variabilité de forme sulcale permet de mieux respecter les spécificités anatomiques individuelles), ou pour investiguer les liens potentiels entre la forme des sillons et le fonctionnement cérébral, notamment la spécialisation des aires corticales. Ensuite, j'ai donné un aperçu des différentes méthodes développées pour investiguer la variabilité des motifs de plissement dans le cerveau mature, en présentant d'abord les méthodes globales et régionales, et dans un deuxième temps les méthodes « sillon-spécifiques » qui s'intéressent à la variabilité d'un pli en particulier. Enfin, j'ai interrogé la littérature sur les spécificités que semble présenter le plissement humain, au regard des études comparées entre humains et autres mammifères dont les primates non-humains, notamment en termes d'asymétries entre les hémisphères cérébraux.

La deuxième section, consacrée au développement des sillons, s'ouvre

sur la compréhension actuelle que nous avons des mécanismes induisant le plissement : question posée selon une triple approche mêlant biologie cellulaire, génétique et biomécanique, qui permet d'explorer des mécanismes qui s'avèrent complémentaires et interdépendantes dans la genèse du plissement. Ensuite, j'ai rappelé les difficultés en lien avec l'imagerie du tout-petit, à la fois chez le fœtus et chez le nouveau-né, afin d'aborder les différentes avancées méthodologiques permettant aujourd'hui d'étudier finement le cerveau en développement par IRM. Enfin, j'ai résumé les connaissances actuelles en termes de développement sulcal chez l'humain, à travers sa chronologie d'apparition, sa dynamique évolutive et ses asymétries, avant de conclure sur les altérations de plissement observées en lien avec la prématurité.

Nous avons l'intention de soumettre cet article à la revue « Developmental Cognitive Neuroscience » (spécialisée en neurosciences cognitives développementales) à l'occasion d'une édition spéciale faisant suite aux symposiums organisés dans le cadre du congrès international « Flux » 2021.

12.4 METHODES ET COHORTE ETUDIEE

Le deuxième chapitre de ma thèse est consacré à la description de ma cohorte d'étude et des méthodes employées pour l'étude de la variabilité en forme sulcale au sein de cette cohorte. Ce chapitre m'a permis de préciser l'étendue de mes contributions méthodologiques au regard de ce qui avait déjà été traité ou implémenté par d'autres membres de mon équipe ou d'équipes partenaires en amont de ma thèse.

La cohorte étudiée est composée de 71 sujets (51 % de garçons) d'âge gestationnel à la naissance compris entre 24 et 28 semaines, et recrutés à l'hôpital « Wilhelmina's Children Hospital, University Medical Center », à Utrecht (Pays-Bas), entre 2008 et 2012. Ces sujets ont été imagés deux fois pendant leur séjour en unité de soin intensive néonatale, une première fois aux alentours de 30s APM et une seconde fois aux alentours de 40s APM. Les sujets ont bénéficié de suivis ultérieurs au cours desquels ont entre autres été évalués leurs scores moteurs, langagiers, et leur latéralité manuelle, entre 24 et 30 mois, puis à 5 ans.

Le prétraitement des images IRM a été opéré en amont de mes études, conformément à la méthodologie détaillée dans Kersbergen et al., 2016. Après segmentation des images (différenciant substance blanche, substance grise et liquide cérébro-spinal), les sillons sont définis comme les surfaces équidistantes aux murs de deux gyri adjacents, délimitées par le haut par la fermeture morphologique de la surface corticale externe (Mangin et al., 1995). Dans le cadre de mes études, la détection des sillons a été rendue légèrement plus sensible pour mieux capturer certains plis en cours de développement, et j'ai corrigé à la main les résultats d'étiquetage automatique grâce au logiciel BrainVISA.

Pour évaluer la variabilité en forme des plis que j'ai étudiés, j'ai bénéficié d'une méthode implémentée préalablement par mon équipe pour l'étude du plissement adulte (Sun et al., 2012; Sun et al., 2016), et que j'ai dû adapter au contexte du cerveau en développement. En résumé, après recalage des cerveaux dans l'espace de Talairach pour compenser la variabilité en forme due aux différentes tailles globales du cerveau, j'ai extrait les objets d'intérêt pour chacune de mes études, dans les hémisphères gauches et droits des sujets aux deux âges. J'ai retourné les objets droits de manière à ce qu'ils soient dans la même orientation que les gauches, puis j'ai calculé une mesure de dissimilarité entre chaque paire d'objets de la cohorte en les recalant deux-à-deux et en calculant la distance résiduelle issue du recalage (j'ai dû optimiser la distance choisie à ma problématique). Les mesures de dissimilarités calculées ont ensuite été rassemblées dans une matrice capturant la variabilité en forme de la cohorte. J'ai ensuite utilisé un algorithme de réduction de dimension, l'Isomap (Tenenbaum, 1999), pour projeter ces données en plus faible dimension, et j'ai été amenée à élaborer une méthode pour choisir les paramètres à retenir pour cet algorithme. Pour chacune des dimensions obtenues, j'ai pu projeter les objets individuels sur leurs coordonnées respectives, et, interpréter la caractéristique de forme capturée par l'algorithme, à l'aide de moyennes glissantes calculées sur les sujets le long de la dimension.

Les dimensions d'Isomap (corrigées par modèle linéaire pour les différences d'âge à l'acquisition) ont ensuite été utilisées pour comparer les positionnements relatifs de différents sous-groupes

(définis en fonction de l'âge ou de l'hémisphère) le long des dimensions, permettant d'évaluer les corrélations entre les deux âges et les positionnements relatifs des objets issus d'hémisphères droits par rapport aux gauches.

12.5 RESULTATS OBSERVES SUR LE SILLON CENTRAL

Cette méthode a tout d'abord été appliquée au sillon central, région intéressante à étudier au regard des capacités motrices des sujets dans la mesure où ce sillon délimite les régions motrice et somatosensorielle primaires (dans les gyri pré- et post-centraux) qui présentent la particularité d'une organisation somatotopique (les différentes parties du corps y étant représentées selon l'homonculus) (Penfield and Rasmussen, 1950; Germann et al., 2019). Étudier ainsi le sillon central à 30 et à 40s APM a permis de décrire la variabilité précoce de forme de ce dernier ainsi que de tester sa capacité prédictive sur le devenir moteur de l'enfant à 5 ans, en termes de latéralité manuelle et de motricité fine évaluée par le movement Assessment Battery for Children (mABC).

Dix caractéristiques de forme ont été capturées dans le sillon central en développement, concernant principalement la taille du sillon, la hauteur, longueur et profondeur de la bosse caractéristique du sillon central au niveau de la région de représentation de la main (« hand-knob »), et la présence d'une deuxième bosse. Parmi ces 10 caractéristiques de forme, 8 montraient une corrélation (ou tout du moins une tendance) entre les deux âges, suggérant un encodage précoce (à 30s APM) de la majorité des caractéristiques de forme du sillon central. De plus, une dimension a montré une distribution asymétrique à 30s APM, mais pas à 40s, indiquant que la bosse était plus profonde à droite qu'à gauche de manière précoce mais plus à l'AET. Ceci peut s'interpréter comme une avance développementale de cette caractéristique à droite qui est ensuite compensée par la gauche avant l'AET, ce qui serait cohérent avec l'avance de sulcation préalablement rapportée au niveau de l'hémisphère droit. À 40s APM, une autre dimension a montré une asymétrie, encodant un passage d'une configuration à une seule bosse pour les sillons droits à une configuration à deux bosses pour les sillons gauches, d'une façon similaire à l'asymétrie capturée chez l'adulte (Sun et al., 2012).

Dans un deuxième temps, afin de tenter de prédire la latéralité ou le devenir moteur des sujets à 5 ans à partir des caractéristiques de forme du sillon central, j'ai entraîné un classifieur à support vectoriel (SVC) avec pour entrées les coordonnées d'Isomap par groupe d'âge et par hémisphère, afin de limiter le nombre de paramètres en liens avec la taille limitée de la cohorte. J'ai comparé les performances de ces classifieurs avec celle d'un classifieur prenant pour entrée une sélection de facteurs cliniques connus pour avoir un impact sur le devenir comportemental et clinique des enfants nés prématurément, et j'ai également évalué la complémentarité entre ces facteurs cliniques et les paramètres de forme. Les résultats obtenus n'ont pas été entièrement concluants, peut-être à cause des limites suivantes : la faible taille de ma cohorte m'a empêchée de paramétrer l'algorithme, de sélectionner les paramètres pertinents ou de considérer conjointement les sillons gauches et droits. Bien que non-significatifs, ces résultats semblaient suggérer une capacité prédictive de la forme sulcale sur le devenir moteur à 5 ans.

Ces travaux ont donné lieu à la publication d'un article dans la revue NeuroImage (de Vareilles et al., 2021).

12.6 RESULTATS OBSERVES AU NIVEAU DE LA SCISSURE SYLVIENNE

À la suite du sillon central, j'ai orienté mes travaux autour de la scissure sylvienne, qui présente la particularité de ne pas être un sillon puisqu'elle se forme par recouvrement du lobe insulaire par les lobes frontal, pariétal et temporal (processus d'opercularisation). Par ailleurs, cette région est le siège d'une majorité des aires corticales impliquées dans le traitement du langage, dont une partie présente une latéralisation fonctionnelle favorisant l'hémisphère gauche (Hickok and Poeppel, 2007).

Tout en reproduisant des asymétries déjà décrites dans la littérature, quant à la longueur (plus longue à gauche) et la courbure (plus courbée à droite) de la scissure sylvienne (Chi et al., 1977b, Dubois et al., 2010), ma méthodologie m'a permis de décrire une caractéristique de forme asymétrique supplémentaire : sa tendance dans l'hémisphère gauche à se courber vers l'arrière et à avoir une branche pariétale. J'ai de plus constaté l'encodage de ces trois caractéristiques asymétriques

dès 30s APM, qui restent stables à 40s APM. Une quatrième caractéristique semblait asymétrique à l'AET : la profondeur de la bosse supramarginale (plus profonde à gauche), dont l'asymétrie n'est pas encore observée à 30s APM. J'ai également capturé deux asymétries transitoires à 30s APM qui ne perdurent pas jusqu'à 40s APM, suggérant que la forme de cette scissure évolue pendant cette période avec des dynamiques différentes dans les deux hémisphères.

Je me suis ensuite intéressée à la forme générale que prennent les sillons autour de la scissure sylvienne à 40s APM, en sélectionnant un ensemble de points appartenant aux sillons proches d'elle dont l'inclusion a été pondérée par leur distance à elle (pondération Gaussienne). L'objet résultant capture les éléments de sillons proches de la scissure sylvienne et permet d'étudier ce que je nomme dans la suite la région périsylvienne. La première dimension de l'Isomap de cette région a démontré une forte asymétrie, capturant un phénomène de plus grande proximité des lobes frontal et temporal dans l'hémisphère gauche par rapport au droit, ainsi que la plus forte courbure à droite de la partie postérieure de la scissure sylvienne, qui impacte la disposition les sillons avoisinants.

Avec une méthodologie similaire, j'ai choisi de m'intéresser à la région frontale inférieure par intérêt pour l'aire fonctionnelle associée, l'aire de Broca, impliquée dans la production du langage et latéralisée à gauche chez 90 % des êtres humains (Knecht et al., 2000). J'ai donc défini un objet représentatif de la région frontale inférieure en pondérant l'inclusion de ses sillons constitutifs (en incluant les branches de la scissure sylvienne) par leur distance au point de branchement antérieur de la scissure sylvienne. La première dimension d'Isomap de l'objet résultant a à nouveau capturé une forte asymétrie, semblant encoder l'enfoncement du rameau horizontal antérieur (plus enfoui à gauche) et la profondeur du sillon frontal inférieur (plus profond à droite).

En corrélant les dimensions des différents objets d'étude, j'ai de plus observé des liens entre les dimensions asymétriques, suggérant une dynamique de forme divergente entre l'hémisphère gauche et droit. La combinaison des observations de forme de la scissure sylvienne, de la région périsylvienne et de la région frontale inférieure m'ont menée à émettre l'hypothèse que le processus d'opercularisation présenterait

une dynamique de formation différente du processus de sulcation, se traduisant notamment par une l'avance de l'hémisphère gauche sur l'hémisphère droit, selon un ordre inverse à celui recensé pour la sulcation.

Cette étude a mené à un article qui n'est pas encore soumis mais que nous avons l'intention de soumettre à la revue Cerebral Cortex.

12.7 Discussion

12.7.1 L'étude du plissement cortical

L'étude du plissement cortical étant un champ d'étude relativement récent, l'effort de recherche a tendance à favoriser les sillons et scissures primaires, qui se forment en premier, sont plus profonds, et dont l'identification est généralement moins ambiguë que celle des sillons issus des vagues secondaire (à partir de 32s APM) et tertiaire (à partir de 38s APM) de plissement (Chi et al., 1977a ; Feess-Higgins & Laroche, 1987). En étudiant le sillon central et la scissure sylvienne, j'ai suivi cette mouvance, également pour des raisons de chronologie d'apparition de ces plis, qui peuvent être extraits dès 30s APM, et pour obtenir des résultats interprétables au vu de la littérature préexistante. J'ai ainsi qualifié la forme du sillon central de manière détaillée à 30 et 40s APM, observé une asymétrie de motif sulcal à 40s APM qui n'avait pas été mis en évidence par simple comparaison de longueur sulcale dans la même cohorte (Kersbergen et al., 2016), et qui ressemble vivement à l'asymétrie capturée chez l'adulte (simple ou double « knob ») (Sun et al., 2012). Au niveau de la scissure sylvienne, nous avons retrouvé des asymétries signalées au préalable (en termes de longueur et de courbure ; Chi et al., 1977b ; Dubois et al., 2010), observé de nouvelles asymétries (tendance à se courber en arrière et à avoir une branche, profondeur de la bosse supramarginale hémisphère gauche), et rapporté des caractéristiques de variabilité en forme qui semblent dépendre de l'hémisphère à 30s APM mais pas à 40s, suggérant une asymétrie développementale précoce qui est compensée avant l'AET. Par ailleurs, pour le sillon central comme la scissure sylvienne, les corrélations entre 30 et 40s APM ont suggéré un encodage précoce de la majorité des caractéristiques de forme.

12.7.2 Considérations sur la pertinence méthodologique

Mes choix méthodologiques ont été faits avec un objectif exploratoire. L'utilisation de l'algorithme d'Isomap a rendu chacune de mes études spécifiques à la cohorte, dans la mesure où l'on ne peut pas projeter de nouveau sujet sur une dimension d'Isomap préétablie. Cette méthode nous a cependant permis de qualifier et quantifier la variabilité en forme de nos différents objets d'étude de manière continue (sans opérer de groupement de type « clustering ») et de façon très détaillée. En contrepartie, l'applicabilité clinique des classifieurs de devenir moteur étant intrinsèquement très limitée, j'ai opté pour un paramétrage prudent des classifieurs dû à la taille réduite de la cohorte, ce qui pourrait expliquer leurs faibles performances. Ces études exploratoires ont néanmoins permis d'identifier une caractéristique de forme d'intérêt qui pourrait par la suite être étudiée à plus grande échelle, sur de nouvelles cohortes, à l'aide de méthodes de paramétrisation non dépendantes de la cohorte d'étude (par exemple Cykowski et al., 2008).

12.7.3 Le développement sulcal précoce

Les observations faites sur le sillon central et la scissure sylvienne suggèrent une continuité globale de l'encodage des caractéristiques de forme des plis primaires entre 30 et 40s APM, ainsi qu'un faible impact de la croissance des sillons secondaires et tertiaires sur la forme des sillons et fissures primaires. Pour la scissure sylvienne, j'ai observé une caractéristique de forme postérieure à la région de l'insula qui montrait une corrélation entre 30s et 40s APM plus importante dans l'hémisphère droit, et j'ai émis l'hypothèse qu'elle découlerait d'un phénomène de sulcation plutôt que d'opercularisation.

12.7.4 Une dynamique différente entre opercularisation et sulcation

La question de la différence de dynamique et d'asymétries entre sulcation et opercularisation s'est posée à l'occasion des études régionales que j'ai menées pendant cette thèse, en lien avec la forme fine de la scissure sylvienne. Les asymétries de la région périsylvienne rapportées de manière très reproductibles chez l'humain, et différentes de celles observées chez le chimpanzé (Hou et al., 2019), pointent vers

un contrôle génétique important des changements morphologiques observés au niveau de cette région. Les fortes asymétries que j'ai capturées dans les régions périsylvienne et frontale inférieure, en lien avec les asymétries de la scissure sylvienne, semblent pointer vers une avance d'opercularisation dans l'hémisphère gauche. Or une précédente étude avait montré une absence de relation entre l'asymétrie de longueur de la partie postérieure de la scissure sylvienne et celle de profondeur du sillon temporal supérieur (Glasel et al., 2011), laissant deviner un contrôle génétique différent entre processus de sulcation (observé pour le sillon temporal supérieur) et celui d'opercularisation (engendrant la scissure sylvienne).

12.7.5 Liens entre asymétries interhémisphériques et latéralisation fonctionnelle

Parmi les asymétries précoces du cerveau en développement, les plus fréquemment rapportées sont l'asymétrie de la scissure sylvienne en faveur de la gauche et l'asymétrie du sillon temporal supérieur en faveur de la droite. En plus des asymétries liées à l'opercularisation que nous avons abordées précédemment, deux asymétries supplémentaires de motifs de plissement ont été identifiées : au niveau du cortex cingulaire (Duan et al., 2019), et du sillon central (démontré dans cette thèse). Ces régions anatomiques sont toutes en lien avec des régions fonctionnelles latéralisées : le sillon temporal supérieur et la scissure sylvienne peuvent être rattachés au traitement du langage, le sillon central à la latéralisation motrice, et les sillons cingulaires à la latéralisation des réponses inhibitrices (Serrien et al., 2013), bien que de manière moins clairement définie que pour le langage et la motricité. Ayant accès aux données de latéralité manuelle à 5 ans des sujets de la cohorte d'étude, j'ai tenté de mettre en relation cette information fonctionnelle/comportementale avec le motif de plissement du sillon central. Cependant, malgré une tentative de sélectionner les sujets présentant une latéralité manuelle « naturelle » (non liée à des phénomènes pathologiques), les résultats obtenus ont montré une complémentarité des facteurs cliniques avec les caractéristiques de forme, suggérant un impact des adversités liées à la prématurité sur la latéralité des sujets. Ceci a remis en perspective le caractère non-représentatif de ma cohorte d'études vis-à-vis d'un développement typique des enfants, la prématurité extrême étant

conue comme ayant un impact sur la latéralisation fonctionnelle (Domellöf, 2011 ; Tseng et al., 2019). Nous ne pouvons donc exclure que la naissance prématurée et les affections périnatales qui y sont liées, ont eu un impact direct ou indirect sur les résultats observés. La prématurité extrême a effectivement été démontrée comme ayant un impact sur la latéralisation fonctionnelle (Domellöf, 2011 ; Tseng et al., 2019).

12.7.6 Conclusion et perspectives

Au cours de ma thèse, j'ai contribué à affiner la description des caractéristiques de forme du sillon central et de la scissure sylvienne, ceci au cours du développement et de manière longitudinale : ceci m'a permis de mettre en évidence leur encodage précoce ainsi que des asymétries importantes entre hémisphères. J'ai par ailleurs évalué la capacité prédictive de la forme du sillon central sur le devenir moteur des enfants, et j'ai capturé des asymétries régionales au niveau des régions périsylviennes qui suggèrent une différence de dynamique développementale entre opercularisation et sulcation.

Pour aller plus loin, il faudrait poursuivre l'effort de description de la variabilité en forme des sillons et de ses relations avec la spécialisation et la latéralisation fonctionnelles dans le cerveau mature, reproduire mes études sur des nouveau-nés sains nés à terme pour identifier l'étendue de la variabilité typique, mais aussi sur de plus grandes cohortes de prématurés pour investiguer davantage les liens entre plissement, prématurité et devenir fonctionnel. La question des différences entre opercularisation et sulcation devrait être également approfondie, ainsi que les liens entre asymétries morphologiques des régions périsylviennes et développement de la latéralisation fonctionnelle pour le traitement du langage. Enfin, les méthodes présentées dans cette thèse pourraient être élargies à d'autres sillons et régions d'intérêt, notamment aux sillons secondaires et tertiaires, dont les motifs pourraient être vecteurs d'information fonctionnelle précieuse (Miller et al., 2021).

13 REFERENCES

Altarelli, I., Leroy, F., Monzalvo, K., Fluss, J., Billard, C., Dehaene-Lambertz, G., Galaburda, A.M., Ramus, F., 2014. Planum temporale asymmetry in developmental dyslexia: Revisiting an old question: Planum Temporale Asymmetry in Dyslexia. Hum. Brain Mapp. 35, 5717–5735. https://doi.org/10.1002/hbm.22579

Anderson, P.J., Doyle, L.W., 2006. Neurodevelopmental Outcome of Bronchopulmonary Dysplasia. Seminars in Perinatology 30, 227–232. https://doi.org/10.1053/j.semperi.2006.05.010

Besl, P.J., McKay, N., 1992. A method for registration of 3-D shapes. IEEE Transactions on Pattern Analysis and Machine Intelligence 14, 239–256. https://doi.org/10.1109/34.121791

Cachia, A., Roell, M., Mangin, J.-F., Sun, Z.Y., Jobert, A., Braga, L., Houde, O., Dehaene, S., Borst, G., 2018. How interindividual differences in brain anatomy shape reading accuracy. Brain Struct Funct 223, 701–712. https://doi.org/10.1007/s00429-017-1516-x

Carrion-Castillo, A., Pepe, A., Kong, X.-Z., Fisher, S.E., Mazoyer, B., Tzourio-Mazoyer, N., Crivello, F., Francks, C., 2020. Genetic effects on planum temporale asymmetry and their limited relevance to neurodevelopmental disorders, intelligence or educational attainment. Cortex 124, 137–153. https://doi.org/10.1016/j.cortex.2019.11.006

Chi, J.G., Dooling, E.C., Gilles, F.H., 1977a. Gyral development of the human brain. Ann Neurol. 1, 86–93. https://doi.org/10.1002/ana.410010109

Chi, J.G., Dooling, E.C., Gilles, F.H., 1977b. Left-Right Asymmetries of the Temporal Speech Areas of the Human Fetus. Archives of Neurology 34, 346–348. https://doi.org/10.1001/archneur.1977.00500180040008

Cunningham, D.J., 1892. Cunningham Memoirs - Contribution to the surface anatomy of the cerebral hemispheres by D.J. Cunningham with a chapter upon cranio-cerebral topography by Victor Horsley.

Cykowski, M.D., Coulon, O., Kochunov, P.V., Amunts, K., Lancaster, J.L., Laird, A.R., Glahn, D.C., Fox, P.T., 2008. The Central Sulcus: an Observer-Independent Characterization of Sulcal Landmarks and Depth Asymmetry. Cerebral Cortex 18, 1999–2009. https://doi.org/10.1093/cercor/bhm224

de Vareilles, H., Rivière, D., Sun, Z.-Y., Fischer, C., Leroy, F., Neumane, S., Stopar, N., Eijsermans, R., Ballu, M., Tataranno, M.-L., Benders, M., Mangin, J.-F., Dubois, J., 2022. Shape variability of the central sulcus in the developing brain: A longitudinal descriptive and predictive study in preterm infants. NeuroImage 251, 118837. https://doi.org/10.1016/j.neuroimage.2021.118837

Del Maschio, N., Sulpizio, S., Fedeli, D., Ramanujan, K., Ding, G., Weekes, B.S., Cachia, A., Abutalebi, J., 2019. ACC Sulcal Patterns and Their Modulation on Cognitive Control Efficiency Across Lifespan: A Neuroanatomical Study on Bilinguals and Monolinguals. Cerebral Cortex 29, 3091–3101. https://doi.org/10.1093/cercor/bhy175

Domellöf, E., Johansson, A.-M., Rönnqvist, L., 2011. Handedness in preterm born children: A systematic review and a meta-analysis. Neuropsychologia 49, 2299–2310. https://doi.org/10.1016/j.neuropsychologia.2011.04.033

Duan, D., Xia, S., Rekik, I., Meng, Y., Wu, Z., Wang, L., Lin, W., Gilmore, J.H., Shen, D., Li, G., 2019. Exploring folding patterns of infant cerebral cortex based on multi-view curvature features: Methods and applications. NeuroImage 185, 575–592. https://doi.org/10.1016/j.neuroimage.2018.08.041

Dubois, J., Benders, M., Cachia, A., Lazeyras, F., Ha-Vinh Leuchter, R., Sizonenko, S.V., Borradori-Tolsa, C., Mangin, J.F., Huppi, P.S., 2008. Mapping the Early Cortical Folding Process in the Preterm Newborn Brain. Cerebral Cortex 18, 1444–1454. https://doi.org/10.1093/cercor/bhm180

Dubois, J., Benders, M., Lazeyras, F., Borradori-Tolsa, C., Leuchter, R.H.-V., Mangin, J.F., Hüppi, P.S., 2010. Structural asymmetries of perisylvian regions in the preterm newborn. NeuroImage 52, 32–42. https://doi.org/10.1016/j.neuroimage.2010.03.054

Engelhardt, E., Inder, T.E., Alexopoulos, D., Dierker, D.L., Hill, J., Essen, D., Neil, J.J., 2015. Regional impairments of cortical folding in premature infants. Ann Neurol. 77, 154–162. https://doi.org/10.1002/ana.24313

Feess-Higgins, A., Laroche, J.C., 1987. Development of the Human Foetal Brain: an Anatomical Atlas. Inserm-CNRS, Masson.

Fischer, C., Operto, G., Laguitton, S., et al., 2012. Morphologist 2012: The New Morphological Pipeline of BrainVISA.

Gajawelli, N., Deoni, S.C.L., Ramsy, N., Dean, D.C., O'Muircheartaigh, J., Nelson, M.D., Lepore, N., Coulon, O., 2021. Developmental changes of the central sulcus morphology in young children. Brain Struct Funct 226, 1841–1853. https://doi.org/10.1007/s00429-021-02292-x

Garel, C., Chantrel, E., Brisse, H., Elmaleh, M., Luton, D., Oury, J.-F., Sebag, G., Hassan, M., 2001. Fetal Cerebral Cortex: Normal Gestational Landmarks Identified Using Prenatal MR Imaging 6.

Germann, J., Chakravarty, M.M., Collins, L.D., Petrides, M., 2019. Tight Coupling between Morphological Features of the Central Sulcus and Somatomotor Body Representations: A Combined Anatomical and Functional MRI Study. Cerebral Cortex bhz208. https://doi.org/10.1093/cercor/bhz208

Glasel, H., Leroy, F., Dubois, J., Hertz-Pannier, L., Mangin, J.F., Dehaene-Lambertz, G., 2011. A robust cerebral asymmetry in the infant brain: The rightward superior temporal sulcus. NeuroImage 58, 716–723. https://doi.org/10.1016/j.neuroimage.2011.06.016

Guo, T., Duerden, E.G., Adams, E., Chau, V., Branson, H.M., Chakravarty, M.M., Poskitt, K.J., Synnes, A., Grunau, R.E., Miller, S.P., 2017. Quantitative assessment of white matter injury in preterm neonates: Association with outcomes. Neurology 88, 614–622. https://doi.org/10.1212/WNL.0000000000003606

Habas, P.A., Scott, J.A., Roosta, A., Rajagopalan, V., Kim, K., Rousseau, F., Barkovich, A.J., Glenn, O.A., Studholme, C., 2012. Early Folding Patterns and Asymmetries of the Normal Human Brain Detected from in Utero MRI. Cerebral Cortex 22, 13–25. https://doi.org/10.1093/cercor/bhr053

Hansen, P., Ballesteros, M., Soila, K., Garcia, L., Howard, J.M., 1993. MR Imaging of the Developing Human Brain. RadioGraphics 13, 21–36.

Hickok, G., Poeppel, D., 2007. The cortical organization of speech processing. Nat Rev Neurosci 8, 393–402. https://doi.org/10.1038/nrn2113

Hill, J., Dierker, D., Neil, J., Inder, T., Knutsen, A., Harwell, J., Coalson, T., Van Essen, D., 2010. A Surface-Based Analysis of Hemispheric Asymmetries and Folding of Cerebral Cortex in Term-Born Human Infants. Journal of Neuroscience 30, 2268–2276. https://doi.org/10.1523/JNEUROSCI.4682-09.2010

Hou, L., Xiang, L., Crow, T.J., Leroy, F., Rivière, D., Mangin, J.-F., Roberts, N., 2019. Measurement of Sylvian Fissure asymmetry and occipital bending in humans and Pan troglodytes. NeuroImage 184, 855–870. https://doi.org/10.1016/j.neuroimage.2018.08.045

Kersbergen, K.J., Leroy, F., Išgum, I., Groenendaal, F., de Vries, L.S., Claessens, N.H.P., van Haastert, I.C., Moeskops, P., Fischer, C., Mangin, J.-F., Viergever, M.A., Dubois, J., Benders, M.J.N.L., 2016. Relation between clinical risk factors, early cortical changes, and neurodevelopmental outcome in preterm infants. NeuroImage 142, 301–310. https://doi.org/10.1016/j.neuroimage.2016.07.010

Knecht, S., Dräger, B., Deppe, M., Bobe, L., Lohmann, H., Flöel, A., Ringelstein, E.-B., Henningsen, H., 2000. Handedness and hemispheric language dominance in healthy humans. Brain 123, 2512–2518. https://doi.org/10.1093/brain/123.12.2512

Kwon, S.H., Scheinost, D., Lacadie, C., Sze, G., Schneider, K.C., Dai, F., Constable, R.T., Ment, L.R., 2015. Adaptive mechanisms of developing brain: Cerebral lateralization in the prematurely-born. NeuroImage 108, 144–150. https://doi.org/10.1016/j.neuroimage.2014.12.032

Le Guen, Y., Leroy, F., Auzias, G., Riviere, D., Grigis, A., Mangin, J.-F., Coulon, O., Dehaene-Lambertz, G., Frouin, V., 2018. The chaotic morphology of the left superior temporal sulcus is genetically constrained. NeuroImage 174, 297–307. https://doi.org/10.1016/j.neuroimage.2018.03.046

Leroy, F., Mangin, J.-F., Rousseau, F., Glasel, H., Hertz-Pannier, L., Dubois, J., Dehaene-Lambertz, G., 2011. Atlas-Free Surface Reconstruction of the Cortical Grey-White Interface in Infants. PLoS ONE 6, e27128. https://doi.org/10.1371/journal.pone.0027128

Leroy, F., Cai, Q., Bogart, S.L., Dubois, J., Coulon, O., Monzalvo, K., Fischer, C., Glasel, H., Van der Haegen, L., Bénézit, A., Lin, C.-P., Kennedy, D.N., Ihara, A.S., Hertz-Pannier, L., Moutard, M.-L., Poupon, C., Brysbaert, M., Roberts, N., Hopkins, W.D., Mangin, J.-F., Dehaene-Lambertz, G., 2015. New human-specific brain landmark: The depth asymmetry of superior temporal sulcus. Proc Natl Acad Sci USA 112, 1208–1213. https://doi.org/10.1073/pnas.1412389112

Mallela, A.N., Deng, H., Brisbin, A.K., Bush, A., Goldschmidt, E., 2020. Sylvian fissure development is linked to differential genetic expression in the pre-folded brain. Sci Rep 10, 14489. https://doi.org/10.1038/s41598-020-71535-4

Mangin, J.-F., Frouin, V., Bloch, I., Régis, J., López-Krahe, J., 1995. From 3D magnetic resonance images to structural representations of the cortex topography using topology preserving deformations. J Math Imaging Vis 5, 297–318. https://doi.org/10.1007/BF01250286

Mangin, J., Poupon, F., Duchesnay, E., Riviere, D., Cachia, A., Collins, D., Evans, A., Regis, J., 2004. Brain morphometry using 3D moment invariants. Medical Image Analysis 8, 187–196. https://doi.org/10.1016/j.media.2004.06.016

Mangin, J.-F., Le Guen, Y., Labra, N., Grigis, A., Frouin, V., Guevara, M., Fischer, C., Rivière, D., Hopkins, W.D., Régis, J., Sun, Z.Y., 2019. "Plis de passage" Deserve a Role in Models of the Cortical Folding Process. Brain Topogr 32, 1035–1048. https://doi.org/10.1007/s10548-019-00734-8

Meng, Y., Li, G., Wang, L., Lin, W., Gilmore, J.H., Shen, D., 2018. Discovering cortical sulcal folding patterns in neonates using large-scale dataset. Hum. Brain Mapp. 39, 3625–3635. https://doi.org/10.1002/hbm.24199

Miller, J.A., D'Esposito, M., Weiner, K.S., 2021. Using Tertiary Sulci to Map the "Cognitive Globe" of Prefrontal Cortex. Journal of Cognitive Neuroscience 33, 1698–1715. https://doi.org/10.1162/jocn_a_01696

Moeskops, P., Benders, M.J.N.L., Chiţă, S.M., Kersbergen, K.J., Groenendaal, F., de Vries, L.S., Viergever, M.A., Išgum, I., 2015. Automatic segmentation of MR brain images of preterm infants using supervised classification. NeuroImage 118, 628–641. https://doi.org/10.1016/j.neuroimage.2015.06.007

Penfield, W., Rasmussen, T., 1950. The cerebral cortex of man; a clinical study of localization of function. Macmillan.

Perrot, M., Rivière, D., Mangin, J.-F., 2011. Cortical sulci recognition and spatial normalization. Medical Image Analysis 15, 529–550. https://doi.org/10.1016/j.media.2011.02.008

Scheinost, D., Lacadie, C., Vohr, B.R., Schneider, K.C., Papademetris, X., Constable, R.T., Ment, L.R., 2015. Cerebral Lateralization is Protective in the Very Prematurely Born. Cerebral Cortex 25, 1858–1866. https://doi.org/10.1093/cercor/bht430

Serrien, D.J., Sovijärvi-Spapé, M.M., 2013. Cognitive control of response inhibition and switching: Hemispheric lateralization and hand preference. Brain and Cognition 82, 283–290. https://doi.org/10.1016/j.bandc.2013.04.013

Sowell, E.R., Thompson, P.M., Rex, D., Kornsand, D., Tessner, K.D., Jernigan, T.L., Toga, A.W., 2002. Mapping Sulcal Pattern Asymmetry and Local Cortical Surface Gray Matter Distribution In Vivo: Maturation in Perisylvian Cortices. Cerebral Cortex 12, 17–26. https://doi.org/10.1093/cercor/12.1.17

Sun, T., Patoine, C., Abu-Khalil, A., Visvader, J., Sum, E., Cherry, T.J., Orkin, S.H., Geschwind, D.H., Walsh, C.A., 2005. Early Asymmetry of Gene Transcription in Embryonic Human Left and Right Cerebral Cortex. Science 308, 1794–1798. https://doi.org/10.1126/science.1110324

Sun, Z.Y., Perrot, M., Tucholka, A., Rivière, D., Mangin, J.-F., 2009. Constructing a Dictionary of Human Brain Folding Patterns. Lecture Notes in Computer Science 5762, 117–124.

Sun, Z.Y., Klöppel, S., Rivière, D., Perrot, M., Frackowiak, R., Siebner, H., Mangin, J.-F., 2012. The effect of handedness on the shape of the central sulcus. NeuroImage 60, 332–339. https://doi.org/10.1016/j.neuroimage.2011.12.050

Sun, Z.Y., Pinel, P., Rivière, D., Moreno, A., Dehaene, S., Mangin, J.-F., 2016. Linking morphological and functional variability in hand movement and silent reading. Brain Struct Funct 221, 3361–3371. https://doi.org/10.1007/s00429-015-1106-8

Sun, Z.Y., Cachia, A., Rivière, D., Fischer, C., Makin, T., Mangin, J.-F., 2017. Congenital unilateral upper limb absence flattens the contralateral hand knob. 2017 Organization for Human Brain Mapping Meeting (OHBM 2017).

Tenenbaum, J.B., 2000. A Global Geometric Framework for Nonlinear Dimensionality Reduction. Science 290, 2319–2323. https://doi.org/10.1126/science.290.5500.2319

Tseng, C.-E.J., Froudist-Walsh, S., Kroll, J., Karolis, V., Brittain, P.J., Palamin, N., Clifton, H., Counsell, S.J., Williams, S.C.R., Murray, R.M., Nosarti, C., 2019. Verbal Fluency Is Affected by Altered Brain Lateralization in Adults Who Were Born Very Preterm. eNeuro 6, ENEURO.0274-18.2018. https://doi.org/10.1523/ENEURO.0274-18.2018

“Mieux vaut regarder là où on ne va pas,
parce que, là où on va,
on saura ce qu’il y a quand on y sera”
Proverbe Shadok, *Jacques Roussel*

“Better look at where we are not headed,
because, where we are going,
we will know what there is when we get there”
Shadok proverb, *Jacques Roussel*

14 ANNEX : PUBLICATION LIST AND CONFERENCE PRESENTATIONS

14.1 PUBLICATION LIST

14.1.1 Published

i. Shape variability of the central sulcus in the developing brain: a longitudinal descriptive and predictive study in preterm infants, 2021. NeuroImage 251, 118837. https://doi.org/10.1016/j.neuroimage.2021.118837

***de Vareilles, H.**, Rivière, D., Sun, Z., Fischer, C., Leroy, F., Neumane, S., Stopar, N., Eijsermans, R., Ballu, M., Tataranno, M., Benders, M., Mangin*, J.F., Dubois*, J.*

ii. A Longitudinal Study of the Evolution of the Central Sulcus' Shape in Preterm Infants using Manifold Learning, 2019 In: Wang Q. et al. (eds) Smart Ultrasound Imaging and Perinatal, Preterm and Paediatric Image Analysis. PIPPI 2019, SUSI 2019. Lecture Notes in Computer Science, vol 11798. Springer, Cham, 4P proceedings article https://doi.org/10.1007/978-3-030-32875-7_16

***de Vareilles, H.**, Sun, Z., Benders, M., Fischer, C., Leroy, F., de Vries, L, Groenendaal, F., Rivière, D., Dubois, J., Mangin, J.F.*

14.1.2 Articles in preparation

i. Exploring the emergence of morphological asymmetries around the brain's sylvian fissure: a longitudinal study of shape variability in preterm infants, Full-length article, intended for Cerebral Cortex

***de Vareilles, H.**, Rivière, D., Pascucci, M., Sun, Z., Fischer, C., Leroy, F., Tataranno, M., Benders, M., Dubois*, J., Mangin*, J.F.*

ii. Development of cortical folds in the human brain: an attempt to review biological hypotheses, neuroimaging investigation and modeling studies, Full-length article, intended for Developmental Cognitive Neuroscience (Flux special edition),

***de Vareilles, H.**, Rivière, D., J., Mangin, J.F., Dubois, J.*

14.1.3 Conference presentations

By reverse chronological order:

i. June 2021: Shape variability of the central sulcus in the developing brain: a longitudinal descriptive and predictive study in preterm infants, in French, NeoBrain2 conference,

   Oral presentation (invited),

   ***de Vareilles, H.**, Rivière, D., Dubois, J., Mangin, J.F.*

ii. June 2021: Disentangling the differential maturation of sensorimotor cortices in newborns compared to adults, OHBM conference,

   Poster,

   *Devisscher, L., Chauvel, M., Rolland, C., Labra , N., Aubrain, K., Leroy, F., **de Vareilles, H.**, Hertz-Pannier, L., Grigis, A., Mangin, J.F., Dubois J.*

iii. June 2021: Exploring the cortex microstructure in newborns: A clustering approach of diffusion MRI parameters, OHBM conference,

   Poster,

   *Ginzburg, F., Chauvel, M., Rolland, C., Aubrain, K., Leroy, F., **de Vareilles, H.**, Devisscher, L., Hertz-Pannier, L., Mangin, J.F., Lebenberg, J., Dubois, J.*

iv. June 2020: Folding Dynamics of the Sylvian Fissure : a Longitudinal Study on Preterms, OHBM conference,

Poster,

***de Vareilles, H.**, Riviere, D., Benders, M., Sun , Z., Fischer, C., Leroy, F., Dubois, J., Mangin, J.F.*

v. June 2020: Exploring the microstructural properties of the newborn sensorimotor network with diffusion MRI, OHBM conference,

Poster,

*Chauvel, M., Rheault, F., Rolland, C., Aubrain, K., Leroy, F., **de Vareilles, H.**, Girard, G., Rivière, D., Hertz-Pannier, L., Mangin, J.F., Descoteaux, M., Dubois, J.*

vi. February 2020: Mapping the developing sensorimotor network in newborns with diffusion MRI, ECMRN conference,

Oral presentation (selected),

*Chauvel, M., Rolland, C., Rheault, F., Aubrain, K., Leroy, F., **de Vareilles, H.**, Girard, G., Rivière, D., Hertz-Pannier, L., Mangin, J.F., Descoteaux, M., Dubois, J.*

vii. November 2019: A Longitudinal Study of the Evolution of the Central Sulcus' Shape in Preterm Infants using Manifold Learning, PIPPI workshop from the MICCAI conference,

Oral presentation (selected) and poster

***de Vareilles, H.**, Sun, Z., Benders, M., Fischer, C., Leroy, F., de Vries, L, Groenendaal, F., Rivière, D.,Dubois, J., Mangin, J.F.*

- Best Presentation Award

viii. June 2019: Folding dynamics of the Central Sulcus : a longitudinal study on preterms, OHBM conference,

Poster,

***de Vareilles, H.**, Sun , Z., Benders, M., Fischer, C., Leroy, F., de Vries, L., Groenendaal, F., Riviere, D., Dubois, J., Mangin, J.F.*